Computational aspects of the Schrödinger equation for multiple excitation in scattering processes

COMPUTATIONAL ASPECTS
OF
THE SCHRÖDINGER EQUATION
FOR
MULTIPLE EXCITATION
IN
SCATTERING PROCESSES

^{40}Ar + ^{238}U
E_{lab} =286MeV

0^+

$\sum_i P_i$

P_i

2^+

4^+

6^+

8^+

10^+

12^+

14^+

1.0

0.1

0.5

0.1

0.01

0.001

0   20   40   60   80

θ_{cm}

L.D. TOLSMA

COMPUTATIONAL ASPECTS OF THE SCHRÖDINGER EQUATION FOR MULTIPLE EXCITATION IN SCATTERING PROCESSES

COMPUTATIONAL ASPECTS
OF THE SCHRÖDINGER EQUATION FOR
MULTIPLE EXCITATION IN SCATTERING PROCESSES

PROEFSCHRIFT

TER VERKRIJGING VAN DE GRAAD VAN DOCTOR IN DE
TECHNISCHE WETENSCHAPPEN AAN DE TECHNISCHE
HOGESCHOOL EINDHOVEN, OP GEZAG VAN DE RECTOR
MAGNIFICUS, PROF. DR. F.N. HOOGE, VOOR EEN
COMMISSIE AANGEWEZEN DOOR HET COLLEGE VAN
DEKANEN IN HET OPENBAAR TE VERDEDIGEN OP
VRIJDAG 13 JUNI 1986 TE 16.00 UUR

DOOR

LAMBERTUS DOMINICUS TOLSMA

GEBOREN TE MAGELANG

INDONESIË

DIT PROEFSCHRIFT IS GOEDGEKEURD DOOR DE PROMOTOREN

Prof. dr. B.J. Verhaar

en

Prof. dr. G.W. Veltkamp

Aan mijn ouders,
Tineke,
Karin en Ellen.

CHAPTER 1

GENERAL INTRODUCTION

Inelastic scattering of charged particles from atoms and nuclei is an important tool for studying the properties of excited states. In general, the quantum-mechanical description of inelastic scattering processes with multiple excitation requires the numerical solution of the Schrödinger equation, reformulated as a set of N coupled linear second-order radial differential equations. By means of this solution, the scattering matrix elements can be calculated and, from them, the excitation probabilities which can be compared with experimental data.

In this thesis computational aspects of solving the Schrödinger equation have been studied for small, as well as for large sets to describe inelastic scattering problems with multiple excitation in nuclear physics.

In the usual approach, the set of coupled equations is solved as many times as the dimension of the set with linearly independent regular starting values for each of the solution vectors. The equations are integrated from the origin to a radius at which all nuclear and coupling interactions become insignificant. By constructing the physical solution as a linear combination of the solution vectors with the appropriate asymptotic behaviour of an incoming partial wave in the entrance channel plus outgoing partial waves in all relevant exit channels, the desired S-matrix elements can be found. This standard procedure is satisfactory for small systems of coupled equations, i.e., for light-ion reactions, but it is particularly time-consuming for large systems associated with heavy-ion collisions. In addition, this procedure generates S-matrix elements which form a complete N x N matrix. However, in the nuclear physics context, often only a restricted number of entrance channels (only one for a zero-spin ground state) is important which means that only a restricted number of columns of the scattering matrix is needed. In these cases, iteration methods can be applied for which the solutions are obtained directly without the need for solving the set of coupled equations N times.

When studying scattering problems by solving the Schrödinger equation numerically, an insight has to be gained into the loss of accuracy in the solutions and S-matrix elements, due to the discretization of the set of differential equations and due to other possible sources of deficiencies. Especially, when solving scattering problems with energies near or below

the Coulomb barrier, special attention has to be paid to the loss of accuracy that results from a tendency of the solution vectors to become "nearly linearly dependent" during integration through a classically forbidden region where rounding errors occur that are inherent in the finite representation of numbers in a computer. This loss of accuracy necessitates "stabilization" of the set of solution vectors in a specific way.

The set of coupled equations can be integrated by means of well-known multistep methods, such as the Numerov method. In applying these metods special attention has to be paid to the behaviour of the solution. The heavier the charged particles in the scattering process and the higher the energy of their relative motion, the more rapidly the solution will oscillate in the classically allowed region and the smaller the step sizes in the multistep methods have to be chosen. Since, in general, these circumstances occur together with large systems of coupled equations and a long range of the Coulomb coupling interaction, the multistep methods can become prohibitively time-consuming.

Until recently, calculations with many coupled equations have been possible only within the semi-classical framework of multiple Coulomb excitation. This approach has a number of limitations. Its accuracy decreases steadily as the excitation energy of the reaction channels increases and the transferred angular momentum becomes larger. At energies significantly above the Coulomb barrier, the computational complexity of accurate semi-classical calculations increases rapidly; alternatively, the accuracy of the simplest semi-classical calculation decreases rapidly. Thus, although semi-classical methods are of great value, their limitations are such that a fully quantum mechanical method that can cope with substantially more than twenty to thirty coupled channels would be a valuable alternative.

In order to meet with the problems that occur in heavy-ion collisions, due to the standard procedure for solving the N coupled radial equations N times and the step-size dependency of the multistep methods, it is advantageous to formulate piecewise analytical solution methods together with iteration methods. In this way, heavy-ion multiple Coulomb excitation, as well as multiple excitation including the effects of the nuclear interaction, can be treated effectively. In these methods, the partial wave radial solution of the Schrödinger equation is decomposed into regular and outgoing components, i.e., it is written as a linear combination of two basis functions which oscillate in the classically allowed region with relatively slowly varying amplitudes. These basis functions

are the solutions of the decoupled radial equations. An appropriately chosen reference potential will allow them to be expressed in terms of piecewise analytic reference solutions. Rewriting the set of coupled differential equations in an integral form, the varying amplitudes satisfy a set of coupled integral equations. The integrals that appear in these equations can be evaluated analytically when piecewise analytic reference solutions are used, provided that they belong to a suitably chosen reference potential. The set of integral equations is solved by means of iteration.

This thesis will be subdivided into the following chapters:

In Chapter 2, the formalism for multiple excitation in inelastic scattering processes will be discussed. The set of coupled radial differential equations is derived for the channel-spin as well as for the spin-orbit representation. The general expression for the set is reduced to the form used in the following chapters in order to study solution methods.

In Chapter 3, the accuracy of the numerical integration process is investigated for small sets, using a multistep integration method. A method for measuring the accuracy of the regular solution subspace, spanned by the solution vectors, is used rather than the accuracy of the solution vectors themselves. This method computes the principal angles between two solution subspaces that are obtained under different numerical conditions. Chapter 4 is also devoted to the integration of small sets but, in order to take into account the long range of the Coulomb coupling effectively, a piecewise analytical solution integration method is applied to the integration range beyond the range of the nuclear potential. It appears that, due to its effectiveness, this method can be used to solve moderately large sets as well.

In Chapter 5, the solution of large sets is investigated in order to describe quantum mechanically heavy-ion multiple Coulomb excitation. The results of an investigation, which includes in addition a nuclear interaction potential, are presented in Chapter 6. In both chapters, the set of coupled differential equations has been rewritten as an equivalent set of coupled integral equations. Using goniometric or Airy functions as piecewise analytic reference solutions, the integrals in this set can be evaluated analytically. Coulomb wave functions can be used as reference solutions too, because the corresponding integrals can be evaluated effectively using recurrence relations. The set of integral equations is solved iteratively with a considerable reduction of computation time compared with conventional calculations described in the two foregoing

chapters, where the set was solved as many times as the dimension of the set. The effectiveness of two iteration schemes, an inward-outward and a sequential or perturbative one, has been investigated in some test cases that deal with multiple excitation of ^{238}U by ^{40}Ar and ^{84}Kr. In general, only a few iterations are needed in the inward-outward scheme. In chapter 5, the excitation probabilities for ^{238}U, Coulomb excited by 385 MeV ^{84}Kr up to a state with $I^{\pi} = 24^{+}$ of the ground-state rotational band (GSB), are shown and they are compared with the excitation probabilities calculated according to the semi-classical theory. In chapter 6, the excitation probabilities for Coulomb-nuclear excitation of ^{238}U by 286 MeV ^{40}Ar and 718 MeV ^{84}Kr up to high spin states of the GSB are calculated and for the former compared with experimental data.

In Chapter 7, the recurrence relations are given satisfied by the electric multipole radial matrix elements or Coulomb integrals which arise in particular in the integral representation of the radial Schrödinger equation. The numerical stability and the accuracy obtained are discussed.

A method for vectorization of coupled-channel Fortran programmes, based upon the integral equation method, is presented for use on the Cyber 205 computer (with one vector-pipeline), in Chapter 8. Results are given for the above-mentioned ^{40}Ar and ^{84}Kr test cases. In these tests with dimensions of the set of 64 and 169 , respectively, it appears that the vector algorithm gives a partial speed-up of 4 to 8, resulting in an overall factor of 2 to 3 speed-up as compared with a highly optimized scalar algorithm.

Chapter 9 presents the results of determining the intrinsic quadrupole and hexadecapole moments of the odd-A nuclei ^{163}Dy and ^{167}Er. In addition, the intrinsic quadrupole moment of ^{176}Lu was determined precisely as part of a general study of the electromagnetic properties of this odd-odd nucleus. These properties are interesting, because ^{176}Lu has been proposed for using the β-decay of its $K,I^{\pi} = 7,7^{-}$ ground state to ^{176}Hf as a cosmic clock for s-process nucleosynthesis. These results were obtained in collaboration with the group of Prof. Dr. Th. W. Elze from the university of Frankfurt (BRD).

Finally, it should be noted that some chapters show overlap. This is due to the fact that chapters 3 to 9 constitute independent papers. Overlap occurs, especially, in the sections which describe the introduction and the formalism.

FORMALISM FOR MULTIPLE EXCITATION IN INELASTIC SCATTERING PROCESSES

1. INTRODUCTION

When we consider inelastic collisions between two nuclei a and A, such a pair of particles will be called a "partition" of the total collection of nucleons involved and will be denoted by a Greek letter such as α. The nuclei a and A may exist in any of a large number of excited states as well as their ground states. Sometimes we will use the symbol α to mean simply the partition a+A, and sometimes it will refer to a particular internal state of that partition too, i.e., a particular state of either nucleus a or A. The term "channel" will be used to refer to a particular internal state of a partition in a particular state of relative motion. This term will also be used flexibly [1].

All processes other than elastic or inelastic scattering will be ignored. Let $\vec{r}$ be the relative position vector of the centers of mass of projectile a and target A and let x_a and x_A be the internal nuclear coordinates. We assume that the Hamiltonian equation of the system has the form

$$H = H_a(x_a) + H_A(x_A) + T + V(\vec{r}, x_a, x_A), \tag{2.1}$$

where H_a, H_A are the internal Hamiltonians of projectile and target and T is the relative kinetic energy operator. The interaction potential V contains the nuclear and Coulomb components $V_N(r)$, $V_C(r)$ of the optical potential and the nuclear and Coulomb transition potentials $V_N(\vec{r}, x_a, x_A)$, $V_C(\vec{r}, x_a, x_A)$ that couple internal excitations of a,A with the relative motion [1]:

$$V(\vec{r}, x_a, x_A) = V_N(r) + V_C(r) + V_N(\vec{r}, x_a, x_A) + V_C(\vec{r}, x_a, x_A). \tag{2.2}$$

The internal states of a and A are eigenstates of the internal Hamiltonians H_a and H_A:

$$\left(H_a - \epsilon_{I_a}^a \right) \phi_{I_a M_a}^a(x_a) = 0,$$

$$\tag{2.3}$$

$$\left(H_A - \epsilon_{I_A}^A \right) \phi_{I_A M_A}^A(x_A) = 0,$$

where the superscripts a,A distinguish different internal states of given

angular momentum and the energies are excitation energies referred to the respective ground states.

The relative orbital angular momentum $\vec{L}_\alpha$ of a and A and their respective angular momenta $\vec{I}_a$ and $\vec{I}_A$ are coupled to the total angular momentum $\vec{J} = \vec{I}_a + \vec{I}_A + \vec{L}_\alpha$. Since the interaction $V(\vec{r}, x_a, x_A)$ is a scalar $\vec{J}$ must be conserved; its magnitude J and projection M on to the z-axis are good quantum numbers. In addition, parity must also be conserved; therefore, π is a good quantum number too. There are three choices for the order of coupling these three angular momenta to their resultant, i.e.,

$$\vec{I}_a + \vec{I}_A = \vec{S}_\alpha, \qquad \vec{S}_\alpha + \vec{L}_\alpha = \vec{J} \tag{2.4a}$$

$$\vec{L}_\alpha + \vec{I}_a = \vec{J}_a, \qquad \vec{J}_a + \vec{I}_A = \vec{J} \tag{2.4b}$$

$$\vec{L}_\alpha + \vec{I}_A = \vec{J}_A, \qquad \vec{J}_A + \vec{I}_a = \vec{J} \tag{2.4c}$$

The coupling scheme should be chosen, where possible, so as to simplify the treatment of scattering. If there is a strong interaction coupling between the two nuclear spins, but not to their relative orbital motion (e.g., one proportional to $\vec{I}_A \cdot \vec{I}_a$ times a scalar function of r), this interaction is diagonal in the channel spin $\vec{S}_\alpha$ and the channel-spin representation (2.4a) will be the most useful one. More often, at least with light ions, the strongest interaction is to couple the spin of the light ion to the relative orbital motion. If this ion is the one labeled a, the spin orbit representation (2.4b) will diagonalize the spin-orbit coupling and will be the most convenient one to use. If both types of coupling are of the same importance, none of the representations will diagonalize both simultaneously. Then, the choice is arbitrary, or it may be made on some other grounds. One of these grounds may be the need to use existing computer programs with a minimum modification. In the next two sections, we will derive coupled radial equations for the channel-spin, as well as, for the spin-orbit representation. In particular, expressions will be given for the coupling matrix elements in both representations, taking into account, the mutual excitation of projectile and target [1]. In section 4, the reduction of these general expressions will be discussed ignoring the projectile excitation, as well as its spin. In section 5, the boundary conditions are treated satisfied by the so-called physical solutions of the coupled radial equations.

2. CONSTRUCTION OF COUPLED-CHANNEL EQUATIONS WITH MUTUAL EXCITATION IN THE 'CHANNEL-SPIN' REPRESENTATION

We introduce the channel eigenstates*

$$\Phi_{I_a,I_A}^{a,A,S_\alpha}(x_a,x_A) = \left[\phi_{I_a}(x_a)\, \phi_{I_A}(x_A) \right]_{S_\alpha M_s} \tag{2.5}$$

corresponding to the channel spin $\vec{S}_\alpha$, where we ignore the effects of antisymmetry between projectile and target nucleons. From now on, the superscripts a and A will be deleted in the notation. A basis state of partition α for given total angular momentum J and parity π can be specified by a definite channel spin S_α and a definite relative orbital angular momentum ℓ_α. Solutions of the Schrödinger equation can be expressed, then, in terms of these channel-spin basis states, in the form of:

$$\psi_M^{J\pi}(\vec{r},x_a,x_A) = \frac{1}{r} \sum_\alpha \psi_\alpha^{J\pi}(r) \left[i^{\ell_\alpha} Y_{\ell_\alpha}(\hat{r}) \left[\phi_{I_a}(x_a)\, \phi_{I_A}(x_A) \right]_{S_\alpha} \right]_{JM} \tag{2.6}$$

with $\alpha \equiv \gamma I_a I_A S_\alpha \ell_\alpha$. We have added a subscript γ to stand for any other labels (besides the spins I_a, I_A) needed to specify the internal states of the two nuclei. In practice, only a restricted number of channels are included in the expansion (2.6). Within the truncated model space so defined, the Schrödinger equation reduces to a finite set of coupled radial equations [1]

$$\left[\frac{d^2}{dr^2} + k_\alpha^2 - \frac{\ell_\alpha(\ell_\alpha+1)}{r^2} - \frac{2\mu}{\hbar^2} V^{opt}(r) \right] \psi_\alpha^{J\pi}(r) = \frac{2\mu}{\hbar^2} \sum_{\alpha'=1}^{N} V_{\alpha\alpha'}(r)\, \psi_{\alpha'}^{J\pi}(r). \tag{2.7}$$

The elements $V_{\alpha\alpha'}(r)$ of the coupling matrix in (2.7) are

$$V_{\alpha\alpha'}(r) = \left\langle \left[i^{\ell_\alpha} Y_{\ell_\alpha} \left[\phi_{I_a} \phi_{I_A} \right]_{S_\alpha} \right]_{JM} \middle| V_N(\vec{r},x_a,x_A) + V_C(\vec{r},x_a,x_A) \middle| \right.$$

$$\left. \left[i^{\ell'_\alpha} Y_{\ell'_\alpha} \left[\phi_{I'_a} \phi_{I'_A} \right]_{S'_\alpha} \right]_{JM} \right\rangle \equiv V_{\alpha\alpha'}^N(r) + V_{\alpha\alpha'}^C(r), \tag{2.8}$$

and $V^{opt}(r) = V_N(r) + V_C(r)$. Because $V_N(\vec{r},x_a,x_A) + V_C(\vec{r},x_a,x_A)$ is a scalar,

---

* A square bracket with two angular-momentum dependent functions in it denotes vector coupling. Thus, e.g., $[\phi_j \phi_{j'}]_{JM} = \sum_{m\,m'} (jmj'm'|JM)\phi_{jm}\phi_{j'm'}$.

the matrix with elements $V_{\alpha\alpha'}(r)$ is diagonal in J and M and in π and is independent of M. Consequently, $\psi_\alpha^{J\pi}(r)$ for different values of the total angular momentum J and different parity π $\left[\pi = \pi_a\pi_A(-)^{\ell_\alpha} = \pi_a'\pi_A'(-)^{\ell'_\alpha}\right]$ are not coupled; a set of coupled equations (2.7) exists for each pair of values J,π. The number of coupled equations in (2.7) is denoted by N and the channel wave number k_α is given by:

$$k_\alpha^2 = \frac{2\mu}{\hbar^2}\left(E - \epsilon_{I_a}^a - \epsilon_{I_A}^A\right). \tag{2.9}$$

In these formulae, E is the center-of-mass energy in the incident ground-state channel and μ is the reduced mass. Closed channels, for which k_α is imaginary will not occur in the following.

The nuclear part of the optical potential will be taken to be of complex Woods-Saxon form, e.g.,

$$V_N(r) = -V(1+e_v)^{-1} - iW(1+e_w)^{-1}, \tag{2.10a}$$

where

$$e_v = \exp\left[(r - R_v)/a_v\right], \tag{2.10b}$$

whilst V, R_v and a_v are the strength, the radius and diffuseness parameters of the real part of the nuclear potential, respectively. The parameters W and e_w have a similar meaning relative to the imaginary part of the nuclear potential.

The Coulomb part of the optical potential is given by the interaction potential of a point charge with a uniform sphe i a ha e ist i ution within the Coulomb radius R_c and zero charge outside it:

$$V_C(r) = Z_aZ_Ae^2 \begin{bmatrix} \frac{1}{2R_c}\left(3 - (\frac{r}{R_c})^2\right) & r < R_c \\ \\ \frac{1}{r} & r > R_c \end{bmatrix} \tag{2.11}$$

where Z_a and Z_A represent the charge numbers of the projectile and target nucleus, respectively.

A complete specification of the coupling matrix $V_{\alpha\alpha'}(r)$ requires the introduction of a detailed model for the internal nuclear states involved and specific assumptions about the nuclear and Coulomb interaction potentials $V_N(\vec{r},x_a,x_A)$ and $V_C(\vec{r},x_a,x_A)$. The evaluation of these matrix elements is the most crucial part of the whole calculation; however, we will not do this. Never-the-less, the nuclear transition potential can

- 8 -

still be written in a general form as [2,3]:

$$V_N(\vec{r}, x_a, x_A) = \sum_{\substack{a,A \\ \lambda_a, \lambda_A, \lambda}} v_{\lambda_a \lambda_A \lambda}^{(a,A)}(r) \; \{[Q_{\lambda_a}^{(a)} Q_{\lambda_A}^{(A)}]_\lambda \cdot i^\lambda Y_\lambda(\hat{r})\}, \qquad (2.12)$$

where the superscripts a,A distinguish terms of different character but with the same tensorial ranks λ_a, λ_A. The operators $Q_{\lambda_a}^{(a)}$ and $Q_{\lambda_A}^{(A)}$ operate only on the coordinates of the nuclei a and A, respectively. The dot in (2.12) indicates a scalar product of two tensor operators of the same rank λ. These tensor operators work on different degrees of freedom of the system, i.e., they commute.

The transition electric-electric multipole Coulomb interaction potential between the charge distributions of a and A is given by [4]:

$$V_C(\vec{r}, x_a, x_A) = (4\pi)^{3/2} \sum_{\lambda_a, \lambda_A, \lambda} (-)^{\lambda_a} \left[\frac{(2\lambda_a + 2\lambda_A)!}{(2\lambda_a + 1)!(2\lambda_A + 1)!(2\lambda + 1)} \right]^{1/2}$$

$$\frac{1}{r^{\lambda_a + \lambda_A + 1}} \{[M_a(E\lambda_a)M_A(E\lambda_A)]_\lambda \cdot i^\lambda Y_\lambda(\hat{r})\}, \qquad (2.13)$$

where the electric multipole moments are defined as:

$$M(E\lambda, \mu) = \int \rho(\vec{r}) \; r^\lambda \; Y_{\lambda\mu}(\hat{r}) \; d\tau \qquad (2.14)$$

with a charge density given by $\rho(\vec{r})$, which for a deformed target nucleus (projectile) may differ from the spherical one associated with (2.11).

If the expression (2.12) is used for the transition nuclear potential, then, the coupling matrix element $V_{\alpha\alpha'}^N(r)$ of (2.8) can be obtained explicitly as [5]:

$$V_{\alpha\alpha'}^N(r) = \sum_{\substack{a,A \\ \lambda_a, \lambda_A, \lambda}} v_{\lambda_a \lambda_A \lambda}^{(a,A)}(r) \; \langle I_a \| Q_{\lambda_a}^{(a)} \| I_a' \rangle \; \langle I_A \| Q_{\lambda_A}^{(A)} \| I_A' \rangle$$

$$G(I_a I_A S_\alpha \ell_\alpha, I_a' I_A' S_\alpha' \ell_\alpha'; \lambda_a \lambda_A \lambda J), \qquad (2.15)$$

where the geometrical factor $G(I_a I_A S_\alpha \ell_\alpha, I_a' I_A' S_\alpha' \ell_\alpha'; \lambda_a \lambda_A \lambda J)$ in the channel-spin representation is defined as:

$$G(I_a I_A S_\alpha \ell_\alpha, I'_a I'_A S'_\alpha \ell'_\alpha; \lambda_a \lambda_A \lambda J) = (4\pi)^{-1/2} \, i^{\ell'_\alpha - \ell_\alpha + \lambda} \, (-)^{J + S_\alpha + \ell_\alpha + \ell'_\alpha}$$

$$\hat{\ell}_\alpha \hat{\ell}'_\alpha \hat{\lambda} \begin{pmatrix} \ell_\alpha & \ell'_\alpha & \lambda \\ 0 & 0 & 0 \end{pmatrix} \begin{Bmatrix} \ell_\alpha & \ell'_\alpha & \lambda \\ S'_\alpha & S_\alpha & J \end{Bmatrix} \hat{S}_\alpha \hat{S}'_\alpha \hat{\lambda} \begin{Bmatrix} I_a & I'_a & \lambda_a \\ I_A & I'_A & \lambda_A \\ S_\alpha & S'_\alpha & \lambda \end{Bmatrix}$$

$$(2.16)$$

with $\hat{x} = (2x+1)^{1/2}$. The reduced matrix elements $\langle I_a \| Q^{(a)}_{\lambda_a} \| I'_a \rangle$ and $\langle I_A \| Q^{(A)}_{\lambda_A} \| I'_A \rangle$ appearing in (2.15) contain the dynamics of the nuclei a and A, respectively, that are involved in the problem [5,6]. Based upon some model, explicit forms can be given for these reduced matrix elements [2]. It is noted that the basis states (2.6) are defined with i^ℓ factors accompanying the spherical harmonics $Y^m_\ell(\theta, \phi)$. A factor i^λ is included explicitly in the scalar product of the two tensor operators (2.12) too. These phase factors ensure convenient time-reversal properties.

In the same way, the coupling matrix element $V^C_{\alpha\alpha'}(r)$ can be derived from (2.13) for the Coulomb transition potential:

$$V^C_{\alpha\alpha'}(r) = (4\pi)^{3/2} \sum_{\lambda_a, \lambda_A, \lambda} (-)^{\lambda_a} \left[\frac{(2\lambda_a + 2\lambda_A)!}{(2\lambda_a + 1)!(2\lambda_A + 1)!(2\lambda + 1)} \right]^{1/2}$$

$$\frac{1}{r^{\lambda_a + \lambda_A + 1}} \langle I_a \| M_a(E\lambda_a) \| I'_a \rangle \langle I_A \| M_A(E\lambda_A) \| I'_A \rangle$$

$$G(I_a I_A S_\alpha \ell_\alpha, I'_a I'_A S'_\alpha \ell'_\alpha; \lambda_a \lambda_A \lambda J), \quad (2.17)$$

where the geometrical factor is again given by (2.16).

3. CONSTRUCTION OF COUPLED-CHANNEL EQUATIONS WITH MUTUAL EXCITATION IN THE 'SPIN-ORBIT' REPRESENTATION

Using an analogy with (2.16), we introduce the spin-orbit basis states according to coupling scheme (2.4b):

$$\psi_M^{J\pi}(\vec{r},x_a,x_A) = \frac{1}{r} \sum_\alpha \psi_\alpha^{J\pi}(r) \left[\left[i^{\ell_\alpha} Y_{\ell_\alpha}(\hat{r}) \Phi_{I_a}(x_a) \right]_{j_a} \Phi_{I_A}(x_A) \right]_{JM} \quad (2.18)$$

with $\alpha \equiv \gamma \ell_\alpha I_a j_a I_A$. If we insert this expansion into the Schrödinger equation, we obtain a finite set of coupled radial equations for the radial functions $\psi_\alpha^{J\pi}(r)$ similar to (2.7)

$$\left[\frac{d^2}{dr^2} + k_\alpha^2 - \frac{\ell_\alpha(\ell_\alpha+1)}{r^2} - \frac{2\mu}{\hbar^2} V^{opt}(r) \right] \psi_\alpha^{J\pi}(r) = \frac{2\mu}{\hbar^2} \sum_{\alpha'=1}^{N} V_{\alpha\alpha'}(r) \psi_{\alpha'}^{J\pi}(r),$$

$$(2.19)$$

where the elements $V_{\alpha\alpha'}(r)$ of the coupling matrix are now given by:

$$V_{\alpha\alpha'}(r) = \left\langle \left[\left[i^{\ell_\alpha} Y_{\ell_\alpha} \Phi_{I_a} \right]_{j_a} \Phi_{I_A} \right]_{JM} \left| V_N(\vec{r},x_a,x_A)+V_C(\vec{r},x_a,x_A) \right. \right.$$

$$\left. \left[\left[i^{\ell'_\alpha} Y_{\ell'_\alpha} \Phi_{I'_a} \right]_{j'_a} \Phi_{I'_A} \right]_{JM} \right\rangle \equiv V_{\alpha\alpha'}^N(r)+V_{\alpha\alpha'}^C(r) \quad (2.20)$$

The nuclear interaction potential $V_N(\vec{r},x_a,x_A)$ can be expanded to:

$$V_N(\vec{r},x_a,x_A) = \sum_{\substack{a,A \\ \lambda_a,\lambda_A,\lambda}} v_{\lambda_a\lambda_A\lambda}^{(a,A)}(r) \left\{ \left[i^\lambda Y_\lambda(\hat{r}) Q_{\lambda_a}^{(a)} \right]_{\lambda_A} \cdot Q_{\lambda_A}^{(A)} \right\}, \quad (2.21)$$

and equivalently the electric-electric Coulomb interaction potential V_C

$$V_C(\vec{r},x_a,x_A) = (4\pi)^{3/2} \sum_{\lambda_a,\lambda_A,\lambda} \left[\frac{(2\lambda_a+2\lambda_A)!}{(2\lambda_a+1)!(2\lambda_A+1)!(2\lambda_A+1)} \right]^{1/2}$$

$$(2.22)$$

$$\frac{1}{r^{\lambda_a+\lambda_A+1}} \left\{ \left[i^\lambda Y_\lambda(\hat{r}) M_a(E\lambda_a) \right]_{\lambda_A} \cdot M_A(E\lambda_A) \right\},$$

The standard reduction formulae for the coupling matrix elements of the scalar product of two commuting tensor operators such as (2.21) and

(2.22) can be used here, too. Then, $V_{\alpha\alpha'}^{N}(r)$ in the spin-orbit representation becomes:

$$V_{\alpha\alpha'}^{N}(r) = \sum_{\substack{a,A \\ \lambda_a,\lambda_A,\lambda}} v_{\lambda_a\lambda_A\lambda}^{(a,A)}(r) \langle I_a \| Q_{\lambda_a}^{(a)} \| I_a' \rangle \langle I_A \| Q_{\lambda_A}^{(A)} \| I_A' \rangle$$

$$G(\ell_\alpha I_a j_a I_A, \ell_\alpha' I_a' j_a' I_A'; \lambda_a \lambda_A \lambda J), \qquad (2.23)$$

where the geometrical factor $G(\ell_\alpha I_a j_a I_A, \ell_\alpha' I_a' j_a' I_A'; \lambda_a \lambda_A \lambda J)$ in the spin-orbit representation is defined as:

$$G(\ell_\alpha I_a j_a I_A, \ell_\alpha' I_a' j_a' I_A'; \lambda_a \lambda_A \lambda J) = (4\pi)^{-1/2} i^{\ell_\alpha'-\ell_\alpha+\lambda} (-)^{J+I_A+\ell_\alpha+j_a'}$$

$$\hat{\ell}_\alpha \hat{\ell}_\alpha' \hat{\lambda} \begin{pmatrix} \ell_\alpha & \ell_\alpha' & \lambda \\ 0 & 0 & 0 \end{pmatrix} \begin{Bmatrix} j_a & j_a' & \lambda_A \\ I_A' & I_A & J \end{Bmatrix} \hat{j}_a \hat{j}_a' \hat{\lambda}_A \begin{Bmatrix} \ell_\alpha & \ell_\alpha' & \lambda \\ I_a & I_a' & \lambda_a \\ j_a & j_a' & \lambda_A \end{Bmatrix}.$$

$$(2.24)$$

In the same way, the coupling matrix element $V_{\alpha\alpha'}^{C}(r)$ in the spin-orbit representation is obtained from (2.22) for the Coulomb transition potential:

$$V_{\alpha\alpha'}^{C}(r) = (4\pi)^{3/2} \sum_{\lambda_a,\lambda_A,\lambda} \left[\frac{(2\lambda_a+2\lambda_A)!}{(2\lambda_a+1)!(2\lambda_A+1)!(2\lambda_A+1)} \right]^{1/2}$$

$$\frac{1}{r^{\lambda_a+\lambda_A+1}} \langle I_a \| M_a(E\lambda_a) \| I_a' \rangle \langle I_A \| M_A(E\lambda_A) \| I_A' \rangle$$

$$G(\ell_\alpha I_a j_a I_A, \ell_\alpha' I_a' j_a' I_A'; \lambda_a \lambda_A \lambda J), \qquad (2.25)$$

where the geometrical factor is given by (2.24)

4. THE COUPLING MATRIX ELEMENTS $V_{\alpha\alpha'}(r)$ FOR $\lambda_a = 0$ and $I_a = 0$

In the preceeding sections, we described the general formalism for inelastic scattering, including mutual excitation. In the next chapters, however, calculation methods and their results will be discussed based upon a formalism that ignores the excitation of the projectile, as well as its spin, if it has any. Therefore, in this section, the expressions for the coupling matrix elements $V_{\alpha\alpha'}(r)$ will be given to which the general expressions (2.15, 2.17) and (2.23, 2.25) of $V^N_{\alpha\alpha'}(r)$ and $V^C_{\alpha\alpha'}(r)$ in the channel-spin and spin-orbit representation, respectively, reduce for $\lambda_a = 0$ and $I_a = 0$.

When the projectile excitation is not considered, or the interaction acts only on the internal degrees of freedom of one nucleus, say A, we may put $\lambda_a = 0$ and $Q^{(a)}_{\lambda_a} = 1$. It is then clear that $\lambda_A = \lambda$ and the reduced matrix elements of the projectile in (2.15) and (2.17) become:

$$\langle I_a \| Q^{(a)}_{\lambda_a} \| I'_a \rangle = (2I_a+1)^{1/2} \, \delta_{I_a I'_a} \tag{2.26}$$

and

$$\langle I_a \| M_a(E\lambda_a) \| I'_a \rangle = \frac{Z_a e}{(4\pi)^{1/2}} (2I_a+1)^{1/2} \, \delta_{I_a I'_a} \, , \tag{2.27}$$

respectively.

The geometrical factor (2.16) in the channel-spin representation reduces for $\lambda_a = 0$ to

$$G(I_a I_A S_\alpha \ell_\alpha, I_a I'_A S'_\alpha \ell'_\alpha; 0\lambda\lambda J) = (4\pi)^{-1/2} \, i^{\ell'_\alpha - \ell_\alpha + \lambda} (-)^{J - S'_\alpha}$$

$$\hat{\ell}_\alpha \hat{\ell}'_\alpha \hat{\lambda} \begin{pmatrix} \ell_\alpha & \ell'_\alpha & \lambda \\ 0 & 0 & 0 \end{pmatrix} \begin{Bmatrix} \ell_\alpha & \ell'_\alpha & \lambda \\ S'_\alpha & S_\alpha & J \end{Bmatrix} \hat{S}_\alpha \hat{S}'_\alpha \begin{Bmatrix} S_\alpha & S'_\alpha & \lambda \\ I'_A & I_A & I_a \end{Bmatrix} . \tag{2.28}$$

This expression reduces further if $I_a = 0$ (then $S_\alpha = I_A$ and $S'_\alpha = 0$) to:

$$G(0I_A I_A \ell_\alpha, 0I'_A I'_A \ell'_\alpha; 0\lambda\lambda J) = (4\pi)^{-1/2} \, i^{\ell'_\alpha - \ell_\alpha + \lambda} (-)^{J + I_A + \ell_\alpha + \ell'_\alpha}$$

$$\hat{\ell}_\alpha \hat{\ell}'_\alpha \hat{\lambda} \begin{pmatrix} \ell_\alpha & \ell'_\alpha & \lambda \\ 0 & 0 & 0 \end{pmatrix} \begin{Bmatrix} \ell_\alpha & \ell'_\alpha & \lambda \\ I'_A & I_A & J \end{Bmatrix} . \tag{2.29}$$

The expression for the geometrical factor (2.24) in the spin-orbit representation reduces for $\lambda_a = 0$ to:

$$G(\ell_\alpha I_a j_a I_A, \ell'_\alpha I_a j'_a I'_A; 0\lambda\lambda J) = (4\pi)^{-1/2} \, i^{\ell'_\alpha - \ell_\alpha + \lambda} \, (-)^{J+I_A+\ell_\alpha+j'_a}$$

$$\hat{\ell}_\alpha \hat{\ell}'_\alpha \, \hat{\lambda} \begin{pmatrix} \ell_\alpha & \ell'_\alpha & \lambda \\ 0 & 0 & 0 \end{pmatrix} \begin{Bmatrix} j_a & j'_a & \lambda \\ I'_A & I_A & J \end{Bmatrix} \hat{j}_a \hat{j}'_a \begin{Bmatrix} \ell_\alpha & \ell'_\alpha & \lambda \\ j'_a & j_a & I_a \end{Bmatrix}. \quad (2.30)$$

For $I_a = 0$ (then $j_a = \ell_\alpha$ and $j'_a = \ell'_\alpha$) it reduces further to the same expression (2.29) that we obtained in the channel-spin representation when $I_a = 0$:

$$G(\ell_\alpha 0 \ell_\alpha I_A, \ell'_\alpha 0 \ell'_\alpha I'_A; 0\lambda\lambda J) = (4\pi)^{-1/2} \, i^{\ell'_\alpha - \ell_\alpha + \lambda} \, (-)^{J+I_A+\ell_\alpha+\ell'_\alpha}$$

$$\hat{\ell}_\alpha \hat{\ell}'_\alpha \, \hat{\lambda} \begin{pmatrix} \ell_\alpha & \ell'_\alpha & \lambda \\ 0 & 0 & 0 \end{pmatrix} \begin{Bmatrix} \ell_\alpha & \ell'_\alpha & \lambda \\ I'_A & I_A & J \end{Bmatrix}. \quad (2.31)$$

In the next chapters, we will study methods for solving a set of coupled radial equations (2.19) without mutual excitation and for spinless projectiles, i.e., for $\lambda_a = 0$ and $I_a = 0$. Then, the expressions for the coupling matrix elements $V^N_{\alpha\alpha'}(r)$ and $V^C_{\alpha\alpha'}(r)$ given by (2.23) and (2.25), respectively, reduce to:

$$V^N_{\alpha\alpha'}(r) = \sum_\lambda v^{(A)}_\lambda(r) \, \langle I_A \| Q^{(A)}_\lambda \| I'_A \rangle \, G(\ell_\alpha 0 \ell_\alpha I_A, \ell'_\alpha 0 \ell'_\alpha I'_A; 0\lambda\lambda J) \quad (2.32)$$

and

$$V^C_{\alpha\alpha'}(r) = Z_a e \sum_\lambda \frac{4\pi}{2\lambda+1} \frac{1}{r^{\lambda+1}} \langle I_A \| M_A(E\lambda_A) \| I'_A \rangle \, G(\ell_\alpha 0 \ell_\alpha I_A, \ell'_\alpha 0 \ell'_\alpha I'_A; 0\lambda\lambda J),$$

$$(2.33)$$

where the geometrical factor $G(\ell_\alpha 0 \ell_\alpha I_A, \ell'_\alpha 0 \ell'_\alpha I'_A; 0\lambda\lambda J)$ is given by (2.31).

5. BOUNDARY CONDITIONS FOR THE SOLUTION FUNCTION $\psi_\alpha^{J\pi}(r)$

In order to obtain solutions $\psi_\alpha^{J\pi}(r)$ of the sets (2.7) or (2.19) of the coupled radial equations of physical interest, i.e., the physical solutions, two boundary conditions have to be fulfilled ($\alpha \equiv I\ell$ when $\lambda_a = 0$ and $I_a = 0$). At the origin $\psi_\alpha^{J\pi}(r)$ should vanish:

$$\lim_{r \to 0} \psi_\alpha^{J\pi(\alpha_0)}(r) = 0, \qquad (2.34a)$$

whilst, for large distances, $\psi_\alpha^{J\pi}(r)$, must represent an ingoing partial wave in the entrance channel plus outgoing partial waves in all the relevant exit channels. The precise asymptotic form defines the scattering matrix elements $S_{\alpha\alpha_0}^{J\pi}$:

$$\psi_\alpha^{J\pi(\alpha_0)}(r) \underset{r \to \infty}{\sim} H_\ell^-(r)\, \delta_{\alpha\alpha_0} - \left[\frac{k_{\alpha_0}}{k_\alpha}\right]^{1/2} H_\ell^+(r)\, S_{\alpha\alpha_0}^{J\pi}, \qquad (2.34b)$$

where the subscript and superscript α_0 correspond to an ingoing wave in the entrance channel for $\alpha = \alpha_0$. In principle, there are N entrance channels. The ingoing and outgoing Coulomb waves $H_\ell^-(r)$ and $H_\ell^+(r)$, respectively, are given in terms of the well-known regular and irregular Coulomb wave functions $F_\ell(r)$ and $G_\ell(r)$, by $H_\ell^\pm(r) = \{G_\ell(r) \pm iF_\ell(r)\}$.

The solution $\{\psi_1^{J\pi}(r),\ldots, \psi_N^{J\pi}(r)\}$ of (2.7) or (2.19) can be considered as a solution vector $\psi^{J\pi}(r)$. The solution vectors constitute a vector space of dimension 2N. This 2N-dimensional space contains an N-dimensional subspace of regular solutions that satisfy the boundary conditions (2.34a). The generation of a basis of N linearly independent solution vectors $\psi_s^{J\pi}(r)$, $s = 1,2,\ldots,N$, for the regular subspace, by solving (2.7) or (2.19), involves the explicit construction of N regular solution vectors, each with a linearly independent choice of starting conditions. The solution vectors $\psi^{J\pi(\alpha_0)}(r)$ that we are looking for, are regular; hence, they are linear combinations of the vectors $\psi_s^{J\pi}(r)$ and are found by considering the boundary condition (2.34b) at a matching radius $r = R_m$ which is sufficiently large for all the potentials except $V_C(r)$ in (2.2) to be negligible.

Thus, the sets (2.7) or (2.19) have to be solved N times. Especially, for large systems this will be time-consuming. In addition, this procedure generates S-matrix elements which form a complete N x N matrix; while in the physics context, often only a restricted number of entrance channels is important which means that only a restricted number of

columns of the scattering matrix is needed. For these cases, iteration methods can be applied and solutions are obtained directly without the need of solving the sets (2.7) or (2.19) N times.

The scattering amplitudes are expressed in terms of the S-matrix elements (see Chap. IX of Ref. [4])

$$f(\theta,\phi)_{I_0 M_0 \rightarrow IM} = \left(\frac{4\pi}{k_{I_0} k_I}\right)^{1/2} \sum_{\ell_0 \ell J} (2\ell_0+1)^{1/2} i^{\ell_0-\ell} (\ell_0 0 I_0 M_0 | JM_0)(\ell m IM | JM_0)$$

$$\frac{1}{2i} \{ \exp[i(\sigma_{\ell_0}+\sigma_\ell)] \ S^{J\pi}_{I\ell;I_0\ell_0} - \delta_{II_0} \delta_{\ell\ell_0} \} Y_{\ell m}(\theta,\phi),$$

(2.35)

in which σ_ℓ is the Coulomb phase shift

$$\sigma_\ell(\eta) = \arg\Gamma(\ell+1+i\eta).$$

(2.36)

From the scattering amplitudes, it is easy to calculate the cross section for state I:

$$\frac{d\sigma_I(\theta)}{d\Omega} = \frac{1}{2I_0+1} \frac{k_I}{k_{I_0}} \sum_{M_0 M} | \ f_{I_0 M_0 \rightarrow IM}(\theta,\phi=0) \ |^2$$

(2.37)

and other observable quantities. The excitation probability, for instance, is given by:

$$P_I(\theta) = \frac{k_I}{k_{I_0}} \frac{d\sigma_I}{d\sigma_R},$$

(2.38)

where σ_R is the Rutherford cross section.

REFERENCES
[1] G.R. Satchler, "Direct Nuclear Reactions", Clarendon Press, Oxford, 1983.
[2] T. Tamura, Rev. Mod. Phys. 37(1965)679.
[3] T. Tamura, Physics Reports 14(1974)59.
[4] K. Alder and A. Winther, "Electromagnetic Excitation", North-Holland Publishing Company, Amsterdam-Oxford, 1975.
[5] A.R. Edmonds, "Angular Momentum in Quantum Mechanics", Princeton University Press, Princeton, New Jersey, 1957.
[6] D.M. Brink and G.R. Satchler, "Angular Momentum", Clarendon Press, Oxford, 1962.

CHAPTER 3

MEASURING THE ACCURACY OF THE SOLUTION SUBSPACE OBTAINED BY
NUMERICAL INTEGRATION OF THE SCHRÖDINGER EQUATION[*]

L.D. TOLSMA

Department of Physics, Eindhoven University of Technology

and

G.W. VELTKAMP

Department of Mathematics, Eindhoven University of Technology,

Eindhoven, The Netherlands

ABSTRACT

In general, the quantum-mechanical description of inelastic scattering processes requires the numerical solution of the radial Schrödinger equation. To investigate the accuracy of the numerical integration process, a method has been used successfully for measuring the accuracy of the regular solution subspace spanned by the solution vectors, rather than the accuracy of the solution vectors themselves. This method computes the principal angles between two solution subspaces obtained under different numerical conditions. One of the subspaces is constructed under optimal conditions so that it is considered to be the reference subspace, the other being the subspace to be investigated. In this method, the quality of a solution subspace obtained by a numerical procedure, can be measured, e.g., the extent to which solution vectors, as a basis of the solution subspace, remain linearly independent in the range from the origin to the matching radius R_m during the integration.

The computation of the principal angles can be used to inspect the loss of accuracy in the integration range originating from the truncation error inherent in the difference formula employed and to detect possible sources of deficiencies in the numerical process for solving the Schrödinger equation. A method has been developed and applied with which deficiencies caused by discontinuities in the potential matrix can be avoided.

The loss of accuracy due to the tendency of the solution vectors to become nearly linearly dependent during the integration through a classically forbidden region as an effect of round-off errors, can be examined by determining the principal angles, as well. This loss of accuracy requires stabilization of the set of solution vectors. We found that the stabilization in only a few well chosen mesh points in our nuclear physics test cases of alpha scattering from ^{28}Si, proved to be sufficient for obtaining an S-matrix accuracy satisfactory for practical purposes.

1. INTRODUCTION

For the quantum-mechanical description of inelastic scattering processes with multiple excitation the radial Schrödinger equation, i.e., a set of coupled linear second-order differential equations, has to be in general solved numerically. In the case of nuclear physics scattering problems with energies near or below the Coulomb barrier, special attention has to be paid to the stability of the solutions since, without precautions, the initial linear independence of the solution vectors will be destroyed. Solving the set of coupled equations with a multistep integration method, the accuracy of the solutions, as well as of the S-matrix elements can be measured by means of the differences in these quantities computed for successively decreasing step sizes.

For the study of stability and accuracy in the solutions of nuclear physics scattering processes, Tamura's code JUPITOR $[1,5]$ has been used. In this code Störmer's multistep integration method has been applied which has a local discretization or truncation error of order h^7; whereas, the global error for a fixed integration interval will be of order h^5. Therefore, an accuracy is expected of order h^4 to h^5. However, even after developing a satisfying stabilization procedure, it appears that the accuracy obtained is of the order h.

A primary aim of this paper is to investigate the reasons for the serious loss of accuracy and to detect the possible sources of deficiencies. For examining the accuracy of the integration process, a method has been used for measuring the accuracy of the regular solution subspace spanned by the solution vectors, rather than the accuracy of the solution vectors themselves. This method computes the principal angles between two solution subspaces obtained under different numerical conditions (varying integration step length and stabilization strategy). One of the subspaces has been constructed under optimal conditions, so that it is considered as the reference subspace, the other being the subspace to be investigated. This seems to be a very sensitive method and the deficiencies have been located with it. It appears that the loss of accuracy is, in part, caused by discontinuities in the second and higher radial derivatives of the Coulomb part of the diagonal potential and in the Coulomb part of the coupling potential and its higher radial derivatives at the Coulomb radius. Another source of deficiency appears to be a programming error in the original version of the code JUPITOR.

After developing and applying a method that avoids the inaccuracies in the solutions due to the discontinuities mentioned, the expected accuracy of the solutions and S-matrix elements can be obtained. It must be stressed that the method presented can also be applied to the general case in which the diagonal, as well as the coupling potential and/or their higher radial derivatives, show discontinuities at some radius.

Along with the loss of accuracy in the solutions and S-matrix elements due to the discretization of the set of differential equations, there is also, a loss of accuracy due to the tendency of the solution vectors to become nearly linearly dependent in combination with the finite representation of numbers in the computer (round-off errors). Gaining an insight into the latter loss of accuracy is the second purpose of this paper. This can be obtained by the method of computing angles between the subspaces spanned by the solution vectors.

In section 2, a concise description of the scattering formalism is given. This description is limited to the formulae needed for this paper. Section 3 is devoted to the integration methods used in JUPITOR to solve the set of differential equations. To maintain the linear independence of the set of solution vectors, a stabilization procedure and a criterion for the need to perform a stabilization are discussed in section 4. In section 5, attention is paid to the boundary conditions at the matching radius. Section 6 describes a method of computing the principal angles between subspaces spanned by the solution vectors. In section 7, a method is derived to avoid the inaccuracies in the solutions due to radial discontinuities in the potential matrix. The results of our investigation are presented and discussed in Section 8 and 9. These results have been obtained for the inelastic scattering of 10 and 104 MeV alpha particles from ^{28}Si. Section 8 contains the results related to the detection of the sources of deficiencies and the avoidance of their inaccuracies in the solutions. In addition, the influence of the deficiencies, and of their removal, on the accuracy of the S-matrix elements will be discussed. From these results that were obtained for successively decreasing step sizes, an insight has been obtained into the accuracy of the integration process. Section 9 treats the results related to the loss of accuracy due to the tendency of the solution vectors to move towards linear dependency. Finally, in section 10, conclusions are drawn.

2. CONCISE DESCRIPTION OF THE SCATTERING FORMALISM

The quantum-mechanical description of inelastic scattering in nuclear physics has been discussed extensively in literature [1-4]. This description leads to a set of coupled second-order differential equations for the partial wave radial functions $\psi_{I\ell}^{J\pi}$, having the following form:

$$[\frac{d^2}{dr^2} + k_I^2 - \frac{\ell(\ell+1)}{r^2} - \frac{2\mu}{\hbar^2} V_{diag}(r)] \; \psi_{I\ell}^{J\pi}(r) = \frac{2\mu}{\hbar^2} \sum_{I'\ell'} V_{I\ell;I'\ell'}^{J\pi}(r) \; \psi_{I'\ell'}^{J\pi}(r),$$

(2.1)

assuming a spinless projectile. Here, J, ℓ and I denote the total angular momentum, the orbital angular momentum and the spin of the target nucleus, respectively. The excitation energy of the target in a state with spin I is $\mathcal{E}_I$. The total angular momentum J, its projection onto the z-axis and the parity π are good quantum numbers. Let E be the center-of-mass energy in the incident channel, then, the wave number k_I and Sommerfeld parameter η_I are given by:

$$k_I^2 = \frac{2\mu}{\hbar^2} (E-\mathcal{E}_I),$$

(2.2a)

$$\eta_I = \frac{2\mu}{\hbar^2} \frac{Z_1 Z_2 e^2}{2k_I},$$

(2.2b)

where μ is the reduced mass, while Z_1 and Z_2 represent the charge numbers of the projectile and target nucleus, respectively.

In the following description of the diagonal potential V_{diag} and the coupling potential $V_{I\ell;I'\ell'}^{J\pi}$, Tamura's paper [1] has been used. This description is limited to the formulae needed in this paper. Tamura's paper is recommended for a more detailed description of the formalism. In the present study, only scattering from a rotational target nucleus has been considered.

The diagonal potential is only the usual optical-model potential, written in two parts as:

$$V_{diag}(r) = V_{diag}^{nucl}(r) + V_{diag}^{Coul}(r),$$

(2.3)

representing the nuclear and Coulomb diagonal potentials, respectively. For the nuclear potential, the Woods-Saxon form has been taken to be:

$$V_{diag}^{nucl}(r) = -V(1+e_v)^{-1} - iW(1+e_w)^{-1},$$

(2.4)

where

$$e_v = \exp[(r-R_v)/a_v],$$

(2.5)

whilst V, R_v and a_v are the strength, the radius and diffusness parameters of the real part of the nuclear potential, respectively. A similar meaning is allocated to W and e_w concerning the imaginary part of the nuclear potential. The Coulomb potential, derived from a constant charge distribution in the target within the Coulomb radius R_c and zero outside it, has the form:

$$V_{diag}^{Coul}(r) = Z_1 Z_2 e^2 \left[\begin{array}{ll} \dfrac{1}{2R_c}\left(3 - \left(\dfrac{r}{R_c}\right)^2\right) & r \leqslant R_c \qquad\qquad (2.6a) \\[2ex] \dfrac{1}{r} & r > R_c \qquad\qquad (2.6b) \end{array} \right.$$

For later reference, it is noted that this potential, together with its first derivative, is continuous at $r = R_c$; however, its second and higher derivatives are discontinuous.

The radially dependent part of the coupling potential can also be written as two different terms:

$$V_{coupl}^{\lambda}(r) = V_{coupl}^{nucl;\lambda}(r) + V_{coupl}^{Coul;\lambda}(r). \qquad\qquad (2.7)$$

They represent the radial dependence of the nuclear and Coulomb coupling potential, respectively. The superscript λ refers to the transferred angular momentum during the scattering process. Since only a rotational target nucleus has been considered, the nuclear coupling potential is given by a Legendre polynomial expansion with expansion coefficients for $\lambda \neq 0$:

$$V_{coupl}^{nucl;\lambda}(r) = -\int_0^1 \left\{ V(1+e_v)^{-1} + iW(1+e_w)^{-1} \right\} Y_{\lambda 0}(\theta)\, d(\cos(\theta)), \qquad (2.8)$$

where

$$e_v = \exp\left[\left\{r - R_v\left(1 + \sum_{\lambda'} \beta_{\lambda'}^{N} Y_{\lambda'0}(\theta)\right)\right\}/a_v\right] \qquad\qquad (2.9)$$

with the nuclear mass deformation parameters $\beta_{\lambda'}^{N}$. A similar expression will hold for e_w. The Coulomb coupling potential is expressed up to second order of the deformation. The radial dependence has the form:

$$V_{coupl}^{Coul;\lambda}(r) = \frac{3Z_1 Z_2 e^2}{(2\lambda+1)R_c}\left[\beta_{\lambda}^{C(1)}\left[\begin{array}{l}\left(\dfrac{r}{R_c}\right)^{\lambda} \\[1.5ex] \left(\dfrac{R_c}{r}\right)^{\lambda+1}\end{array}\right. + \beta_{\lambda}^{C(2)}\left[\begin{array}{ll}(1-\lambda)\left(\dfrac{r}{R_c}\right)^{\lambda} & r \leqslant R_c \quad (2.10a) \\[1.5ex] (\lambda+2)\left(\dfrac{R_c}{r}\right)^{\lambda+1} & r > R_c \quad (2.10b)\end{array}\right],$$

where the parameters $\beta_\lambda^{C(1)}$ and $\bar{\beta}_\lambda^{C(2)}$ describe the charge deformation in first and second order, respectively. Also, for later reference, we note that the right-hand side of (2.10) and its higher radial derivatives are discontinuous at $r = R_c$.

To obtain solutions for $\psi_{I\ell}^{J\pi}(r)$, two boundary conditions have to be fulfilled. At the origin $\psi_{I\ell}^{J\pi}(r)$ should vanish:

$$\lim_{r\to 0} \psi_{I\ell}^{J\pi(I_0\ell_0)}(r) = 0, \tag{2.11a}$$

whilst, for large distances, $\psi_{I\ell}^{J\pi}(r)$, must represent an ingoing partial wave in the entrance channel plus outgoing partial waves in all the relevant exit channels. The precise asymptotic form defines the scattering matrix elements $S_{I\ell;I_0\ell_0}^{J\pi}$:

$$\psi_{I\ell}^{J\pi(I_0\ell_0)}(r) \underset{r\to\infty}{\sim} \delta_{II_0}\delta_{\ell\ell_0}H_\ell^-(\eta_{I_0};k_{I_0}r) - \left[\frac{k_{I_0}}{k_I}\right]^{1/2} S_{I\ell;I_0\ell_0}^{J\pi} H_\ell^+(\eta_I;k_Ir).$$
$$\tag{2.11b}$$

The ingoing and outgoing Coulomb waves H_ℓ^- and H_ℓ^+, respectively, are given in terms of the well-known regular and irregular Coulomb wave functions F_ℓ and G_ℓ, by $H_\ell^\pm = (G_\ell \pm iF_\ell)$. The indices I_0, ℓ_0 correspond to an ingoing wave in the entrance channel for $I = I_0$ and $\ell = \ell_0$.
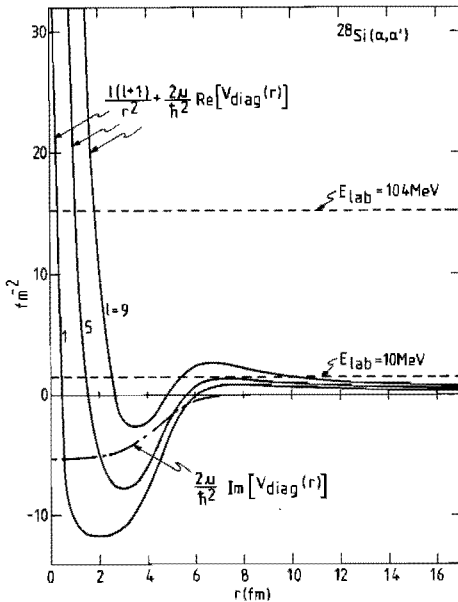
Fig.1. The sum of the centrifugal potential for three different ℓ-values and the real part of $V_{diag}(r)$. Also, the behaviour of the imaginary part of $V_{diag}(r)$ is shown. Two laboratory energies of 10 and 104 MeV are indicated and correspond respectively, to an energy near the Coulomb barrier and one well above it.

In Figure 1, the sum of the centrifugal potential for three different ℓ-values and the real part of $V_{diag}(r)$ is plotted as a function of r. Also, the behaviour of the imaginary part of $V_{diag}(r)$ is shown. Two laboratory energies of 10 and 104 MeV for inelastic alpha scattering from ^{28}Si are indicated and correspond respectively, to an energy near the Coulomb barrier and one well above it. These energies are the energies of two test cases from which the different items treated in this paper will be clarified. Section 8 contains more details about these test cases, such as the optical model parameters employed to plot Figure 1.

The set of coupled equations (2.1) has to be solved for each J value in a whole range of J values. From the scattering matrix elements obtained for these J values, the cross section of the ground state and each excited state, as well as other observable quantities, can be calculated.

3. INTEGRATION OF THE SET OF DIFFERENTIAL EQUATIONS

The set of differential equations (2.1) is rewritten in a more convenient form:

$$\frac{d^2}{dr^2} \psi_c(r) = \sum_{c'=1}^{n} A_{cc'}(r) \psi_{c'}(r), \qquad c = 1,2,\ldots,n \qquad (3.1)$$

where the various channels are represented by the channel number c, assuming that there are n channels. The quantities $A_{cc'}$ are the elements of a matrix A which will be called the potential matrix. Denoting the entrance channel by the sub- and superscript i, the boundary conditions (2.11) can be written as:

$$\lim_{r \to 0} \psi_c^i(r) = 0, \qquad c = 1,2,\ldots,n \qquad (3.2a)$$

$$\psi_c^i(r) \underset{r \to \infty}{\sim} H_i^- \delta_{ci} - \left[\frac{k_i}{k_c}\right]^{1/2} H_c^+ S_{ci}, \qquad c = 1,2,\ldots,n \qquad (3.2b)$$

where k_c is the wave number in channel c. In principle, there are n entrance channels.

The solution $\{\psi_1(r),\ldots,\psi_n(r)\}$ of (3.1) can be considered as a solution vector $\psi(r)$. The solution vectors constitute a vector space of dimension 2n. This 2n-dimensional space contains an n-dimensional

subspace of regular solutions that satisfy the boundary conditions (3.2a). In order to generate a basis of n linearly independent solution vectors $\psi_s(r)$, $s = 1, \ldots n$, for the regular subspace by solving (3.1), suitable initial conditions have to be specified. For these, the following can be chosen:

$$\lim_{r \to 0} (k_c r)^{-(\ell_c+1)} \psi_{cs}(r) = \frac{1}{(2\ell_c+1)!!} \delta_{cs}, \tag{3.3}$$

where $\psi_{cs}(r)$ denotes the component c of the solution vector $\psi_s(r)$ and ℓ_c is the orbital angular momentum in channel c. These solution vectors form the columns of a solution matrix $\Psi(r) = \left[\psi_1(r), \ldots, \psi_s(r), \ldots, \psi_n(r) \right]$ with $\psi_s(r) \in \mathbb{C}^n$.

The solution vectors $\psi^i(r)$ that we are looking for, are regular; hence, they are linear combinations of the $\psi_s(r)$ which are found by taking into account the boundary condition (3.2b) at the matching radius R_m. Also, this yields the scattering matrix elements S_{ci}; more details will be given in section 5.

The regular solution vectors $\psi_s(r)$ are constructed by numerical integration from the origin to the matching radius R_m. In Tamura's code JUPITOR [5] use is made of Euler's and Störmer's multistep integration methods which need the knowledge of the solution vectors in two and five prior mesh points of the integration range.

Euler's method is used to initiate the radial integration. The use of this or a similar two-point method is essential, since it is not possible to specify the values of the solution vectors near the origin at more than two mesh points. One of these points can be the origin, where all the solution vectors have to be eliminated; another mesh point is r_1 close to the origin, where a value to the solution vectors can be given according to (3.3):

$$\psi_{cs}(r_1) = \frac{1}{(2\ell_c+1)!!} (k_c r_1)^{\ell_c+1} \delta_{cs}. \tag{3.4}$$

Using matrix notation for both the solution and potential, Euler's method becomes:

$$\Psi(r) = 2\Psi(r-h) - \Psi(r-2h) + h^2 B(r-h), \tag{3.5}$$

where $B(x) = A(x)\Psi(x)$. The local truncation error of this formula is of

order h^4. Here, r is a mesh point and h the mesh or step size.

Störmer's method can be applied, provided that r is not in the vicinity of the origin:

$$\Psi(r) = 2\Psi(r-h) - \Psi(r-2h) + \frac{h^2}{240}\left[299B(r-h) - 176B(r-2h) + 194B(r-3h)\right.$$
$$\left. - 96B(r-4h) + 19B(r-5h)\right]. \qquad (3.6)$$

The local truncation error of this formula is of order h^7. This error will be introduced at each step. However, the propagation of the local truncation error after many integration steps gives a global error in the solution, at a matching radius R_m, of the order h^5, neglecting starting errors and round-off errors [6,7]. In order to keep starting errors small enough, Euler's method has been used in the starting region with a reduced step length.

To calculate the first derivative of the solution, at some mesh point r, the formula :

$$\Psi'(r) = \frac{1}{12h}\left[\Psi(r-2h) - 8\Psi(r-h) + 8\Psi(r+h) - \Psi(r+2h)\right] \qquad (3.7)$$

has been used; it has a truncation error of order h^4.

4. STABILIZATION PROCEDURE

In the preceding section, it was shown that n linearly independent solution vectors ψ_s can be generated by choosing appropriate initial values. These solution vectors form the columns of a solution matrix Ψ with components denoted by ψ_{cs}. Integrating through a classically forbidden region, the components with negative local kinetic energy will generally consist of an exponentially growing part and an exponentially decreasing part. The former is responsible for the tendency to destroy the initially generated linear independence of the solution vectors. The longer the integration continues through a classically forbidden region, the stronger this tendency will be; for instance, it will occur in scattering problems of nuclear physics with energies near or below the Coulomb barrier.

This section will be subdivided into three subsections. In the first, a description of the stabilization procedure is given. The second subsection shows how this procedure is implemented in our program. In the third subsection, a criterion for the linear independence of the set of

solution vectors ψ_s is discussed and its use, restoring this independence by stabilization, is shown from our test cases.

4.1 Description of a stabilization procedure

To maintain the linear independence of the solution vectors ψ_s, the following stabilization procedure was applied. At some mesh point R, called a stabilization point, the components in the solution vectors were reordered in order of decreasing real part of the local relative kinetic energy. This reordering allows permutations of the rows and the columns, both of the potential matrix A and the solution matrix Ψ by the same permutation. To be precise, a permutation matrix P was determined such that the diagonal entries in the matrix $P^T \text{Re}(-A(R))P$ had decreasing order.

First we set:

$$\Lambda^2 = \text{diag}(A(R)) \tag{4.1a}$$

which defines a diagonal matrix

$$\Lambda^2 = \text{diag}(\lambda_1^2, \ldots, \lambda_c^2, \ldots, \lambda_n^2) \tag{4.1b}$$

with entries λ_c^2, where

$$\lambda_c = \left[-\varepsilon_c(R) - i\chi_c(R) \right]^{1/2}. \tag{4.2}$$

The real part ε_c of the local kinetic energy in channel c is given by

$$\varepsilon_c(r) = k_c^2 - \frac{\ell_c(\ell_c+1)}{r^2} - \frac{2\mu}{\hbar^2} \text{Re}\left[V_{\text{diag}}(r) + V_{cc}(r)\right], \tag{4.3a}$$

whereas, the imaginary part χ_c is given by

$$\chi_c(r) = -\frac{2\mu}{\hbar^2} \text{Im}\left[V_{\text{diag}}(r) + V_{cc}(r)\right], \tag{4.3b}$$

where $V_{cc}(r)$ is a diagonal element of the coupling potential in (2.1). We see that, the ε_c values will be (much) larger than the χ_c values, in a large part of the classically forbidden region; therefore, the reordering has been based on the ε_c values. This would be the case for the next considerations, too.

Secondly, we reorder Λ^2

$$P^T \Lambda^2 P \equiv \Omega^2 = \text{diag}(\omega_1^2, \ldots, \omega_c^2, \ldots, \omega_n^2) \tag{4.4}$$

with increasing real parts of the entries ω_c^2.

If $\Phi = P^T \Psi P$ is the correspondingly reordered Ψ-matrix, it satisfies

$$\frac{d^2\Phi(r)}{dr^2} = P^T A(r) P \; \Phi(r)$$
$$= (\Omega^2 + Z(r)) \; \Phi(r), \tag{4.5}$$

where

$$Z(r) = P^T \left[A(r) - \text{diag}(A(R)) \right] P. \tag{4.6}$$

If negative $\varepsilon_c(R)$ values occur, the most rapidly growing components of a column of Φ will be located the furthest down this column.

To explain the stabilization procedure, let

$$\tilde{\Phi}(r) = \Phi(r) \; U, \tag{4.7}$$

where U is a nonsingular matrix. Then $\tilde{\Phi}(r)$ satisfies (4.5)

$$\frac{d^2\tilde{\Phi}(r)}{dr^2} = (\Omega^2 + Z(r)) \; \tilde{\Phi}(r). \tag{4.8}$$

If we neglect the contribution of $Z(r)$ in (4.8), the solution matrix $\tilde{\Phi}(r)$ would be

$$\tilde{\Phi}(r) = \frac{1}{2} \exp(-(r-R)\Omega) \left[\Phi(R) - \Omega^{-1}\Phi'(R) \right] U$$
$$+ \frac{1}{2} \exp(+(r-R)\Omega) \left[\Phi(R) + \Omega^{-1}\Phi'(R) \right] U, \tag{4.9}$$

where the prime denotes differentiation with respect to the argument r. In the case of negative $\varepsilon_c(R)$ values, the coefficients of the exponentially growing components are in the coefficient matrix

$$\left[\Phi(R) + \Omega^{-1}\Phi'(R) \right] U. \tag{4.10}$$

The matrix U can be constructed so that this matrix becomes zero below the diagonal in the rows where the $\varepsilon_c(R)$ values (renumbered to correspond to the reordering of channels) are negative [8]; thus:

$$\left[\tilde{\Phi}(R) + \Omega^{-1}\tilde{\Phi}'(R) \right]_{cc'} = 0 \tag{4.11a}$$

for all c and c' such that

$$\hat{c} < c < n,$$
$$1 < c' < c, \tag{4.11b}$$

where $\hat{c}$ is determined by

$$\epsilon_{\hat{c}}(R) < 0 < \epsilon_{\hat{c}-1}(R).\tag{4.11c}$$

In other words, a new set of linearly independent solution vectors $\tilde{\phi}_{c'}$ is obtained that — assuming $Z(r) = 0$ — has the following properties:

If $\epsilon_{c'}(R) \gg |\chi_{c'}(R)|$ then, all components of $\tilde{\phi}_{c'}$ oscillate.

If $\epsilon_{c'}(R) \ll -|\chi_{c'}(R)|$ then, no component of $\tilde{\phi}_{c'}$ grows faster than $\exp((r-R)\omega_{c'})$, the fastest growing one being component $\tilde{\phi}_{c'c'}$.

However, due to $Z(r) \neq 0$, for $r > R$, there will be a coupling between the components of a solution vector and, therefore, the differential equation for a declining component may contain exponentially growing coupling terms. The influence of the latter terms on this component depends upon r and the ratio of the entries of $Z(r)$ and Ω^2 and they will determine where the next stabilization point will be located.

4.2 Practical implementation of the stabilization procedure

To carry out the above-described stabilization procedure, firstly, we must specify the permutation matrix P. The matrix A is premultiplied by a product

$$I_{\hat{c}}\cdots I_c\cdots I_{n-1}I_n\tag{4.12}$$

of $n-\hat{c}+1$ elementary matrices I_c for $\hat{c} \leqslant c \leqslant n$, where the entries of I_n are chosen such that the premultiplication of the matrix $Re(-A)$ by I_n causes the interchange of the row with the smallest local kinetic energy and the row at position n. Premultiplication by I_{n-1} interchanges the row with the smallest energy but one and the one at position n-1. This is continued for all rows up to and including row $\hat{c}$. Let

$$P = I_n I_{n-1}\cdots I_c\cdots I_{\hat{c}}.\tag{4.13}$$

Secondly, we postmultiply Ψ and Ψ' by a diagonal matrix D such that columns of

$$\begin{bmatrix} \Psi \\ \Lambda^{-1}\Psi' \end{bmatrix} D^{-1}\tag{4.14}$$

have approximately the same length. It should be noted that when one of the elements of Λ becomes very small, an average value has to be taken.

Moreover, we define the matrix:

$$\Pi = P^T \big[\Psi(R) + \Lambda^{-1} \Psi'(R) \big] D^{-1} P. \tag{4.15}$$

Then, to ensure that ΠU has "upper triangular form", the matrix U can be chosen as a product of elementary Householder matrices [9,10,11]:

$$U = U_n U_{n-1} \cdots U_c \cdots U_{\hat{c}}, \tag{4.16}$$

in which c runs over the components of (4.15) with negative local kinetic energy. Here

$$U_c = I - 2w_c w_c^H, \tag{4.17}$$

where the matrix I is the n-by-n identity matrix and the unit column vector w_c with n components can be constructed from row c of

$$\Pi^{(c)} = \Pi\, U_n U_{n-1} \cdots U_{c+1} \tag{4.18}$$

by [12]:

$$2Kw_c^H = (\pi_{c1}^{(c)}, \pi_{c2}^{(c)}, \ldots, \pi_{cc}^{(c)} + S\pi_{cc}^{(c)}/|\pi_{cc}^{(c)}|, 0, \ldots 0), \tag{4.19}$$

where, only for this equation, the capitals K and S are used to define positive constants, given by the expressions

$$S^2 = \sum_{s=1}^{c} \left| \pi_{cs}^{(c)} \right|^2, \qquad 2K^2 = S^2 + S \left| \pi_{cc}^{(c)} \right|. \tag{4.20}$$

By constructing the unitary transformation matrix U in this way, a stable solution matrix $\tilde{\Phi}$ is obtained

$$\tilde{\Phi} = P^T \Psi D^{-1} P U \tag{4.21}$$

in terms of the permuted original solution matrix ΨD^{-1}. Backward permutation gives

$$\tilde{\Psi} = P \tilde{\Phi} P^T = \Psi D^{-1} \mathbb{U}, \tag{4.22}$$

where the stabilization matrix $\mathbb{U}$ is written as

$$\mathbb{U} = \mathbb{U}_n \mathbb{U}_{n-1} \cdots \mathbb{U}_c \cdots \mathbb{U}_{\hat{c}} \tag{4.23}$$

with the permuted Householder matrices

$$\mathbb{U}_c = P U_c P^T. \tag{4.24}$$

However, in our program, a slightly different approach has been followed. We used the permutation matrices P_c defined as

$$P_c = I_n I_{n-1} \cdots I_c \tag{4.25}$$

with $P_{\hat{c}} \equiv P$ and correspondingly we changed the definition of $\amalg_c$ given by (4.24) in:

$$\amalg_c = P_c U_c P_c^T. \tag{4.26}$$

This means that

$$PU = \left[I_n I_{n-1} \cdots I_c \cdots I_{\hat{c}} \right] \left[U_n U_{n-1} \cdots U_c \cdots U_{\hat{c}} \right] \tag{4.27}$$

in (4.21), has been replaced by the product

$$I_n \tilde{U}_n I_{n-1} \tilde{U}_{n-1} \cdots I_c \tilde{U}_c \cdots I_{\hat{c}} \tilde{U}_{\hat{c}} \tag{4.28}$$

in order to obtain a stable solution matrix $\tilde{\Psi}$, as given by (4.22). Here, $\tilde{U}_c$ corresponds to the unitary matrix (4.17) for which the unit column vector w_c has been constructed, in the same way as (4.19), from row c of

$$\Pi^{(c)} = P_c^T [\Psi(R) + \Lambda^{-1} \Psi'(R)] D^{-1} I_n \tilde{U}_n \cdots I_{c+1} \tilde{U}_{c+1} I_c \tag{4.29}$$

instead of (4.18).

We note that, although the index c only runs over the components with negative local kinetic energy, in principle, it is also possible to let c run over all the components of the solution vectors, including those with positive local kinetic energy.

This stabilization procedure has been applied to Störmer's multistep integration formula (3.6). For this purpose, the solution matrix Ψ is calculated up to and including the mesh point R+2h. The diagonal matrix D and Householder matrices $U_n, U_{n-1}, \ldots, U_c, \ldots, U_{\hat{c}}$ are determined from the solution matrix and its derivative at mesh point R. The derivative of the solution matrix is determined by means of Eq. (3.7). The solution matrices at the mesh points of Störmer's formula can now be transformed according to (4.22)

$$\tilde{\Psi}(R+kh) = \Psi(R+kh) D^{-1}(R) \amalg(R) \tag{4.30}$$

for k = -2,-1,0,1,2. Using the stabilized solution matrices (4.30) in Störmer's formula, a stable solution matrix can be obtained from mesh point R+3h onwards.

4.3 Criterion for the linear independence of the set of solution vectors

   To discuss a criterion for the linear independence of the set of solution vectors ψ_s, we have to consider the matrix $F \in \mathbb{C}^{2n \times n}$ given by (4.14)

$$F = \begin{bmatrix} \psi \\ \Lambda^{-1} \psi' \end{bmatrix} D^{-1}, \tag{4.31}$$

where D is a normalizing diagonal matrix which will be chosen later. Due to the initial conditions (3.3), the set of solution vectors ψ_s is initially linearly independent. Then the matrix F has rank n. A Singular Value Decomposition of this matrix yields n non-zero singular values

$$\sigma_1 \geqslant \sigma_2 \geqslant \dots \dots \geqslant \sigma_n > 0. \tag{4.32}$$

It is shown in [11] that F can be written as

$$F = \sum_{i=1}^{n} \sigma_i u_i v_i^T, \tag{4.33}$$

where the vectors u_i and v_i are, respectively, the i-th left singular vector and the i-th right singular vector.

   Using the 2-norm, the condition number of F can be expressed in terms of its largest and smallest singular values

$$\kappa_2(F) = \sigma_1 / \sigma_n. \tag{4.34a}$$

We see that $\kappa_2(F) \geqslant 1$. If F has a small condition number, then F is said to be well-conditioned. If, on the contrary, $\kappa_2(F)$ is large, then F is said to be ill-conditioned. If the columns of F are orthogonal and D is chosen so that these columns are normalized in the 2-norm, then [11]

$$\kappa_2(F) = 1. \tag{4.34b}$$

   If the set of solution vectors becomes nearly linearly dependent, – which, in general, happens gradually during the integration process – then, the matrix F becomes ill-conditioned. This implies that F becomes nearly rank deficient, i.e., F is near to a matrix of rank lower than n. To quantify this, let

$$E = \sigma_n u_n v_n^T, \tag{4.35}$$

then rank $(F-E) = n-1$ and

$$\frac{\|E\|_2}{\|F\|_2} = \frac{\sigma_n}{\sigma_1} = \frac{1}{\kappa_2(F)} \; . \tag{4.36}$$

Hence, the ratio (4.36) gives an indication of the distance, in a relative sense, of F to the set of matrices with rank lower than n.

These considerations lead to the introduction of a linear independence number of a set of solution vectors ψ_s defined by

$$\nu(F) = \left\{\frac{1}{\kappa_2(F)} \;\middle|\; \begin{array}{l} \text{F given by (4.31) with D such that} \\ \text{the columns of F have the same length} \end{array} \right\} \tag{4.37}$$

This number can be used as a criterion for the need to perform a stabilization in order to restore the linear independence of a set of solution vectors.

Figures 2 and 3 show the independence numbers $\nu(F)$ as functions of r, with F given by (4.31) and determined without any stabilization during the integration process, for our test cases with projectile energies of 10 and 104 MeV, respectively. A more detailed description of the test cases will be given in section 8. In the figures, the numbers $\nu(F)$ are plotted on a logarithmic scale at the mesh points $R = 5h, 10h, \ldots, 3.4$ fm for $h = 1/5, 1/10, 1/20, 1/40$ and $1/80$ fm and the corresponding curves are denoted by $\nu_{1/h}$. The solid line curves correspond to a multipole expansion of the deformed nuclear and Coulomb potentials, given by (2.8) and (2.10), respectively, up to degree $\lambda = 8$. The broken line curves correspond to an expansion up to degree $\lambda = 4$.

Looking at Figures 2 and 3 the following remarks can apply:

Firstly, close to the origin, the set of solution vectors ψ_s is linearly independent to a reasonable extent. However, a little further up the integration range, the linear independency deteriorates. This happens less quickly, the larger the step size h.

Secondly, in the classically forbidden region, the curves of both figures are nearly identical which means that in this region, the linear independence number is not dependent upon the energy of the incoming particle. However, the higher this energy, the smaller the classically forbidden region will be. For a projectile energy of 104 MeV, this region ends at $r = 1.9$ fm, as shown in Figure 3 (see also Figure 1). In the classically allowed region, the curves are horizontal.

Thirdly, comparing the curves with solid and broken lines, the behaviour
of the linear independence number depends on the maximum degree of the
expansion of the deformed potential. This means that the number of non-
zero elements and their entries in the potential matrix A of (3.1)
determine the behaviour of $\nu(F)$. It seems that the values of the matrix
elements themselves are of less importance, although they depend upon the
deformation parameters β_λ.

Fourthly, at the radii of about 1.0 and 1.5 fm, the curves ν_{80} and
ν_{40}, respectively, decrease to a value of the order of the machine
precision of our computer. For a Burroughs 7900, the single floating-
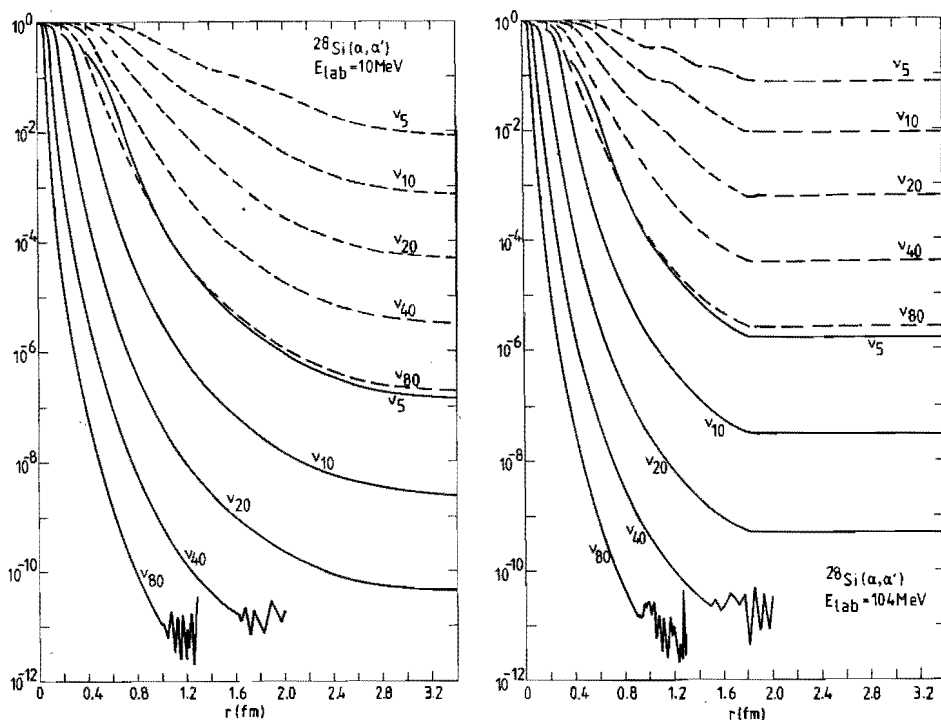
Figs. 2 and 3. In these figures, plots of the linear independence numbers
$\nu_{1/h}$ determined with step sizes h = 1/5, 1/10, 1/20, 1/40, 1/80 fm and
without any stabilization during the integration process, are shown for
energies of 10 and 104 MeV, respectively. The solid line curves corres-
pond to a multipole expansion of the deformed nuclear and Coulomb poten-
tials up to degree λ = 8. The broken line curves correspond to an expan-
sion up to degree λ = 4.

point numbers are represented by a normalized mantissa of 13 octal digits; thus, the machine precision is equal to $\frac{1}{2} 8^{1-13} \approx 0.7 \; 10^{-11}$. If the value of $\nu(F)$ is of the order of the machine precision then, the set of solution vectors ψ_s has completely lost its linear independency and corresponds to the erratic behaviour of $\nu(F)$ beyond this point.

Figure 4 illustrates how $\nu(F)$ can be used to indicate when stabilization is needed to maintain the linear independence of a set of solution vectors ψ_s at some level. The figure shows two curves of $\nu(F)$ calculated for h = 1/80 fm, λ = 8 and projectile energy of 10 MeV. For the curve denoted by $\nu_{80}^{(-2)}$, the criterion $\nu(F) < 10^{-2}$ has been used, for the other, denoted by $\nu_{80}^{(-4)}$, we used $\nu(F) < 10^{-4}$. The behaviour of $\nu_{80}^{(-2)}$ and $\nu_{80}^{(-4)}$ for r < 3.4 fm shows that only in two and one mesh points, respectively, a stabilization is needed to maintain the imposed conditions of the curves. We see that after a stabilization, $\nu(F)$ nearly regains its original value of unity.
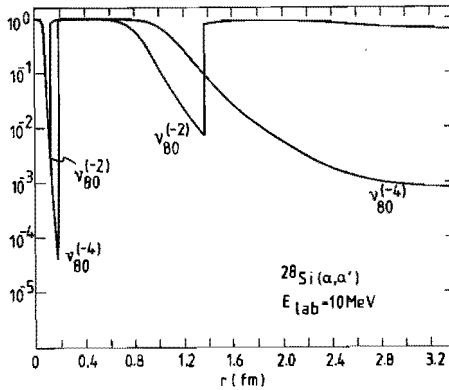
Fig.4. This figure illustrates how the linear independence number ν can be used to indicate when stabilization is needed to maintain the linear independence of a set of solution vectors at a certain level. Two plots of ν, calculated for h = 1/80 fm, are shown. For the curve that is denoted by $\nu_{80}^{(-2)}$, the criterion $\nu < 10^{-2}$ has been used, for the other, denoted by $\nu_{80}^{(-4)}$, $\nu < 10^{-4}$ was used. The behaviour of the curves for r < 3.4 fm shows that a stabilization is needed in a few mesh points only, to maintain the imposed conditions. After a stabilization, ν nearly regains its original value of unity.

Finally, in practice, we state that it seems only necessary to stabilize the solution matrix at a few mesh points in a classically forbidden region of the integration range in order to maintain the linear independence at some prescribed level. However, if necessary the program can carry out the stabilization procedure after every 5 step lengths in the integration range, including the classically allowed region.

In section 9, the influence of $v(F)$ deviating from 1 on the loss of accuracy in the solutions and S-matrix elements will be discussed.

5. MATCHING THE BOUNDARY CONDITIONS AT RADIUS R_m

The integration of a set of coupled equations (3.1) is performed up to some mesh point of the integration range. This mesh point has to be chosen so that the nuclear potential at this point, as well as in general, the Coulomb part of the coupling potential are both negligible. Here, the set of coupled equations reduces to a set of decoupled equations of which the solutions are known, since they are given by the boundary conditions (3.2b). This point in the integration range is called the matching radius R_m.

As described in section 3, the set of n coupled equations is solved ṅ times in order to satisfy the boundary conditions (3.2b) at R_m. Satisfying these conditions needs a set of 2n linear equations, because a column of n S-matrix elements related to outgoing partial waves in all the relevant exit channels has to be determined for each ingoing partial wave in the entrance channel, as well as, a column of n normalization coefficients of the solutions. Since in principle, there are n entrance channels, complete n-by-n scattering and normalization matrices can be generated. The boundary conditions (3.2b) and their derivatives with respect to $k_c r$ are usually taken in order to obtain a set of 2n linear equations. In that case the matching relationship at radius R_m in matrix notation can be written as

$$\begin{bmatrix} \Psi \\ \Psi' \end{bmatrix} N = \begin{bmatrix} H^{(-)} \\ H^{(-)'} \end{bmatrix} - \begin{bmatrix} H^{(+)} \\ H^{(+)'} \end{bmatrix} K^{-1/2} S K^{1/2}, \qquad (5.1)$$

where N is the normalization matrix, and $H^{(\pm)}$ and $K^{1/2}$ are diagonal matrices defined by

$$H^{(\pm)} = diag(H_1^{(\pm)}, \ldots, H_c^{(\pm)}, \ldots, H_n^{(\pm)}) \qquad (5.2)$$

$$K^{1/2} = diag(k_1^{1/2}, \ldots, k_c^{1/2}, \ldots, k_n^{1/2}). \qquad (5.3)$$

The solution matrix Ψ contains the solution vectors ψ_s, $s = 1,\ldots,n$ as discussed in section 3.

The Wronskian of two solution matrices Φ and Ψ is defined by

$$W(\Phi,\Psi) = \Phi^T\Psi' - \Phi'^T\Psi. \tag{5.4}$$

Using the Wronskian

$$W(H^{(-)}, H^{(+)}) = H^{(-)}H^{(+)'} - H^{(-)'}H^{(+)} = 2iI, \tag{5.5}$$

the normalization and scattering matrices are given by

$$N = -2i\left[W(H^{(+)}, \Psi)\right]^{-1} \tag{5.6}$$

and

$$S = W(H^{(-)}, K^{1/2}\Psi)\left[W(H^{(+)}, K^{1/2}\Psi)\right]^{-1}, \tag{5.7}$$

respectively. Equation (5.7) shows that the S-matrix does not depend upon the normalization of the solution matrix, i.e., upon the choice of the normalization matrix N in (5.1).

Based upon considerations of invariance of the scattering process under time reversal, it can be proved that the S-matrix is symmetric. It follows from the matching conditions (5.1) and the definition (5.4) that

$$S - S^T = \frac{1}{2}\, W(K^{1/2}\Psi\, N\, K^{-1/2},\, K^{1/2}\Psi\, N\, K^{-1/2}) \tag{5.8}$$

which relates the asymmetry of the S-matrix to the Wronskian of the normalized solution matrix with itself. It can be proved that the Wronskian of any two regular solution matrices at every point of the integration range is equal to zero, when taking into account the symmetry of the A-matrix in (3.1) and the regularity of the solution matrix at the origin. Hence, deviations from zero of the Wronskian of the normalized solution matrix with itself, determined during the integration, tell us something about the influence of the unwanted irregular solution matrix and might be used as a measure for the accuracy of the regular solutions. In this connection, it has to be realized that the solution matrix was stabilized several times during the integration process and had to be normalized at the end. Therefore, deviations from zero in the sense of equation (5.8) can only be determined after ending the integration process.

To make a calculation that achieves the above-suggested possibility for measuring the accuracy of the solution matrix, we assume that during the integration process the stabilization procedure had been applied at the mesh points $R_1,\ldots,R_p,\ldots,R_t$. The point R_{t+1} corresponds to the

matching radius R_m. The normalized solution matrix between the points R_p and R_{p+1} can then be written as

$$\Psi^{(p)}{}_{(r)N} = \Psi^{(p-1)}{}_{(r)}\left[D^{-1(p)}\mu^{(p)}\right]\left[D^{-1(p+1)}\mu^{(p+1)}\right]..\left[D^{-1(t)}\mu^{(t)}\right]_N \qquad (5.9)$$

referring to (4.22) and where $\Psi^{(p-1)}$ corresponds to the unnormalized solution matrix between R_p and R_{p+1} in case no stabilizations are performed at the points $R_p,...,R_t$. The matrix N is the normalization matrix given by (5.6). The solution (5.9) will be called the physical solution.

   After ending the integration, the physical solution matrix can be calculated at every mesh point of the integration range and the Wronskian of the physical solution matrix with itself can be determined. However, measuring of the accuracy of the solution matrix at the mesh points between the origin and R_p by means of this Wronskian will be perturbed by possible deficiencies occuring at the mesh points between R_p and R_m. This perturbation is inherent in the use of the physical solution matrix, as shown by equation (5.9). In other words, errors in the physical solution at the mesh points below R_p are introduced by what happens at the mesh points above R_p including the matching radius. Since this is really the case, as will be shown in one of the following sections, this method is not suited to our purpose. The method of computing angles between subspaces spanned by the solution vectors which will be treated in the next section, does not have this disadvantage and can detect deficiencies below R_p independently of those which occur in the remainder of the integration range. Moreover, in contrast to this method, the S-matrix and Wronskian give only an indirect measure of the lost accuracy during the integration process.

   As has been already noted, the S-matrix does not depend upon the normalization of the solution matrix. Or, stated positively, the S-matrix is entirely determined by the regular subspace spanned by the solution vectors at the matching radius. Therefore, the accuracy of the S-matrix should be examined by studying the accuracy of this subspace measured by calculating the angles between it and a reference subspace.

6. COMPUTING ANGLES BETWEEN SUBSPACES SPANNED BY THE SOLUTION VECTORS
   In this section, a method for computing angles between subspaces spanned by solution vectors (and their derivatives) will be discussed.

By computing these angles, differences between the subspaces spanned by two solution matrices Ψ and $\Psi + \delta\Psi$, which were obtained by variants of the numerical process, can be investigated. To this end, the following two matrices F and G $\in \mathbb{C}^{2n \times n}$ are defined

$$
F = \begin{bmatrix} \Psi \\ \Lambda^{-1}\Psi' \end{bmatrix}_{r = R} , \qquad G = \begin{bmatrix} \Psi + \delta\Psi \\ \Lambda^{-1}(\Psi' + \delta\Psi') \end{bmatrix}_{r = R} , \qquad (6.1)
$$

where the prime denotes a differention of the components ψ_{cs} with respect to r. The matrices F and G consist of n linearly independent columns.

The linearly independent columns of the matrices F and G span n-dimensional subspaces S_F and $S_G \subset \mathbb{C}^{2n}$, respectively. Differences between the subspaces S_F and S_G are characterized by the principal angles $\Theta_1, \ldots, \Theta_n \in [0, \pi/2]$ between S_F and S_G. In [13] these angles are defined for k = 1, 2, ..., n recursively by:

$$
\cos(\Theta_k) = \max_{u \in S_F} \max_{v \in S_G} u^H v = u_k^H v_k , \qquad (6.2a)
$$

with

$$
\|u\|_2 = \|v\|_2 = 1 \qquad (6.2b)
$$

and subject to the constraints

$$
u^H u_i = 0, \quad v^H v_i = 0, \qquad i = 1, 2, \ldots, k-1. \qquad (6.2c)
$$

It can be seen that $0 \leqslant \Theta_1 \leqslant \ldots \leqslant \Theta_n \leqslant \pi/2$. The vectors $\{u_1, \ldots, u_n\}$ and $\{v_1, \ldots, v_n\}$ form unitary bases for S_F and S_G, respectively, and are called the principal vectors of the subspace pair (S_F, S_G).

To compute the principal angles and vectors, the QR-decompositions of the matrices F and G need to be determined

$$
F = Q_F R_F, \qquad Q_F^H Q_F = I_n, \qquad R_F \in \mathbb{C}^{n \times n}, \qquad (6.3a)
$$

$$
G = Q_G R_G, \qquad Q_G^H Q_G = I_n, \qquad R_G \in \mathbb{C}^{n \times n}, \qquad (6.3b)
$$

where Q_F and Q_G have orthonormal columns and R_F and R_G are upper triangular. The n columns of Q_F and Q_G form unitary bases for the subspaces S_F and S_G, respectively. The matrix I_n denotes the n-by-n identity matrix of dimension n. For these decompositions, either the method of Householder transformations or the modified Gram-Schmidt method can be used.

Subsequently, by means of unitary matrices U and V, the Singular Value Decomposition of the product matrix $Q_F^H Q_G$ is determined

$$U^H(Q_F^H Q_G)V = \text{diag}(\sigma_1, \ldots, \sigma_n), \tag{6.4}$$

which yields the singular values $\sigma_1 \geqslant \sigma_2 \geqslant \ldots \geqslant \sigma_n \geqslant 0$.

It can be shown that the principal angles Θ_k and principal vectors of the subspace pair (S_F, S_G) are given by [13]

$$\cos(\Theta_k) = \sigma_k \tag{6.5a}$$

$$\{u_1, \ldots, u_n\} = Q_F U \tag{6.5b}$$

$$\{v_1, \ldots, v_n\} = Q_G V. \tag{6.5c}$$

The principal angles depend on the subspaces S_F and S_G only, which implies that they are invariant against postmultiplication of the matrices F and/or G by any regular matrix. The main advantage of determining the principal angles is that they give a measure for the nearness of the subspaces S_F and S_G, independently of the bases representing them; thus, looking at the equations (5.1) and (5.9), the principal angles are not influenced by the normalization matrices N, the scaling matrices D or the stabilization matrices $\mathbb{U}$. In particular the latter maintain or restore the quality of the bases of the subspaces in the sense of being orthogonal, as much as possible, but do not affect the subspaces themselves.

This method for computing the principal angles between the subspaces S_F and S_G, i.e., between solution spaces represented by Ψ and $\Psi + \delta\Psi$, has been applied inspecting the accuracy loss along the integration interval and detecting possible sources of deficiencies in the numerical process. It is a very sensitive method for this purpose, as is seen in the test cases we studied and illustrated in the Figures 6.a and 7.a, where the largest principal angle between S_F and S_G, in the sense just mentioned, is plotted as a function of r for four different combinations of subspaces. It is shown clearly that the behaviour of the curves at r = 4 and 17 fm is discontinuous and which corresponds to deficiencies of the numerical process. More details will be given in section 8.

In the next section, a method will be developed for avoiding inaccuracies in the solution vectors, due to one of the deficiencies.

7. AVOIDING INACCURACIES IN THE SOLUTION VECTORS AT COULOMB RADIUS R_c

The Störmer integration method (3.6) contains higher derivatives of the solutions at mesh point r-h [6,14] implicitly. To guarantee a local truncation error of order h^7, the higher derivatives up to and including the sixth order have to be continuous. However, the second and higher radial derivatives of the Coulomb part of the diagonal potential (2.6) and the Coulomb part of the coupling potential (2.10), as well as its higher derivatives are discontinuous at the Coulomb radius R_c. This means that the potential function $A_{cc'}(r)$ in (3.1) is neither continuous, nor continuously differentiable for $r = R_c$. This causes discontinuities in the second and higher derivatives of the solutions.

In this section, a method will be presented that avoids these inaccuracies in the solutions due to the discontinuities at radius R_c. The method can be applied to the general case, too, in which the diagonal and the coupling potential and/or their higher radial derivatives are discontinuous at some radius. In deriving the method, it was supposed that the radius R_c coincides with a mesh point. The approach presented here differs from the one published recently [15].

Using vector and matrix notation, the set of differential equations (3.1) for $r \leqslant R_c+2h$ is written as

$$\Psi''(r) = A(r)\Psi(r), \qquad\qquad r \leqslant R_c+2h \qquad (7.1a)$$

and for $r \geqslant R_c-2h$ as

$$\widetilde{\Psi}''(r) = \widetilde{A}(r)\widetilde{\Psi}(r), \qquad\qquad r \geqslant R_c-2h \qquad (7.1b)$$

The radial dependence of the Coulomb part of A(r) in (7.1a) corresponds to (2.6a) and (2.10a) taken for $r \leqslant R_c+2h$; whereas, this part of $\widetilde{A}(r)$ in
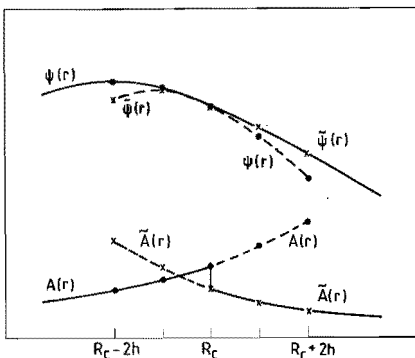
Fig.5. This figure illustrates a possible radial dependence of the potential matrices A(r) and $\widetilde{A}(r)$ in the vicinity of the radius R_c. The behaviour of a component of the solution vector has been given diagrammatically.

(7.1b) corresponds to (2.6b) and (2.10b) taken for $r \geqslant R_c - 2h$. Figure 5 illustrates a possible radial dependence of both $A(r)$ and $\tilde{A}(r)$ in the vicinity of the radius R_c. In this figure, the behaviour of a component of the solution vector has been given diagrammatically. Integrating from the origin up to $R_c + 2h$, the solutions $\Psi(R_c + kh)$ for $k = -2, -1, 0, 1, 2$ will be known with an accuracy of order h^5 and using (3.7), the derivative of the solutions in R_c can be calculated with an accuracy of at least order h^4. Further integration without loss of accuracy requires knowledge of $\tilde{\Psi}(R_c + kh)$ for $k = -2, \ldots, 2$ with an accuracy of order h^5.

Taking $x = r - R_c$, the equations (7.1) can be written as

$$\Psi''(x) = A(x)\Psi(x), \qquad\qquad x < 2h \qquad (7.2a)$$

and

$$\tilde{\Psi}''(x) = \tilde{A}(x)\tilde{\Psi}(x). \qquad\qquad x > -2h. \qquad (7.2b)$$

Define for the mesh points $x_k = kh$:

$$\Psi_k^{(m)} = (d/dx)^m \Psi(x_k), \qquad\qquad (7.3a)$$

$$A_k^{(m)} = (d/dx)^m A(x_k). \qquad\qquad (7.3b)$$

The problem which has to be solved requires the determination of $\tilde{\Psi}_k$ with known Ψ_k and given A_k and $\tilde{A}_k$ for $k = 0, \pm 1, \pm 2$. The continuity condition at $x = 0$ gives:

$$\tilde{\Psi}_0 = \Psi_0, \qquad\qquad (7.4a)$$

$$\tilde{\Psi}_0^{(1)} = \Psi_0^{(1)}. \qquad\qquad (7.4b)$$

In order to derive expressions for the other $\tilde{\Psi}_k$, define the differences

$$\Delta\Psi_k = \tilde{\Psi}_k - \Psi_k, \qquad\qquad (7.5a)$$

$$\Delta A_k = \tilde{A}_k - A_k \qquad\qquad (7.5b)$$

and expand $\Delta\Psi_k$ in a Taylor series about $x = 0$ using (7.4)

$$\Delta\Psi_k = \frac{(kh)^2}{2!}\Delta\Psi_0^{(2)} + \frac{(kh)^3}{3!}\Delta\Psi_0^{(3)} + \frac{(kh)^4}{4!}\Delta\Psi_0^{(4)} + O(h^5). \qquad (7.6)$$

Using

$$\Delta\Psi_k^{(2)} = \tilde{\Psi}_k^{(2)} - \Psi_k^{(2)} = \tilde{A}_k\tilde{\Psi}_k - A_k\Psi_k$$

$$= \tilde{A}_k(\tilde{\Psi}_k - \Psi_k) + (\tilde{A}_k - A_k)\Psi_k = \tilde{A}_k\Delta\Psi_k + \Delta A_k\Psi_k, \tag{7.7}$$

gives

$$\Delta\Psi_0^{(2)} = \Delta A_0\Psi_0, \tag{7.8}$$

$$\Delta\Psi_0^{(3)} = (\Delta A\Psi)_0^{(1)} = \Delta A_0^{(1)}\Psi_0 + \Delta A_0\Psi_0^{(1)} \tag{7.9a}$$

$$= \frac{1}{2h}(\Delta A_1\Psi_1 - \Delta A_{-1}\Psi_{-1}) + O(h^2), \tag{7.9b}$$

$$\Delta\Psi_0^{(4)} = \tilde{A}_0\Delta\Psi_0^{(2)} + (\Delta A\Psi)_0^{(2)}$$

$$= \tilde{A}_0\Delta A_0\Psi_0 + \Delta A_0^{(2)}\Psi_0 + 2\Delta A_0^{(1)}\Psi_0^{(1)} + \Delta A_0\Psi_0^{(2)} \tag{7.10a}$$

$$= \tilde{A}_0\Delta A_0\Psi_0 + \frac{1}{h^2}(\Delta A_1\Psi_1 + \Delta A_{-1}\Psi_{-1} - 2\Delta A_0\Psi_0) + O(h^2). \tag{7.10b}$$

Substituting (7.8), (7.9a) and (7.10a) in (7.6), the expressions for the differences $\Delta\Psi_k$ for $k = \pm1, \pm2$ obtain the form:

$$\Delta\Psi_{\pm1} = \frac{1}{2}h^2\Delta A_0\Psi_0 \pm \frac{1}{6}h^3(\Delta A_0^{(1)}\Psi_0 + \Delta A_0\Psi_0^{(1)})$$

$$+ \frac{1}{24}h^4(\tilde{A}_0\Delta A_0\Psi_0 + \Delta A_0^{(2)}\Psi_0 + 2\Delta A_0^{(1)}\Psi_0^{(1)} + \Delta A_0\Psi_0^{(2)}) + O(h^5), \tag{7.11a}$$

$$\Delta\Psi_{\pm2} = 2h^2\Delta A_0\Psi_0 \pm \frac{4}{3}h^3(\Delta A_0^{(1)}\Psi_0 + \Delta A_0\Psi_0^{(1)})$$

$$+ \frac{2}{3}h^4(\tilde{A}_0\Delta A_0\Psi_0 + \Delta A_0^{(2)}\Psi_0 + 2\Delta A_0^{(1)}\Psi_0^{(1)} + \Delta A_0\Psi_0^{(2)}) + O(h^5). \tag{7.11b}$$

Alternatively, substituting (7.8), (7.9b) and (7.10b) in (7.6), the expressions for the differences become:

$$\Delta\Psi_{\pm 1} = \frac{h^2}{24} \left[10\Delta A_0 \Psi_0 + (1\pm 2)\Delta A_1 \Psi_1 + (1\mp 2)\Delta A_{-1}\Psi_{-1} \right]$$

$$+ \frac{h^4}{24} \tilde{A}_0 \Delta A_0 \Psi_0 + O(h^5), \tag{7.12a}$$

$$\Delta\Psi_{\pm 2} = \frac{2h^2}{3} \left[\Delta A_0 \Psi_0 + (1\pm 1)\Delta A_1 \Psi_1 + (1\mp 1)\Delta A_{-1}\Psi_{-1} \right]$$

$$+ \frac{2h^4}{3} \tilde{A}_0 \Delta A_0 \Psi_0 + O(h^5). \tag{7.12b}$$

It appears that the expressions (7.11) are rather more accurate than (7.12).

8. RESULTS OF DETECTING DEFICIENCIES, THEIR AVOIDANCE AND THE ACCURACY OF THE INTEGRATION PROCESS

In the next two sections, the results of our investigation will be presented; they were obtained by calculating the inelastic scattering of 10 and 104 MeV alpha particles from ^{28}Si. A multiple excitation of ^{28}Si, with spin sequence $0^+ - 2^+$(1.78 MeV) $- 4^+$(4.61 MeV), has been induced by the alpha particles. This means that the number of coupled equations n in the set (3.1) becomes 9. This set has been solved for a total angular momentum value J = 5 and a matching radius R_m = 17 fm. A purely rotational model is assumed with deformation parameters $\beta_2^N = \beta_2^C = -0.329$ and $\beta_4^N = \beta_4^C = -0.108$. The deformed nuclear and Coulomb potentials, given by (2.8) and (2.10), respectively, are expanded up to degree λ = 8. The optical model parameters are V = 89.749 MeV, W = 31.46 MeV, r_v = 1.443 fm, r_w = 1.429 fm, r_c = 1.317 fm and a_v = 0.628 fm, a_w = 0.729 fm. The test case with 104 MeV alpha projectiles corresponds to one of the test cases mentioned in the Karlsruhe report [5].

In the first subsection, the results will be presented for detecting the sources of deficiencies in the numerical process by means of the calculation of angles between subspaces spanned by the solution vectors. Also, the effects of avoiding the deficiencies, in part by the application of the method explained in the preceding section, will be shown. In the second subsection, the influence on the accuracy of the S-matrix elements by the deficiencies and their removal, will be discussed. Finally, in the third subsection, a figure will be shown and discussed in which the results of calculations from both preceding

subsections have been combined. By means of this figure, preliminary conclusions can be drawn concerning the accuracy of the integration process. These results, presented in all three subsections, have been based on calculations obtained for successively decreasing step sizes.

8.1 Angles between the subspaces spanned by the solution vectors.

The set of differential equations (3.1) was solved with step sizes $h = 1/5, 1/10, 1/20, 1/40$ and $1/80$ fm. The unnormalized solution vectors and their derivatives at the mesh points $R = 5h, 10h, \ldots, R_m$ for $h = 1/5$, $1/10, 1/20, 1/40$ and $1/80$ fm were used to construct the solution matrices G. These matrices will be identified by a subscript corresponding to $1/h = 5, 10, 20, 40$ and 80. The matrices G_{80} will be considered as "reference matrices", since they conform with the highest accuracy. The solution vectors have been stabilized at the mesh points mentioned in order to ensure that they were as linearly independent as possible.

Subsequently, subspaces $S_5, \ldots, S_{80}$ were associated, successively, with the matrices $G_5, \ldots, G_{80}$. The principal angles between the subspaces $S_{1/h}$ and S_{80}, with $1/h = 5, \ldots, 40$ were computed with the method explained in section 6 at the mesh points $R = 5h, 10h, \ldots, R_m$. In Figures 6a,b and 7a,b, the largest principal angles $\theta_{1/h}$ between $S_{1/h}$ and S_{80} are plotted on a logarithmic scale for projectile energies of 10 and 104 MeV, respectively.

The solutions related to the curves in Figures 6a and 7a were obtained by means of Tamura's code JUPITOR in its original form. The curves in Figure 6a clearly show discontinuities at $r = 4.0$ fm, which corresponds to the Coulomb radius R_c and at the matching radius $R_m = 17.0$ fm. The curves in Figure 7a show a pronounced discontinuity at the Coulomb radius only. The discontinuity at R_c arises if the Coulomb potential is approximated to be due to a homogeneously distributed nuclear charge within a sharp radius R_c. This potential is then not continuously differentiable at this point (see (2.6) and (2.10)), also, some of the terms are discontinuous (see (2.10)). The discontinuity in the curves at R_c can be removed by using the method given in section 7. This method avoids inaccuracies in the solutions due to the deficient behaviour of the Coulomb potential at R_c. This is clearly shown by the curves of figures 6b and 7b; they behave steadily at the Coulomb radius.

The discontinuity in the curves of Figure 6a at R_m appears to be caused by a programming error in Tamura's code [5]. In the subroutine
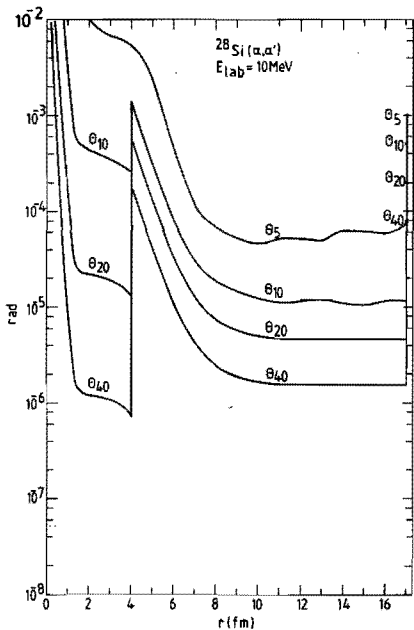
Fig.6a. The largest principal angles $\Theta_{1/h}$ between the solution subspaces $S_{1/h}$ and S_{80}, $1/h$ = 5, 10, 20, 40. The curves clearly show discontinuities at the Coulomb radius R_c = 4 fm and the matching radius R_m = 17 fm.
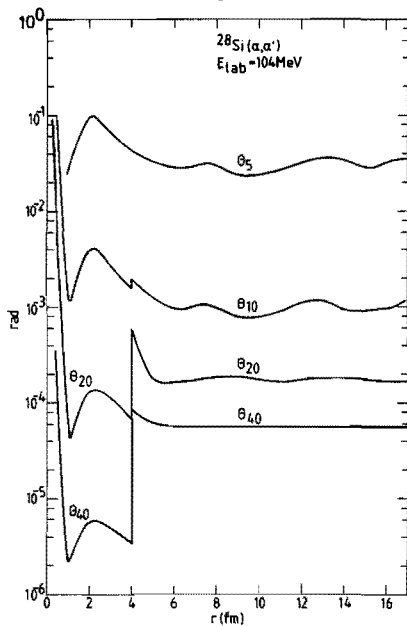
Fig.7a. The same as Figure 6a, except that the discontinuity at the matching radius R_m does not show up in the case of 104 MeV.
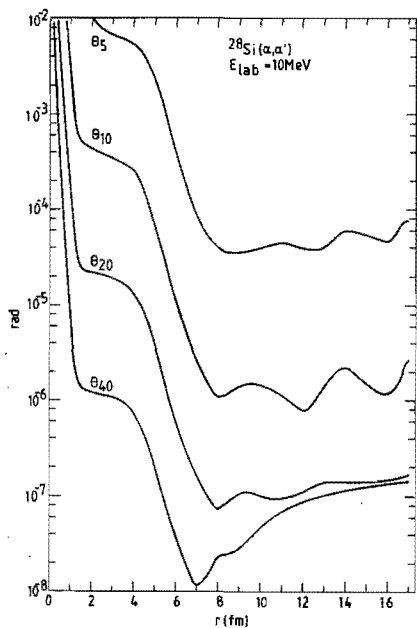
Fig.6b. The same as Figure 6a, but the deficiencies causing the discontinuities now have been removed.
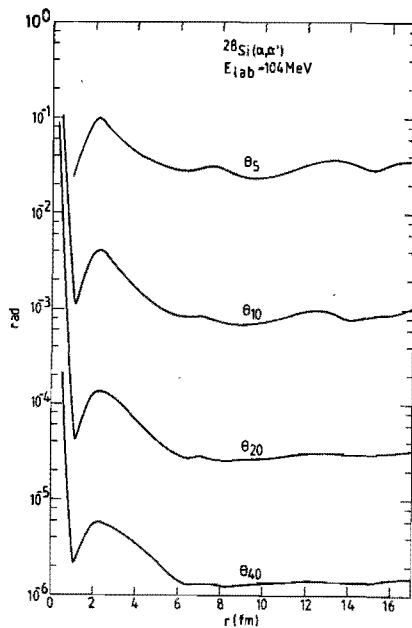
Fig.7b. The same as Figure 7a, but the discontinuity at the Coulomb radius R_c now has been removed.

COUPLE at line 926 the conditional statement should read
IF(NX-(NXCPLE+2)) 1330,1330,1610 instead of IF(NX-NXCPLE+2).,.,.. Conse-
quently, the non-diagonal elements of the potential matrix A in (3.1)
become reduced to zero in fact. Since for projectile energies near the
Coulomb barrier these elements at R_m are still important compared to the
diagonal elements, their effect of becoming zero will be reflected in the
behaviour of the principal angles. A similar discontinuity does not
appear in the curves of Figure 7a at R_m, because for energies well above
the Coulomb barrier, the relative importance of the non-diagonal elements
at this radius is much less.

8.2 S-matrix elements for successively decreasing step sizes.

    In this subsection, the influence on the accuracy of the S-matrix
elements by the deficiencies and their removal will be discussed. This
will be performed for an arbitrarily chosen element of the S-matrix,
namely, $S^5_{45;05}$ which will be used along with others for calculating the
cross sections of the 4^+ state. In Tables 1 and 2, the values calculated
for this S-matrix element are shown as a function of successively
decreasing step sizes h, labelled by t (tests) for the projectile
energies of 10 and 104 MeV, respectively. The values resulted from the
same calculations as those for the principal angles in the previous
subsection. The tables show, in columns 3, 4 and 5 respectively, the real
and imaginary parts of $S^5_{45;05}$, as well as, the modulus of
$(S^5_{45;05} - S^5_{05;45})$, denoted by "asym" in seven decimal figures. In columns
6, 7 and 8, the absolute values of the differences between the successive
entries in columns 3, 4 and 5, respectively, are given in five decimal
figures. The numbers in parentheses at the top of the columns denote the
powers of 10 by which the underlying numbers have to be multiplied. Both
tables are subdivided into four different parts that correspond to the
calculations which were performed with or without the presence of radial
discontinuities in the potential matrix A in (3.1) at R_c and R_m. The
values in parts a are influenced by both discontinuities. Those in parts
b and c are influenced only by the discontinuity at R_m and R_c,
respectively. The influence of both discontinuities have been removed in
parts d as shown.

    Tables 1 and 2 give rise to the following conclusions related to the
influence of the deficiencies on the accuracy of the S-matrix elements:

    Firstly, the discontinuity in the potential matrix A at R_m is the main

Table 1. S-matrix element for 10 Mev alpha scattering from $^{28}Si(0^+-2^+-4^+)$ as a function of successively decreasing step sizes h.

t	1/h	$S^5_{45;05}(t)$			$\left\| S^5_{45;05}(t) - S^{5}_{45;05}(t+1) \right\|$		
	fm^{-1}	real	imag	|asym|	real	imag	|asym|
		(-3)	(-3)	(-6)	(-5)	(-5)	(-6)
a) With discontinuities in potential matrix A at R_c = 4fm and R_m = 17fm.
1	5	.6127480	-.2479657	.2283326	.69039	.39919	.17426
2	10	.6196519	-.2439738	.0540680	.29780	.23112	.04096
3	20	.6226299	-.2416626	.0131061	.13444	.12202	.00984
4	40	.6239743	-.2404424	.0032611	.06353	.06235	.00240
5	80	.6246096	-.2398189	.0008627			
b) With discontinuity in potential matrix A at R_m.
1	5	.6125957	-.2480221	.2416972	.69514	.40783	.18690
2	10	.6195471	-.2439438	.0548013	.30286	.22974	.04168
3	20	.6225757	-.2416464	.0131256	.13716	.12118	.00989
4	40	.6239473	-.2404346	.0032368	.06488	.06195	.00220
5	80	.6245961	-.2398151	.0010354			
c) With discontinuity in potential matrix A at R_c.
1	5	.6256308	-.2393349	.0073168	.02961	.01113	.00624
2	10	.6253347	-.2392236	.0010758	.00597	.00199	.00096
3	20	.6252750	-.2392037	.0001156	.00277	.00085	.00006
4	40	.6252473	-.2391952	.0000523	.00136	.00039	.00001
5	80	.6252337	-.2391913	.0000669			
d) Without any discontinuity in potential matrix A.
1	5	.6254759	-.2393937	.0177432	.02462	.01993	.01611
2	10	.6252297	-.2391944	.0016341	.00089	.00067	.00150
3	20	.6252208	-.2391877	.0001338	.00005	.00003	.00008
4	40	.6252203	-.2391874	.0000570	.00000	.00001	.00011
5	80	.6252203	-.2391875	.0001710			

Table 2. S-matrix element for 104 Mev alpha scattering from $^{28}Si(0^+-2^+-4^+)$ as a function of successively decreasing step sizes h.

t	1/h fm^{-1}	$S^5_{45;05}(t)$ real (−2)	imag (−2)	|asym| (−4)	$\left\| S^5_{45;05}(t) - S^{5(t+1)}_{45;05} \right\|$ real (−2)	imag (−2)	|asym| (−4)
a) With discontinuities in potential matrix A at R_c = 4fm and R_m = 17fm.							
1	5	.1931047	−.4105927	.6898895	.21452	.39530	.63340
2	10	.4076243	−.0152959	.0564886	.00044	.01163	.05441
3	20	.4080613	−.0036645	.0020782	.00061	.00096	.00201
4	40	.4086671	−.0027067	.0000687	.00028	.00040	.00007
5	80	.4089502	−.0023105	.0000017			
b) With discontinuity in potential matrix A at R_m.							
1	5	.2031317	−.4191230	.7032578	.20771	.40675	.64599
2	10	.4108368	−.0123757	.0572717	.00157	.01027	.05516
3	20	.4092644	−.0021086	.0021127	.00005	.00019	.00204
4	40	.4092181	−.0019220	.0000697	.00000	.00001	.00006
5	80	.4092158	−.0019163	.0000061			
c) With discontinuity in potential matrix A at R_c.							
1	5	.1931483	−.4105629	.6894037	.21447	.39529	.63300
2	10	.4076221	−.0152734	.0564087	.00044	.01162	.05435
3	20	.4080594	−.0036535	.0020609	.00061	.00095	.00200
4	40	.4086661	−.0027012	.0000644	.00028	.00039	.00006
5	80	.4089496	−.0023077	.0000012			
d) Without any discontinuity in potential matrix A.							
1	5	.2031763	−.4190919	.7027446	.20766	.40674	.64556
2	10	.4108344	−.0123530	.0571892	.00157	.01026	.05509
3	20	.4092625	−.0020975	.0020943	.00005	.00018	.00203
4	40	.4092171	−.0019165	.0000647	.00000	.00000	.00006
5	80	.4092152	−.0019135	.0000042			

reason why the accuracy obtained for the energies near the Coulomb barrier is of order h only. This is shown in parts a and b of the columns 6 and 7 of Table 1. The accuracy of the solutions and their derivatives at R_m are of the order h too, whereas, $|S_{45;05}^5 - S_{05;45}^5|$ is of the order h^2 which appears in parts a and b of columns 8. This effect does not appear in the corresponding parts of Table 2, due to the relatively unimportant non-diagonal elements of the potential matrix A at R_m for those energies well above the Coulomb barrier. This is also the reason for the differences between parts b and d of the columns 6,7 and 8 of Table 2 being very small or even zero.

Secondly, the influence of the discontinuity in the potential matrix A at R_c has only minor importance when compared to that at R_m for energies near the Coulomb barrier. For energies well above it, this discontinuity gives rise to only a small deviation. However, for both energies, the discontinuity at R_c departs from the expected order of accuracy. This is shown in part c of columns 6 and 7 in the tables.

Thirdly, only after removing both discontinuities in the potential matrix A does the accuracy of the S-matrix elements become of the order h^4 to h^5. This is shown in part d of the columns 6 and 7 in the tables.

Fourthly, from part d in the tables, we see that the entries of column 5, i.e., $|S_{45;05}^{5(t)} - S_{05;45}^{5(t)}|$ values are about an order of magnitude smaller than the estimate $|S_{45;05}^{5(t)} - S_{45;05}^{5(5)}|$ for the error in $S_{45;05}^{5(t)}$. This means that a high degree of symmetry in the S-matrix elements does not guarantee an equal high accuracy of these elements.

Finally, the differences between the calculations with and without either discontinuities are rather small and the former will have little serious consequence for the calculations in our test cases in practice.

From now onwards, the calculations have been performed without any discontinuity in the potential matrix.

8.3 About the accuracy of the integration process.

In this subsection, we look for a relationship between the asymmetry of the S-matrix and the largest principal angle between the solution subspaces when they are used as a measure of the accuracy of the integration process. Examining this relationship, the modulus of the largest element of $(S-S^T)$ is plotted in Figure 8 on a double logarithmic scale as a function of the step size h. The values of the moduli are denoted by full dots. The largest principal angles, $\theta_{1/h}$, $1/h = 5$, 10, 20 and 40,
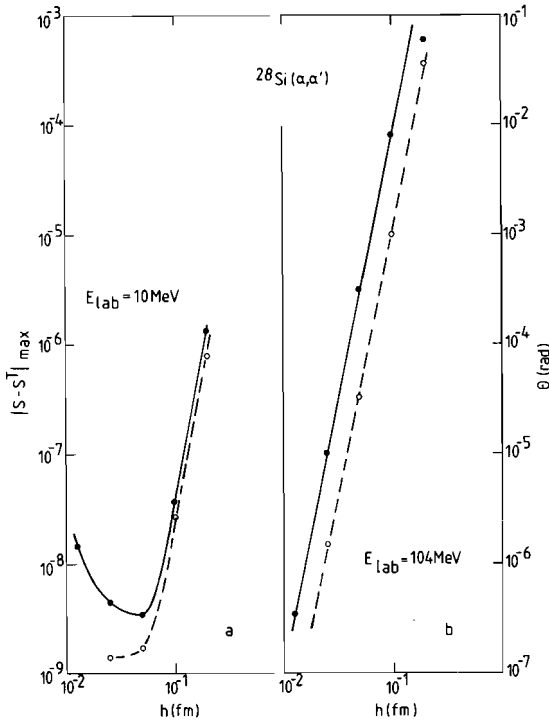
Fig.8. The modulus of the largest element of $(S-S^T)$ (full dots), and the largest principal angle $\Theta_{1/h}$, $1/h = 5, 10, 20, 40$ at the matching radius R_m (open dots), plotted as functions of the step size h. The slopes of the straight parts of the curves are all between 4.8 and 5.1 indicating that Störmer's difference method does give rise to a global truncation error of order h^5.

defined in subsection 8.1, at the matching radius R_m are also plotted in the figure. They are indicated by open dots. Parts a and b of the figure refer to projectile energies of 10 and 104 MeV, respectively.

Looking at Figure 8, the following preliminary conclusions that relate to the accuracy of the integration process itself can be drawn:

Firstly, the slopes of the straight parts of the curves are all between 4.8 and 5.1 indicating that Störmer's difference method does give rise to a global truncation error of order h^5. This is not only indicated by the moduli of the largest elements of $(S-S^T)$ (solid lines), but also, by the largest principal angles at R_m (broken lines). Therefore, both quantities can be used to measure the accuracy; however, during the integration process, only the largest principal angle can serve as such a measure, as opposed to the largest element of $(S-S^T)$, which has been pointed out in section 5. In other words, only the largest principal angle is capable of describing the development of a global error during the course of the integration. Once more, this is confirmed by the curves $\Theta_{1/h}$, $1/h = 5,...,40$ in Figures 6b and 7b, that also show an $O(h^5)$ character along most of the integration range. The declining

behaviour of the curves during the first part of the integration corresponds to a damping of the global truncation error, probably caused by the rising character of the solutions here.

Secondly, for energies well above the Coulomb barrier, the accuracy of the numerical process for all step sizes is fully determined by the global truncation error due to the particular difference equation used. For energies near the Coulomb barrier, the errors are considerably less and the $O(h^5)$ character appears only with the larger step sizes. For smaller step sizes, the truncation errors are so small that round-off errors are dominant. This is shown in Figure 8a by those parts of the curves deviating from a straight line at the smaller step sizes. Looking at the curve θ_{40} in Figure 6b, we can see that these round-off errors are accumulated during the second half of the integration range.

Finally, we can observe that the largest element of $(S-S^T)$ is a factor of one to two orders of magnitude smaller than the largest principal angle.

Here, we wish to state that, historically, the disappointing behaviour of the S-matrix elements for successively decreasing step sizes, as shown by part a of Tables 1 and 2, motivated us to investigate the integration process.

9. RESULTS RELATING TO THE LOSS OF ACCURACY DUE TO THE TENDENCY OF THE
   SOLUTION VECTORS TOWARDS LINEAR DEPENDENCY

In this section, we present the results of our investigations related to the loss of accuracy due to the tendency of the solution vectors to become nearly linearly dependent during the integration through a classically forbidden region. This loss of accuracy is a consequence of the finite representation of numbers in the computer (round-off errors) and it would not occur if this representation is infinitely precise.

The tendency of the solution vectors towards linear dependency is illustrated in Figures 9 and 10 for projectile energies of 10 and 104 MeV, respectively. In these figures, the principal angles $\theta_1,\dots,\theta_9$ (as given by (6.2)) between two solution subspaces are plotted on a logarithmic scale as a function of r. The solution matrices associated with these subspaces were calculated for h = 1/80 fm in order to keep the truncation error as small as possible. One of the solution matrices was stabilized at all the mesh points R = 5h, 10h,...,R_m, in order to ensure that the solution vectors remained as linearly independent as possible.

The other solution matrix has not been stabilized at all. The first
subspace can be considered as the reference subspace and the second one
the subspace to be investigated. Figure 9 shows that, at 10 MeV, three
principal angles obtain a value of $\pi/2$ which indicates that the dimension
of the initial nine dimensional solution subspace has been reduced to
six. Figure 10 shows that, at 104 MeV, dimension reduction of the
solution subspace is less drastic. A dimension reduction of the solution
subspace means that the representation of the physical solution as a
linear combination of the solution vectors has completly lost its
accuracy.
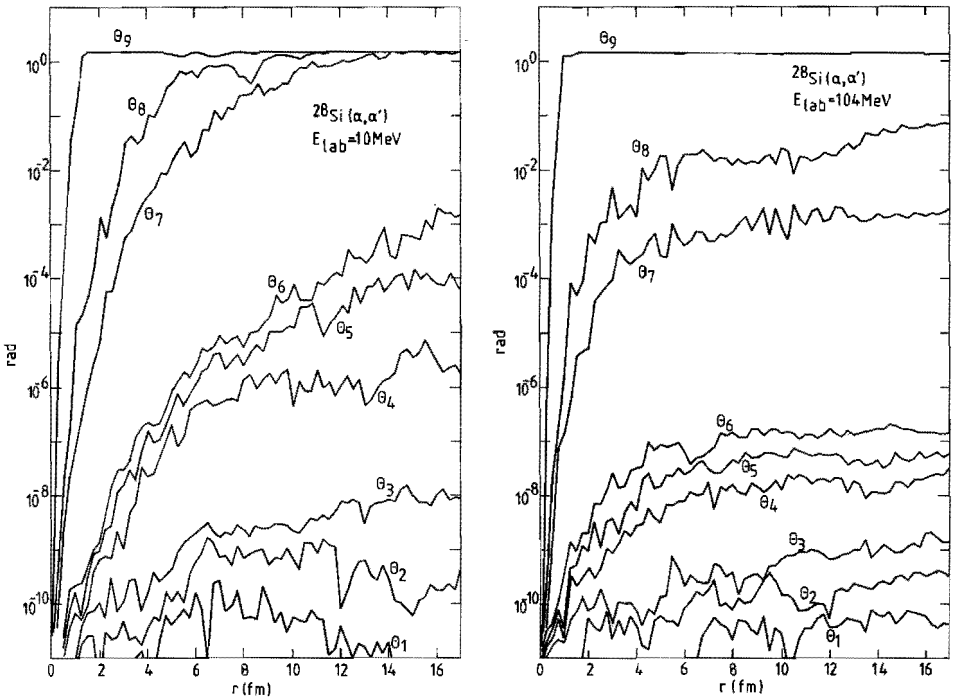
Figs. 9 and 10. These figures illustrate the tendency of the solution
vectors towards linear dependency by showing the principal angles
$\theta_1,\ldots,\theta_9$ between a reference subspace and a subspace to be investigated,
for energies of 10 and 104 MeV, respectively. The two solution matrices
associated with these subspaces were calculated for h = 1/80 fm; the
first one was stabilized at all the mesh points R = 5h, 10h,..., R_m,
whereas, the second one has not been stabilized at all. Principal angles
obtain a value of $\pi/2$ which indicates that the dimension of the initial
nine dimensional solution subspace has been reduced.

In order to keep such a loss of accuracy within given bounds, the integration through a classically forbidden region necessitates the stabilization of the solution matrix Ψ. This will be necessary in only a few mesh points. In Figure 4, this is shown for a small part of the integration range near the origin. For the whole integration range, it is shown in the Figures 11 and 12 for projectile energies of 10 and 104 MeV, respectively. In these two figures, the linear independence numbers are plotted logarithmically as a function of r for two different cases denoted by $\nu_{80}^{(0)}$ and $\nu_{80}^{(-2)}$ which were calculated for h = 1/80 fm. For the curve that is denoted by $\nu_{80}^{(0)}$, the solution matrix has been stabilized at
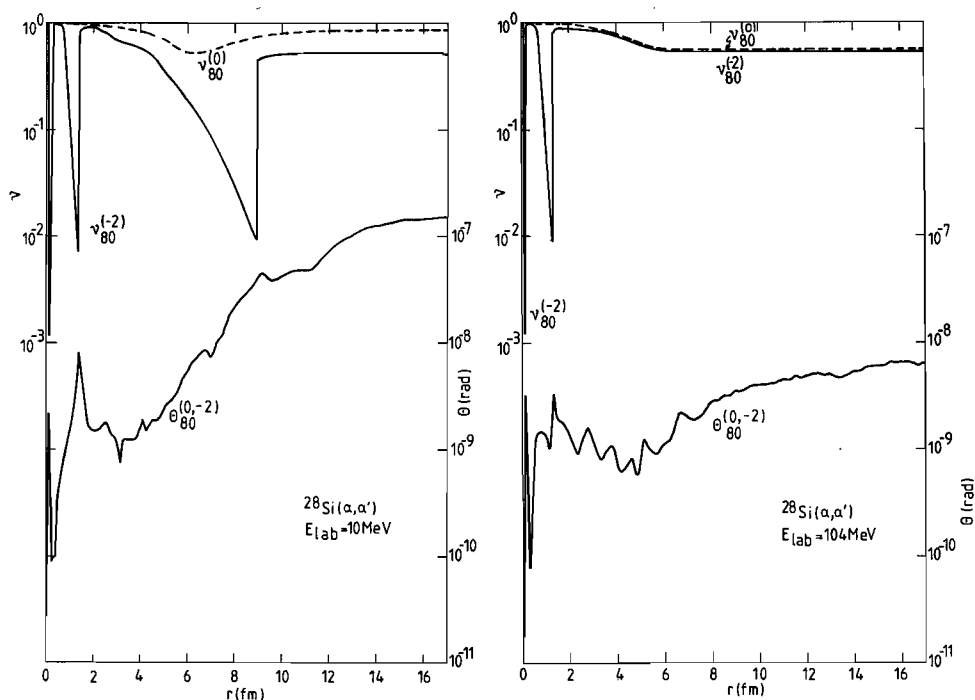
Figs. 11 and 12. In these figures, two plots of the linear independence number ν calculated for h = 1/80 fm, are shown for energies of 10 and 104 MeV, respectively. For the curve that is denoted by $\nu_{80}^{(0)}$ (broken line), the solution matrix has been stabilized at all the mesh points R = 5h, 10h, ..., R_m, while for the other one, denoted by $\nu_{80}^{(-2)}$ (solid line), stabilization is performed only at those mesh points in which $\nu < 10^{-2}$. The largest principal angle between the two subspaces associated with the solution matrices belonging to the curves $\nu_{80}^{(0)}$ and $\nu_{80}^{(-2)}$ is denoted by $\theta_{80}^{(0,-2)}$.

all the mesh points R = 5h, 10h,...,R_m, while for the other one, denoted by $v_{80}^{(-2)}$, stabilization is performed only at those mesh points in which $v < 10^{-2}$. In these cases the solution matrices, called F and G respectively, have been constructed from (4.31) at the above mesh points. The largest principal angle between the subspaces associated with F and G, denoted by $\Theta_{80}^{(0,-2)}$, is plotted on a logarithmic scale in Figures 11 and 12 too.

When looking at these figures, the following remarks can be made:

Firstly, during a decline of $v_{80}^{(-2)}$ as a function of r, the errors are growing, as visualized by an increasing behaviour of $\Theta_{80}^{(0,-2)}$.

Secondly, during the first part of the integration range (r < 4 fm) $\Theta_{80}^{(0,-2)}$ shows an erratic behaviour; however, beyond this part, as shown by Figure 11, $\Theta_{80}^{(0,-2)}$, it rises smoothly during the decline of $v_{80}^{(-2)}$; the value at R_m is determined here mainly.

Thirdly, in the classically allowed region, $v_{80}^{(-2)}$ behaves constantly; however, here $\Theta_{80}^{(0,-2)}$ still rises steadily until it reaches its final value at R_m.

From these remarks, we can conclude that the loss of accuracy is caused mainly by a build-up of round-off errors during the course of integration beyond the initial region. To understand this, we will discuss the increase of the largest principal angle in some integration interval and how it relates to an accumulated condition number to be defined later.

If the round-off is the only source of errors in some interval of the solution matrices F and G leading to perturbations E_F and E_G in F and G, respectively, it can be expected [13] that, in this interval, $\Theta_{80}^{(0,-2)}$ will increase by

$$\Delta\Theta_{80}^{(0,-2)} \sim \left\{ \frac{1}{v(F)} \frac{\|E_F\|}{\|F\|} + \frac{1}{v(G)} \frac{\|E_G\|}{\|G\|} \right\}. \tag{9.1}$$

This means that round-off errors in the solution matrices, generally, will lead to perturbations in the corresponding solution spaces. If these perturbations are measured by the largest principal angle between the perturbated and the unperturbated spaces, in fact, these angles may be larger than the relative errors in the solution matrices by a factor of the order of the condition number of the solution matrices. The relative errors are likely to be of the order of the machine precision (macheps) of our computer (see subsection 4.3).

This suggests that a solution matrix contains less information about
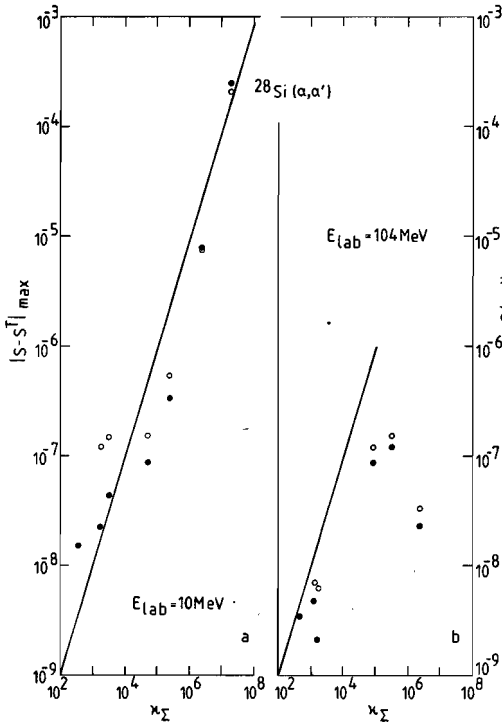
Fig.13. The largest principal angle $\theta_{80}^{(0,-t)}$, $t = 1, 2, ..., 6$ at the matching radius R_m (open dots) and the modulus of the largest element of $(S-S^T)$ (full dots), plotted as functions of the accumulated condition number κ_Σ. For energies near the Coulomb barrier, round-off errors are accumulated during the course of the integration. For energies well above the Coulomb barrier, this is less so.

the subspace it represents, when it becomes more ill-conditioned. It should be stressed that stabilization does not overcome this loss of accuracy; it only reduces the condition number and, therefore, the effect of round-off errors in the next integration interval.

Now, let us define an accumulated condition number as:

$$\kappa_\Sigma = \sum_{\text{at all } R} 1/\nu \tag{9.2}$$

by summing the condition numbers of the solution matrices calculated at all the mesh points. Then, combination of (9.1) and (9.2) suggests that at the matching radius R_m

$$\theta_{80}^{(0,-2)}(R_m) \sim \kappa_\Sigma \cdot \text{macheps}. \tag{9.3}$$

To find an experimental relationship between the build-up of round-off errors and the accumulated condition number, we performed "runs", in which stabilization is carried out only when $\nu < 10^{-t}$. In this way, principal angles $\theta_{80}^{(0,-t)}$ and accumulated condition numbers $\kappa_\Sigma^{(-t)}$ were calculated for $t = 1,2,...,6$. In Figure 13, the largest principal angle $\theta_{80}^{(0,-t)}$, $t = 1,2,...,6$, at the matching radius R_m (open dots) and the

modulus of the maximum element of $(S-S^T)$ (full dots) are plotted on a double logarithmic scale as functions of $\kappa_\Sigma^{(-t)}$. For energies near the Coulomb barrier, we can see from Figure 13a that the position of the full and open dots conforms with (9.3). Clearly, this shows that round-off errors were accumulated during the course of the integration. However, for energies well above the Coulomb barrier, this was less so, as is shown in Figure 13b. We note that, as shown in both figures, the moduli of the largest element of $(S-S^T)$ correspond quite well to the largest principal angles at R_m. This is in contrast to the cases shown in Figure 8, where it was not the noise level, but the amount of truncation error that varied. We cannot explain this difference yet.

Subsequently, we pay attention to a peculiar phenomenon concerning the asymmetry of the S-matrix. It seems that errors in the calculated elements $S_{I\ell;I_0\ell_0}^J$ for $\ell > \ell_0$ are generally larger than those for $\ell < \ell_0$. In other words, the errors in the low-ℓ to high-ℓ transition elements are larger than in the corresponding inverse transition elements. At the same time it appears that, for many elements, this effect will increase as the values $|\ell - \ell_0|$ increase. Roughly, this means that most of the entries below the diagonal of the S-matrix have larger errors than those above the diagonal. This phenomenon has been encountered in many coupled-channel calculations and can be explained [16]. In our discussion of this phenomenon, we will consider the F-norm (Frobenius norm) of the part $D_>^{(-t)}$ of $(S^{(0)} - S^{(-t)})$ for which $\ell > \ell_0$

$$\| D_>^{(-t)} \|_F = \left[\sum_{\ell > \ell_0} \left| (S_{I\ell;I_0\ell_0}^{J(0)} - S_{I\ell;I_0\ell_0}^{J(-t)}) \right|^2 \right]^{1/2}, \qquad (9.4)$$

where $S^{(0)}$ is the S-matrix calculated by stabilizing the solution matrix Ψ at all the mesh points $R = 5h, 10h, \ldots, R_m$; whereas, $S^{(-t)}$ denotes the S-matrix obtained by stabilizing Ψ at these mesh points when only $\nu < 10^{-t}$, $t = 1, 2, \ldots, 6$. In the same way $\| D_<^{(-t)} \|_F$ for $\ell < \ell_0$ can be defined. Tables 3 and 4 contain these F-norms and their differences as functions of the accumulated condition numbers $\kappa_\Sigma^{(-t)}$ for projectile energies of 10 and 104 MeV, respectively. The S-matrices have been calculated with $h = 1/80$ fm.

Looking at Tables 3 and 4, we can see that, for $t \leqslant 2$, i.e., with two or three stabilizations of Ψ, very accurate values for the S-matrix

Table 3. F-norms (9.4) for 10 Mev alpha scattering from $^{28}Si(0^+-2^+-4^+)$ as a function of the accumulated condition number $\kappa_\Sigma^{(-t)}$.

t	$\kappa_\Sigma^{(-t)}$	$\|D_>^{(-t)}\|_F$	$\|D_<^{(-t)}\|_F$	$\|D_>^{(-t)}\|_F - \|D_<^{(-t)}\|_F$
		(-3)	(-3)	(-3)
1	$.17 \ 10^4$	.0000364	.0001751	-.0001387
2	$.31 \ 10^4$	.0000253	.0000715	-.0000462
3	$.55 \ 10^5$	.0001523	.0000559	.0000964
4	$.28 \ 10^6$	.0005935	.0002768	.0003168
5	$.24 \ 10^7$	.0106600	.0022983	.0083617
6	$.19 \ 10^8$	.3101392	.0072964	.3028428

Table 4. F-norms (9.4) for 104 MeV alpha scattering from $^{28}Si(0^+-2^+-4^+)$ as a function of the accumulated condition number $\kappa_\Sigma^{(-t)}$.

t	$\kappa_\Sigma^{(-t)}$	$\|D_>^{(-t)}\|_F$	$\|D_<^{(-t)}\|_F$	$\|D_>^{(-t)}\|_F - \|D_<^{(-t)}\|_F$
		(-6)	(-6)	(-6)
1	$.13 \ 10^4$	.0035279	.0043661	-.0008383
2	$.16 \ 10^4$	.0027832	.0032752	-.0004920
3	$.82 \ 10^5$	.1243626	.0061164	.1182462
4	$.82 \ 10^5$	.1243626	.0061164	.1182462
5	$.31 \ 10^6$	.1488424	.0084672	.1403752
6	$.23 \ 10^7$	.0334215	.0035366	.0298849

elements are obtained. The tables show that, for $t > 2$, $\|D_>^{(-t)}\|_F$ is larger than $\|D_<^{(-t)}\|_F$ and that the difference between the two grows with increasing $\kappa_\Sigma^{(-t)}$ values. This indicates that the calculated elements $S_{I\ell;I_0\ell_0}^J$ for $\ell > \ell_0$ are affected more by the perturbation of the solution space at R_m, than those for $\ell < \ell_0$. This effect will be stronger, as stabilizing of Ψ is delayed. The increasing character of the elements with $\ell > \ell_0$ in the physical solution matrix for a classically forbidden region, apparently, provides the main contribution to the perturbation of the solution space at R_m.

Finally, we can remark that, on the contrary, the errors in the

S-matrix originating from the truncation error, inherent in the difference formula employed, behave quite symmetrically, in the sense that the asymmetry $\|S^{(h)} - (S^{(h)})^T\|_F$ in the S-matrix obtained by integration with a step length h is an order of magnitude smaller than the estimate $\|S^{(h)} - S^{(1/80)}\|_F$ for the error in $S^{(h)}$. This reaffirms our opinion that it is dangerous to conclude from a high degree of symmetry in an obtained S-matrix that its elements contain small errors.

10. CONCLUSIONS

    The following conclusions can be drawn:

1.   The quantum mechanical description of inelastic collisions between particles requires, in general, the numerical solution of the radial Schrödinger equation. For investigating the accuracy of the numerical integration process, a method has been successfully used for measuring the accuracy of the regular solution subspace spanned by the solution vectors, rather than the accuracy of the solution vectors themselves. This method computes the principal angles between two solution subspaces that are obtained under different numerical conditions (varying length of integration step and stabilization strategy). One of the subspaces is constructed under optimal conditions, so that it is considered as the reference subspace, the other being the subspace to be investigated. In this method, the quality of a solution subspace, obtained by a numerical procedure, can be measured, e.g., the extent to which solution vectors, as a basis of the solution subspace, remain linearly independent in the range from the origin to the matching radius R_m, during the integration.

2.   The method of computing the principal angles enables us to inspect the loss of accuracy in the integration range originating from the truncation error inherent in the difference formula employed and to detect possible sources of deficiencies in the numerical process for solving the Schrödinger equation. It appears to be a very sensitive method for the latter purpose.

3.   A method has been developed with which inaccuracies in the solutions due to a deficiency caused by discontinuities in the potential matrix can be avoided. After applying this method, the accuracy of the solution vectors and the S-matrix elements agreed with the order of the global truncation error belonging to the multistep integration method used.

4.   The largest principal angle at the matching radius, as well as the modulus of the largest element of $(S - S^T)$, can be used as measures of

the global truncation error in the integration process. During the execution of this process, however, only the local largest principal angle can serve as such a measure. In other words, only the largest principal angle is capable of recording the development of the global truncation error during the course of integration. Also, the effect of other types of errors can be recorded in a like manner.

5.   The largest principal angle can be used to investigate the loss of accuracy as a result of a tendency by the solution vectors to become nearly linearly dependent during the integration through a classically forbidden region as an effect of round-off errors inherent in the finite representation of numbers in a computer. This loss of accuracy necessitates stabilization of the set of solution vectors. This process can be effectively monitored by introducing a so-called "linear independence number ν" for the set of solution vectors. In this way, we found that stabilizing the set of solution vectors in a few well chosen mesh points only, for our nuclear physics test cases of alpha scattering from ^{28}Si, proved to be adequate for obtaining an S-matrix accuracy that is quite satisfactory.

REFERENCES

[1] T. Tamura, Revs. Mod. Phys. 37(1965)679.

[2] N.K. Glendenning, in Nuclear Structure and Nuclear Reactions, Proc. of the International School of Physics "Enrico Fermi", edited by M. Jean and R.A. Ricci, Academic Press, New York, 1969, p. 332.

[3] J. Raynal, in Computing as a Language of Physics, edited by A. Salam (IAEA, Vienna, 1972), p. 292.

[4] G.R. Satchler, "Direct Nuclear Reactions", Clarendon Press, Oxford University, 1983.

[5]   T. Tamura, Oak Ridge National Laboratory Report No.ORNL-4152(1967);
      H. Rebel and G.W. Schweimer, Kernforschungszentrum Karlsruhe Report
      No. KFK-1333(1971).

[6]   P. Henrici, "Discrete Variable Methods in Ordinary Differential
      Equations", John Wiley and Sons, New York, 1962.

[7]   M.A. Melkanoff, J. Raynal and T. Sawada, Methods Comput. Phys. 6,
      Academic Press, New York, 1969.

[8]   R.G. Gordon, J. Chem. Phys. 51(1969)14.

[9]   J.H. Wilkinson, "The Algebraic Eigenvalue Problem", pp. 152,233,
      Oxford University Press, London, 1965.

[10] A.R. Gourlay and G.A. Watson, "Computational Methods for Matrix
      Eigenproblems", John Wiley and Sons, Chichester, 1973.

[11] G.H. Golub and C.F. van Loan, "Matrix Computations", North Oxford
      Academic, Oxford, 1983.

[12] L.D. Tolsma, J. Comput. Phys. 17(1975)384.

[13] A. Björck and G.H. Golub, Math. Comp. 27(1973)579; Ref[11], p. 428.

[14] N.M. Clarke, Comput. Phys. Commun. 27(1982)365.

[15] E. Onset and L.L. Salcedo, Anales de Fisica A80(1984)109;
      E. Onset and L.L. Salcedo, J. Comput. Phys. 57(1985)361.

[16] W.J.G. Thijssen, B.J. Verhaar and A.M. Schulte,
      Phys. Rev. C23(1981)1984.

A Fast Method for Nuclear Coupled-Channels Calculations Including Coulomb Excitation

L. D. TOLSMA

*Eindhoven University of Technology, Department of Physics,
Cyclotron laboratory, Eindhoven, the Netherlands*

Received September 11, 1974

To reduce the computation time in nuclear coupled-channels calculations including Coulomb excitation, the applicability of Gordon's numerical method has been investigated to the integration range beyond the range of the nuclear potential. It turns out that a considerable reduction of computation time can be obtained. The larger the integration range and the relative wave number, pertinent to a given reaction process and reaction energy, the larger is this reduction. This is illustrated by two test cases dealing with α and ^{16}O scattering near the Coulomb barrier. Consequently, although the method is sometimes also of considerable advantage in the case of scattering of light particles, it seems to be especially suitable to heavy ion scattering problems.

1. INTRODUCTION

The inclusion of the contribution of Coulomb excitation in coupled-channels calculations of nuclear scattering problems often increases the computation time considerably. To reduce this time we have investigated the applicability of a method for solving systems of coupled linear second-order differential equations, introduced by R. G. Gordon in connection with atomic and molecular scattering and bound state problems [1, 2]. For most collisions between atoms and ions at thermal energies, the de Broglie wavelength associated with the relative motion is short as compared to the long range of the interatomic potential. This range can then be divided into intervals which are sufficiently small to approximate the potential matrix by a linearly varying reference potential matrix and which on the other hand contain a sufficient number of de Broglie wavelengths. This enables one to write the general solution vector in e.g., the classically allowed region as a linear combination of two rapidly oscillating Airy functions with slowly varying coefficient vectors. An important advantage of Gordon's method is connected with the fact that part of the numerical procedure is independent of energy. Apart from a possible decrease of computation time at a single scattering

384

energy [3], an additional amount of time is thus saved when the calculation is repeated at a slightly different energy.

In Section 2, we give a concise formulation of Gordon's method. In Section 3, the application of Gordon's method to nuclear scattering problems is discussed. To study this applicability, the method has been implemented in Tamura's code JUPITOR. In the resulting code JUPIGOR, the integration range is divided into a part up to the radius where the nuclear interaction has died out and a large part where only the Coulomb interaction operates. From preliminary calculations it appeared that Gordon's method is not efficient over the first part: the step size has to be taken too small. This part is therefore dealt with by a conventional step-by-step method. Subsequently, the remaining integration range is divided into steps such that the Coulomb interaction matrix is linearized, up to a few percent over one step. Here Gordon's method turns out to be very efficient and to reduce computation time considerably.

In Section 4, we present the results of our study on the 11.5, 16.5, 21.5 MeV ^{122}Te(α, α')^{122}Te [12] and 39, 44, 49 MeV ^{58}Ni(^{16}O, ^{16}O')^{58}Ni [13] inelastic scattering problems. Preliminary results of our investigation on the 10–16 MeV ^{114}Cd(α, α')^{114}Cd inelastic scattering problem have been published elsewhere [14].

2. A Concise Formulation of Gordon's Method

The Schrödinger equation for the partial wave radial function in potential scattering is, in conventional notation,

$$\left\{ \frac{d^2}{dr^2} + k^2 - \frac{2m}{\hbar^2} V(r) - \frac{l(l+1)}{r^2} \right\} \psi(r) = 0. \tag{2.1}$$

This equation can be rewritten into the form

$$(d^2\psi/dr^2) + \{k^2 - U(r)\} \psi = 0. \tag{2.2}$$

Consider some interval of the integration range with the midpoint at radius $\bar{r}$. Although in Gordon's method several forms can be used for the reference potential, we follow him in choosing a linear one of the form

$$U_0(r) = \overline{U}(\bar{r}) + (r - \bar{r})(dU/dr)|_{r=\bar{r}}, \tag{2.3}$$

where $\overline{U}$ is the average value of the potential over the interval. Using (2.3) as potential in (2.2) gives us the Airy functions Ai and Bi as a set of two linearly independent solutions. As shown by Gordon these functions can be efficiently evaluated numerically. The general reference solution may now be written as

$$\psi_0(r) = Ai[\alpha(\beta + r)] a + Bi[\alpha(\beta + r)] b, \tag{2.4}$$

with the constants

$$\alpha = \left(\frac{dU}{dr}\Big|_{r=\bar{r}}\right)^{1/3}, \qquad \beta = \frac{\overline{U}(\bar{r}) - k^2}{dU/dr\,|_{r=\bar{r}}} - \bar{r}. \qquad (2.5)$$

The constant coefficients a and b are determined by conditions of continuity at the interval boundaries. For instance, if they would be adapted to the value and derivative of the exact solution $\psi(r)$ at the "left-hand" boundary r_l,

$$a = \pi\{Bi'[\alpha(\beta + r_l)]\,\psi(r_l) - \alpha^{-1}\,Bi[\alpha(\beta + r_l)]\,\psi'(r_l)\}, \qquad (2.6a)$$

$$b = \pi\{\alpha^{-1}\,Ai[\alpha(\beta + r_l)]\,\psi'(r_l) - Ai'[\alpha(\beta + r_l)]\,\psi(r_l)\}, \qquad (2.6b)$$

where the prime denotes differentiation with respect to the argument.

Including the difference between the true potential and the reference potential one obtains corrections $\Delta a(r)$ and $\Delta b(r)$ to the coefficients a and b. The solution of the Schrödinger Eq. (2.2) can now be approximated by the reference solution (2.4) plus a correction term

$$\psi(r) \approx Ai[\alpha(\beta + r)]\{a + \Delta a(r)\} + Bi[\alpha(\beta + r)]\{b + \Delta b(r)\}, \qquad (2.7)$$

where the varying coefficients, to first order in $[U(r) - U_0(r)]$ are given by

$$\Delta a(r) = -\pi \int_{r_l}^{r} Bi[\alpha(\beta + r')]\{U(r') - U_0(r')\}\,\psi_0(r')\,dr', \qquad (2.8a)$$

$$\Delta b(r) = \pi \int_{r_l}^{r} Ai[\alpha(\beta + r')]\{U(r') - U_0(r')\}\,\psi_0(r')\,dr'. \qquad (2.8b)$$

These coefficients remain small as long as the reference potential is a good approximation to the true potential. Thus, in the classically allowed region the solution (2.7) has been written as a linear combination of two rapidly oscillating Airy functions with slowly varying coefficients. The integrals in (2.8) can be evaluated analytically.

In the case of n coupled equations the differential operator and k^2 in (2.2) stand for diagonal $(n \times n)$ matrices while the potential is in general a nondiagonal $(n \times n)$ matrix $U(r)$. To obtain a reference potential matrix a similarity transformation is performed which reduces $U(\bar{r})$ to diagonal form

$$X^{-1}U(\bar{r})\,X = \text{diag}(\lambda_c), \qquad (2.9)$$

where X is the transformation matrix and λ_c are the eigenvalues. In other words $U(\bar{r})$ has been transformed from a *free* basis into a *local* basis such that it is diagonal. As reference potential matrix the following diagonal matrix is chosen

$$U_0(r) = [X^{-1}\overline{U}(\bar{r})\,X]_{\text{diag}} + (r - \bar{r})[X^{-1}(dU/dr)|_{r=\bar{r}}\,X]_{\text{diag}}, \qquad (2.10)$$

where $\bar{U}(\bar{r})$ is the average value of the potential matrix over the interval and the subscript "diag" means that only the diagonal elements are retained. With this diagonal matrix the set of reference equations becomes uncoupled and the Airy functions are again the linearly independent exact solutions. Writing the Airy functions in diagonal matrix form, the general reference solution vector in the *local* basis is given by

$$\boldsymbol{\psi}_0 = \mathbf{Ai}\,\mathbf{a} + \mathbf{Bi}\,\mathbf{b}. \tag{2.11}$$

The constant coefficient vectors $\mathbf{a}$ and $\mathbf{b}$ are once more determined by boundary conditions like (2.6). The solution vector of the coupled equations may now be approximated by

$$\boldsymbol{\psi} \approx \mathbf{Ai}(\mathbf{a} + \Delta\mathbf{a}) + \mathbf{Bi}(\mathbf{b} + \Delta\mathbf{b}), \tag{2.12}$$

where the varying coefficient vectors are determined by

$$\Delta\mathbf{a} = -\pi \int_{r_l}^{r} \mathbf{Bi}\{\mathbf{U} - \mathbf{U}_0\}\,\boldsymbol{\psi}_0\,dr', \tag{2.13a}$$

$$\Delta\mathbf{b} = \pi \int_{r_l}^{r} \mathbf{Ai}\{\mathbf{U} - \mathbf{U}_0\}\,\boldsymbol{\psi}_0\,dr'. \tag{2.13b}$$

The continuity condition for the solution vector in the free basis leads to a relation between the local solution vector in interval p and that in interval $p+1$, both taken at the common boundary point:

$$\boldsymbol{\psi}_{p+1} = \mathbf{X}_{p+1}^{-1}\mathbf{X}_p\boldsymbol{\psi}_p \equiv \mathbf{T}_p\boldsymbol{\psi}_p. \tag{2.14}$$

Note that the following quantities are independent of energy:

the diagonalized potential matrix $\mathbf{X}^{-1}\bar{\mathbf{U}}\mathbf{X}$,
the transformed derivative potential matrix $\mathbf{X}^{-1}(d\mathbf{U}/dr)\,\mathbf{X}$,
the transformation matrix $\mathbf{T}_p$.

These quantities can therefore be used at other values of the energy, which turns out to save more than half of the computation time.

The general solution vector can be written as a linear combination of n independent solution vectors. These solution vectors can be collected as the columns of a solution matrix $\boldsymbol{\Psi}$. The component c of the vector s (solution) is denoted by ψ_{cs}. Suppose that the components in the solution vectors are arranged in order of decreasing local relative kinetic energy. Integrating through a classically forbidden region, the components with negative kinetic energy will in general consist of an exponentially growing and an exponentially decreasing part. The former is responsible for a tendency to destroying the initially taken linear indepen-

dence of the solution vectors. To maintain this linear independence, the solution matrix can be stabilized by an unitary transformation such that the exponentially growing components below the diagonal with local negative kinetic energy are eliminated. In this way a stable solution matrix $\tilde{\Psi}$ is obtained

$$\tilde{\Psi}^* = \Psi^* \mathcal{U}, \qquad (2.15)$$

in terms of the original solution matrix Ψ. The unitary matrix $\mathcal{U}$ can be chosen [4] as a product of elementary unitary Hermitian matrices: $\mathbf{P}_n \mathbf{P}_{n-1} ... \mathbf{P}_c ...$, in which c runs over the components with local *negative* kinetic energy and with

$$\mathbf{P}_c = \mathbf{I} - 2\mathbf{w}_c \mathbf{w}_c^\dagger. \qquad (2.16)$$

The unit column vector $\mathbf{w}_c$ with n components can be constructed from row c of Ψ:

$$2K\mathbf{w}_c^\dagger = (\psi_{c1}^*, \psi_{c2}^*, ..., \psi_{cc}^* + S\psi_{cc}^*/|\psi_{cc}|, 0, ..., 0), \qquad (2.17)$$

where K and S are defined as positive constants, given by the expressions

$$S^2 = \sum_{s=1}^{c} \psi_{cs} \psi_{cs}^*, \qquad 2K^2 = S^2 + S\,|\psi_{cc}|. \qquad (2.18)$$

It can easily be shown that the solution matrix $\tilde{\Psi}$ obtained has vanishing elements below the diagonal in the rows c up to and including n, while the corresponding elements of the derivative of $\tilde{\Psi}$ become small. If on the other hand a different choice is made for $\mathbf{w}_c$ by replacing ψ_{cs} by ψ_{cs}' in Eq. (2.17), the abovementioned results for $\tilde{\Psi}$ and $\tilde{\Psi}'$ are interchanged. Clearly, it is possible to eliminate the exponentially growing solution by means of the linear combination $k_c \psi_{cs} + \psi_{cs}'$. The wave number k_c is defined as $(|\lambda_c|)^{1/2}$ in terms of one of the negative eigenvalues λ_c in Eq. (2.9).

In Gordon's method [1] the solution vectors are real. In view of our preference for the use of complex solution vectors in Section 3, we have given the above-mentioned formulae in an adapted notation. Furthermore, we note that in Gordon's code an approximation to $[\mathbf{X}^{-1} \bar{\mathbf{U}}(\bar{r}) \mathbf{X}]_{\text{diag}}$ in Eq. (2.10) is used. In Section 3 this approximation is not made. We use in Eq. (2.9) $\bar{\mathbf{U}}(\bar{r})$ instead of $\mathbf{U}(\bar{r})$.

3. The Application of Gordon's Method to Nuclear Scattering Problems

The Calculational Procedure

The coupled-channels formalism for inelastic scattering in nuclear physics has been discussed extensively in the literature [5–8]. This formalism leads to a set of

coupled differential equations for the radial wave functions u_{Il}^J of the following form

$$\left[\frac{\hbar^2}{2m}\left(\frac{d^2}{dr^2} - \frac{l(l+1)}{r^2}\right) + (E - \epsilon_I) - \frac{z_1 z_2 e^2}{r} + V^{\mathrm{opt}}\right] u_{Il}^J(r)$$

$$= \sum_{I'l'} V_{Il;I'l'}^J(r)\, u_{I'l'}^J(r), \qquad (3.1)$$

assuming a spinless projectile. Here J, l and I denote the total angular momentum, the orbital angular momentum and the spin of the target nucleus in the state with excitation energy ϵ_I, respectively. The coupling potential is denoted by $V_{Il;I'l'}^J$, the optical model potential by V^{opt}, whereas z_1 and z_2 are the charge numbers of the projectile and target nucleus, respectively. The total angular momentum J, its projection on the z-axis and the parity are good quantum numbers.

If n is the number of coupled equations (3.1) for a given J, the solution satisfying the usual boundary conditions [6] can be written as a linear combination of n independent regular solutions $u_{Il}^{J(\nu)}$

$$\sum_{\nu=1}^{n} a^{(\nu)} u_{Il}^{J(\nu)} \underset{r \to \infty}{\sim} (2l+1)^{1/2}\, e^{i\sigma_l}\left[\delta_{II_i}\delta_{ll_i}F_l + \left(\frac{k_i}{k}\right)^{3/2} C_{I_i l_i; Il}^J\{G_l{}^J + iF_l\}\right], \quad (3.2)$$

where G_l and F_l are the irregular and regular Coulomb wave functions and σ_l the partial-wave Coulomb phase shift. The subscript i refers to the initial channel. A similar set of equations holds for the derivatives of the respective functions and together with Eq. (3.2) they supply the matching and normalization conditions. The calculated matrix elements $C_{I_i l_i; Il}^J$ are used in the calculation of the elastic and inelastic scattering amplitudes.

To study the applicability of Gordon's method, it has been implemented in Tamura's code JUPITOR [9]. In the resulting code JUPIGOR, the integration range is divided into a part up to the radius where the nuclear interaction has died out, to be called the coupling radius r_{cp} and a large part up to the matching radius r_m where only the Coulomb interaction operates.

From preliminary calculations for a single channel case with a complex nuclear potential, it appeared that Gordon's method is not efficient up to the radius r_{cp}. The step size has to be taken too small, because the nuclear potential varies too fast over this range to be efficiently linearized. This part is therefore dealt with by a conventional method with a step size of 0.1 to 0.2λ [10], where λ is the de Broglie wavelength. In JUPITOR the step-by-step Störmer method is used for this purpose. Subsequently, we divide the remaining integration range into steps such that the potential is linearized up to a few per cent over one step. In the next subsection the procedure followed in choosing the step sizes will be dealt with.

Choosing Step Sizes

Taking a perturbation potential matrix $[U(r) - U_0(r)]$ which is quadratic in r on the diagonal and linear in r for the off-diagonal elements, the perturbation integrals (2.13) can be evaluated analytically. Notwithstanding this, the calculation of these first-order corrections to the reference solution needs extended matrix multiplications. As a consequence, the calculation of the solution (2.12) requires about two or three times as much computational effort as does the calculation of the reference solution (2.11) alone. In view of this it is useful to avoid the calculation of the perturbation integrals in cases where this is possible.

In Gordon's method the step size is taken such that the perturbation integrals are small enough to keep the accuracy of the reference solution at some required level. For some potential and total angular momentum this requires the calculation of these integrals once; for subsequent calculations at different energies, with the same potential and total angular momentum, the reference solution can then be calculated efficiently using the same intervals and applying the energy independent matrices following Eq. (2.14) of Section 2.

In our application of Gordon's method we prefer to prescribe the step size without the calculation of the perturbation integrals. Over the integration range $r_{cp} < r < r_m$ the potential of each uncoupled equation of set (3.1) has a radial dependence of the form $2\eta k r^{-1} + l(l + 1) r^{-2}$, where η is the Coulomb parameter. Preparatory calculations have shown that in the case of an uncoupled equation a sufficient accuracy of the final results can be obtained by choosing the step sizes
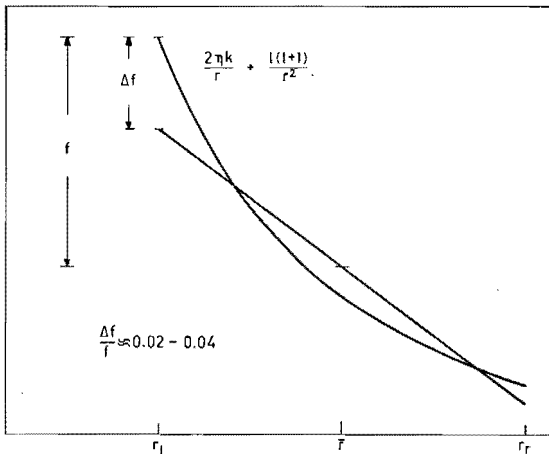
FIG. 1. The step sizes over the integration range from r_{cp} to r_m are chosen by linearizing the potential up to a few percent over one step.

such that over one step the maximal deviation of the actual potential with respect to the linearized potential equals a few percent of the difference between the actual potential and the average potential (see Fig. 1). In the case of coupled equations it is evident that coinciding intervals have to be chosen in all channels of the same coupled J set. The step size is determined according to the abovementioned method, applied to a similar potential form $2\eta k r^{-1} + l(l + 1) r^{-2}$, in which now an average value of l over the coupled channels has been taken into account. For the test cases to be dealt with in Section 4 the first steps have a size of about 1 fm, the last few about 8 fm, depending on the value of r_m.

The radial region around the classical turning points of the individual equations deserves special attention, because the coupling between the equations is most effective here. This complication occurs for such high J values that some or all of the turning points are beyond r_{cp}. In the region of turning points more rigorous linearizing conditions are imposed.

In this way we can work with the reference solution avoiding the calculation of the perturbation integrals (2.13). For subsequent calculations with the same total angular momentum and Coulomb interaction but with a different energy and/or nuclear interaction the reference solution can be evaluated using the same step sizes and applying again the energy independent matrices following Eq. (2.14).

4. Results and Discussion

In this section the results of two test cases will be presented. In both cases the multiple excitation of a "vibrational" nucleus with one-phonon and two-phonon triplet states is considered. The excitation is induced by inelastic scattering of alpha and ^{16}O particles, respectively, near the Coulomb barrier. The code JUPIGOR allows independent variation of each of the optical potential deformation parameters β, involved in the coupling of the levels considered. In addition, the corresponding reduced electric multipole matrix elements can be introduced independently. In view of the purpose of this paper, however, we preferred to consider the following simple choice. The coupling potential has been expanded up to and including the first order in the deformation. A purely harmonic vibrational model is assumed. As a consequence, the deformation parameters β_{02}, β_{20}, β_{22} and β_{24}, defined by Tamura [11], have been taken equal, whereas $\beta'_{00} = \beta'_{02} = \beta'_{04} = 0$. The common β value is given below. Some of the calculated C-matrix elements for alpha and ^{16}O scattering have been collected in Tables I and II, respectively. In Fig. 2 the reduction of computation time for Gordon's method compared with Störmer's method, is given as a function of the matching radius r_m for a total angular momentum value $J = 5$.

Multiple Excitation of ^{122}Te *by* 11.5, 16.5, *and* 21.5 MeV ^{4}He

In this case, the Coulomb parameter and wave number are about 8.0 and 1.7, respectively. The optical model parameters are: $V = 250$ MeV, $W = 37.6$ MeV, $r_v = r_w = r_c = 1.333$ fm, $a_v = a_w = 0.582$ fm. The abovementioned deformation parameters are taken equal to 0.15.

Calculations were carried out for several total angular momentum J values. However, we have concentrated our attention in this article on $J = 5$ and 30, because the results for these two J values turn out to be representative for the general properties of low and high J values. Furthermore, calculations were performed for several r_m values distributed between 25 and 200 fm. It appears that in most practical calculations for this reaction with energies near the Coulomb barrier, the contribution of Coulomb excitation to the C-matrix elements can only be neglected if r_m is chosen equal to about 100 fm or larger. In the following we shall confine ourselves to such r_m values. In addition, to study the extent of linear independence of the solution vectors, calculations were also carried out in the $J = 30$ case for different r_{cp} values.

In Table I the C-matrix elements are presented for $J = 5$ and 30 at laboratory energies of 16.5 and 21.5 MeV. The rows containing the C-matrix elements calculated with our code JUPIGOR are denoted by G, those with Tamura's code JUPITOR by T. The results have been obtained with r_{cp} and r_m values of 15 and 100 fm, respectively.

First, we discuss the $J = 5$ ($I_i = 0$; $l_i = 5$) results for $E_{\text{lab}} = 16.5$ MeV ($G - 1$, $T - 1$, $T - 2$, $T - 3$) and $E_{\text{lab}} = 21.5$ MeV ($G - 2$, $T - 4$). Row $G - 1$ contains the C-matrix elements, obtained with a step size of 0.10 fm for Störmer's method up to r_{cp} and 33 steps according to Gordon's method for the remaining integration up to r_m. The rows $T - 1$, $T - 2$, and $T - 3$ contain the elements calculated with step sizes of 0.05, 0.10 and 0.20 fm, respectively, for Störmer's method over the whole integration range. Comparing $G - 1$ with $T - 1$, we see that in most C-matrix elements a 3-figure correspondence is obtained. Variations of of r_m beyond 100 fm lead to changes in the C-matrix elements $G - 1$ of a fraction of 1%. To get an indication of the computational efficiencies we have compared $G - 1$ with $T - 2$, the latter results being almost identical to $T - 1$. For $r_m = 100$ fm this gives a reduction of the computation time by a factor of about 9 (Fig. 2). Row $G - 2$ contains the C-matrix elements obtained at at $E_{\text{lab}} = 21.5$ MeV using the same intervals from r_{cp} to r_m as in $G - 1$ and applying the energy independent matrices as expressed in Section 2 (following Eq. (2.14)), which already have been calculated for $G - 1$. In this way the computation time is reduced by a total factor of about 20 (Fig. 2). As evident from Table I, the correspondence of $G - 2$ with $T - 4$ is satisfactory. A similar correspondence is obtained at an energy of 11.5 MeV. These results have not been presented.

Next, we discuss the $J = 30$ ($I_i = 0$; $l_i = 30$) results for $E_{lab} = 16.5$ MeV ($G - 3$, $T - 5$, $T - 6$, $T - 7$) and $E_{lab} = 21.5$ MeV ($G - 4$, $T - 8$). Row $G - 3$ contains the C-matrix elements obtained with a step size of 0.20 fm for Störmer's part ($r_{cp} = 15$ fm, $r_m = 100$ fm). This step size can be taken relatively large because of the monotonous behaviour of the solution vector up to r_{cp}. Gordon's method needs in this case 44 steps. The rows $T - 5$, $T - 6$ and $T - 7$ contain the elements calculated with step sizes of 0.05, 0.10 and 0.20 fm, respectively. Comparing these results the correspondence can be considered as satisfactory except for some elements, particularly the elastic channel and the $I_f = 4$, $l_f = 32,34$ elements. Calculations for r_m beyond 100 fm give rise to variations of the $G - 3$ elements within one per cent, apart from some elements which show variations of a few percent. The C-matrix elements of the elastic channel and the small elements for $I_f = 4$, $l_f = 32,34$, which are not expected to contribute significantly to cross sections, show larger relative variations, but remain of the same order of magnitude.

The abovementioned discrepancy in the C-matrix element of the elastic channel can be understood by considering that the elastic component of the solution vector in Eq. (3.2), divided by $(2l + 1)^{1/2} \exp(i\sigma_i)$, corresponds at this high J value with the regular Coulomb wave function F_i in about four figures. Consequently, the relatively small value of the C-matrix element is obtained by subtracting two quantities, which agree up to about four figures, and is rather sensitive to small variations in the elastic component of the solution vector. However, we believe that in most practical calculations this discrepancy has no consequences.

The discrepancy for $I_f = 4$, $l_f = 32,34$ cannot be explained on this basis: the accuracy of the C-matrix elements of the inelastic channels is more directly related to the accuracy of the inelastic components of the solution vector. We believe that the $T - 5$ and $T - 6$ values for these C-matrix elements are too large due to a numerical instability in the Störmer procedure, originating from a tendency of the solution vectors to become linearly dependent for high angular momenta. To confirm this we have carried out addition calculations for different r_{cp} values ($r_m = 100$ fm).

For r_{cp} values up to about 15 fm, it turns out that in all C-matrix elements a 3 à four-figure correspondence is obtained, whereas for $r_{cp} = 20$ fm some C-matrix elements begin to show agreement to within two-figures. The correspondence for the r_{cp} values larger than 20 fm remains acceptable, except for the $I_f = 4$, $l_f = 32,34$ elements. We note that for $J = 30$ the radial region of the classical turning points of the individual equations lies between $r \approx 21$ and $r \approx 26$ fm. For $r_{cp} = 25$ fm the $I_f = 4$, $l_f = 32,34$ elements still have the same order of magnitude, but they deviate more and more for r_{cp} values of 30 and 35 fm, lying in the classically allowed region, especially when a step size of 0.05 fm is taken over the integration range up to r_{cp}. In this case they become of the same order of magnitude as in the case $T - 5$ of Table I.

Looking at the *solution vectors*, it turns out that for r_{cp} values of about 5 fm and larger the Störmer procedure generates some solution vectors, which show a tendency to become linearly dependent. We conclude, however, that by using Gordon's stabilization transformation in the classically forbidden region for sufficiently small r_{cp} values, this tendency can be suppressed, which then leads to reliable values of the C-matrix elements.

The Störmer procedure used in Tamura's code does not contain a facility to maintain linear independence. However, we believe that in principle it is possible to apply Gordon's stabilization procedure to the Störmer method. In this case the potential matrix needs only to be diagonalized to determine the arrangement of the components in the solution vectors in order of decreasing relative kinetic energy. It is not necessary to transform the solution vectors into a local basis. Presumably, stabilization is only needed in a few points of the classically forbidden region. We have not realized these ideas in the Störmer procedure to stabilize the solution vectors below r_{cp}. The reason is that in general and also in our test cases, the linear dependence enters only for high J values. However, note that in our code JUPIGOR r_{cp} has been chosen such that the nuclear potential can be neglected outside r_{cp}. In the first instance one may be inclined to conclude from this that it is less meaningful to take r_{cp} smaller than 15 fm, the value of r_{cp} which has been taken for the results in the table. For high J values, however, the nuclear potential no longer contributes significantly to the C-matrix elements. (This is already the case for $J \approx 15$.) In these cases a small r_{cp} value can be recommended to guarantee the linear independence of the solution vectors, as well as for reasons of computational efficiency. For practical cross section calculations it is therefore advantageous to take r_{cp} for the high J values considerably below 15 fm, e.g., 1 fm, or even smaller. In JUPIGOR this is actually done.

The C-matrix elements in row $G - 4$ are calculated by using the energy independent matrices, which already have been determined in $G - 3$. The correspondence with $T - 8$ is satisfactory, except for the abovementioned discrepancies. About a similar correspondence is obtained at an energy of 11.5 MeV.

Multiple Excitation of ^{58}Ni by 39, 44 and 49 MeV ^{16}O

This case has a Coulomb parameter and wave number of about 21 and 4.5, respectively. The optical model parameters are: $V = 22.69$ MeV, $r_v = 1.30$ fm, $a_v = 0.533$ fm, $W = 2.35$ MeV, $r_w = 1.37$ fm, $a_w = 0.375$ fm, and $r_c = 1.25$ fm [13]. The deformation parameters are taken equal to 0.18. The values of r_{cp} and r_m have again been taken as 15 and 100 fm, respectively. In Table II the C-matrix elements are presented as before for $J = 5$ and 30 at laboratory energies of 44 and 49 MeV.

We discuss now the $J = 5$ ($I_i = 0$, $l_i = 5$) results for $E_{lab} = 44$ MeV ($G - 1$, $T - 1$, $T - 2$, $T - 3$) and $E_{lab} = 49$ MeV ($G - 2$, $T - 4$). Comparing $G - 1$

TABLE I

A Sample $C^J_{I_i l_i; I_f l_f}$ for $^{122}Te(\alpha,\alpha')$ with target states $0^+ - 2^+(0.564) - 0^+(1.357) - 2^+(1.257) - 4^+(1.180)$

$I_i = 0$ $l_i = 5$	I_f l_f															
	0	5	2	3	2	5	2	7	0	5	2	3	2	5	2	7
E_{lab}=16.5 MeV	(-1)	(0)	(-2)	(-1)	(-1)	(-1)	(-1)	(-2)	(-3)	(-3)	(-2)	(-2)	(-3)	(-3)	(-3)	(-4)
G-1[a] .100[b] 33[c]	[l].631 [r].144		.714	.563	.275	-.234	-.213	-.996	-.876	-.837	.212	.199	-.718	-.705	.266	.197
T-1[d] .050[e]	.629	.144	.714	.563	.275	-.234	-.213	-.997	-.876	-.837	.212	.199	-.718	-.705	.267	.192
T-2 .100	.628	.144	.715	.563	.275	-.234	-.213	-.997	-.877	-.838	.212	.199	-.719	-.706	.267	.196
T-3 .200	.581	.143	.620	.560	.272	-.234	-.214	-.997	-.759	-.780	.212	.123	-.626	-.652	.282	-.072
E_{lab}=21.5 MeV	(-1)	(0)	(-1)	(-1)	(-2)	(-1)	(-1)	(-2)	(-2)	(-1)	(-2)	(-2)	(-2)	(-2)	(-2)	(-2)
G-2 .100 33	-.412	.446	.291	.170	.875	-.270	-.348	-.982	.383	-.112	.653	.622	.233	-.652	-.834	-.202
T-4 .100	-.412	.446	.291	.170	.874	-.270	-.348	-.981	.382	-.112	.653	.622	.233	-.652	-.834	-.201

	I_f l_f									
	4	1	4	3	4	5	4	7	4	9
E_{lab}=16.5 MeV	(-2)	(-2)	(-2)	(-2)	(-3)	(-3)	(-3)	(-3)	(-3)	(-3)
G-1 .100 33	-.464	-.119	.176	.120	-.449	-.552	.383	.132	-.275	-.405
T-1 .050	-.464	-.119	.176	.120	-.450	-.551	.384	.132	-.277	-.406
T-2 .100	-.464	-.119	.176	.120	-.450	-.553	.384	.133	-.277	-.406
T-3 .200	-.466	-.092	.173	.122	-.377	-.469	.413	.101	-.274	-.408
E_{lab}=21.5 MeV	(-1)	(-3)	(-2)	(-2)	(-2)	(-2)	(-2)	(-2)	(-4)	(-2)
G-2 .100 33	-.118	-.447	.522	.586	.353	-.620	-.695	-.252	.124	.840
T-4 .100	-.118	-.442	.522	.586	.353	-.620	-.695	-.252	.159	.840

$I_i = 0$ $l_i = 30$	I_f l_f														
	0	30	2	28	2	30	2	32	0	30	2	28	2	30	2	32
E_{lab}=16.5 MeV	(-3)	(-3)	(-1)	(-3)	(-2)	(-2)	(-3)	(-2)	(-4)	(-4)	(-4)	(-4)	(-5)	(-6)	(-4)	(-5)
G-3[a] .200[b] 44[c]	.342	.158	.108	.424	.559	-.309	.813	-.131	.346	.108	.569	.823	-.299	-.162	.107	-.200
T-5[d] .050[e]	.052	.155	.107	.410	.559	-.309	.821	-.129	.346	.108	.559	.824	-.270	-.477	.153	.247
T-6 .100	-.032	.156	.107	.408	.559	-.309	.809	-.130	.342	.108	.559	.824	-.298	-.489	.109	-.565
T-7 .200	-4.65	.177	.107	.317	.556	-.313	.794	-.130	.342	.104	.565	.818	-.207	-.409	.113	-.242
E_{lab}=21.5 MeV	(-3)	(-3)	(-1)	(-2)	(-2)	(-2)	(-2)	(-2)	(-4)	(-4)	(-4)	(-3)	(-5)	(-5)	(-4)	(-5)
G-4 .200 44	.034	.222	.118	.165	.834	-.291	.168	-.168	.539	.485	.438	.156	-1.01	-.625	.240	.730
T-8 .100	-.217	.224	.118	.166	.833	-.292	.168	-.168	.537	.485	.454	.157	-.954	-.616	.245	.781

	I_f l_f									
	4	26	4	28	4	30	4	32	4	34
E_{lab}=16.5 MeV	(-4)	(-3)	(-4)	(-4)	(-4)	(-4)	(-4)	(-5)	(-5)	(-5)
G-3 .200 44	-.125	.178	.412	.804	.309	.210	.105	-.012	.194	-.137
T-5 .050	-.149	.177	.415	.801	.369	.208	-.002	1.21	71.0	-76.3
T-6 .100	-.149	.177	.415	.801	.369	.209	.119	-.258	-3.65	-4.03
T-7 .200	-.134	.177	.420	.796	.369	.206	.104	-.046	.511	-5.40
E_{lab}=21.5 MeV	(-4)	(-3)	(-4)	(-3)	(-4)	(-4)	(-4)	(-4)	(-5)	(-5)
G-4 .200 44	-.891	.208	.245	.141	.530	.644	.214	.102	.596	-.629
T-8 .100	-.675	.218	.255	.141	.530	.644	.214	.111	6.97	-2.42

[a] Rows containing JUPIGOR results. [b] Step size for Störmer's method up to r_{cp}. [c] Number of steps from r_{cp} to r_m.
[d] Rows containing JUPITOR results. [e] Step size for Störmer's method over the whole integration range.
[l] Left entries mean: $Re C^J = .631_{10}^{-1}$, [r] right entries mean: $Im C^J = .144_{10}^{0}$, where additional exponents have been added between brackets above the columns.

TABLE II

A Sample $C^{J}_{I_i l_i, I_f l_f}$ for $^{58}Ni(^{16}O, ^{16}O')$ with target states $0^+ - 2^+(1.454) - 0^+(2.943) - 2^+(2.775) - 4^+(2.459)$

$I_i = 0$ $l_i = 5$									I_f l_f							
	0	5	2	3	2	5	2	7	0	5	2	3	2	5	2	7
E_{lab}=44.0 MeV	(0)	(0)	(-1)	(-1)	(-1)	(-1)	(-1)	(-1)	(-3)	(-2)	(-2)	(-2)	(-2)	(-2)	(-2)	(-2)
G-1[a] .050[b] 32[c]	l.118	r.380	.493	.246	-.264	-.272	.102	.407	-.896	.906	.343	-.587	-.218	.545	.285	-.516
T-1[d] .025[e]	.118	.380	.494	.246	-.264	-.272	.102	.406	-.873	.906	.343	-.588	-.218	.545	.284	-.517
T-2 .050	.118	.380	.495	.244	-.265	-.272	.103	.407	-.848	.906	.341	-.588	-.216	.545	.282	-.517
T-3 .100	.095	.362	.520	.160	-.301	-.222	.164	.380	-.485	.882	.243	-.615	-.129	.556	.197	-.538
E_{lab}=49.0 MeV	(-1)	(0)	(-2)	(-1)	(-2)	(-1)	(-2)	(-1)	(-2)	(-2)	(-2)	(-2)	(-2)	(-4)	(-2)	(-2)
G-2 .050 32	-.373	.505	.894	.204	-.260	-.189	-.340	.217	-.821	.188	.766	-.319	-.482	-.760	.415	.228
T-4 .050	-.376	.505	.909	.204	-.268	-.189	-.336	.217	-.819	.191	.764	-.321	-.461	-.572	.415	.226

		I_f l_f								
	4	1	4	3	4	5	4	7	4	9
E_{lab}=44.0 MeV	(-2)	(-2)	(-2)	(-2)	(-2)	(-2)	(-2)	(-2)	(-2)	(-2)
G-1 .050 32	-.768	.366	.560	-.226	-.537	.203	.504	-.212	-.539	.181
T-1 .025	-.769	.366	.560	-.226	-.537	.203	.504	-.212	-.539	.182
T-2 .050	-.767	.368	.559	-.227	-.536	.205	.503	-.213	-.538	.184
T-3 .100	-.686	.468	.506	-.301	-.487	.276	.453	-.280	-.491	.256
E_{lab}=49.0 MeV	(-1)	(-2)	(-2)	(-3)	(-2)	(-2)	(-2)	(-2)	(-2)	(-2)
G-2 .050	-.117	.234	.751	-.222	-.570	-.160	.320	.331	.103	-.438
T-4 .050	-.117	.238	.750	-.250	-.570	-.158	.321	.300	.101	-.438

$I_i = 0$ $l_i = 30$		I_f l_f														
		0	30	2	28	2	30	2	32	0	30	2	28	2	30	2	32
E_{lab}=44.0 MeV		(-2)	(-2)	(-1)	(-1)	(-2)	(-1)	(-2)	(-2)	(-3)	(-3)	(-2)	(-3)	(-5)	(-3)	(-3)	(-4)
G-3[a] .200[b] 36[c]		.605	.326	.479	-.200	-.200	-.214	-.678	-.187	-.256	-.616	.154	-.868	-.283	-.234	-.222	-.295
T-5[d] .025[e]		.600	.325	.479	-.199	-.200	-.213	-.667	-.184	-.256	-.614	.154	-.865	.086	-.233	-.221	-.276
T-6 .050		.459	.324	.479	-.200	-.205	-.213	-.667	-.182	-.257	-.612	.153	-.868	.028	-.233	-.221	-.271
T-7 .100		-7.66	.916	.438	-.266	-.513	-.205	-.677	-.079	-.330	-.556	.136	-1.05	-3.18	-.225	-.216	.038
E_{lab}=49.0 MeV		(-1)	(-2)	(-1)	(-1)	(-2)	(-1)	(-2)	(-2)	(-3)	(-2)	(-2)	(-4)	(-3)	(-3)	(-3)	(-3)
G-4 .200 36		.110	.496	.606	-.108	.472	-.267	-.705	-.467	.191	-.102	.267	-.720	.174	-.233	-.276	-.235
T-8 .050		.122	.496	.605	-.106	.472	-.266	-.701	-.464	.191	-.102	.266	-.620	.178	-.233	-.273	-.233

	I_f l_f									
	4	26	4	28	4	30	4	32	4	34
E_{lab}=44.0 MeV	(-2)	(-2)	(-2)	(-3)	(-3)	(-3)	(-3)	(-3)	(-4)	(-4)
G-3 .200 36	.200	.422	.191	-.323	.121	-.812	-.243	-.149	-.796	.587
T-5 .025	.201	.420	.190	-.322	.119	-.811	-.243	-.146	-.783	.595
T-6 .050	.202	.419	.189	-.327	.117	-.810	-.243	-.145	-.799	.586
T-7 .100	.254	.379	.179	-.579	.001	-.800	-.254	-.107	-.673	.672
E_{lab}=49.0 MeV	(-3)	(-2)	(-2)	(-3)	(-3)	(-2)	(-3)	(-3)	(-3)	(-4)
G-4 .200 36	.403	.628	.268	.720	.729	-.101	-.213	-.384	-.151	.211
T-8 .050	.391	.624	.267	.728	.728	-.101	-.213	-.382	-.150	.183

[a] Rows containing JUPIGOR results. [b] Step size for Störmer's method up to r_{cp}. [c] Number of steps from r_{cp} to r_m.
[d] Rows containing JUPITOR results. [e] Step size for Störmer's method over the whole integration range.
[l] Left entries mean: $\mathrm{Re} C^J = .118_{10}^{\;0}$, right entries mean: $\mathrm{Im} C^J = .380_{10}^{\;0}$, where additional exponents have been added between brackets above the columns.

with $T - 1$ we see that in most C-matrix elements a three-figure correspondence is obtained. However, the comparison with $T - 2$ gives only small discrepancies and may be used to determine the reduction of the computation time. For $r_m = 100$ fm this reduction is about a factor of 18 (Fig. 2). The C-matrix elements of row $G - 2$ at $E_{\text{lab}} = 49$ MeV have again been obtained by applying energy independent matrices. The reduction of the computation time is now a total factor of about 42 (Fig. 2). The agreement with $T - 4$ is satisfactory. A similar agreement is evident from the results at an energy of 39 MeV, which have been left out in Table II.
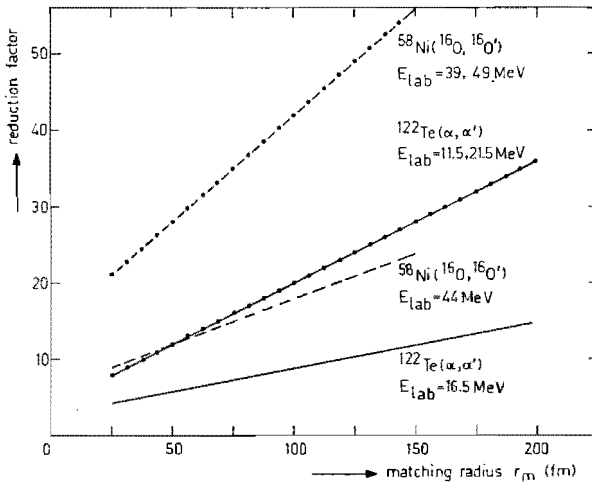
FIG. 2. Reduction factor of computation time for Gordon's method compared with Störmer's method, applied to the integration range from r_{cp} to r_m for a total angular momentum value $J = 5$. The solid and dashed curves represent the results of alpha and oxygen particles scattering, respectively. The dotted curves represent the results obtained by applying energy independent matrices already calculated for a different energy.

Finally, considering the $J = 30$ ($I_i = 0$, $l_i = 30$) results for $E_{\text{lab}} = 44$ MeV ($G - 3$, $T - 5$, $T - 6$, $T - 7$) and $E_{\text{lab}} = 49$ MeV ($G - 4$, $T - 8$) similar conclusions can be drawn as in the preceding $J = 30$ case. Note, however, that the type of discrepancy observed for some C-matrix elements is absent here.

5. Conclusion

In describing a nuclear reaction process including Coulomb excitation by means of a coupled-channels calculation, the analysis often involves the solution of a large set of coupled linear second-order differential equations. It turns out that a con-

siderable reduction of computation time can be obtained by applying Gordon's numerical method, especially if the calculation is to be carried out for various energies and/or optical model parameter sets. The larger the integration range and the relative wave number, pertinent to the reaction process, the larger is this reduction. Consequently, although the method is also of considerable advantage in some light particle scattering cases, it seems to be especially suitable to heavy ion scattering problems. Furthermore, a comparison of the results in this paper with those recently published by the present author [14], indicates that the reduction factor increases also with the dimension of the set of coupled equations to be solved.

REFERENCES

1. R. G. GORDON, *J. Chem. Phys.* **51** (1969), 14.
2. R. G. GORDON, *in* "Methods in Computational Physics: 10, Atomic and Molecular Scattering" (B. Alder, S. Fernbach, and M. Rotenberg, eds.), p. 81, Academic Press, New York, 1971.
3. A. C. ALLISON, *J. Comput. Phys.* **6** (1970), 378.
4. J. H. WILKINSON, "The Algebraic Eigenvalue Problem," pp. 152, 233, Oxford University Press, London, 1965.
5. B. BUCK, *Phys. Rev.* **130** (1963), 712.
6. T. TAMURA, *Revs. Mod. Phys.* **37** (1965), 679.
7. U. SMILANSKY, *Nucl. Phys. A* **112** (1968), 185.
8. K. ALDER AND H. K. A. PAULI, *Nucl. Phys. A* **128** (1969), 193.
9. T. TAMURA, Oak Ridge National Laboratory Report No. ORNL-4152 (1967); H. REBEL AND G. W. SCHWEIMER, Kernforschungszentrum Karlsruhe Report No. KFK-1333 (1971).
10. P. E. HODGSON, "The Optical Model of Elastic Scattering," p. 43, Oxford University Press, London, 1963.
11. T. TAMURA, *Prog. Theor. Phys. Supplement No.* **37–38** (1966), 383.
12. M. SAMUEL AND U. SMILANSKI, Proc. Int. Conf. Reac. Complex Nuclei, Nashville, (R. L. Robinson, *et al.*, Eds.), Vol. I, p. 188, North-Holland Publ. Co., Amsterdam, 1974.
13. P. R. CHRISTENSEN, I. CHERNOV, E. E. GROSS, R. STOKSTAD, AND F. VIDEBAECK, *Nucl. Phys. A* **207** (1973), 433.
14. L. D. TOLSMA, Proc. Int. Conf. Nucl. Phys., Munich, (J. de Boer and H. J. Mang, Eds.), Vol. I, p. 385, North-Holland Publ. Co., Amsterdam, 1973.

CHAPTER 5

Solving coupled equations by iteration for heavy ion multiple Coulomb excitation

L. D. Tolsma

Department of Physics, Eindhoven University of Technology, Eindhoven, The Netherlands

The set of coupled linear second-order differential equations which has to be solved for quantum-mechanical calculations of inelastic scattering processes with multiple excitation can be rewritten as an equivalent set of coupled first-order integral equations. When Airy functions are used as piecewise analytic reference solutions, it makes it possible to evaluate analytically the integrals that arise in the set of integral equations. This set can be solved iteratively with a considerable reduction of computation time in cases of heavy ion scattering, when compared to quantum-mechanical coupled-channel calculations of the conventional type. The efficiency of two iteration schemes, an inward-outward and a perturbative one, has been investigated for some test cases dealing with multiple Coulomb excitation of ^{238}U by Kr and Pb. It turns out that, for heavy ion scattering, only the inward-outward iteration scheme has a practical importance. Finally, the excitation probabilities for ^{238}U, Coulomb excited by 385 MeV Kr up to $I = 24\hbar$, are shown for a reduced $E2$ transition matrix element of 3.5 eb and they are compared with the excitation probabilities calculated according to the semiclassical theory.

NUCLEAR REACTIONS Solving coupled equations by iteration; quantum mechanically calculated excitation probabilities for heavy ion multiple Coulomb excitation.

I. INTRODUCTION

For collisions between heavy ions, the asymptotic de Broglie wavelength associated with the relative motion is very short as compared to the long range of the strong Coulomb interaction. In general also many open channels are involved to a significant extent. In heavy ion multiple Coulomb excitation, the rotational bands of a deformed target nucleus can be excited up to $I \gtrsim 20\hbar$. The analysis of such excitations can be performed according to the semiclassical theory, in which the influence of the energy transfer and the change in orbital angular momentum during the collision are neglected in principle.[1] However, for an accurate analysis of the excitations of the high-spin states, or a study of the deviations with respect to semiclassical theories in more general circumstances,[2] it is advisable to have the disposal of fully quantum-mechanical calculations of the cross sections. These coupled-channel calculations of conventional type are not feasible yet, due to the tremendous amount of computation time needed. An attempt has been made to find a solution to this problem by investigating the application of a method for solving systems of coupled linear second-order differential equations by iteration.

The efficiency of this method, as in Gordon's method,[3] depends upon the possibility to divide the integration range into intervals which are sufficiently small to approximate the potential by some more simply varying reference potential but which, on the other hand, contains a sufficient-

ly large number of de Broglie wavelengths. For heavy ion collisions, both conditions are fulfilled. A further element of the method is the decomposition of the partial wave radial solution into regular and outgoing components. This means that the solution in, e.g., the classically allowed region is written as a linear combination of two rapidly oscillating base functions with more or less slowly varying amplitudes. The chosen reference potential allows these base functions to be expressed in terms of piecewise analytic reference solutions. Taking the reference potential over the interval as a linear one, these reference solutions are given by Airy functions.[3]

The Schrödinger equation for the partial wave radial solution is rewritten in an integral form which leads to a system of coupled first-order integral equations for the amplitudes. These amplitudes are obtained by means of an iteration procedure. Two iteration schemes, an inward-outward[4,5] and a perturbative one,[6] have been investigated. When compared to previous applications of these iteration schemes, the advantage of the new method is that the integrals are evaluated analytically.

Although the results are presented for some Coulomb excitation inelastic scattering problems, it is possible in principle to include the influence of a nuclear interaction. Inelastic heavy ion scattering cases involving an optical potential are now being investigated.

In the next section, a concise formulation is given for the quantum-mechanical theory of in-

elastic scattering as applied to multiple Coulomb excitation. In Sec. III, the calculation procedure is discussed and the two iteration schemes are described. In Sec. IV the results of the study that considers the above-mentioned amplitudes is presented, plus the scattering matrix elements for the heavy ion multiple Coulomb excitation of ^{238}U by 385 MeV Kr and 1000 MeV Pb. Both iteration schemes are illustrated by figures and a table which show the rate of convergence and the accuracy achieved. In Sec. V, the excitation probabilities for ^{238}U, Coulomb excited by 385 MeV Kr up to $I = 24\hbar$, is shown for a reduced $E2$ transition matrix element of 3.5 eb and is compared with results from the semiclassical theory with energy-symmetrized classical orbits.[1] In the last section some conclusions are drawn.

II. CONCISE QUANTUM-MECHANICAL FORMULATION OF INELASTIC SCATTERING

In general, the quantum-mechanical description of inelastic scattering leads to a set of coupled second-order differential equations of the partial wave radial functions ψ_{lI}^{J} of the following form:

$$\left[\frac{d^2}{dr^2} + k_I^2 - \frac{2\eta_I k_I}{r} - \frac{l(l+1)}{r^2}\right]\psi_{lI}^{J}(r)$$
$$= \sum_{l'I'} V_{lI;\,l'I'}^{J}(r)\,\psi_{l'I'}^{J}(r), \quad (2.1)$$

for a spinless projectile. Here J, l, and I denote the total angular momentum, the orbital angular momentum, and the spin of the target nucleus with excitation energy ϵ_I, respectively. The total angular momentum J, its projection on the z axis and the parity are good quantum numbers. The wave number k_I and Sommerfeld parameter η_I are given by

$$k_I^2 = \frac{2\mu}{\hbar^2}(E - \epsilon_I),$$
$$\eta_I = \frac{2\mu}{\hbar^2}\frac{Z_1 Z_2 e^2}{2k_I}, \qquad (2.2)$$

where μ is the reduced mass, while Z_1 and Z_2 represent the charge numbers of the projectile and target nucleus, respectively. The coupling potential for the special case of multiple Coulomb excitation is given by[7]

$$V_{lI;\,l'I'}^{J}(r) = \frac{2\mu}{\hbar^2}Z_1 e\sqrt{4\pi}\sum_{\lambda}\left(\frac{(2l+1)(2l'+1)}{2\lambda+1}\right)^{1/2}(-1)^{J+I'+\lambda}\langle I'\,\|M(E\lambda)\|\,I\rangle\begin{pmatrix}l & l' & \lambda \\ 0 & 0 & 0\end{pmatrix}\begin{Bmatrix}J & l' & I' \\ \lambda & I & l\end{Bmatrix}\frac{1}{r^{\lambda+1}},$$

$$(2.3)$$

where $\langle I'\,\|M(E\lambda)\|\,I\rangle$ denotes the reduced matrix element of the electric 2^{λ}-pole moment of the target.

To obtain the solutions for $\psi_{lI}^{J}(r)$, two boundary conditions have to be fulfilled. At the origin, they must vanish and for large distances they must be related to an ingoing partial wave in the entrance channel plus outgoing partial waves in all relevant exit channels. The precise asymptotic form defines a scattering matrix. We follow Alder and Winther's convention[7] for defining an R matrix by the following asymptotic condition:

$$\psi_{lI}^{J(l_0 I_0)} \underset{r\to\infty}{\sim} H_I^-(\eta_I; k_I, r)\,\delta_{II_0}\delta_{ll_0}$$
$$- \left[\frac{k_{I_0}}{k_I}\right]^{1/2}R_{lI;\,l_0 I_0}^{J}H_I^+(\eta_I; k_I, r). \quad (2.4)$$

The ingoing and outgoing Coulomb waves H_I^- and H_I^+, respectively, are given by $H_I^{\pm} = (G_I \pm iF_I)$, in terms of the well-known regular and irregular Coulomb wave functions F_I and G_I. The indices I_0, l_0 correspond to an ingoing wave in the entrance channel for $I = I_0$ and $l = l_0$.

The dimension N of the set (2.1) is determined largely by the maximum value $I_{\max}$ of the target spin. Considering the excitation of a ground state rotational band with spin sequence $0^+, 2^+, 4^+, \ldots,$ $I_{\max}$, N is given by

$$N = \sum (I_n + 1). \qquad (2.5)$$

This means that for $I_{\max} = 20$, N becomes 121 and for even higher values of $I_{\max}$, N assumes huge values. In conventional coupled-channel calculations, the set (2.1) has to be solved N times for each J value in order to satisfy the boundary conditions. Especially for large systems this is time consuming. In addition, this procedure generates R-matrix elements which form a complete $N \times N$ matrix. However, in the nuclear physics context of a case with a zero-spin ground state, only one column of this matrix is needed, namely those elements which connect the ground state entrance channel to all the experimentally relevant exit channels. This is the motivation to study iteration methods for which the solutions $\psi_{lI}^{J}(r)$ are obtained directly without the need for solving the set (2.1) N times.

The scattering amplitudes are expressed in terms of the R-matrix elements[7]

$$f(\theta, \phi)_{I_0 M_0 \to I M} = \frac{\sqrt{4\pi}}{(k_{I_0} k_I)^{1/2}} \sum_{l_0 l J} (2l_0 + 1)^{1/2} i^{l_0 - l} \langle l_0\, 0 I_0 M_0 | J M_0 \rangle \langle l m\, I M | J M_0 \rangle$$

$$\times \frac{1}{2i} \{ \exp[i(\sigma_{l_0} + \sigma_l)] R^J_{II;\, I_0 l_0} - \delta_{II_0} \delta_{l l_0} \} Y_{lm}(\theta, \phi), \tag{2.6}$$

in which σ_l is the Coulomb phase shift

$$\sigma_l(\eta) = \arg \Gamma(l + 1 + i\eta). \tag{2.7}$$

From the scattering amplitudes it is easy to calculate the cross section for state I

$$\frac{d\sigma_I(\theta)}{d\Omega} = \frac{1}{2I_0 + 1} \frac{k_I}{k_{I_0}} \sum_{M_0 M} |f_{I_0 M_0 \to I M}(\theta, \phi = 0)|^2 \tag{2.8}$$

and other observable quantities. The excitation probability, for instance, is given by[2]

$$P_I(\theta) = \frac{k_I}{k_{I_0}} \frac{d\sigma_I}{d\sigma_R}, \tag{2.9}$$

where σ_R is the Rutherford cross section.

III. THE CALCULATION PROCEDURE

The Schrödinger equation (2.1) is rewritten in the more convenient form

$$\left[\frac{d^2}{dr^2} + k_i^2 - U_{ii}(r) \right] \psi_i(r) = \sum_{j \neq i}^{N} U_{ij}(r) \psi_j(r), \quad i = 1, 2, \ldots, N \tag{3.1}$$

and the boundary condition (2.4) as

$$\psi_i^k(r) \underset{r \to \infty}{\sim} \delta_{ik} H_i^- - \left[\frac{k_k}{k_i} \right]^{1/2} R_{ik} H_i^+. \tag{3.2}$$

The superscript and subscript k denotes the entrance channel.

When considering some interval of the integration range with its midpoint at radius $\bar{r}$ and expanding the potential function in a Taylor series, the equation is the following:

$$\left[\frac{d^2}{dr^2} + k_i^2 - \sum_{m=0}^{2} \frac{(r - \bar{r})^m}{m!} \frac{d^m U_{ii}(r)}{dr^m} \Big|_{r = \bar{r}} \right] \psi_i(r) = \sum_{j \neq i}^{N} \left[\sum_{m=0}^{2} \frac{(r - \bar{r})^m}{m!} \frac{d^m U_{ij}(r)}{dr^m} \Big|_{r = \bar{r}} \right] \psi_j(r). \tag{3.3}$$

Subsequently, introducing an average value for the components of the first derivatives at the left-hand side,

$$\left[\frac{d^2}{dr^2} + k_i^2 - U_{ii}(\bar{r}) - (r - \bar{r}) \frac{dU_{av}(r)}{dr} \Big|_{r = \bar{r}} \right] \psi_i(r)$$

$$= \left\{ (r - \bar{r}) \left[\frac{dU_{ii}(r)}{dr} \Big|_{r = \bar{r}} - \frac{dU_{av}(r)}{dr} \Big|_{r = \bar{r}} \right] + \frac{(r - \bar{r})^2}{2} \frac{d^2 U_{ii}(r)}{dr^2} \Big|_{r = \bar{r}} \right\} \psi_i(r)$$

$$+ \sum_{j \neq i}^{N} \left[\sum_{m=0}^{2} \frac{(r - \bar{r})^m}{m!} \frac{d^m U_{ij}(r)}{dr^m} \Big|_{r = \bar{r}} \right] \psi_j(r) \tag{3.4}$$

or, in more convenient notation,

$$\left[\frac{d^2}{dr^2} + k_i^2 - \bar{U}_{ii}(\bar{r}) - (r - \bar{r}) \frac{dU_{av}(r)}{dr} \Big|_{r = \bar{r}} \right] \psi_i(r) = \sum_{j}^{N} W_{ij}(r) \psi_j(r), \tag{3.5}$$

where $\bar{U}_{ii}$ is introduced as the average value of the diagonal potential for the interval. The potential form at the left-hand side is the reference potential. The reason for introducing an average value of the first derivatives will become clear later in this paper.

If the right-hand side of Eq. (3.5) is replaced by zero, each of the resulting decoupled equations has two linearly independent solutions:

1. The regular solution $G_i(r)$. It is defined to vanish at the origin and by the asymptotic form

$$G_i(r) \underset{r \to \infty}{\sim} \frac{i}{2\sqrt{k_i}} [H_i^-(\eta_i; k_i r) - R_i^0 H_i^+(\eta_i; k_i r)] .$$

(3.6a)

2. The irregular outgoing wave solution $G_i^+(r)$. This is defined by the asymptotic form

$$G_i^+(r) \underset{r \to \infty}{\sim} \frac{1}{\sqrt{k_i}} H_i^+(\eta_i; k_i r) .$$

(3.6b)

Owing to the special form of the left-hand side of Eq. (3.5), the solutions (3.6) can be expressed in terms of Airy functions which can be efficiently evaluated numerically, as shown by Gordon[3]

$$G_i(r) = \text{Ai}[\alpha(\beta_i + r)] a_i + \text{Bi}[\alpha(\beta_i + r)] b_i \quad (3.7a)$$

and

$$G_i^+(r) = \text{Ai}[\alpha(\beta_i + r)] a_i^+ + \text{Bi}[\alpha(\beta_i + r)] b_i^+ , \quad (3.7b)$$

with the constants

$$\alpha = \left(\frac{dU_{av}(r)}{dr} \Big|_{r=\bar{r}} \right)^{1/3} ,$$

$$\beta_i = \frac{\bar{U}_{ii}(\bar{r}) - k_i^2}{dU_{av}(r)/dr|_{r=\bar{r}}} - \bar{r} .$$

(3.8)

The constant coefficients a_i, b_i and a_i^+, b_i^+ are determined by conditions of continuity at the interval boundaries.

Now the Green's function which belongs to the coupled differential Eq. (3.5) can be introduced; it is regular at the origin and has an outgoing wave asymptotic form of

$$G_i(r, r') = -G_i(r_<) G_i^+(r_>) .$$

(3.9)

where $r_<$ and $r_>$ are the smaller and the larger values of r and r', respectively.

With an ingoing wave in the entrance channel k, the coupled differential Eq. (3.5) can be written as a set of N coupled integral equations

$$\psi_i^k(r) = G_i(r) \left[\frac{2}{i} \delta_{ik} - \int_r^\infty G_i^+(r') \sum_{j=1}^N W_{ij}(r') \psi_j^k(r') dr' \right] - G_i^+(r) \left[\int_0^r G_i(r') \sum_{j=1}^N W_{ij}(r') \psi_j^k(r') dr' \right] .$$

(3.10a)

Equivalently,

$$\psi_i^k(r) \equiv G_i(r) c_i(r) - G_i^+(r) c_i^+(r) ,$$

(3.10b)

with the boundary conditions

$$c_i(\infty) = \frac{2}{i} \delta_{ik}$$

(3.11a)

and

$$c_i^+(0) = 0 .$$

(3.11b)

In practice, however, instead of Eq. (3.11b) the approximate condition

$$c_i^+(r_0) = \int_0^{r_0} G_i(r') \sum_{j=1}^N W_{ij}(r') \psi_j^k(r') dr' = 0$$

(3.11c)

is used for a relatively small r_0, in order to prevent the set of integral equations becoming singular.

The choice of r_0 is very important. It must be neither too small nor too large. Of course, the R-matrix elements have to be independent of the actual value of r_0. In Sec. IV this subtle point is discussed in more detail. The asymptotic value of the outgoing coefficients $c_i^+(r)$ are related to the R-matrix elements

$$c_i^+(\infty) = R_{ik} - R_i^0 \delta_{ik} .$$

(3.12)

The set of coupled integral equations (3.10) can be solved by iteration. We have concentrated our investigation on the behavior of the amplitudes $c_i(r)$ and $c_i^+(r)$ instead of the wave function itself. This has been done for two iteration schemes.

A. Inward-outward iteration scheme

In this scheme, the following set of coupled integral equations for the amplitudes $c_i(r)$ and $c_i^+(r)$ are considered:

$$c_i(r) = \frac{2}{i} \delta_{ik} - \int_r^\infty G_i^+(r') \sum_{j=1}^N W_{ij}(r') G_j(r') c_j(r') dr' + \int_r^\infty G_i^+(r') \sum_{j=1}^N W_{ij}(r') G_j^+(r') c_j^+(r') dr' ,$$

(3.13a)

$$c_i^+(r) = \int_0^r G_i(r') \sum_{j=1}^N W_{ij}(r') G_j(r') c_j(r') dr' - \int_0^r G_i(r') \sum_{j=1}^N W_{ij}(r') G_j^+(r') c_j^+(r') dr'$$

(3.13b)

for $i = 1, 2, \ldots, N$. This scheme was proposed by Alder, Roesel, and Morf[4] and Ichimura et al.[5] They used a differential form of these equations.

When solving these equations iteratively, a start is made at infinity (in practice a few hundred or even thousand fm), where the $c_j(r)$ values are known, due to the boundary condition (3.11a), but the $c_j^+(r)$ are not. However, the product $G_i^+ W_{ij} G_j^+$ oscillates rapidly over the classically allowed region of the integration range which tends to nullify the contribution of the term with $c_j^+(r)$. This will also be apparent from some of the figures in the next section. It is, therefore, justifiable to take the value of these coefficients equal to zero as a first guess. Now, a first approximation to $c_i(r)$ can be generated by the inward integration of

Eq. (3.13a) from infinity to r_0. The obtained values of $c_i(r)$, together with the initial condition (3.11c), are used in an outward integration of Eq. (3.13b) from r_0 to infinity, where the term with $c_i(r)$ is now considered as a known inhomogeneous function. This outward integration gives a first approximation to $c_i^+(r)$ with a value at infinity, which corresponds to a first approximation of the R-matrix elements.

The iteration procedure continues as a second inward integration of Eq. (3.13a) using the calculated values of $c_i^+(r)$ and so forth, until convergence is obtained for $c_i^+(\infty)$. In the cases tested, only a few steps in the iteration process were needed.

B. Perturbative iteration scheme

The set of coupled integral equations for the amplitudes $c_i(r)$ and $c_i^+(r)$ can also be written as

$$c_i(r) = \frac{2}{i}\delta_{ik} + \int_0^r G_i^+(r') \sum_{j=1}^N W_{ij}(r')[G_j(r')c_j(r') - G_j^+(r')c_j^+(r')]dr'$$

$$- \int_0^\infty G_i^+(r') \sum_{j=1}^N W_{ij}(r')[G_j(r')c_j(r') - G_j^+(r')c_j^+(r')]dr', \tag{3.14a}$$

$$c_i^+(r) = \int_0^r G_i(r') \sum_{j=1}^N W_{ij}(r')[G_j(r')c_j(r') - G_j^+(r')c_j^+(r')]dr'. \tag{3.14b}$$

In this scheme, which was proposed by Raynal,[6] the coupling potential W is considered as a perturbation.

To illustrate the iteration procedure the results for the nth step of the iteration in case $k = 1$ are written as

$$c_i^{(n)}(r) = \frac{2}{i}\delta_{i1} + \int_0^r G_i^+(r')X_i^{(n)}(r')dr' - \int_0^\infty G_i^+(r')X_i^{(n)}(r')dr' \tag{3.15a}$$

$$c_i^{+(n)}(r) = \int_0^r G_i(r')X_i^{(n)}(r')dr', \tag{3.15b}$$

where

$$X_i^{(n)} = W_{i1}[G_1 c_1^{(n-1)} - G_1^+ c_1^{+(n-1)}] + \sum_{j=2}^{i-1} W_{ij}[G_j c_j^{(n)} - G_j^+ c_j^{+(n)}] + \sum_{j=i}^N W_{ij}[G_j c_j^{(n-1)} - G_j^+ c_j^{+(n-1)}] \tag{3.16a}$$

for $i = 2, 3, \ldots, N$ and

$$X_i^{(n)} = W_{11}[G_1 c_1^{(n-1)} - G_1^+ c_1^{+(n-1)}] + \sum_{j=2}^N W_{1j}[G_j c_j^{(n)} - G_j^+ c_j^{+(n)}] \tag{3.16b}$$

for $i = 1$.

The calculation of Eq. (3.15) starts with $i = 2$, using (3.16a) under the initial conditions

$$c_j^{(0)}(r_0) = \frac{2}{i}\delta_{j1}, \quad c_j^{+(0)}(r_0) = 0. \tag{3.17}$$

This component must be integrated to infinity, due to the third term in (3.15a), before the calculation can be continued for $i = 3$. The iteration step ends with the integration of the first component using (3.16b).

We have also investigated a perturbative scheme with the initial conditions

$$c_j^{(0)}(\infty) = \frac{2}{i}\delta_{j1}, \quad c_j^{+(0)}(\infty) = 0, \tag{3.18}$$

and adapted integral expressions for $c_i^{(n)}(r)$ and $c_i^{+(n)}(r)$. However, in the cases tested, the results varied little from those obtained with the initial conditions (3.17).

To solve Eqs. (3.13) and (3.14) we use the relatively slow variation of the amplitudes $c_i(r)$ and

$c_i^*(r)$ with respect to the rapid oscillations of the functions $G_i(r)$ and $G_i^*(r)$ in the classically allowed region. This behavior is understood by noting that $c_i(r)$ and $c_i^*(r)$ nearly lose their r dependence on the midpoint of an interval. This dependence is weak as long as the difference between the true potential and the reference potential is small. Thus, a choice of step size has to be made so that small variations of $c_i(r)$ and $c_i^*(r)$ over an interval can be neglected.

Assuming that in the first iteration step we have already integrated Eq. (3.13a), for example, from the right up to r_r and using the values of $c_i(r_r)$, this equation yields a first-order contribution to $c_i(r_1)$ at the "left-hand" boundary r_1, provided integrals of the form

$$\int_{r_1}^{r_r} G_i(r)(r-\bar r)^m G_j(r) dr \qquad (3.19)$$

are determined. Expressing $G_i(r)$ [and also $G_i^*(r)$] in Airy functions and introducing an average value for the first derivatives [see (3.4)] when the constant α becomes independent of the channels, integrals are obtained of the form

$$\int_{r_1}^{r_r} (r-\bar r)^m \text{Ai}[\alpha(\beta_i + r)] \, \text{Bi}[\alpha(\beta_j + r)] dr . \qquad (3.20)$$

This type of integral can be evaluated analytically. The analytical expressions for the integrals of $m = 0, 1, 2$; $\beta_i = \beta_j$ and for $m = 0, 1$; $\beta_i \neq \beta_j$ were given by Gordon,[3] while the expression for $m = 2$ and $\beta_i \neq \beta_j$ is given in the Appendix.

IV. RESULTS AND DISCUSSION

In this section we present results with respect to the amplitudes $c(r), c^*(r)$ and the R-matrix elements for two heavy ion scattering test cases. In these cases, the multiple Coulomb excitation of the ground-state rotational band of a doubly even nucleus with the corresponding spin sequence has been considered. The reduced transition matrix elements which are used were calculated according to the simple rotational model starting from given values of the reduced $E2$ and $E4$ matrix elements, $\langle 2^+ \| M(E2) \| 0^+ \rangle$ and $\langle 4^+ \| M(E4) \| 0^+ \rangle$, respectively. Before starting our investigation on the heavy ion test cases, we made for a light ion test case[B] a comparison between iteratively calculated R-matrix elements and those calculted with a conventional coupled-channel computer program (AROSA[B]). It turns out that a three- to four-figure correspondence is obtained.

Multiple Coulomb excitation of ^{238}U by 385 MeV Kr. (Ref. 10)

For this case, the Sommerfeld parameter and wave number are approximately 244 and 29, re-

spectively. The target spin sequence is $0^+, 2^+, 4^+, \ldots, 20^+$ ($N = 121$). In Fig. 1 the values of the complex R-matrix element, with a set of quantum numbers and hypothetical $E2$ and $E4$ values as mentioned in the figure, are plotted with a logarithmic radial scale in the complex plane, for successive iteration steps of both schemes. This figure shows as a surprising result the very rapid convergence of the inward-outward iteration scheme when compared to the perturbative one. It is seen that the perturbative values jump from one quadrant to the other while approaching the convergence limit only after more than about thirteen steps. On the contrary, the inward-outward scheme has a starting value which already nearly coincides with the convergence limit. It appears that for larger values of the reduced $E2$ transition matrix element, the rate of convergence for the perturbative iteration scheme is poorer. For the more realistic reduced $E2$ element of 3.5 eb, it diverges. The inward-outward scheme needs only a few steps to converge in this case. Therefore, from now on we concentrate our investigation on the inward-outward iteration scheme, using an $E2$ element equal to 3.5 eb.

Figure 2 shows the behavior of the amplitudes $c(r)$ and $c^*(r)$, during the first and final iteration step, for the set of quantum numbers $I_0 = 0$, $I = 2$, $l_0 = l = 100$. Numerically speaking, the fourth iteration step gives at least a three-figure agreement
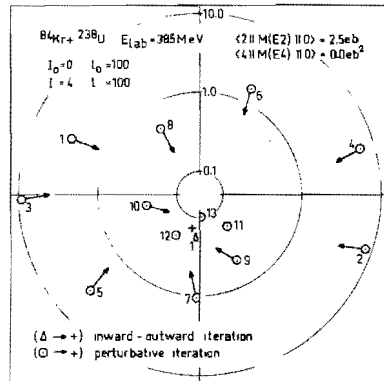
FIG. 1. A R-matrix element for a heavy ion scattering case, plotted with a logarithmic radial scale in the complex plane and calculated for successive iteration steps according to the inward-outward iteration scheme and the perturbative one. The convergence limit is indicated by a cross (+). Note the rapidity of convergence of the inward-outward scheme.
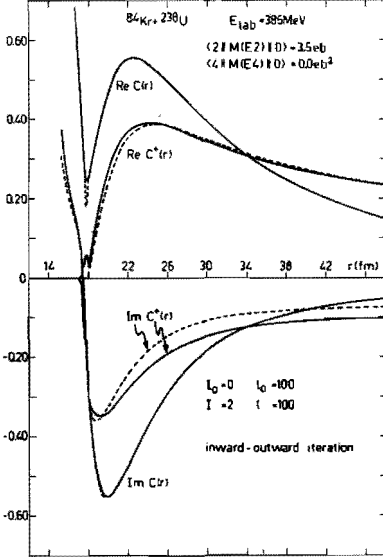
FIG. 2. This figure illustrates the inward-outward
iteration scheme for a heavy ion scattering case. The
amplitudes $c(r)$ and $c'(r)$ are plotted as a function of r
for the first iteration step (– – –) and the final one (——).
The difference between the first and final iteration steps
for $c(r)$ is visible only in the neighborhood of the classi-
cal turning points. The location of the latter is given in
Fig. 3.

with the final result. We note that the influence of
$c'(r)$, obtained in an outward integration, on $c(r)$
during the next inward integration over the classi-
cally allowed region is rather weak. Only in the
region around the classical turning points of the
decoupled set of equations the difference between
the first and final iteration steps is visible in the
figure. Clearly, even one iteration step yields a
reasonable result. To study the behavior of the
amplitudes in more detail, the imaginary parts of
$c(r)$ and $c^*(c)$ are plotted in Fig. 3 on a larger r
scale for the above-mentioned set of quantum num-
bers and, additionally, for $I_0 = 0$, $I = 6$, $I_0 = l = 100$.
Both sets, but especially the latter, suggest that
the step sizes must be chosen with care over a
limited part of the integration range outside the
turning points, due to the tendency of the ampli-
tudes to oscillate here. In connection with the
foregoing, the general behavior of the amplitudes
may be summarized as follows: They change
monotonically inside the innermost turning point
and tend to oscillate outside it before approaching
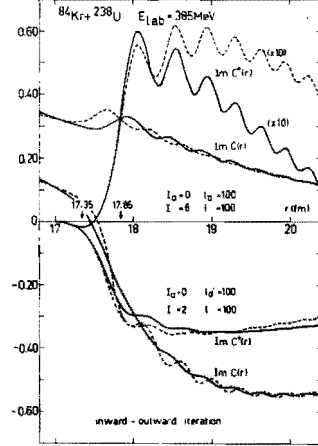
FIG. 3. The same as Fig. 2, but the imaginary parts of
$c(r)$ and $c^*(r)$ are now plotted on a larger r scale for two
different sets of quantum numbers. The inner- and outer-
most classical turning points are indicated by arrows.

FIG. 4. This figure shows the behavior of the imaginary
part of $c(r)$ for two different values of the starting point
r_0, plotted as a function of r for the first part of the in-
tegration range and for successive iteration steps.

constant values in the asymptotic region.

In the previous section, it is stated that the starting point r_0 has to be taken so that its choice does not affect the value of the R-matrix elements asymptotically. It seems that, on the one hand, making r_0 too small gives rise to diverging asymptotic values of these elements, while on the other hand, for large values of r_0 the R-matrix elements become dependent on r_0. However, in the present case, the margin is rather large, as can be seen from Fig. 4. This figure shows for two different r_0 values the imaginary part of $c(r)$, which is plotted as a function of r for the first part of the integration range and for successive iteration steps. The upper part of the figure corresponds to starting values of the components $\psi_i^k(r)$ in the solution vector of about $\exp(-20)$, while the lower part corresponds to values of about $\exp(-30)$. It is seen that outside the starting point the amplitude for successive iteration steps changes very rapidly; nevertheless, it converges for both r_0 values to the same value at about 15.5 fm, far inside the innermost turning point of the decoupled set of equations. As Fig. 3 shows, this turning point is located at 17.35 fm. The behavior of $c^+(r)$ and the real part of $c(r)$ are similar. In general, such a behavior guarantees a stable iteration process, since it means that numerically speaking the components $\psi_i^k(r)$, due to (3.10b), obtain a significant value inside the innermost turning point. Comparing the R-matrix elements at infinity for the present two r_0 values, it is seen that a two- to three-figure correspondence is obtained, illustrating the degree of independence on r_0.

Also, a comparison is made with a conventional coupled-channel calculation in the sense of Sec. II. For this, only the computer program JUPIGOR[11] was available. It uses Airy functions as piecewise analytic reference solutions too. The results are presented in Table I. Comparing the significant R-matrix elements, a two- to three-figure correspondence is obtained, even for the high-spin states. Calculations of the modulus give rise to discrepancies of about one per cent. In view of the uncertainties in experimental excitation probabilities,[12] such an accuracy may be called satisfactory. Note that there is a considerable reduction of computation time. With our computer, the average computation time for one integration step when solving a system of 121 coupled equations takes about 140 sec for a conventional coupled-channel calculation; but for the inward-outward scheme it takes about 4.3 sec, including four iteration steps. Every extra iteration step takes about 0.3 sec.

Finally, it should be noted that iteration schemes based on the integral form of the Schrödinger equa-

tion, have been studied elsewhere in light particle problems for inelastic scattering as well as for rearrangement.[13] In that study, an analysis of the kernel eigenvalue problem was made in order to understand the convergence properties. In this study such an analysis was not made; however, it is believed that the striking difference in convergence properties of the two iteration schemes, examined here, has to be sought in the fact that in the inward-outward scheme, the amplitudes $c(r)$ and $c^+(r)$ are iterated independently, while this is not the case in the perturbative scheme.

Multiple Coulomb excitation of ^{238}U by 1000 MeV Pb

This case has been studied to investigate the stability of the inward-outward iteration scheme for very heavy ion multiple excitations. The Sommerfeld parameter and wave number are now 542 and 53, respectively. The target spin sequence chosen is $0^+, 2^+, 4^+, \ldots, 32^+$ ($N = 289$). Figure 5 illustrates the behavior of the imaginary parts of the amplitudes $c(r)$ and $c^+(r)$ during the first and the final iteration step, for a set of quantum numbers mentioned in the figure. It turns out that in this case, too, only a few iteration steps are needed. Numerically speaking, the sixth iteration step gives at least a three-figure agreement with the final result. In this figure, the amplitudes are plotted as a function of r for the region in the neighborhood of the classical turning points, as is done in Fig. 3 for the excitation by ^{84}Kr. Comparing both figures shows a similar behavior, although the amplitudes in Fig. 5 have a slightly more oscillatory dependence on the integration variable r.

The insensitivity of the R-matrix elements to the starting point r_0 has also been investigated for the present case. This is illustrated in Fig. 6, where for two different r_0 values the imaginary part of $c(r)$ is plotted as a function of r for the first part of the integration range and for successive iteration steps. The upper and lower part of the figure correspond to starting values of the components $\psi_i^k(r)$ in the solution vector of about $\exp(-20)$ and $\exp(-30)$, respectively. It is seen that, as in Fig. 4, the amplitude converges for both r_0 values to the same value at about 19.6 fm, sufficiently inside the innermost turning point, which is located at 20.64 fm. The amplitude $c^+(r)$ and the real part of $c(r)$ show a similar behavior. This behavior guarantees a stable iteration process. The degree of independence on r_0 is illustrated by comparing asymptotically the R-matrix elements for both r_0 values. This comparison shows a two- to three-figure correspondence.

It must be noted that in a similar case to that

TABLE I. Selected $R^f_{l_i \, 0 l_0}$ values for ^{84}Kr + ^{238}U with $E_{lab} = 385$ MeV, $\langle 2 \| M(E2) \| 0 \rangle = 3.5$ eb, $\langle 4 \| M(E4) \| 0 \rangle = 0.0$ eb^2. The values for a quantum-mechanical coupled-channel calculation of conventional (Conv. C. C.) type (JUPIGOR), as well as the values for an inward-outward iterative (Inw.-Outw. Iter.) calculation after four iteration steps are given. The significant elements show a correspondence of about two and sometimes three figures, even for the high-spin states. The computation time per integration step, solving a system of 121 coupled equations for $I_{max} = 20$, takes about 140 sec for the former calculation, while for the latter, it takes about 4.3 sec. Left entries mean real parts, middle entries mean imaginary parts, and right entries mean the moduli. Additional exponents have been added in parentheses above the columns.

$J = l_0 = 100$

$I = 0$

	$l = l_0$		
	(0)	(0)	(0)
Conv. C. C.	0.120	0.197	0.231
Inw.-Outw. Iter.	0.119	0.195	0.229
			0.9%

$I = 4$

	$l = l_0 - 4$			$l = l_0 - 2$			$l = l_0$			$l = l_0 + 2$			$l = l_0 + 4$		
	(0)	(-1)	(0)	(0)	(-1)	(0)	(-1)	(-1)	(-1)	(-1)	(-1)	(-1)	(-1)	(0)	(0)
Conv. C. C.	0.113	-0.560	0.126	-0.103	0.163	0.105	0.919	-0.135	0.929	-0.776	0.535	0.943	0.171	-0.117	0.118
Inw.-Outw. Iter.	0.116	-0.533	0.127	-0.103	0.152	0.104	0.906	-0.141	0.917	-0.777	0.515	0.932	0.196	-0.118	0.119
			0.8%			0.8%			1.3%			1.2%			1.0%

$I = 8$

	$l = l_0 - 8$			$l = l_0 - 4$			$l = l_0$			$l = l_0 + 4$			$l = l_0 + 8$		
	(0)	(-1)	(0)	(-1)	(-1)	(0)	(-1)	(-1)	(-1)	(-1)	(-1)	(-1)	(-1)	(-1)	(-1)
Conv. C. C.	0.120	0.971	0.154	0.685	0.766	0.103	0.648	0.624	0.900	0.727	0.296	0.785	0.714	-0.400	0.819
Inw.-Outw. Iter.	0.119	0.995	0.155	0.682	0.785	0.104	0.644	0.628	0.899	0.713	0.324	0.783	0.714	-0.388	0.813
			0.6%			1.2%			0.1%			0.3%			0.7%

$I = 12$

	$l = l_0 - 12$			$l = l_0 - 6$			$l = l_0$			$l = l_0 + 6$			$l = l_0 + 12$		
	(-1)	(0)	(0)	(-1)	(-1)	(-1)	(-2)	(-1)	(-1)	(-1)	(0)	(0)	(0)	(0)	(0)
Conv. C. C.	-0.157	0.126	0.127	0.165	-0.825	0.841	-0.713	0.895	0.898	-0.216	-0.105	0.107	0.104	0.144	0.178
Inw.-Outw. Iter.	-0.159	0.127	0.128	0.167	-0.835	0.851	-0.765	0.903	0.906	-0.200	-0.106	0.108	0.104	0.147	0.180
			0.7%			1.2%			0.9%			1.0%			1.2%

$I = 16$

	$l = l_0 - 16$			$l = l_0 - 8$			$l = l_0$			$l = l_0 + 8$			$l = l_0 + 16$		
	(-2)	(0)	(0)	(-2)	(-1)	(-1)	(-2)	(-1)	(-1)	(-1)	(-1)	(-1)	(-1)	(-1)	(-1)
Conv. C. C.	-0.375	-0.156	0.156	0.608	-0.836	0.838	0.190	-0.889	0.699	-0.108	-0.583	0.593	-0.364	-0.592	0.695
Inw.-Outw. Iter.	-0.328	-0.157	0.157	0.656	-0.835	0.837	0.252	-0.700	0.701	-0.099	-0.579	0.588	-0.365	-0.600	0.702
			0.6%			0.1%			0.3%			0.8%			1.0%

$I = 20$

	$l = l_0 - 20$			$l = l_0 - 10$			$l = l_0$			$l = l_0 + 10$			$l = l_0 + 20$		
	(-2)	(-1)	(-1)	(-2)	(-1)	(-1)	(-3)	(-1)	(-1)	(-2)	(-1)	(-1)	(-2)	(-1)	(-1)
Conv. C. C.	-0.365	0.722	0.723	0.232	-0.304	0.305	0.218	0.189	0.189	-0.224	-0.104	0.106	0.381	0.704	0.800
Inw.-Outw. Iter.	-0.337	0.721	0.722	0.231	-0.301	0.302	0.105	0.188	0.188	-0.215	-0.102	0.104	0.383	0.714	0.809
			0.2%			1.0%			0.8%			1.9%			1.1%
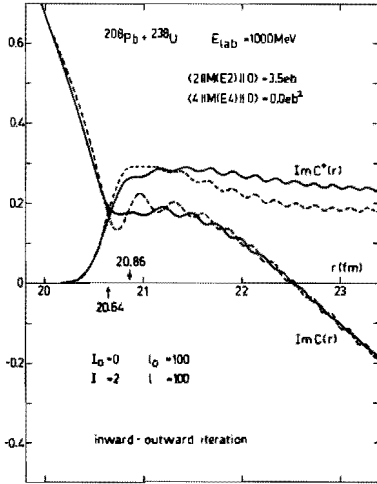
FIG. 5. This figure illustrates the inward-outward iteration scheme for a very heavy ion scattering case. The imaginary parts of the amplitudes $c(r)$ and $c^*(r)$ are plotted as a function of r for the first iteration step (---) and the final one (——). This has been done for the region in the neighborhood of the inner- and outermost classical turning points, which are indicated by arrows. The amplitudes show a slightly more oscillatory dependence on r as compared to the amplitudes in Fig. 3.

illustrated in Fig. 5, but with a target spin sequence of $0^+, 2^+, 4^+, \ldots, 24^+$, the inward-outward iteration scheme does not converge. Apparently, it can be considered as a further condition for a stable iteration process that the coupling scheme of the differential equations includes all experimentally relevant target states.

In conclusion, the inward-outward iteration scheme is successful and manageable even for multiple Coulomb excitation induced by very heavy ion collisions where it shows a rapid convergence.

V. COULOMB EXCITATION PROBABILITIES OF ^{84}Kr + ^{238}U at 385 MeV

To calculate the scattering amplitudes, cross sections, and excitation probabilities, use is made of some subroutines provided by the program AROSA.[8] However, it is necessary to adapt these subroutines due to the large number of J values needed in the partial-wave sums.

For the calculation of the cross sections (2.8) and excitation probabilities (2.9), a target spin sequence of $0^+, 2^+, 4^+, \ldots, 24^+$ ($N = 169$) and reduced

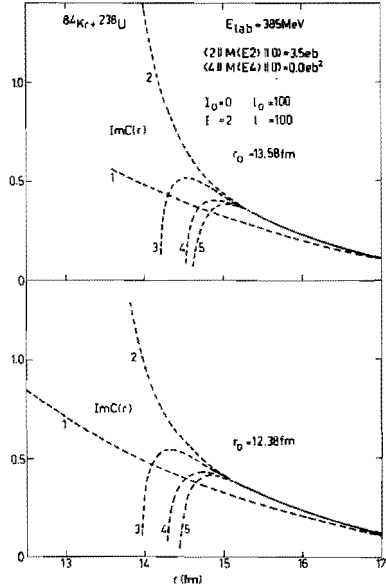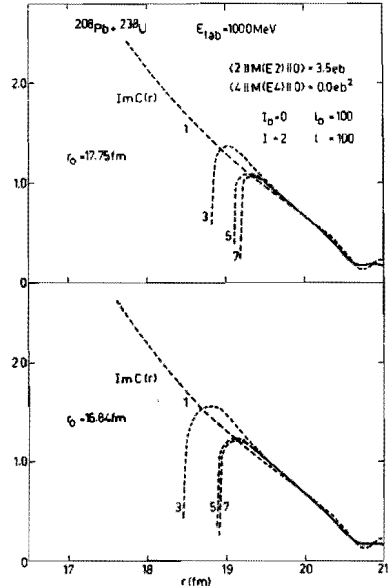
FIG. 6. This figure shows for the same very heavy ion scattering case as in Fig. 5, the behavior of the imaginary part of $c(r)$ for two different values of the starting point r_0, plotted as a function of r for the first part of the integration range and for successive iteration steps.

$E2$ and $E4$ transition matrix elements equal to 3.5 eb and 0.0 eb^2, respectively, have been taken. The R-matrix elements were calculated for the following sequence: $J = 0, 40, (1); \ 42, 100, (2); \ 104, 196, (4); \ 204, 516, (8); \ 532, 1332, (16)$. The values in parentheses indicate J steps. The values of the missing R-matrix elements are obtained by interpolation.

It is well known that the number of target states, which are coupled, is reduced at high J values. To illustrate this behavior, in Fig. 7 the absolute values of some R-matrix elements are plotted against J. These values are multiplied by the weight $(2J + 1)^{1/2}$, with which the R-matrix elements appear in the expression of the scattering amplitudes (2.6). It appears that the full set of coupled differential equations is necessary only up to a J value equal to about 200. For higher J values the dimension of the set can be gradually decreased.

In Figs. 8(a) and 8(b) the quantum-mechanical (QM) Coulomb excitation probabilities, calculated in the center-of-mass system, are plotted for all target states included as a function of the scattering angle θ. In addition, the probabilities are plotted from calculations based upon the semi-
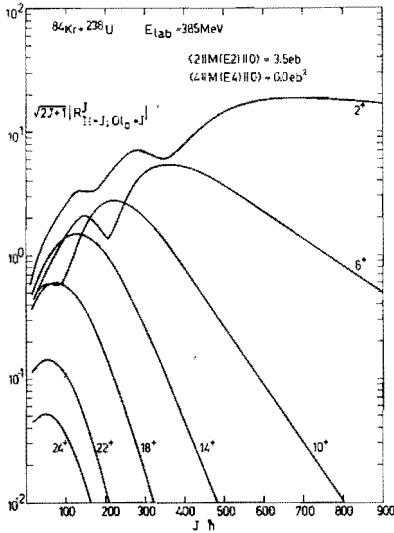
FIG. 7. The absolute values of some R-matrix elements, multiplied by a weight factor, are plotted against J for several spin states of the target.

classical (SC) theory with energy-symmetrized classical orbits.[14] Comparing both probabilities, it is seen that, as expected, the difference between the QM and SC probabilities for the low-spin states [Fig. 8(a)] is small, although significant. The difference is somewhat larger for the other states. Looking at Fig. 8(b), it is noted that at backward angles, the QM and SC probabilities for $I^{\pi} = 10^{+}$ coincide. For $I^{\pi} = 12^{+}$, 14^{+}, and 16^{+} the QM probability becomes larger than the SC value, for $I^{\pi} = 18^{+}$ they coincide again, while for $I^{\pi} = 20^{+}$, 22^{+}, and 24^{+} the SC probability increases relative to the QM probability. It is observed that the systematics of the differences between the QM and SC excitation probabilities, depending upon the excited target state and scattering angle, shows up quite clearly in the present study.

VI. CONCLUSIONS

The description of a heavy ion nuclear scattering process, especially of multiple Coulomb excitation, by means of a quantum-mechanical coupled-channel calculation of conventional type is not feasible at present, since the analysis involves the solution of a very large set of coupled linear second-order differential equations, which has to be solved as many times as the dimension of the set

to form a full set of linearly independent solutions.

Rewriting the set of coupled differential equations in integral form, transforms it into an equivalent set of coupled first-order integral equations. Approximating the potential energy over a radial interval by a linear reference potential, makes it possible to use Airy functions as piecewise analytic reference solutions. This opens up the possibility of evaluating analytically the integrals appearing in the set of first-order integral equations. This set can be solved iteratively which, in cases of heavy ion scattering, gives a considerable reduction of computation time as compared to the above-mentioned coupled-channel calculations. The efficiency of two iteration schemes, an inward-outward and a perturbative one, was examined. It appears that for heavy ion scattering only the inward-outward scheme has practical importance, since it converges for any realistic value of the deformation parameters and needs only a few iteration steps. The accuracy which can be achieved is sufficient for practical purposes. Finally, it is concluded that the piecewise analytical approach by inward-outward iteration enables one to describe quantum-mechanically heavy ion scattering processes which are of increasing importance. Additionally, it opens up a favorable study procedure for heavy ion collisions.

APPENDIX

We consider integrals over Airy functions of the form

$$\int R^{m} A[\alpha(\beta_{1}+R)] \, B[\alpha(\beta_{2}+R)] dR \, ,$$

where A and B are the Airy functions or any linear combinations of them. Integrals involving $m = 0, 1, 2$; $\beta_{1} = \beta_{2}$ and $m = 0, 1$; $\beta_{1} \neq \beta_{2}$ were given by Gordon.[3] The analytical expression for the integral with $m = 2$ and $\beta_{1} \neq \beta_{2}$ may also be derived:
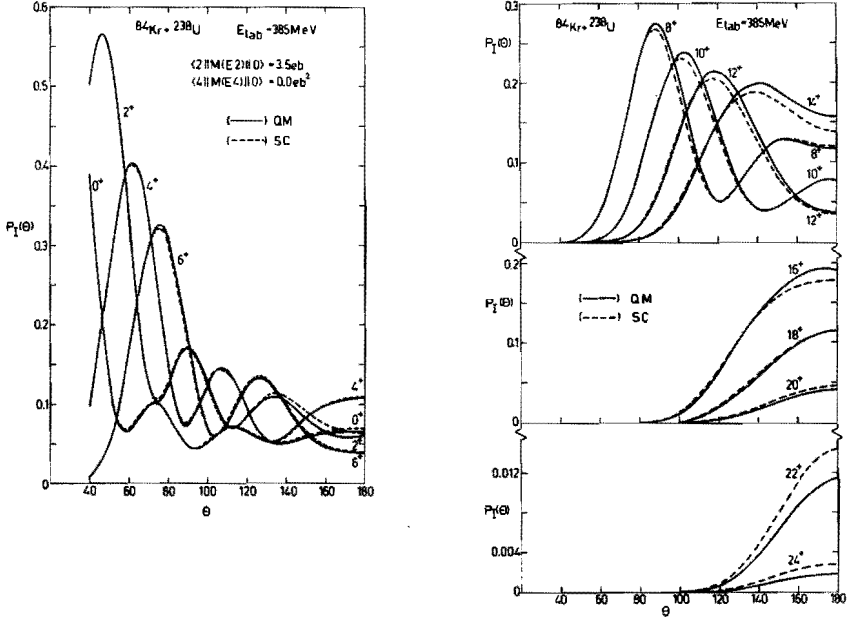
FIG. 8. (a) The quantum-mechanical (QM) and semiclassical (SC) Coulomb excitation probabilities P_f, calculated in the center-of-mass system, are plotted as a function of the scattering angle θ for the low-spin states of the target. (b) The same as (a), but the excitation probabilities P_f are now plotted as a function of the scattering angle θ for the high-spin states of the target. The difference between the QM and SC excitation probabilities depends upon both the excited target state and scattering angle.

$$\int R^2 A\left[\alpha(\beta_1+R)\right] B\left[\alpha(\beta_2+R)\right] dR$$

$$= -\frac{1}{\alpha^6(\beta_1-\beta_2)^4}\left\{12(\beta_1+\beta_2)+[24+2\alpha^3(\beta_1+\beta_2)(\beta_1-\beta_2)^2]R+4\alpha^3(\beta_1-\beta_2)^2R^2\right\}\left\{A\left[\alpha(\beta_1+R)\right] B\left[\alpha(\beta_2+R)\right]\right\}$$

$$+\frac{4}{\alpha^5(\beta_1-\beta_2)^3}\left\{\beta_2 A'\left[\alpha(\beta_1+R)\right] B\left[\alpha(\beta_2+R)\right]-\beta_1 A\left[\alpha(\beta_1+R)\right] B'\left[\alpha(\beta_2+R)\right]\right\}$$

$$+\frac{1}{\alpha^6(\beta_1-\beta_2)^5}\left\{[24+2\alpha^3(\beta_1+\beta_2)(\beta_1-\beta_2)^2]+12\alpha^3(\beta_1-\beta_2)^2R+\alpha^6(\beta_1-\beta_2)^4R^2\right\}$$

$$\times\left\{A'\left[\alpha(\beta_1+R)\right] B\left[\alpha(\beta_2+R)\right]-A\left[\alpha(\beta_1+R)\right] B'\left[\alpha(\beta_2+R)\right]\right\}$$

$$+\frac{4}{\alpha^7(\beta_1-\beta_2)^4}\left[6+\alpha^3(\beta_1-\beta_2)^2R\right]\left\{A'\left[\alpha(\beta_1+R)\right] B'\left[\alpha(\beta_2+R)\right]\right\},$$

where the prime denotes differentiation with respect to the argument. The constant β does not contain F as in (3.8).

[1] K. Alder and A. Winther, *Electromagnetic Excitation* (North-Holland, Amsterdam, 1975).

[2] J. de Boer, G. Dannhauser, H. Massmann, F. Roessel, and A. Winther, J. Phys. G **3**, 889 (1977); M. W. Guidry, R. Donangelo, J. O. Rasmussen, and J. P. Boisson, Nucl. Phys. **A295**, 482 (1978).

[3] R. G. Gordon, J. Chem. Phys. **51**, 14 (1969); R. G. Gordon, in *Methods in Computational Physics: 10, Atomic and Molecular Scattering*, edited by B. Alder, S. Fernbach, and M. Rotenberg (Academic, New York, 1971), p. 81.

[4] K. Alder, F. Roesel, and R. Morf, Nucl. Phys. **A284**, 145 (1977).

[5] M. Ichimura, M. Igarashi, S. Landowne, C. H. Dasso, B. S. Nilsson, R. A. Broglia, and A. Winther, Phys. Lett. **67B**, 129 (1977).

[6] J. Raynal, *Computing as a Language of Physics* (IAEA, Vienna, 1972), p. 281.

[7] See Chap. IX of Ref. 1.

[8] F. Roesel, J. X. Saladin, and K. Alder, Comp. Phys. Commun. **8**, 35 (1974).

[9] H. J. Wollersheim, W. Wilcke, Th.W. Elze, and D. Pelte, Phys. Lett. **48B**, 323 (1974).

[10] E. Grosse, J. de Boer, R. M. Diamond, F. S. Stephens, and P. Tjøm, Phys. Rev. Lett. **35**, 565 (1975).

[11] L. D. Tolsma, J. Comp. Phys. **17**, 384 (1975).

[12] M. W. Guidry, E. Eichler, N. R. Johnson, G. D. O'Kelley, R. J. Sturm, and R. O. Sayer, Phys. Rev. C **12**, 1937 (1975).

[13] P. J. R. Soper, Phys. Rev. C **10**, 1282 (1974).

[14] A. Winther and J. de Boer, in *Coulomb Excitation*, edited by K. Alder and A. Winther (Academic, New York, 1970), p. 303.

CHAPTER 6

SOLVING COUPLED EQUATIONS BY ITERATION FOR HEAVY ION
MULTIPLE COULOMB-NUCLEAR EXCITATION

L.D. Tolsma

Department of Physics, Eindhoven University of Technology

Eindhoven, The Netherlands

ABSTRACT

   To describe quantum mechanically multiple Coulomb-nuclear excitation
in heavy-ion reactions, the set of coupled differential equations of the
partial-wave radial solutions is rewritten in integral form. Decomposing
these solutions into two basis functions, the corresponding amplitudes of
these functions satisfy a set of coupled integral equations. Expressing
the basis functions in terms of appropriately chosen piecewise analytic
reference solutions, the integrals appearing in this set can be evaluated
analytically. The coupled set of amplitude equations is solved itera-
tively. The efficiency of two iteration methods, the inward-outward and
the sequential one, has been investigated for test cases dealing with
multiple Coulomb and nuclear excitation of ^{238}U by 286 MeV ^{40}Ar and
718 MeV ^{84}Kr up to high spin states of the ground-state rotational band.
Padé approximants to the S-matrix elements were also included in both of
the iteration methods. It turns out that the inward-outward iteration
method converges much faster than the sequential one. In many cases, the
inward-outward method does not need Padé acceleration at all, while the
sequential method does. It happens that convergent cases in the
inward-outward method diverge in the sequential method aided by Padé
approximants.

   Numerical studies of the excitation probabilities as a function of the
scattering angle for the aforementioned heavy-ion reactions show that the
probability functions of the members of the ground-state rotational band,
satisfy a general rule at near-grazing angles, previously formulated for
the excitation probability as a function of the energy near the Coulomb
barrier for backward scattering from a deformed rotor.

> NUCLEAR REACTIONS Solving coupled radial equations by iteration.
>
>   Quantum mecanically calculated excitation probabilities for
>
>   heavy-ion multiple Coulomb-nuclear excitation.

1. INTRODUCTION

The quantum-mechanical description of inelastic scattering of charged particles from nuclei requires the solution of the Schrödinger equation, which can be reformulated as a set of N coupled linear second-order differential equations of the partial-wave radial functions. Such a description becomes computationally complex when heavy ions are involved in the scattering process, mainly due to:

1. The rapidly oscillating behaviour of the solution function within the classically allowed region of the integration range.

2. The long range of the Coulomb coupling. Therefore, the integration of the set of coupled equations should be carried out over long ranges.

3. The large number of coupled equations or channels that, in general, should be considered.

4. The large number of partial waves that should be included when calculating the quantities observed.

In the usual approach, the set of coupled equations is solved as many times as the dimension of the set with linearly independent regular starting values at the origin for each of the solution vectors. The equations are integrated from the origin to a radius at which all nuclear and coupling interactions become insignificant. By constructing the physical solution as a linear combination of the solution vectors with the appropriate asymptotic behaviour of an incoming partial wave in the entrance channel plus outgoing partial waves in all the relevant exit channels, the desired S-matrix elements can be found. This standard procedure is satisfactory for small systems of coupled equations, i.e., for light-ion reactions but is particularly time-consuming for the large systems associated with heavy-ion collisions. In addition, this procedure generates S-matrix elements which form a complete N x N matrix. However, in the nuclear physics context, often only a restricted number of entrance channels (only one for a zero-spin ground state) is important which means that only a restricted number of columns of the scattering matrix is needed. In these cases, iteration methods can be applied for which the solutions are obtained directly without the need for solving the set of coupled equations N times.

The set of coupled equations can be integrated by means of the well-known multistep methods, such as the Numerov method. In applying these methods special attention has to be paid to the behaviour of the solution. The heavier the charged particles in the scattering process and the

higher the energy of their relative motion, the more rapidly the solution will oscillate in the classically allowed region and the smaller the step sizes in the multistep methods have to be chosen. Since, these circumstances occur, in general, together with large systems of coupled equations and a long range of the Coulomb coupling, the multistep methods can become prohibitively time-consuming.

In order to cope with the problems that occur in heavy-ion collisions, due to the standard procedure for solving the N coupled radial equations N times and due to the step-size dependency of the multistep methods, it is advantageous to formulate piecewise analytical solution methods together with iteration methods. In this way, an efficient treatment of heavy-ion multiple, Coulomb excitation has been discussed in a previous paper [1]. It was shown that the partial-wave radial solution of the Schrödinger equation can be decomposed into regular and outgoing components, i.e., can be written as a linear combination of two basis functions which oscillate in the classically allowed region with relatively slowly varying amplitudes. These basis functions are the solutions of the decoupled radial equations. An appropriately chosen reference potential will allow them to be expressed in terms of piecewise analytic reference solutions. The efficiency of these methods depends upon the possibility of dividing the integration range into intervals which are sufficiently small to approximate the potential by some simpler varying reference potential, but which, on the other hand, contains a sufficiently large number of oscillations of the solution. It was also shown that, after rewriting the set of coupled differential equations into an integral form, the varying amplitudes satisfy a set of coupled integral equations. The integrals that arise in these equations can be evaluated analytically when Airy functions are used as piecewise analytic reference solutions corresponding to a linear reference potential [2]. The set of integral equations was solved by means of an iteration procedure. Two iteration schemes, an inward-outward [3,4] and a sequential or perturbative one [5,6] were investigated. It appeared that only the inward-outward iteration scheme is of practical importance.

In an extended study about techniques for heavy-ion coupled channels calculations which include nuclear and Coulomb interactions, various iterative methods were compared in order to solve the coupled radial equations in the interior region of configuration space [7,8]. The Born-Neumann series, the method of moments, Austern's modification of the

Sasakawa method and the sequential iteration were studied, but not the inward-outward iteration. The conclusion was drawn that sequential iteration with Padé acceleration is the most rapidly convergent and efficient method. The integration of the set of coupled equations itself was carried out by means of a multistep method.

In this paper we report the continuation of our investigation into the numerical solution of the radial Schrödinger equation in order to describe heavy-ion multiple excitation including nuclear interactions. This was done within the framework of the iterative piecewise analytical solution method too. The approximation of the potential by a linear reference potential implies the generation of complex Airy functions [9,10] for the intervals of the integration region where the optical potential contributes significantly to the total interaction. However, since the numerical evaluation of complex Airy functions is rather computer-time consuming, approximation of the potential by a constant reference potential has been investigated for this part of the integration range [11]. It appears that this approach is much more efficient, because the corresponding reference solutions are goniometric functions. In addition, Coulomb wave functions has been used as piecewise analytic reference solutions within the long range of the Coulomb coupling. The Coulomb integrals that arise in the coupled integral equations for the amplitudes can be efficiently evaluated using their recursion relations [12]. The efficiency of both iteration methods, the inward-outward and the sequential one, has been investigated, for test cases dealing with multiple Coulomb and nuclear excitation of ^{238}U by 286 MeV ^{40}Ar and 718 MeV ^{84}Kr up to high spin states of the ground-state rotational band. Padé approximants to the S-matrix elements were also included in both of the iteration methods. It turns out that the inward-outward iteration method is still the most rapidly convergent one and, even in many cases it does not need Padé acceleration at all, while the sequential iteration method does. The first results of our investigation have been published already [13,14].

The set of coupled second-order differential equations of the partial-wave radial functions can be rewritten equivalently into two sets of coupled first-order differential equations of the above-mentioned amplitudes. In a study [15], these sets were solved iteratively by neglecting in the pure Coulomb coupling region of the integration range, the rapidly oscillating contributions to the equations. The inward-outward iteration

method was used. As an application of this approach, rotational model
calculations were performed for a case of multiple Coulomb-nuclear
excitation of ^{238}U by 340 MeV ^{40}Ar.

In section 2, a concise quantum-mechanical description of inelastic
scattering is given. Section 3 is devoted to the iterative piecewise
analytical solution method. Several forms of the reference potentials and
the corresponding reference solutions are described. The inward-outward
iteration method, as well as the sequential method are explained. Section
4 contains the results of our investigation related to the behaviour of
the amplitudes and the rate of convergence of both iteration methods. In
section 5, the excitation probabilities for ^{238}U, excited by 286 MeV ^{40}Ar
and 718 MeV ^{84}Kr, are shown. Finally, in section 6, conclusions are drawn
and a final remark is made.

2. CONCISE DESCRIPTION OF THE SCATTERING FORMALISM

The coupled equations to be solved for the partial-wave radial
functions $\psi_{I\ell}^{J\pi}(r)$ are:

$$\left[\frac{d^2}{dr^2} + k_I^2 - \frac{\ell(\ell+1)}{r^2} - \frac{2\mu}{\hbar^2} V_{diag}(r)\right] \psi_{I\ell}^{J\pi}(r) = \frac{2\mu}{\hbar^2} \sum_{I'\ell'} V_{I\ell;I'\ell'}^{J\pi}(r) \psi_{I'\ell'}^{J\pi}(r),$$

$$(2.1)$$

assuming a spinless projectile. Here, J,ℓ and I denote the total angular
momentum, the orbital angular momentum and the spin of the target
nucleus, respectively. The excitation energy of the target is ε_I, in a
state with spin I. The total angular momentum J, its projection onto the
z-axis and the parity π are good quantum numbers and, therefore, the
equations (2.1) refer to a single combination of (J,π) for the system.
Let E be the center-of-mass energy in the incident channel, then, the
asymptotic wave number k_I is given by:

$$k_I^2 = \frac{2\mu}{\hbar^2} (E-\varepsilon_I),$$

$$(2.2a)$$

and the Sommerfeld parameter η_I which will be needed later, by:

$$\eta_I = \frac{2\mu}{\hbar^2} \frac{Z_P Z_T e^2}{2k_I},$$

$$(2.2b)$$

where μ is the reduced mass, while Z_P and Z_T represent the charge numbers
of the projectile and target nucleus, respectively.

The diagonal potential is just the usual optical-model potential which is
written in two parts as:

$$V_{diag}(r) = V^N_{diag}(r) + V^C_{diag}(r),$$ (2.3)

representing the nuclear and Coulomb diagonal potentials, respectively.
For the nuclear potential, the Woods-Saxon form was taken:

$$V^N_{diag}(r) = -V(1+e_v)^{-1} - iW(1+e_w)^{-1},$$ (2.4)

where

$$e_v = \exp\left[(r-R_v)/a_v\right],$$ (2.5a)

whilst V, R_v and a_v are the strength, the radius and diffuseness para-
meters of the real part of the nuclear potential, respectively. Denoting
the projectile and target masses by A_P and A_T respectively, the radius
R_v is given by:

$$R_v = r_v \left[A_P^{1/3} + A_T^{1/3}\right],$$ (2.5b)

where r_v is the real optical radius parameter. A similar explanation
applies to W and e_w concerning the imaginary part of the nuclear
potential. The Coulomb potential, derived from a constant charge distri-
bution in the target within the Coulomb radius R_c and zero outside it,
has the form:

$$V^C_{diag}(r) = Z_P Z_T e^2 \left[\begin{array}{ll} \frac{1}{2R_c}\left(3 - (\frac{r}{R_c})^2\right) & r < R_c \quad (2.6a) \\ \frac{1}{r} & r > R_c \quad (2.6b) \end{array}\right.$$

$$\text{with } R_c = r_c A_T^{1/3},$$ (2.6c)

where r_c is the Coulomb radius parameter.

Representing the coupling or transition potential by a multipole
expansion of the deformed optical model and assuming rotational eigen-
states for the nuclear wave functions, the elements $V^{J\pi}_{I\ell;I'\ell'}(r)$ of the
coupling matrix will have the form:

$$V^{J\pi}_{I\ell;I'\ell'}(r) = \sum_\lambda V^\lambda_{cpl}(r)\, G_\lambda(I\ell,I'\ell';J),$$ (2.7)

where the geometrical factor $G_\lambda(I\ell,I'\ell';J)$ is given by:

$$G_\lambda(I\ell,I'\ell';J) = (4\pi)^{-1/2} \, i^{\ell'-\ell+\lambda} \, (-1)^{J+\lambda} \, \hat{I} \, \hat{I}' \, \hat{\ell} \, \hat{\ell}' \, \hat{\lambda}$$

$$\begin{pmatrix} I' & \lambda & I \\ 0 & 0 & 0 \end{pmatrix} \begin{pmatrix} \ell & \lambda & \ell' \\ 0 & 0 & 0 \end{pmatrix} \begin{Bmatrix} I & \ell & J \\ \ell' & I' & \lambda \end{Bmatrix}, \qquad (2.8)$$

assuming couplings within the ground-state rotational band (GSB) only. Here, the symbol $\hat{x}$ stands for $(2x+1)^{1/2}$.

The radially dependent part of the coupling potential can be described with two different terms, too:

$$V_{cpl}^\lambda(r) = V_{cpl}^{N;\lambda}(r) + V_{cpl}^{C;\lambda}(r). \qquad (2.9)$$

They represent the radial dependence of the nuclear and Coulomb coupling potential, respectively. The superscript λ refers to the transferred angular momentum during the scattering process. Since, only a rotational target nucleus has been considered, the nuclear coupling potential is given by a Legendre polynomial expansion with expansion coefficients for $\lambda \neq 0$ [16]:

$$V_{cpl}^{N;\lambda}(r) = -4\pi \int_0^1 \{ V(1+e_v)^{-1} + iW(1+e_w)^{-1} \} \, Y_{\lambda 0}(\theta) \, d(\cos(\theta)), \qquad (2.10)$$

where

$$e_v = \exp[(r - R_v(\theta))/a_v]. \qquad (2.11a)$$

The radius $R_v(\theta)$ is assumed to be given by:

$$R_v(\theta) = r_v \left[A_P^{1/3} + A_T^{1/3} \{ 1 + \sum_{\lambda'} (\beta_{\lambda'}^N, Y_{\lambda'0}(\theta) - \frac{(\beta_{\lambda'}^N,)^2}{4\pi}) \} \right] \qquad (2.11b)$$

with the nuclear mass deformation parameters $\beta_{\lambda'}^N$ [17]. The last term in the summation maintains volume to this order in the deformation parameters. A similar expression holds for e_w. The Coulomb coupling potential is expressed up to the second order in the deformation. The radial dependence has the form:

$$V_{cpl}^{C;\lambda}(r) = \frac{3Z_P Z_T e^2}{(2\lambda+1)R_c} \{ \beta_\lambda^{C(1)} \begin{bmatrix} (\frac{r}{R_c})^\lambda \\ (\frac{R_c}{r})^{\lambda+1} \end{bmatrix} + \beta_\lambda^{C(2)} \begin{bmatrix} (1-\lambda)(\frac{r}{R_c})^\lambda & r \leqslant R_c \quad (2.12a) \\ (\lambda+2)(\frac{R_c}{r})^{\lambda+1} & r > R_c \quad (2.12b) \end{bmatrix} \},$$

where the parameters $\beta_\lambda^{C(1)}$ and $\beta_\lambda^{C(2)}$ describe the charge deformation in the first and second orders, respectively.

To obtain solutions for $\psi_{I\ell}^{J\pi}(r)$, two boundary conditions have to be fulfilled. At the origin $\psi_{I\ell}^{J\pi}(r)$ should vanish:

$$\lim_{r\to 0} \psi_{I\ell}^{J\pi(I_0\ell_0)}(r) = 0, \tag{2.13a}$$

whilst, for large distances, $\psi_{I\ell}^{J\pi}(r)$ must represent an ingoing partial wave in the entrance channel plus outgoing partial waves in all the relevant exit channels. The precise asymptotic form defines the scattering matrix elements $S_{I\ell;I_0\ell_0}^{J\pi}$:

$$\psi_{I\ell}^{J\pi(I_0\ell_0)}(r) \underset{r\to\infty}{\sim} \delta_{II_0}\delta_{\ell\ell_0} H_\ell^-(\eta_{I_0};k_{I_0}r) - \left[\frac{k_{I_0}}{k_I}\right]^{1/2} S_{I\ell;I_0\ell_0}^{J\pi} H_\ell^+(\eta_I;k_I r).$$

$$\tag{2.13b}$$

The ingoing and outgoing Coulomb waves H_ℓ^- and H_ℓ^+, respectively, in terms of the well-known regular and irregular Coulomb wave functions F_ℓ and G_ℓ, are $H_\ell^\pm = (G_\ell \pm iF_\ell)$. The indices I_0, ℓ_0 correspond to an ingoing wave in the entrance channel for $I = I_0$ and $\ell = \ell_0$.

The set of coupled equations (2.1) has to be solved for each J value in a full range of J values. From the scattering matrix elements obtained for these J values, the cross section for the ground state and each excited state, as well as other observable quantities, can be calculated [1].

3. ITERATIVE PIECEWISE ANALYTICAL SOLUTION METHOD

The Schrödinger equation (2.1) can be rewritten in the form:

$$\left[\frac{d^2}{dr^2} + k_i^2 - U_{ii}(r)\right] \psi_i(r) = \sum_{j\neq i}^{N} U_{ij}(r)\,\psi_j(r), \quad i = 1,2,\ldots,N \tag{3.1}$$

and the boundary condition (2.13b) as:

$$\psi_i^k(r) \underset{r\to\infty}{\sim} \delta_{ik} H_i^- - \left[\frac{k_k}{k_i}\right]^{\frac{1}{2}} S_{ik} H_i^+. \tag{3.2}$$

The superscript and subscript k refer to the entrance channel.

Considering some interval of the integration range with its midpoint at a radius $\bar{r}$ and introducing a reference potential $U^{rf}(r)$ for that

interval, equation (3.1) becomes:

$$[\frac{d^2}{dr^2} + k_i^2 - U_{ii}^{rf}(r)] \psi_i(r) = \sum_{j=1}^{N} W_{ij}(r) \psi_j(r), \quad i = 1,2,\ldots,N \quad (3.3)$$

where the right-hand side contains the difference between the true poten-
tial and the reference potential [1]. Replacing the right-hand side of
equation (3.3) by zero, several forms of the reference potential and the
corresponding solutions can be considered. The form that will be used in
practice depends upon the location of the integration range:

3.1 Constant reference potential [2,11]

$$U_{ii}^{rf}(r) = \bar{U}_{ii}, \quad (3.4)$$

where $\bar{U}_{ii}$ is introduced as the average value of the potential over the
interval. For $k_i^2 > \bar{U}_{ii}$ the reference solutions $A_i(r)$ and $B_i(r)$ are
goniometric functions:

$$A_i(r) = \sin[\gamma_i(r-\bar{r})] \quad (3.5a)$$

$$B_i(r) = \cos[\gamma_i(r-\bar{r})], \quad (3.5b)$$

with $\gamma_i = (k_i^2 - \bar{U}_{ii})^{1/2}$ and for $k_i^2 < \bar{U}_{ii}$ the solutions are

$$A_i(r) = \sinh[\delta_i(r-\bar{r})] \quad (3.6a)$$

$$B_i(r) = \cosh[\delta_i(r-\bar{r})], \quad (3.6b)$$

in which $\delta_i = (\bar{U}_{ii} - k_i^2)^{1/2}$.

3.2 Linear reference potential [2]

$$U_{ii}^{rf}(r) = \bar{U}_{ii} + (r-\bar{r}) \left.\frac{dU_{av}(r)}{dr}\right|_{r=\bar{r}}, \quad (3.7)$$

where again $\bar{U}_{ii}$ is the average potential over that interval. It should
be noted that, for the first derivative, an average value for the
components of the first derivative has been taken. This has to do with

the analytical evaluation of integrals (3.23a) later in this paper[1].
The reference solutions are the Airy functions Ai and Bi:

$$A_i(r) = Ai[\alpha(\beta_i + r)] \tag{3.8a}$$

$$B_i(r) = Bi[\alpha(\beta_i + r)], \tag{3.8b}$$

with the constants

$$\alpha = \left[\frac{dU_{av}(r)}{dr}\bigg|_{r=\bar{r}}\right]^{1/3} \quad \text{and} \quad \beta_i = \frac{\bar{U}_{11} - k_i^2}{dU_{av}(r)/dr\big|_{r=\bar{r}}} - \bar{r}. \tag{3.9}$$

3.3 Coulomb reference potential

$$U_{11}^{rf}(r) = \frac{2\eta_i k_i}{r} + \frac{\ell_i(\ell_i+1)}{r^2} \tag{3.10}$$

with the Sommerfeld parameter η_i and wave number k_i. The reference so-
lutions are the regular and irregular Coulomb wave functions F_ℓ and G_ℓ:

$$A_i(r) = F_{\ell_i}(\eta_i; k_i r) \tag{3.11a}$$

$$B_i(r) = G_{\ell_i}(\eta_i; k_i r). \tag{3.11b}$$

When $\eta = 0$, the reference solutions reduce to the spherical Bessel and
Neumann functions which were used by Sams and Kouri [18].

3.4 Integral representation of the coupled radial differential equations

If the right-hand side of equation (3.3) is replaced by zero, each of
the resulting decoupled equations will have two linearly independent
solutions:

1. The regular solution $G_i(r)$, which vanishes at the origin and is
   asymptotically defined as:

$$G_i(r) \underset{r \to \infty}{\sim} \frac{1}{2\sqrt{k_i}} \left[H_i^-(\eta_i; k_i r) - S_i^0 H_i^+(\eta_i; k_i r)\right]. \tag{3.12a}$$

2. The irregular outgoing wave solution $G_i^+(r)$, which is defined by the
   asymptotic form:

$$G_i^+(r) \underset{r \to \infty}{\sim} \frac{1}{\sqrt{k_i}} H_i^+(\eta_i; k_i r). \tag{3.12b}$$

Owing to the the special form of the left-hand side of equation (3.3), the solutions (3.12) can be expressed in terms of the linearly independent reference solutions $A_i(r)$ and $B_i(r)$ that belong to a specific form of the reference potential $U_{ii}^{rf}(r)$:

$$G_i(r) = A_i(r)a_i + B_i(r)b_i \qquad (3.13a)$$

and

$$G_i^+(r) = A_i(r)a_i^+ + B_i(r)b_i^+. \qquad (3.13b)$$

The constant coefficients a_i, b_i and a_i^+, b_i^+ are determined by conditions of continuity at the interval boundaries.

Subsequently, the Green's function which belongs to equation (3.3) can be constructed; it is regular at the origin and has asymptotically an outgoing wave form:

$$G_i(r,r') = -G_i(r_<) \, G_i^+(r_>), \qquad (3.14)$$

where $r_<$ and $r_>$ are the smaller and the larger values of r and r', respectively. With an ingoing wave in the entrance channel k, the set of coupled differential equation (3.3) can be rewritten as an equivalent set of N coupled integral equations:

$$\psi_i^k(r) = G_i(r) \left[\frac{2}{i} \delta_{ik} - \int_r^\infty G_i^+(r') \sum_{j=1}^N W_{ij}(r') \, \psi_j^k(r') \, dr' \right]$$

$$- G_i^+(r) \left[\int_0^r G_i(r') \sum_{j=1}^N W_{ij}(r') \, \psi_j^k(r') \, dr' \right], \qquad (3.15a)$$

$$\equiv G_i(r) \, c_i(r) - G_i^+(r) \, c_i^+(r). \qquad (3.15b)$$

The boundary conditions are:

$$c_i(\infty) = \frac{2}{i} \delta_{ik} \, , \qquad (3.16a)$$

$$c_i^+(0) = 0. \qquad (3.16b)$$

In practice, however, instead of (3.16b) the approximate but numerically

adequate physical boundary condition:

$$c_i^+(r_0) = 0 \qquad\qquad\qquad (3.16c)$$

is used for a relatively small r_0, in order to prevent the set of integral equations becoming singular.

The asymptotic value of the outgoing coefficients $c_i^+(r)$ are related to the S-matrix elements:

$$c_i^+(\infty) = S_{ik} - S_i^0 \, \delta_{ik}. \qquad\qquad\qquad (3.17)$$

The set of coupled integral equations (3.15) can be solved by iteration. We have concentrated our investigation on the behaviour of the coefficients $c_i(r)$ and $c_i^+(r)$, instead of the wave function itself. They may be considered as the amplitudes of the functions $G_i(r)$ and $G_i^+(r)$, respectively. Two iteration methods, the inward-outward and the sequential method have been investigated.

3.4.1 Inward-outward iteration method

In the inward-outward iteration method, the following set of coupled integral equations for the amplitudes $c_i(r)$ and $c_i^+(r)$ was considered:

$$c_i(r) = \frac{2}{i} \delta_{ik} - \int_r^\infty G_i^+(r') \sum_{j=1}^N W_{ij}(r') \, G_j(r') \, c_j(r') \, dr'$$

$$+ \int_r^\infty G_i^+(r') \sum_{j=1}^N W_{ij}(r') \, G_j^+(r') \, c_j^+(r') \, dr' , \qquad (3.18a)$$

$$c_i^+(r) = \int_0^r G_i(r') \sum_{j=1}^N W_{ij}(r') \, G_j(r') \, c_j(r') \, dr'$$

$$- \int_0^r G_i(r') \sum_{j=1}^N W_{ij}(r') \, G_j^+(r') \, c_j^+(r') \, dr' , \qquad (3.18b)$$

for $i = 1,2,\ldots,N$. This method was proposed by Alder, Roesel and Morf [3] and Ichimura et al.[4]. They used a differential form of these equations. For solving these equations iteratively, a start should be made at infinity, where the $c_j(r)$ values are known, due to the boundary condition (3.16a), although the $c_j^+(r)$ are not. However, the product $G_i^+ W_{ij} G_j^+$

oscillates rapidly over the classically allowed region of the integration range and tends to nullify the contribution of the term with $c_j^+(r)$. This will be apparent from Fig. 1. It is, therefore, justifiable to make the value of the coefficients $c_j^+(r)$ equal to zero in (3.18a) as a first estimate. Then, the first approximation of $c_i(r)$ can be generated by an inward integration of (3.18a). The values of $c_i(r)$ obtained, together with the initial condition (3.16c), can be used for an outward integration of (3.18b), where the term with $c_j(r)$ is now considered as a known inhomogeneous function. This outward integration gives a first approximation of $c_i^+(r)$ with a value at infinity, which corresponds to the first approximation of the S-matrix elements according to (3.17). The iteration procedure continues as a second inward integration of (3.18a) using the calculated values of $c_i^+(r)$ as known inhomogeneous functions and so forth, until convergence is obtained for $c_i^+(\infty)$.

   For later reference, it should be noted that, in solving the set of integral equations (3.18a) for the vector $c(r)$, the coupling between its components $c_i(r)$ is retained during each step of the iteration procedure, along with the coupling implied by the "inhomogeneous" part containing the vector $c^+(r)$. The same holds mutatis mutandis for the components of the vector $c^+(r)$.

3.4.2 Sequential iteration method

   Alternatively, the set of coupled integral equations for the amplitudes $c_i(r)$ and $c_i^+(r)$ can be written as:

$$c_i(r) = \frac{2}{i} \delta_{ik} + \int_0^r G_i^+(r') \sum_{j=1}^N W_{ij}(r') \left[G_j(r')c_j(r') - G_j^+(r')c_j^+(r') \right] dr'$$

$$- \int_0^\infty G_i^+(r') \sum_{j=1}^N W_{ij}(r') \left[G_j(r')c_j(r') - G_j^+(r')c_j^+(r') \right] dr',$$

$$(3.19a)$$

$$c_i^+(r) = \int_0^r G_i(r') \sum_{j=1}^N W_{ij}(r') \left[G_j(r')c_j(r') - G_j^+(r')c_j^+(r') \right] dr'.$$

$$(3.19b)$$

In the sequential iteration method, which was proposed by Raynal [5,6], the coupling potential W is considered to be a perturbation.

To illustrate the iteration procedure, the results for the n-th step of the iteration for $k = 1$ are written as:

$$c_i^{(n)}(r) = \frac{2}{i}\,\delta_{i1} + \int_0^r G_i^+(r')\,X_i^{(n)}(r')\,dr' - \int_0^\infty G_i^+(r')\,X_i^{(n)}(r')\,dr' \tag{3.20a}$$

$$c_i^{+(n)}(r) = \int_0^r G_i(r')\,X_i^{(n)}(r')\,dr' \,, \tag{3.20b}$$

where

$$X_i^{(n)} = W_{i1}\left[G_1 c_1^{(n-1)} - G_1^+ c_1^{+(n-1)}\right] + \sum_{j=2}^{i-1} W_{ij}\left[G_j c_j^{(n)} - G_j^+ c_j^{+(n)}\right]$$

$$+ \sum_{j=1}^{N} W_{ij}\left[G_j c_j^{(n-1)} - G_j^+ c_j^{+(n-1)}\right] \tag{3.21a}$$

for $i = 2, 3, \ldots, N$ and

$$X_i^{(n)} = W_{11}\left[G_1 c_1^{(n-1)} - G_1^+ c_1^{+(n-1)}\right] + \sum_{j=2}^{N} W_{1j}\left[G_j c_j^{(n)} - G_j^+ c_j^{+(n)}\right] \tag{3.21b}$$

for $i = 1$.

The calculation of Eqs. (3.20) starts with $i = 2$, using (3.21a) under the initial conditions

$$c_j^{(0)}(0) = \frac{2}{i}\,\delta_{j1}, \qquad c_j^{+(0)}(0) = 0. \tag{3.22}$$

This component must be integrated to infinity, due to the third term in (3.20a), before the calculation can be continued for $i = 3$. The iteration step ends with the integration of the first component using (3.21b).

Note, also for later reference, that in solving the set of integral equations (3.19) according to an iteration procedure illustrated by (3.20), in fact, a set of coupled equations is replaced by a set of uncoupled inhomogeneous equations with driving terms specified by the known functions (3.21). The basic idea behind this iteration method is solving the N inhomogeneous equations (3.20) in some definite sequential order; each improved solution $\left[G_j(r)c_j^{(n)}(r) - G_j^+(r)c_j^{+(n)}(r)\right]$ is immediately inserted in the inhomogeneous term of the subsequent equations, as given by the second term in (3.21a) and (3.21b).

3.4.3 Radial integrals

To solve equations (3.18) and (3.19), we make use of the relatively slow variation of the amplitudes $c_i(r)$ and $c_i^+(r)$ with respect to the rapid oscillations of the functions $G_i(r)$ and $G_i^+(r)$ in the classically allowed region. The r-dependence of the amplitudes is weak, as long as the difference between the true potential and the reference potential is small. Thus, a choice of step size has to be made so that small variations of $c_i(r)$ and $c_i^+(r)$ over an interval can be neglected.

Supposing that the true potential has been expanded in a Taylor series around $r = \bar{r}$ and assuming that, in the first iteration step, we have already integrated (3.18a), for instance, from the right up to r_r and using the value of $c_i(r_r)$, this equation yields a first-order contribution to $c_i(r_\ell)$ at the "left-hand" boundary r_ℓ, provided integrals of the form

$$\int_{r_\ell}^{r_r} G_i(r) \, (r-\bar{r})^m \, G_j(r) \, dr \qquad (3.23a)$$

are determined with $m = 0,1,2$. Expressing $G_i(r)$, as well as $G_i^+(r)$, in the reference solutions of the constant or linear reference potentials, integrals will be obtained which can be evaluated analytically. If Airy functions are used for this purpose, then, an average value for the first derivatives has to be introduced.

In the case of a Coulomb reference potential, integrals of the form

$$\int_{r_\ell}^{r_r} G_i(r) \, r^{-(\lambda+1)} \, G_j(r) \, dr \qquad (3.23b)$$

are obtained for $\lambda = 2,3,4,\ldots$. Expressing $G_i(r)$, as well as $G_i^+(r)$, in the regular and irregular Coulomb wave functions as the corresponding reference solutions, these integrals can be effectively evaluated by making use of recursion relations [12].

4. RESULTS AND DISCUSSION

In this section, we present the results related to the amplitudes $c(r)$, $c^+(r)$ and the S-matrix elements for the multiple Coulomb-nuclear excitation of ^{238}U by 718 MeV ^{84}Kr. In this case with $\eta = 178.3$ and $k = 39.7$ fm^{-1}, the rotational model has been considered for the target

nucleus with a spin sequence according to the ground-state rotational band up to $I^{\pi} = 24^{+}$ (N = 169). The optical potential parameters were chosen as:

$$V = 50.0 \text{ MeV}, \qquad W = 32.0 \text{ MeV},$$

$$r_V = 1.129 \text{ fm}, \qquad r_W = 1.211 \text{ fm}, \qquad r_C = 1.400 \text{ fm}, \qquad (4.1)$$

$$a_V = 1.10 \text{ fm}, \qquad a_W = 0.43 \text{ fm},$$

corresponding to the optical potential parameters for elastic scattering of ^{84}Kr from ^{208}Pb [19], because the parameters for ^{238}U were not known at the time that the calculations were made.

The nuclear mass and charge deformation parameters β_{λ}^{N} and $\beta_{\lambda}^{C(1)}$ appearing, respectively, in (2.11) and (2.12) are:

$$\beta_2^N = 0.2370, \qquad \beta_4^N = 0.0,$$

$$(4.2)$$

$$\beta_2^{C(1)} = 0.2121, \qquad \beta_4^{C(1)} = 0.0.$$

Figure 1 shows the behaviour of the real parts of the amplitudes c(r)
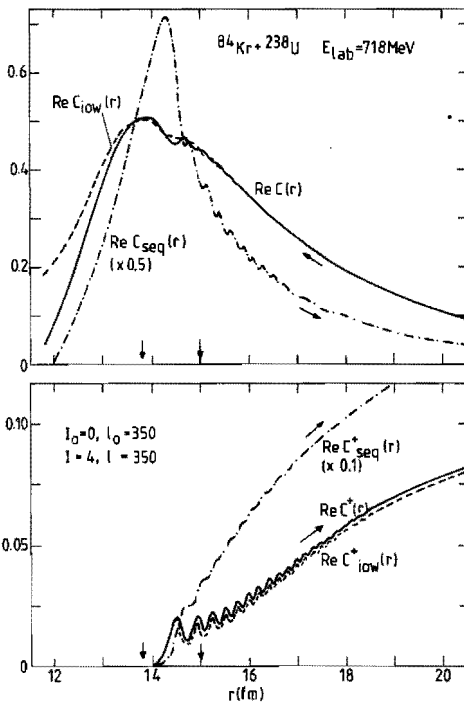
Fig. 1. This figure shows the real parts of the amplitudes c(r) and c^{+}(r) calculated in the inward-outward method, as well as in the sequential method. The dashed curves indicate the first inward-outward iteration step, the dashed-dot curves the first sequential step, whereas the full curves result from the final iteration step for both methods. The inner and outermost classical turning points are indicated by vertical arrows. This figure shows the very rapid convergence of the inward-outward iteration method when compared to the sequential one.

and $c^+(r)$ calculated in the inward-outward method, as well as in the sequential method as a function of r for the set of quantum numbers $I_0 = 0$, $I = 4$, $\ell_0 = \ell = 350$. The orbital angular momentum corresponds to a near-grazing partial wave. The dashed curves indicate the results of the first inward-outward iteration step, the dashed-dot curves the first sequential one, whereas the full curves result from the final iteration step for both schemes. The inner and outermost classical turning points are indicated by vertical arrows. This figure shows the very rapid convergence of the inward-outward iteration scheme when compared to the sequential one. It is seen that the curves of the first inward-outward step nearly coincide with the curves of the final step. It takes only a few iteration steps to obtain convergence. However, the difference between the first and final sequential iteration steps is much larger; a lot more iteration steps are needed to obtain convergence.

We note that in the inward-outward scheme the influence of $c^+(r)$, obtained in an outward integration, on $c(r)$ during the next inward integration over the classically allowed region is rather weak. Only in the region around the classical turning points of the decoupled set of equations is the difference between the first and final iteration steps visible in the figure. It can be seen that the amplitudes have an oscillating behaviour over a limited part of the integration range outside the turning points. The step sizes must be chosen with care [20], since they have to be such that small variations of $c(r)$ and $c^+(r)$ over an interval can be neglected. This means that the step sizes in this region which includes the range of the optical potential for most of the orbital angular momenta, have to be made rather small. Here, the use of a constant reference potential is the most effective one; the calculations can be carried out about 9 times faster when compared to the use of a linear reference potential.

The tendency of $c(r)$ and $c^+(r)$ to oscillate just outside the turning points is a general feature of these amplitudes. As a consequence, especially for light-ion scattering problems, it seems to be more effective to generate the solutions $G_i(r)$ and $G_i^+(r)$, in this part of the integration range, directly with a multistep integration method using a fixed step length [21]. The integrals appearing in (3.18) and (3.19) are then determined numerically according to commonly used methods. In this way, some calculations for the reaction $^{208}Pb(\alpha,\alpha')^{208}Pb(3^-$, 2.6146 MeV) $E_{lab} = 21.0$ MeV have been made.

Thus, looking at the figure, the general behaviour of the amplitudes may
be summarized as follows: they behave monotonically inside the innermost
turning point and tend to oscillate outside it before approaching
constant values in the asymptotic region. This behaviour determined our
strategy for choosing the step sizes: they were chosen such that a
constant reference potential could be used up to just a few fm outside
the outermost turning point (including the optical potential), a linear
reference potential for the region of strong Coulomb coupling interaction
($\approx$ 50fm), and a Coulomb reference potential for the last part of the
integration range (up to $\approx$ 1000 fm or more).

   In Table 1, the convergence properties of the modulus of the S-matrix
elements $S_{4,200;0,200}^{200}$ and $S_{4,350;0,350}^{350}$ for the multiple Coulomb-nuclear
excitation are shown as a function of an iteration number n for the
inward-outward method, as well as for the sequential iteration method.
The numbers in parentheses at the top of the columns (or alongside)
denote the powers of 10 by which the underlying numbers have to be multi-
plied. Table 2 shows the same, but now the multiple excitation is caused
by the Coulomb interaction only. In order to accelerate the convergence,
use can be made of Padé approximants. It seems that sequences of the Padé
approximants for the S-matrix elements accelerate the convergence of the
original sequence when it converges, and continue to converge under many
circumstances in which the original sequence diverges [5,8]. The tables
contain also the results of calculations which take these approximants
into account.

   Table 1 shows that the four original sequences (without Padé accelera-
tion) converge; the inward-outward sequences much faster than the
sequential ones. This is even so when compared to the sequential sequen-
ces with Padé acceleration. It is seen that the inward-outward method
requires only a few iterations to converge for the selected partial waves
and does not need Padé acceleration at all.

   Table 2 contains the iteration sequences of physically hypothetical
(Coulomb excitation only) but numerically interesting S-matrix elements.
It shows that the sequential method diverges completely. Even with the
aid of Padé approximants they do not converge to the right values. Also
in this case, the inward-outward method needs only a few iterations for a
J-value equal to 350. However, for lower J-values the rate of conver-
gence becomes less. The evaluation of the Padé approximants can accele-
rate the convergence in these cases. This is illustrated in the table for

TABLE 1

Convergence properties of the modulus of two S-matrix elements for the multiple Coulomb-nuclear excitation of ^{238}U by 718 MeV ^{84}Kr are shown as a function of an iteration number n for the inward-outward, as well as for the sequential iteration method.

a)	$\left|S^{J=200}_{4,200;0,200}\right|$			b)	$\left|S^{J=350}_{4,350;0,350}\right|$		
n	Inward-outward	Sequential		Inward-outward		Sequential	
	+Padé	+Padé		+Padé		+Padé	
	(-04) (-04)	(-04)	(-04)	(00)	(00)	(00)	(00)
1	0.8809	13.604		0.2522		2.9526	
2	0.8788	48.973		0.2630		6.2808	
3	0.8788 0.8788	55.332	10.440	0.2629	0.2629	5.6258	1.2146
4		34.512	4.4840	0.2628	0.2628	3.8127	0.5459
5		13.642	1.4770	0.2628	0.2628	1.7690	0.1608
6		3.0750	0.6801			0.7991	0.2378
7		1.6980	0.8564			0.4452	0.2662
8		0.7055	0.8416			0.2320	0.2633
9		0.8625	0.8502			0.2970	0.2624
10		0.8498	0.8496			0.2446	0.2625
11		0.8492	0.8495			0.2721	0.2626
12		0.8495	0.8495			0.2582	0.2626
13		0.8495				0.2643	
14						0.2619	
15						0.2628	
16						0.2625	
17						0.2626	
18						0.2626	

$J = 200$. It seems that for much lower J-values the inward-outward iteration method diverges too, even with the aid of Padé approximants ($J \lesssim 100$, see also Fig. 2).

In conclusion, these numerical studies show as a general feature of both iteration methods that the more important the left-hand side of equation (3.3) is relative to its right-hand side, the higher the rate of

TABLE 2

The same as table 1, but now the multiple excitation is caused by the Coulomb interaction only.

a)	$\left|S^{J=200}_{4,200;0,200}\right|$				b)	$\left|S^{J=350}_{4,350;0,350}\right|$			
n	Inward-outward +Padé		Sequential +Padé			Inward-outward +Padé		Sequential +Padé	
	(00)	(00)		(01)		(00)	(00)	(00)	(00)
1	0.6028		.24(2)			0.2376		8.1810	
2	0.0560		.38(3)			0.2451		31.075	
3	0.2441	0.1858	.23(4)	3.0083		0.2431	0.2430	48.045	4.9820
4	0.1980	0.1992	.77(4)	0.4792		0.2434	0.2433	47.268	1.6410
5	0.1975	0.1987	.19(5)	1.1744		0.2434	0.2434	34.329	0.8351
6	0.1966	0.1989	.46(5)	1.1744				21.303	0.0600
7	0.2027	0.1992	.13(6)	1.1744				13.342	0.3064
8	0.1980	0.1992	.38(6)	0.8344				8.7680	0.2646
9	0.1983		.10(7)	1.8518				6.9470	0.2181
10	0.2000		.26(7)	1.2877				4.9176	0.2379
11	0.1990		.67(7)	0.0608				4.0631	0.2370
12	0.1989		.17(8)	0.1516				2.5842	0.2377
13	0.1994		.45(8)	0.1516				2.0063	0.2377
14	0.1992		.11(9)					1.3799	
15	0.1992		.28(9)					0.8721	
16			.71(9)					0.8730	
17			.2(10)					0.2809	
18			.5(10)					0.5803	

convergence will be. This rate is much higher for the inward-outward iteration method compared to the sequential one, because in solving the set of coupled integral equations (3.18) for the amplitudes, the coupling between their components is still retained during the iteration procedure, as opposed to solving the set of coupled integral equations (3.19) which is replaced by a set of "uncoupled inhomogeneous" equations. The latter are solved considering the inhomogeneous terms as perturbations. The sequential iteration method solves the equations in a certain

sequential order, instead of in a straightforward way equivalent to the Born-Neumann series.

Finally, in Fig. 2, the S-matrix elements $S^J_{4,\ell=J;0,\ell_0=J}$ are plotted in the complex plane as a function of J. The solid curves indicate the results for the Coulomb-nuclear excitation. The S-matrix elements were calculated for the sequence: J = 88,216(16); 224,264(8); 268,296(4); 298,368(2); 372,400(4); 408,472(8); 488,552(16); 584,712(32) and partly given in the figure. The dashed curves indicate the results for a pure Coulomb interaction. These S-matrix elements were calculated for the sequence: J = 88,344(4);   352,472(8);   488,552(16); 584,712(32); 776,1992(64). The values in parentheses indicate J steps. In practice, however, it seems to be necessary to calculate the S-matrix elements only
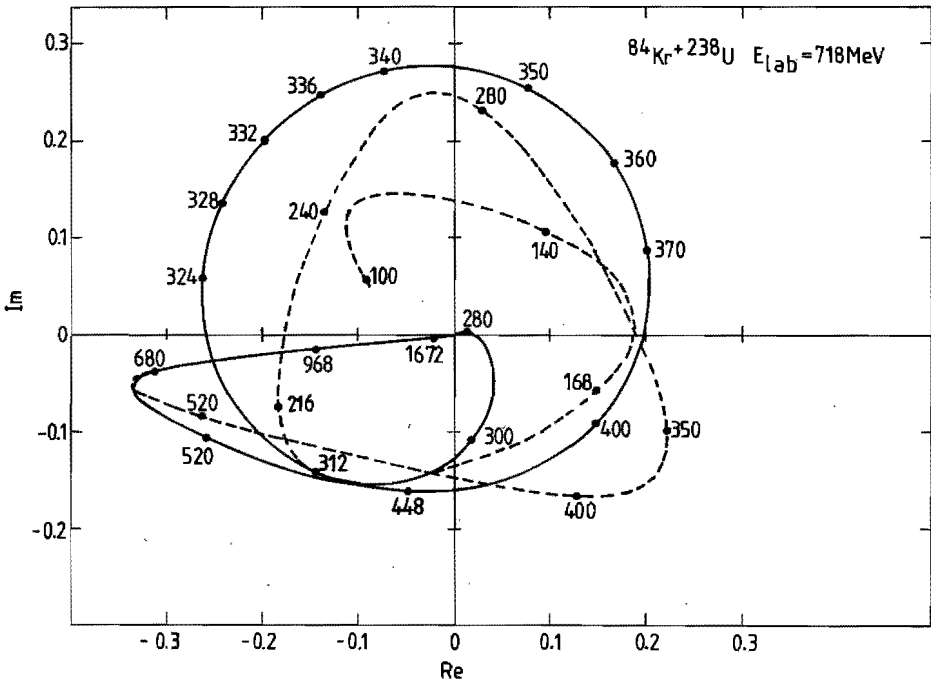
Fig. 2. The S-matrix elements $S^J_{4,\ell=J;0,\ell_0=J}$ are plotted in the complex plane as a function of J. The solid curves indicate the results for the Coulomb-nuclear excitation, while the dashed curves do the same for a pure Coulomb interaction. The figure shows clearly that the influence of the nuclear interaction is felt up to rather high J values.

for a more limited number of appropriately spaced J values. The values of
the missing S-matrix elements are obtained by interpolation. The figure
shows clearly that the influence of the nuclear interaction is felt up to
rather high J values ($\approx$ 648). Since the number of target states which are
coupled is reduced at high J values, the full set of coupled differential
equations is calculated only up to a J value equal to about 472. For
higher J values the dimension of the set can be gradually decreased.

5. COULOMB-NUCLEAR EXCITATION PROBABILITIES OF ^{40}Ar+^{238}U and ^{84}Kr+^{238}U

In this section the quantum-mechanical excitation probabilities [1],
calculated in the center-of-mass system, are presented for the multiple
Coulomb-nuclear excitation of ^{238}U induced by ^{40}Ar and ^{84}Kr up to high
spin states of the ground-state rotational band (GSB). Also, the proba-
bilities will be presented when pure Coulomb excitation is considered.

In Fig. 3, the probabilities for 286 MeV ^{40}Ar are plotted as a
function of the scattering angle Θ for the GSB-states up to the one with
$I^{\pi} = 14^{+}$. The optical potential parameters are: V = 73.0 MeV, W = 80.3
MeV, $r_v = r_w$ = 1.131 fm, r_c = 1.4 fm, and $a_v = a_w$ = 0.624 fm. The solid
curves show the probabilities for Coulomb-nuclear excitation (β_2^N = 0.237,
β_4^N = 0.067, $\beta_2^{C(1)}$ = 0.2121, $\beta_4^{C(1)}$ = 0.0667). The dashed curves represent
the result expected for pure Coulomb excitation. The figure shows that at
scattering angles smaller than the grazing angle Θ_{gr} of about 52^0, the
probabilities are completely determined by multiple Coulomb excitation.
At this angle, the interference between the Coulomb and nuclear inter-
actions begins to set in and corresponds to an orbital angular momentum
$\ell_{gr} \approx$ 200, given by the classical orbit relation $\ell = \eta\cot(\theta/2)$.
Furthermore, at angles $\Theta < \Theta_{gr}$, which correspond to orbits much larger
than ℓ_{gr}, the angular distribution for elastic scattering deviates consi-
derably from the typical Fresnel shape by falling below the Rutherford
cross section. The quarter-point angle, i.e., the scattering angle where
the summed probabilities for all final rotational states equals 1/4, is
about 70^0 and corresponds to an orbital angular momentum $\ell_{1/4} \approx$ 138.

Similar calculations of the excitation probabilities have been
performed with the same above-mentioned optical potential parameters for
340 MeV ^{40}Ar projectiles [15]. Comparing the probabilities, given in this
paper, with ours, it seems that the extrema in the 0^+, 2^+ and 4^+ probabi-
lity functions, occuring at smaller angles of course, have the same value
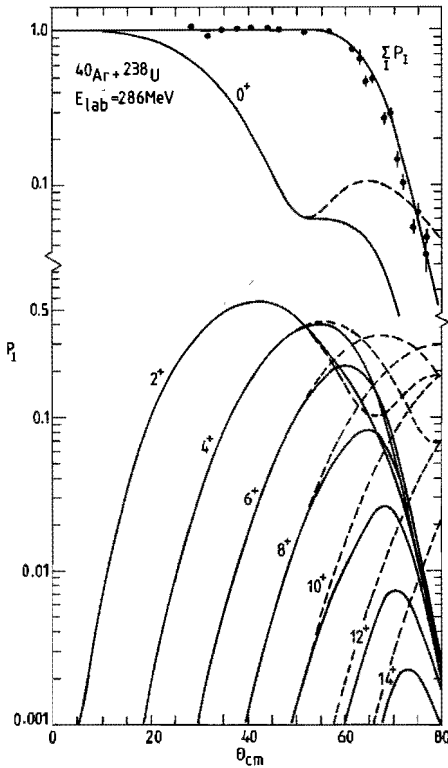
Fig. 3. The quantum-mechanical excitation probabilities P_I are plotted against the scattering angle Θ_{cm} for the target states up to $I^{\pi} = 14^{+}$. The solid curves show the probabilities for Coulomb-nuclear excitation. The parameter set is given in the text. The dashed curves indicate the result expected for pure Coulomb excitation.

in magnitude as our calculated values. However, the maxima of the 6^{+} and 8^{+} functions are about a factor of 1.8 and 4 smaller, respectively. Thus, the excitation probabilities for the high-lying members of the GSB in ^{238}U are larger for 286 MeV than for 340 MeV ^{40}Ar projectiles. This means that the interference between the Coulomb and nuclear interactions for high spin states probably can be investigated, at energies near the Coulomb barrier, most favourably.

The figure shows also the elastic scattering experimental data [22]. It is remarkable how they disagree with the elastic 0^{+} curve, while on the contrary the agreement with the curve of summed probabilities is worth mentioning. Apparently, the measurements do not represent elastic data only, but also quasi-elastic data from the low-lying members of the GSB. A precise measurement of the elastic scattering angular distribution of 90 MeV ^{18}O on ^{184}W has given indications for this [23].

In Figs. 4a and 4b, the excitation probabilities for 718 MeV ^{84}Kr are displayed for the GSB-states up to $I^{\pi} = 16^{+}$. The optical potential and

deformation parameters are given by (4.1) and (4.2), respectively. It is seen in these figures, that for scattering angles smaller than the grazing angle of about 37^0 the probabilities are completely determined by multiple Coulomb excitation. Coulomb-nuclear interference starts to set in at this angle which corresponds to $\ell_{gr} \approx 532$. The quarter-point angle is about 55^0 corresponding to $\ell_{1/4} \approx 342$. Large interference effects are seen in this case.

Relating to the behaviour of the probability functions in the Figs. 3 and 4 at near-grazing scattering angles where the Coulomb-nuclear inter-ference sets in, it can be noted that:

For most of the probability functions the initial Coulomb-nuclear interference is constructive (destructive) if the pure Coulomb excitation probability function for increasing scattering angles is approaching a minimum (maximum).

It is remarkable that this behaviour satisfies a general rule previously formulated for the behaviour of the excitation probability as a function of the projectile energy near the Coulomb barrier for backward scattering from a deformed rotor [24] and based upon a semiclassical model [17]. In this model, it is assumed that the nuclear interaction can be approxi-mated by a smooth complex potential which is largely real in the surface region.

These calculations show clearly that the excitation probabilities of excited states at scattering angles in the Coulomb-nuclear interference region can serve as sensitive probes to study peripheral processes at the deformed nuclear surface. This can be done very effectively with the method described in this paper [25]. When the S-matrix elements are calculated once for a full range of appropriately spaced J values, only those S-matrix elements with a J value corresponding to an orbital angular momentum between $\ell_{1/4} - \Delta\ell_{1/4}$ and ℓ_{gr}, have to be recaculated with a new value of the parameter set in order to fit the experimental data at scattering angles in the interference region. The value of $\Delta\ell_{1/4}$ can be chosen relatively small. The larger the absorption in the reaction at smaller than "quarter-point" distances, the smaller this value can be taken. Thus, in practice only a restricted number of J values is needed, as can be seen in figure 2 for ^{84}Kr + ^{238}U.
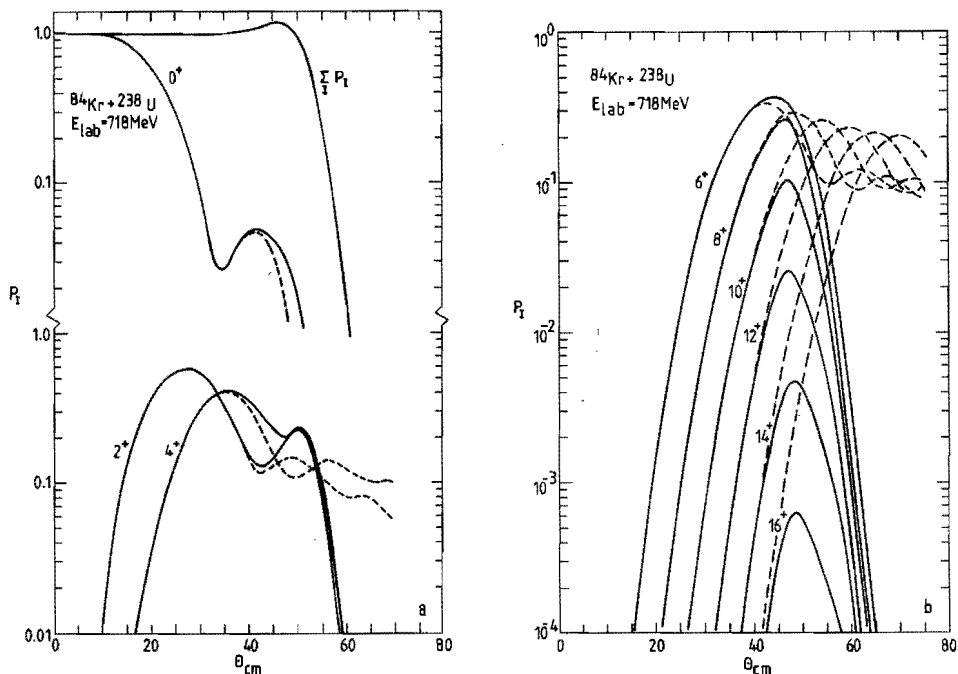
Fig. 4. (a)The quantum-mechanical excitation probabilities P_I are plotted against the scattering angle θ_{cm} for the low-lying GSB target states. The solid curves show the Coulomb-nuclear probabilities. The parameter set is given in the text. The dashed curves show the result expected for pure Coulomb excitation. Large interference effects are seen. (b) The same as (a), but now for the high-lying members of the GSB.

6. CONCLUSIONS AND FINAL REMARK

   To describe quantum mechanically multiple Coulomb-nuclear excitation in heavy-ion reactions, the set of coupled differential equations of the partial-wave radial solutions is rewritten in integral form. Decomposing these solutions into two basis functions the corresponding amplitudes of these functions satisfy a set of coupled integral equations. Expressing the basis functions in terms of appropriately chosen piecewise analytic reference solutions, the integrals appearing in this set can be evaluated analytically. The coupled set of amplitude equations is solved itera-tively. The efficiency of two iteration methods, the inward-outward and the sequential one, has been investigated for test cases dealing with

multiple Coulomb and nuclear excitation of ^{238}U by 286 MeV ^{40}Ar and 718 MeV ^{84}Kr up to high spin states of the ground-state rotational band. Padé approximants to the S-matrix elements were also included in both of the iteration methods. It turns out that the inward-outward iteration method converges much faster than the sequential one. In many cases, the inward-outward method does not need Padé acceleration at all, while the sequential method does. It even happens sometimes that convergent cases in the inward-outward method diverge in the sequential method aided by Padé approximants. This large difference in convergence may be explained by noting that in the inward-outward method the coupling between the amplitudes is retained during the iteration procedure, as opposed to the sequential method where the set of coupled equations is replaced by a set of "uncoupled inhomogeneous" equations. The latter are solved in a certain sequential order, treating the inhomogeneous terms as perturbations.

Our numerical studies of the excitation probabilities as a function of the scattering angle for the aforementioned heavy-ion reactions show that the probability functions of the members of the ground-state rotational band, satisfy a general rule at near-grazing angles, previously formulated for the excitation probability as a function of the energy near the Coulomb barrier for backward scattering from a deformed rotor.

Finally, we turn to a conclusion drawn by M. Rhoades-Brown et al. [8] in connection with the relative efficiency which they obtained for the sequential method plus Padé acceleration, compared to the method studied by us previously [1]. Based on estimates of time requirements for a case with 121 coupled equations (example 2 of Table I in Ref. [8]), which calculation was not yet attempted by them, they came to the conclusion that their approach should be some 200 times faster than the conventional method, while our approach is some 30 times faster than the conventional method. Related to this conclusion, the following should be noted:

1. The conventional method they used to compare their iteration results with, is based upon the Numerov multistep integration method, whereas the conventional method used in our comparison is based upon Gordon's piecewise analytic reference solutions method [26]. One integration step in this method includes many step sizes of a multistep integration method. In some circumstances, a considerable reduction of computation time (20 times for medium-weight ions and much more for heavy ions) can be obtained compared to a conventional multistep method.

2. They present estimates of time requirements for the sequential, as well as for the conventional multistep method. However, the number of couplings per equation is taken 9 for the former, whereas for the latter 121 couplings are taken into account. This seems incorrect: it overestimates the conventional method with a factor of about 13.

Therefore, our conclusion is that the way in which Rhoades-Brown et al. estimate the relative efficiency and which favours their method compared to ours, is disputable. It shows that the comparison of efficiencies of methods or approaches is a delicate question without running the corresponding codes on the same computer under the same conditions such as the required accuracy. We showed from practical test cases that our approach is very efficient [25].

REFERENCES

[1] L.D. Tolsma, Phys. Rev. C20(1979)592.

[2] R.G. Gordon, J. Chem. Phys. 51(1969)14;
R.G. Gordon, Quantum Scattering Using Piecewise Analytic Solutions, in: Methods in Computational Physics 10, Atomic and Molecular Scattering, edited by B. Alder, S. Fernbach and M. Rotenberg, (Academic, New York, 1971), p.81.

[3] K. Alder, F. Roesel and R. Morf, Nucl. Phys. A284(1977)145.

[4] M. Ichimura, M. Igarashi, S. Landowne, C.H. Dasso, B.S. Nilsson, R.A. Broglia and A. Winther, Phys. Lett. 67B(1977)129.

[5] J. Raynal, in Computing as a Language of Physics, edited by A. Salam (IAEA, Vienna, 1972), p. 292.

[6] J. Raynal, Phys. Rev. C23(1981)2571.

[7] M. Rhoades-Brown, M.H. Macfarlane and S.C. Pieper, Phys. Rev. C21(1980)2417.

[8] M. Rhoades-Brown, M.H. Macfarlane and S.C. Pieper, Phys. Rev. C21(1980)2436.

[9] W. Moon, Comput. Phys. Commun. 22(1981)411.

[10] J.J. Leunissen, Eindhoven University of Technology, Department of
     Physics, Internal Report No. VDF-NK-79/07 (1979).

[11] L.Gr. Ixaru, Comput. Phys. Commun. 20(1980)97.
     L.Gr. Ixaru, "Numerical Methods", D. Reidel Publishing Company,
     Dordrecht, 1984.

[12] L.D. Tolsma, to be published in Comput. Phys. Commun.

[13] L.D. Tolsma, Solving Coupled Equations by Iteration for Heavy Ion
     Collisions, Proc. Int. Conf. Nuclear Physics, Berkeley, 1(1980)637;

[14] L.D. Tolsma, Proc. Int Conf. Nuclear Physics, Florence, 1(1983)D170.

[15] A.J. Baltz, Phys. Rev. C25(1982)240.

[16] T. Tamura, Rev. Mod. Phys. 37(1965)679.

[17] M.W. Guidry, H. Massmann, R. Donangelo and J.O. Rasmussen,
     Nucl. Phys. A274(1976)183.

[18] W.N. Sams and D.J. Kouri, J. Chem. Phys. 51(1969)4809;
     W.N. Sams and D.J. kouri, J. Chem. Phys. 51(1969)4815.

[19] R. Vandenbosch, M.P. Webb, T.D. Thomas, S.W. Yates
     and A.M. Friedman, Phys. Rev. C13(1976)1893.

[20] L.D. Tolsma, J. Comput. Phys. 17(1975)384.

[21] N.M. Clarke, Comput. Phys. Commun. 27(1982)365.

[22] J.R. Birkelund, J.R. Huizenga, H. Freiesleben, K.L. Wolf, J.P. Unik
     and V.E. Viola Jr., Phys. Rev. C13(1976)133.

[23] C.E. Thorn, M.J. LeVine, J.J. Kolata, C. Flaum, R.D. Bond
     and J.C. Sens, Phys. Rev. Lett. 38(1977)384.

[24] M.W. Guidry, P.A. Butler, R. Donangelo, E. Grosse, Y. El Masri,
     I.Y. Lee, F.S. Stephens, R.M. Diamond, L.L. Riedinger, C.R. Bingham,
     A.C. Kahler, J.A. Vrba, E.L. Robinson and N.R. Johnson,
     Phys. Rev. Lett. 40(1978)1016.

[25] L.D. Tolsma, Comput. Phys. Commun. 37(1985)245;
     L.D. Tolsma, Solving Large Sets of Coupled Equations Iteratively by
     Vector Processing on the Cyber 205 Computer, in: Supercomputer
     Applications, edited by A.H.L. Emmen (North-Holland, Amsterdam,
     1985), p. 227.

[26] L.D. Tolsma, J. Comput. Phys. 17(1975)384.

RECURRENCE RELATIONS FOR COULOMB EXCITATION ELECTRIC MULTIPOLE RADIAL MATRIX ELEMENTS[*]

L.D. TOLSMA

Department of Physics, Eindhoven University of, Technology,

P.O.Box 513, Eindhoven, The Netherlands

PROGRAM SUMMARY

Nature of the physical problem

The radial Schrödinger equation which has to be solved for the quantum mechanical description of inelastic collisions between charged particles can be rewritten as an equivalent set of coupled integral equations. The partial wave radial function is written as a linear combination of two linearly independent basis functions with more or less slowly varying amplitudes. For large r values of the integration region or for high ℓ values of the orbital angular momentum these amplitudes consist of electric multipole radial matrix elements, i.e., integrals $I_{\ell,\ell'}^{(\lambda)}$ over a finite interval $[R_1, R_2]$ and with an integrand containing a product of the Coulomb wave functions $X_\ell(\eta, kr)$ and $Y_{\ell'}(\eta', k'r)$ and a form factor $r^{-\lambda-1}$, where $\lambda \geq 1$. Such integrals have to be determined for one or more radial intervals when solving the set of integral equations [1,2]. The calculation of the excitation probabilities for analysing experimental data needs the solution of the Schrödinger equation and, thus, the knowledge of these integrals for a few hundred or even thousand partial waves, especially, for heavy ion collisions.

Method of solution

Radial matrix elements $I_{\ell,\ell'}^{(\lambda)}$, of any multipolarity satisfy recurrence

relations. Diagonal ($\ell'=\ell$) and upper-diagonal ($\ell'=\ell+1$) matrix elements are calculated using an upward recursion, starting with four initial integrals. Each of these four initial values is obtained by a call to the subprogram CLMINT [3]. Using the diagonal and upper-diagonal matrix elements in their turn as initial values, the remaining lower and upper-diagonal matrix elements are calculated by a sidewards recursion with ℓ,ℓ' values for which $|\ell - \ell'| < \lambda$. The diagonal and upper-diagonal matrix elements can also be calculated by solving a pentadiagonal system of linear equations obtained by combining and rearranging two recurrence relations. Four boundary values of the radial matrix elements are required: two for low ℓ values and two for high ℓ values. Each of these four boundary values is also obtained by a call to CLMINT.

Restrictions on the complexity of the problem

If the recurrence relations of the radial matrix elements are used in an upward or downward recursion, then they are susceptible to error growth. This growth depends largely on the ratio of k and k'. The more this ratio differs from unity, the more the recurrence relations will lose their accuracy due to the cancellation of terms. This loss of accuracy is not encountered when two recurrence relations are combined and rearranged into a pentadiagonal system of linear equations which can be solved by standard methods.

Typical running time

The running time is mainly determined by the computation time for the initial or boundary radial matrix elements required by CLMINT, i.e., it depends on whether the radial matrix elements are calculated by an upward recursion or by solving a system of linear equations. The output of the test runs gives the processor time of both alternatives. The computation time for the initial or boundary radial matrix elements depends largely on the parameters and the lower limit R_1 [3]. These integrals are generated efficiently by CLMINT for parameters encountered in heavy ion scattering processes.

REFERENCES
[1] L.D. Tolsma, Phys. Rev. C20(1979)592.
[2] L.D. Tolsma, Comput. Phys. Commun. 37(1985)245.
[3] H.F. Arnoldus, Comput. Phys. Commun. 32(1984)421.

LONG WRITE-UP

1. INTRODUCTION

Inelastic scattering of charged particles from atoms and nuclei is an important tool for studying the properties of excited states. In general, the quantum-mechanical description of inelastic scattering processes with multiple excitation requires the numerical solution of the radial Schrödinger equation, i.e., a set of coupled linear second-order differential equations. This set can be rewritten as an equivalent set of coupled integral equations [1-6]. In this integral formalism, the partial wave radial function is written as a linear combination of two basis functions with coefficients or amplitudes containing the integrals. Both linearly independent basis functions are the solutions of the decoupled Schrödinger equation that can be solved for some form of the potential [5,8,9]. These basis functions oscillate within the classically allowed region of the integration range which, in general, occurs rapidly depending on the energy of the incoming particle. On the contrary, the amplitudes, satisfying a set of coupled integral equations, vary more or less slowly in this region.

Both electromagnetic and nuclear interactions play important roles in the study of the inelastic scattering of light and heavy ions from nuclei with projectile energies comparable to the Coulomb barrier. However, the range of the electromagnetic interaction, especially for low multipolarities, is much longer than the range of the nuclear interaction. Therefore, the form of the potential for large r values corresponds to the Coulomb interaction only and the basis functions can be written here in terms of the Coulomb wave functions. This holds for high ℓ values of the orbital angular momentum too. Under these circumstances, solution of the set of coupled integral equations on an interval $[R_1, R_2]$ requires the determination of integrals of the form

$$I_{\ell,\ell'}^{(\lambda)} = \int_{R_1}^{R_2} X_\ell(\eta,kr)\, Y_{\ell'}(\eta',k'r)\, \frac{dr}{r^{\lambda+1}} , \qquad (1.1)$$

where $X_\ell(\eta,kr)$ and $Y_{\ell'}(\eta',k'r)$ denote the regular and/or irregular Coulomb wave functions and λ corresponds to the electric multipole moment. Thus, there are four possible combinations. The orbital angular momenta ℓ and ℓ' refer to the entrance and exit channels, respectively. A similar convention applies to the asymptotic wave number of the relative

motion k and to the Sommerfeld parameter η. The vector addition rule imposes the condition that $|\ell - \ell'| \leqslant \lambda$. The integrals (1.1) are called the electric 2^{λ}-pole radial matrix elements or Coulomb integrals. Such integrals have to be determined for one or more radial intervals when solving the set of integral equations. They play a role in DWBA calculations too. Then $X_{\ell}(\eta,kr)$ and $Y_{\ell'}(\eta',k'r)$ correspond to the regular Coulomb wave functions and the interval boundaries are: $R_1 = 0$, $R_2 = \infty$.

In order to take all the strength of the electromagnetic interaction into account, the following requirements should be fulfilled:

1. In the case of multiple excitations, in general, many channels should be considered.

2. The integration of the set of coupled equations should be carried out for long distances.

3. Many partial waves should be included when calculating the scattering amplitudes.

The heavier the charged particles in the scattering process, the larger will be the set of coupled equations, the longer will be the integration distances and the larger will be the number of partial waves. Requirement (1) can be met by using iteration procedures for solving the set of coupled integral equations [2-7]. Requirement (2) can be fulfilled since, without much effort, integrals (1.1) with large boundary values R_1 and R_2 for large intervals can be determined [10-13]. The problem of the large number of partial waves can be overcome by using recurrence relations that the integrals (1.1) satisfy [14-16].

A primary aim of this paper is to provide a program that calculates the radial matrix elements for any multipolarity by means of recurrence relations in a numerically stable and reliable manner. The recurrence relations used are presented in section 2. They need initial values of the integrals which in our case are obtained by a call to the subprogram CLMINT [13]. This subprogram efficiently generates integrals (1.1) for k and η values that are commonly encountered in heavy ion scattering problems. It must be stressed that the initial values obtained by another method can be used too [16]. In section 3, special attention is paid to the numerical stability of the recurrence relations, since they are susceptible to error growth due to the finite representation of numbers in the computer (rounding errors). It seems that this stability is largely dependent on the ratio of the wave numbers k and k' in (1.1). The more this ratio deviates from unity, the more unstable are the

relations. Section 4 describes a method for computing the integrals in cases in which the ratio of k and k' differs substantially from unity. This method is based upon the solution of a set of linear equations.

2. RECURRENCE RELATIONS FOR THE RADIAL MATRIX ELEMENTS

Using the recurrence relations for the Coulomb wave functions given by Eqs. (14.2.1 – 14.2.3) of Ref. [17] and partial integration of (1.1), many recurrence relations for the radial matrix elements can be derived [10,11,16], among which three, four and five-term relationships. We start with the following five-term one:

$$
\frac{(\ell+\ell'-\lambda)}{(2\ell'+1)}(\ell+1)^2 \left[\ell^2+\eta^2\right]^{\frac{1}{2}} \left[\ell'^2+\eta'^2\right]^{\frac{1}{2}} I^{(\lambda)}_{\ell-1,\ell'-1}
$$

$$
+ \eta'(\ell+1)^2\left[\ell^2+\eta^2\right]^{\frac{1}{2}} \left(\frac{\ell'}{\ell} - \frac{(\ell-\lambda)}{(\ell'+1)}\right) I^{(\lambda)}_{\ell-1,\ell'}
$$

$$
- \left\{\eta\eta'\left(\frac{\ell'}{\ell}(\ell+1)^2+\ell\ell'\frac{(\ell+1)^2(2\ell+1)}{(\ell'+1)^2(2\ell'+1)}\right) + \ell\ell'(\ell+1)^2\left(\frac{\eta}{\eta'}\frac{(2\ell+1)}{(2\ell'+1)}+\frac{\eta'}{\eta}\right)\right\} I^{(\lambda)}_{\ell,\ell'}
$$

$$
+ \eta\ell'\frac{(\ell+1)(2\ell+1)}{(\ell'+1)(2\ell'+1)} \left[(\ell'+1)^2+\eta'^2\right]^{\frac{1}{2}} \left(\frac{\ell(\ell+1)}{(\ell'+1)} - (\ell'+1+\lambda)\right) I^{(\lambda)}_{\ell,\ell'+1}
$$

$$
+ \ell\ell'\frac{(\ell+\ell'+2+\lambda)(\ell+1)}{(2\ell'+1)(\ell'+1)} \left[(\ell+1)^2+\eta^2\right]^{\frac{1}{2}} \left[(\ell'+1)^2+\eta'^2\right]^{\frac{1}{2}} I^{(\lambda)}_{\ell+1,\ell'+1}
$$

$$
= \frac{\ell'(\ell+1)^2}{k'} \left[\ell^2+\eta^2\right]^{\frac{1}{2}} J^{(\lambda)}_{\ell-1,\ell'} - \frac{\ell\ell'(\ell+1)^2(2\ell+1)}{k\,(\ell'+1)(2\ell'+1)} \left[(\ell'+1)^2+\eta'^2\right]^{\frac{1}{2}} J^{(\lambda)}_{\ell,\ell'+1},
$$

$$(2.1)$$

where the J's in the inhomogeneous terms are given by:

$$
J^{(\lambda)}_{\ell,\ell'} = \left.\frac{X_\ell(\eta,kr)\,Y_{\ell'}(\eta',k'r)}{r^{\lambda+1}}\right|_{R_1}^{R_2}.
$$

$$(2.2)$$

Using (2.1) with $\ell' = \ell$, gives rise to a recurrence relation between five integrals of the form:

$$
\frac{(2\ell-\lambda)(\ell+1)^2}{(2\ell+1)} \left[\ell^2+\eta^2\right]^{\frac{1}{2}}\left[\ell^2+\eta'^2\right]^{\frac{1}{2}} I^{(\lambda)}_{\ell-1,\ell-1} + \eta'(\lambda+1)(\ell+1)\left[\ell^2+\eta^2\right]^{\frac{1}{2}} I^{(\lambda)}_{\ell-1,\ell}
$$

$$
- \left\{\eta\eta'\left(\ell^2+(\ell+1)^2\right)+\ell^2(\ell+1)^2\left(\frac{\eta}{\eta'}+\frac{\eta'}{\eta}\right)\right\} I^{(\lambda)}_{\ell,\ell} - \eta(\lambda+1)\ell\left[(\ell+1)^2+\eta'^2\right]^{\frac{1}{2}} I^{(\lambda)}_{\ell,\ell+1}
$$

$$
+ \frac{(2\ell+2+\lambda)\ell^2}{(2\ell+1)}\left[(\ell+1)^2+\eta^2\right]^{\frac{1}{2}}\left[(\ell+1)^2+\eta'^2\right]^{\frac{1}{2}} I^{(\lambda)}_{\ell+1,\ell+1}
$$

$$
= \frac{\ell(\ell+1)^2}{k'} \left[\ell^2+\eta^2\right]^{\frac{1}{2}} J^{(\lambda)}_{\ell-1,\ell} - \frac{\ell^2(\ell+1)}{k}\left[(\ell+1)^2+\eta'^2\right]^{\frac{1}{2}} J^{(\lambda)}_{\ell,\ell+1} . \qquad (2.3a)
$$

By symmetry, ℓ can be interchanged with ℓ', η with η' and k with k' in (2.1) to yield a recurrence relation which is used with $\ell' = \ell+1$. Multiplying the relationship obtained by $(2\ell+1)/(\ell(\ell+2)^2)$ to give a recurrence relation of the form:

$$\frac{(2\ell+1-\lambda)}{\ell}[\ell^2+\eta^2]^{\frac{1}{2}}[(\ell+1)^2+\eta'^2]^{\frac{1}{2}} I_{\ell-1,\ell}^{(\lambda)} + \frac{\eta(\lambda-1)(2\ell+1)}{\ell(\ell+1)}[(\ell+1)^2+\eta'^2]^{\frac{1}{2}} I_{\ell,\ell}^{(\lambda)}$$

$$- \left\{4\eta\eta'+(\ell+1)\left((2\ell+1)\frac{\eta}{\eta'}+(2\ell+3)\frac{\eta'}{\eta}\right)\right\} I_{\ell,\ell+1}^{(\lambda)}$$

$$- \frac{\eta'(\lambda-1)(2\ell+3)}{(\ell+1)(\ell+2)}[(\ell+1)^2+\eta^2]^{\frac{1}{2}} I_{\ell+1,\ell+1}^{(\lambda)}$$

$$+ \frac{(2\ell+3+\lambda)}{(\ell+2)}[(\ell+1)^2+\eta^2]^{\frac{1}{2}}[(\ell+2)^2+\eta'^2]^{\frac{1}{2}} I_{\ell+1,\ell+2}^{(\lambda)}$$

$$= \frac{(2\ell+1)}{k}[(\ell+1)^2+\eta'^2]^{\frac{1}{2}} J_{\ell,\ell}^{(\lambda)} - \frac{(2\ell+3)}{k'}[(\ell+1)^2+\eta^2]^{\frac{1}{2}} J_{\ell+1,\ell+1}^{(\lambda)} . \qquad (2.3b)$$

The integrals in the recurrence relations (2.3a) and (2.3b) are represented pictorially by the dots (•) in the Figs. 1a and 1b, respectively. Starting with four initial values of the integrals, the diagonal ($\ell'=\ell$) and upper-diagonal ($\ell'=\ell+1$) values are determined by upward recursion.
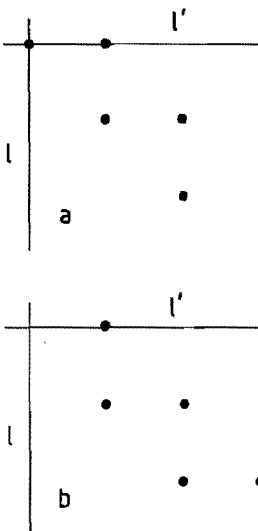
Fig. 1. Pictorial represen-
tation of the integrals in
Eqs. (2.3a and b). The ori-
gin is chosen arbitrarily.
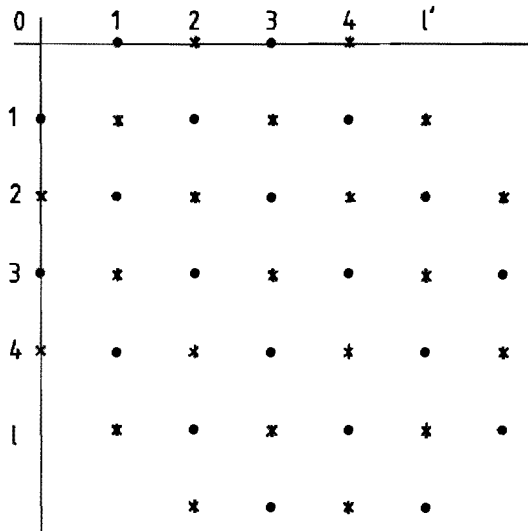
Fig. 2. Pictorial representation of
the integrals for $\lambda = 1,3$ (dots) and
for $\lambda = 2,4$ (stars) under the
condition of $\lambda-|\ell-\ell'| \geq 0$ and even.

However, the vector addition rule requires in general, that the integers $\lambda - |\ell - \ell'|$ have to be ≥ 0 and, in our applications, also even. In Fig. 2 these integrals are represented pictorially by dots (•) for odd λ-values and by stars (*) for even λ-values. To be more specific, in the figure for $\lambda = 1$, one lower and one upper-dotdiagonal are obtained; for $\lambda = 2$, the main, one lower and one upper-stardiagonal, for $\lambda = 3$, two lower and two upper-dotdiagonals, for $\lambda = 4$, the main, two lower and two upper-stardiagonals, etc. To generate these integrals a sidewards recurrence scheme has been set up using the integrals on the diagonal and upper-diagonal as the initial values, up to ℓ and ℓ' values for which $|\ell - \ell'| = \lambda$ at the edge of the band (see Fig. 2). This will be called the λ-inplane recursion, in contrast to λ-up recursion which will not be considered here.

When calculating the integrals on the lower-diagonal ($\ell' = \ell - 1$), use has been made of the relationship:

$$\frac{k'\lambda}{(2\ell+1)\ell}\left[\ell^2 + \eta'^2\right]^{\frac{1}{2}} I^{(\lambda)}_{\ell,\ell-1} - \frac{\eta k}{\ell}\left(\frac{\ell+\lambda}{\ell+1} - 1\right) I^{(\lambda)}_{\ell,\ell} - \frac{k}{\ell}\left[\ell^2+\eta^2\right]^{\frac{1}{2}} I^{(\lambda)}_{\ell-1,\ell}$$

$$+ \frac{k'(2\ell+1+\lambda)}{(2\ell+1)(\ell+1)}\left[(\ell+1)^2 + \eta'^2\right]^{\frac{1}{2}} I^{(\lambda)}_{\ell,\ell+1} = -J^{(\lambda)}_{\ell,\ell} \qquad\qquad \underset{\ell,\ell}{*\!-\!\!-\!\!\bullet} \qquad (2.4a)$$

and

$$\frac{k\lambda}{(2\ell-1)\ell}\left[\ell^2+\eta^2\right]^{\frac{1}{2}} I^{(\lambda)}_{\ell,\ell-1} + \frac{\eta k}{\ell}\left(\frac{\ell-\lambda}{\ell-1} - 1\right) I^{(\lambda)}_{\ell-1,\ell-1} + \frac{k'}{\ell}\left[\ell^2+\eta'^2\right]^{\frac{1}{2}} I^{(\lambda)}_{\ell-1,\ell}$$

$$- \frac{k(2\ell-1-\lambda)}{(2\ell-1)(\ell-1)}\left[(\ell-1)^2+\eta^2\right]^{\frac{1}{2}} I^{(\lambda)}_{\ell-2,\ell-1} = -J^{(\lambda)}_{\ell-1,\ell-1} \;\cdot \qquad \underset{\ell-1,\ell-1}{\big|\!\bullet} \quad (2.4b)$$

The integrals below the lower-diagonal can be determined by a relationship of the form:

$$\frac{k(\ell-\ell'+\lambda)}{(2\ell+1)(\ell+1)}\left[(\ell+1)^2+\eta^2\right]^{\frac{1}{2}} I^{(\lambda)}_{\ell+1,\ell'} + \left(\frac{\eta k(\ell'+1-\lambda)}{\ell(\ell+1)} - \frac{\eta'k'}{(\ell'+1)}\right) I^{(\lambda)}_{\ell,\ell'}$$

$$- \frac{k(\ell+\ell'+1-\lambda)}{(2\ell+1)\ell}\left[\ell^2+\eta^2\right]^{\frac{1}{2}} I^{(\lambda)}_{\ell-1,\ell'}$$

$$+ \frac{k'}{(\ell'+1)}\left[(\ell'+1)^2+\eta'^2\right]^{\frac{1}{2}} I^{(\lambda)}_{\ell,\ell'+1} = -J^{(\lambda)}_{\ell,\ell'} \;\cdot \qquad\qquad \underset{\ell,\ell'}{\big|\!\bullet} \qquad (2.5)$$

The integrals above the upper-diagonal are obtained by a version of this relationship in which ℓ is exchanged with ℓ', k with k' and η with η'.

Finally, we note that Eqs. (2.3a) and (2.3b) for $\lambda = 1$ give Raynal's formulae (37a) and (37b) of Ref. [16], respectively [18].

3. ON THE STABILITY OF THE RECURRENCE RELATIONS

The recurrence relations that satisfy the Coulomb wave functions in the integrand of the Coulomb integrals are only accurate if the quantities obtained from them do not decrease monotonously; they are then said to be stable. Coulomb wave functions change their behaviour at the turning point given by

$$\rho_T = \eta + \left[\eta^2 + \ell(\ell+1)\right]^{\frac{1}{2}}. \tag{3.1}$$

For $kr < \rho_T$, the regular Coulomb wave function decreases, while the irregular Coulomb wave function increases, for increasing ℓ. Thus a downward recursion is stable for the former and an upward recursion for the latter. For $kr > \rho_T$, the functions are always of the order of unity and, therefore, both recursions are stable.

These stability considerations hold for the recurrence relations of the Coulomb integrals too. However, it seems that the stability of these relations depends largely upon the ratio of k and k' as well. The more this ratio differs from unity, the more the recurrence relations are likely to lose accuracy due to the cancellation of terms. Equation (2.3b) can be used for $\lambda = 1$ to investigate the stability as it depends on k/k'; it is written as:

$$(2\ell+4)\, S_\ell(\eta)\, S_{\ell+1}(\eta')\, I_{\ell+1} - \left[(2\ell+1)\frac{k'}{k}S_\ell^2(\eta') + (2\ell+3)\frac{k}{k'}S_\ell^2(\eta)\right] I_\ell$$

$$+ 2\ell\, S_{\ell-1}(\eta)\, S_\ell(\eta')\, I_{\ell-1} = -\frac{(2\ell+3)}{k'}\, S_\ell(\eta)\, J_{\ell+1} + \frac{(2\ell+1)}{k}\, S_\ell(\eta')\, J_\ell \,, \tag{3.2}$$

where

$$S_\ell(\eta) \equiv \left[1 + \frac{\eta^2}{(\ell+1)^2}\right]^{\frac{1}{2}}, \qquad I_\ell \equiv I_{\ell,\ell+1}^{(1)} \quad \text{and} \quad J_\ell \equiv J_{\ell,\ell}^{(1)}. \tag{3.3}$$

It is noted that (2.3b) is decoupled from (2.3a) for $\lambda = 1$.

Consider (3.2) for $\ell \gg \eta$ and η' because, in general, stability problems occur for large ℓ values. Then, this equation can be approximated by

$$I_{\ell+1} - \alpha\, I_\ell + I_{\ell-1} = -\frac{1}{k'}\, J_{\ell+1} + \frac{1}{k}\, J_\ell \,, \tag{3.4}$$

where

$$\alpha = \frac{k'}{k} + \frac{k}{k'} \ .$$ (3.5)

The general solution of (3.4) is a linear combination of any pair of linearly independent homogeneous solutions and a particular solution of the inhomogeneous difference equation. The homogeneous part of (3.4), namely:

$$I_{\ell+1} - \alpha I_\ell + I_{\ell-1} = 0$$ (3.6)

can be recognized as a Poincaré difference equation of order 2 with [19]

$$\Phi(\rho) = \rho^2 - \alpha\rho + 1$$ (3.7)

as its characteristic polynomial. Let ρ_1 and ρ_2 be the roots of $\Phi(\rho) = 0$, then

$$\rho_{1,2} = \frac{\alpha}{2} \pm \left\{ \left(\frac{\alpha}{2}\right)^2 - 1 \right\}^{\frac{1}{2}}.$$ (3.8)

The general solution of (3.6) is of the form

$$I_\ell = c_1 \rho_1^\ell + c_2 \rho_2^\ell \ ,$$ (3.9)

where c_1 and c_2 are determined from the initial conditions, e.g., the values of I_0 and I_1. Substituting $\alpha = e^\theta + e^{-\theta}$ in (3.8), gives three different cases depending on the magnitude of α relative to 2 [20]:

$$I_\ell = \begin{cases} \left[\dfrac{I_1 - I_0 e^{-\theta}}{2\sinh(\theta)}\right] e^{\ell\theta} - \left[\dfrac{I_1 - I_0 e^{\theta}}{2\sinh(\theta)}\right] e^{-\ell\theta} \ , & \alpha > 2, \quad 2\cosh(\theta) = \alpha \\ & \hspace{4cm} (3.10a) \\ \ell I_1 - (\ell-1) I_0 & , \quad \alpha = 2 \hspace{1cm} (3.10b) \\ \left[\dfrac{I_1 - I_0 e^{-i\theta}}{2\sin(\theta)}\right] e^{i\ell\theta} - \left[\dfrac{I_1 - I_0 e^{i\theta}}{2\sin(\theta)}\right] e^{-i\ell\theta} \ , & \alpha < 2, \quad 2\cos(\theta) = \alpha \\ & \hspace{4cm} (3.10c) \end{cases}$$

A particular solution of (3.4) can be constructed by upward recursion, putting I_0 and I_1 equal to zero as starting values. It obtains the same structure as the homogeneous solution. Since α is given by (3.5), it obtains a value greater than two for $k' \neq k$. Consequently, the homogeneous, as well as this particular solution, has for $\ell \gg \eta, \eta'$ an exponential behaviour. The greater $\theta = \text{arccosh}(\alpha/2)$, the faster they will increase.

TABLE 1

$$\int_{R_1}^{R_2} F_\ell(\eta, kr) \frac{1}{r^2} F_{\ell+1}(\eta', k'r)dr \quad \text{calculated by upward recursion with}$$

$$k = 20.2, \quad k' = 20.0 \text{ fm}^{-1}, \quad \alpha = 2.0000990, \quad \theta = 0.0099503,$$

$$\eta' = 100, \quad R_1 = 50, \quad R_2 = 1000 \text{ fm}$$

ℓ	Homogeneous solution (3.2)	Particular solution (3.2)	Inhomogeneous solution (3.2)	Calculated by CLMINT
0				.76025184(-03)
1				.75465483(-03)
2	.74898849(-03)	-.14030570(-07)	.74897446(-03)	.74897446(-03)
3	.74325684(-03)	-.34597983(-07)	.74322224(-03)	.74322224(-03)
4	.73746395(-03)	-.49608806(-07)	.73741434(-03)	.73741434(-03)
10	.70164788(-03)	.15848483(-05)	.70323272(-03)	.70323272(-03)
50	.46639846(-03)	.10025890(-03)	.56665735(-03)	.56665734(-03)
100	.29395997(-03)	.27920531(-03)	.57316528(-03)	.57316528(-03)
150	.24557573(-03)	.44972935(-03)	.69530507(-03)	.69530506(-03)
200	.27205249(-03)	.56121168(-03)	.83326417(-03)	.83326416(-03)
250	.35652820(-03)	.56398933(-03)	.92051754(-03)	.92051752(-03)
300	.50617154(-03)	.44030855(-03)	.94648008(-03)	.94648006(-03)
350	.74653404(-03)	.11715096(-03)	.86368500(-03)	.86368496(-03)
400	.11239398(-02)	-.48828549(-03)	.63565430(-03)	.63565423(-03)
450	.17142789(-02)	-.14171720(-02)	.29710690(-03)	.29710679(-03)
500	.26390403(-02)	-.27765884(-02)	-.13754809(-03)	-.13754825(-03)
550	.40917620(-02)	-.46639718(-02)	-.57220985(-03)	-.57315793(-03)
600	.63807262(-02)	-.72549701(-02)	-.87424384(-03)	-.87459489(-03)
650	.99975505(-02)	-.10883732(-01)	-.88618107(-03)	-.88618168(-03)
700	.15727328(-01)	-.16196527(-01)	-.46919919(-03)	-.46920015(-03)
750	.24825585(-01)	-.24527402(-01)	.29818368(-03)	.29818216(-03)
800	.39302831(-01)	-.38382541(-01)	.92028946(-03)	.92028706(-03)
850	.62382496(-01)	-.62012538(-01)	.36995777(-03)	.36995344(-03)

This will be illustrated with calculations for the different solutions of (3.2). The results are presented in Tables 1 and 2. The first columns of these tables contain the homogeneous solution of (3.2) for $\alpha = 2.0000990$ and $\alpha = 2.0090909$, respectively. (The numbers in parentheses denote the

TABLE 2

$$\int_{R_1}^{R_2} F_\ell(\eta,kr) \frac{1}{r^2} F_{\ell+1}(\eta',k'r)dr \quad \text{calculated by upward recursion with}$$

$$k = 22, \quad k' = 20 \text{ fm}^{-1}, \quad \alpha = 2.0090909, \quad \theta = 0.0953102,$$

$$\eta' = 100, \quad R_1 = 50, \quad R_2 = 1000 \text{ fm}$$

ℓ	Homogeneous solution (3.2)	Particular solution (3.2)	Inhomogeneous solution (3.2)	Calculated by CLMINT
0				.92563155(-04)
1				.92672150(-04)
2	.92776701(-04)	-.22888868(-07)	.92753812(-04)	.92753812(-04)
3	.92879707(-04)	-.53846401(-07)	.92825860(-04)	.92825859(-04)
4	.92984066(-04)	-.72114109(-07)	.92911952(-04)	.92911948(-04)
10	.93800222(-04)	.17600872(-05)	.95560309(-04)	.95560284(-04)
50	.15025824(-03)	-.96979881(-04)	.53278363(-04)	.53276911(-04)
100	.10189443(-02)	-.11192354(-02)	-.10029114(-03)	-.10029025(-03)
150	.19771036(-01)	-.19669954(-01)	.10108267(-03)	.10109828(-03)
200	.72225574(00)	-.72235723(00)	-.10148861(-03)	-.10092014(-03)
250	.38020759(02)	-.38020709(02)	.50218758(-04)	.80148920(-04)
300	.24939521(04)	-.24939542(04)	-.20441507(-02)	-.80882462(-04)
350	.18823517(06)	-.18823531(06)	-.14810279(00)	.78088342(-04)
400	.15613038(08)	-.15613051(08)	-.12290854(02)	-.91111798(-04)
450	.13837781(10)	-.13837792(10)	-.10893259(04)	.10558075(-03)
500	.12871636(12)	-.12871647(12)	-.10132700(06)	-.70596447(-04)
550	.12415805(14)	-.12415814(14)	-.97738638(07)	-.17157634(-04)
600	.12316249(16)	-.12316258(16)	-.96954921(09)	.98012132(-04)
650	.12490099(18)	-.12490108(18)	-.98323489(11)	.50702183(-04)
700	.12892791(20)	-.12892802(20)	-.10149353(14)	.30547595(-04)
750	.13502195(22)	-.13502206(22)	-.10629083(16)	.78447955(-04)
800	.14310477(24)	-.14310488(24)	-.11265372(18)	.48430286(-04)
850	.15319781(26)	-.15319793(26)	-.12059907(20)	-.48633213(-04)

powers of 10 by which the preceding numbers have to be multiplied.) This solution has been obtained by upward recursion of the homogeneous part of (3.2) with the integrals I_0 and I_1 as starting values. They show a monotonous behaviour. The second columns of both tables contain the

particular solution, obtained by upward recursion of (3.2) with I_0 and I_1 equal to zero as starting values. They show a monotonous behaviour too. The third columns contain the inhomogeneous solution of (3.2) obtained by summation of the homogeneous and the particular solutions.   The fourth columns contain the values of the Coulomb integrals calculated by a call on CLMINT. They are used here as a reference for the correct solution. Their accuracy, for the lower ℓ values, is to seven figures at least and, for the higher ones, about six figures [13].

Comparison of the third and fourth columns of Table 1, shows that, for $\alpha = 2.0000990$, the solution obtained by upward recursion is stable up to a maximum ℓ value equal to 850, demanding an accuracy of at least five figures. The same applies for smaller α values. However, for $\alpha = 2.0090909$, a similar correspondance only exists between the third and fourth columns of Table 2 up to a maximum ℓ value equal to about 150. Therefore, the conclusion can be drawn that the more α differs from two, the sooner accuracy is lost due to rounding errors in the summation of the homogeneous and the particular solutions. Although the accuracy of these solutions themselves is quite satisfactory, their tendency to become equal in magnitude with an opposite sign and their finite representation in the computer causes a loss of accuracy of the inhomogeneous solution. This is clearly shown by the first and second columns and from the result of their summation in the third column of Table 2. We note that, since the general solution has an oscillatory behaviour, as seen in the fourth columns of Tables 1 and 2, also, since α is always greater than two, this loss of accuracy will not only occur with upward recursion but with downward recursion as well.

It is not difficult to see that the above-mentioned maximum ℓ values depend on the accuracy of the initial integrals too, with which the recursion starts. The greater this accuracy, the larger these ℓ values will be.

In this section, the dependence of stability on the ratio k/k' has been investigated using a special recurrence relation for $\lambda = 1$. However, we believe that this dependence is similar for relations like those in Eqs. (2.3), (2.4) and (2.5), i.e., that it is a general feature of the present recurrence relations.

In the next section, a stable recurrence procedure has been developed whose stability is not dependent on the value of α.

4. A STABLE RECURRENCE PROCEDURE

In order to develop a stable algorithm, the recurrence relations (2.3a) and (2.3b) will be written in the following condensed form in which the superscript (λ) is suppressed

$$a_\ell I_{\ell-1,\ell-1} + s_\ell I_{\ell-1,\ell} + b_\ell I_{\ell,\ell} + t_\ell I_{\ell,\ell+1} + c_\ell I_{\ell+1,\ell+1} = y_\ell \quad (4.1a)$$

$$p_\ell I_{\ell-1,\ell} + d_\ell I_{\ell,\ell} + q_\ell I_{\ell,\ell+1} + e_\ell I_{\ell+1,\ell+1} + r_\ell I_{\ell+1,\ell+2} = z_\ell \quad (4.1b)$$

Comparing these expressions with Eqs. (2.3a) and (2.3b), respectively, will define the coefficients and the inhomogeneous terms. Instead of solving an initial value problem by upward or downward recursion, a boundary value problem can be set up to find the solution of (4.1). This requires the solution of a pentadiagonal system of linear equations

$$
\begin{bmatrix}
b_1 & t_1 & c_1 & & & & \\
d_1 & q_1 & e_1 & r_1 & & \text{\Large 0} & \\
a_2 & s_2 & b_2 & t_2 & c_2 & & \\
 & p_2 & d_2 & q_2 & e_2 & r_2 & \\
 & & \cdot & \cdot & \cdot & \cdot & \cdot \\
 & & & \cdot & \cdot & \cdot & \cdot & \cdot \\
 & \text{\Large 0} & & & a_L & s_L & b_L & t_L \\
 & & & & & p_L & d_L & q_L
\end{bmatrix}
\begin{bmatrix}
I_{1,1} \\
I_{1,2} \\
I_{2,2} \\
I_{2,3} \\
\cdot \\
\cdot \\
\cdot \\
I_{L,L} \\
I_{L,L+1}
\end{bmatrix}
=
\begin{bmatrix}
y_1 - a_1 I_{0,0} & -s_1 I_{0,1} \\
z_1 & -p_1 I_{0,1} \\
I_{2,2} \\
I_{2,3} \\
\cdot \\
\cdot \\
y_L - c_L I_{L+1,L+1} \\
z_L - e_L I_{L+1,L+1} - r_L I_{L+1,L+2}
\end{bmatrix}
$$

$$(4.2)$$

This solution can be produced by a standard method provided by the NAG-library, for example. The required boundary integrals $I_{0,0}$, $I_{0,1}$, $I_{L+1,L+1}$ and $I_{L+1,L+2}$ are calculated by a call on the subroutine CLMINT.

This procedure is very stable, even for extreme k/k' ratios. However, it is considerably more computer-time consuming than the upward recursion, mainly due to the need to determine the boundary integrals with high ℓ values. The results of a calculation such as this are mentioned in Tables 3a and 3b. The first columns of these tables contain the solution of the set of linear equations (4.2) for $\alpha = 2.0000990$ and $\alpha = 2.0090909$, respectively. The second columns correspond to the fourth columns of

TABLE 3

$$\int_{R_1}^{R_2} F_\ell(\eta, kr) \frac{1}{r^2} F_{\ell+1}(\eta', k'r)dr$$ calculated by solving a pentadiagonal

system of linear equations with

a) $k = 20.2$, $k' = 20.0$ fm^{-1},   b) $k = 22$, $k' = 20$ fm^{-1},

   $\alpha = 2.0000990$, $\theta = 0.0099503$, $\alpha = 2.0090909$, $\theta = 0.0953102$,

   $\eta' = 100$, $R_1 = 50$, $R_2 = 1000$ fm $\eta' = 100$, $R_1 = 50$, $R_2 = 1000$ fm

ℓ	solution of system (4.2)	Calculated by CLMINT	solution of system (4.2)	Calculated by CLMINT
0		.76025184(-03)		.92563155(-04)
50	.56665735(-03)	.56665734(-03)	.53278469(-04)	.53276911(-04)
100	.57316527(-03)	.57316528(-03)	-.10029034(-03)	-.10029025(-03)
150	.69530506(-03)	.69530506(-03)	.10109823(-03)	.10109828(-03)
200	.83326415(-03)	.83326416(-03)	-.10092005(-03)	-.10092014(-03)
250	.92051751(-03)	.92051752(-03)	.80149136(-04)	.80148920(-04)
300	.94648005(-03)	.94648006(-03)	-.80882976(-04)	-.80882462(-04)
350	.86368495(-03)	.86368496(-03)	.78087827(-04)	.78088342(-04)
400	.63565422(-03)	.63565423(-03)	-.91112025(-04)	-.91111798(-04)
450	.29710678(-03)	.29710679(-03)	.10558073(-03)	.10558075(-03)
500	-.13754827(-03)	-.13754825(-03)	-.70596446(-04)	-.70596447(-04)
550	-.57221013(-03)	-.57315793(-03)	-.17157216(-04)	-.17157634(-04)
600	-.87424428(-03)	-.87459489(-03)	.98012135(-04)	.98012132(-04)
650	-.88618176(-03)	-.88618168(-03)	.50702227(-04)	.50702183(-04)
700	-.46920028(-03)	-.46920015(-03)	.30547687(-04)	.30547595(-04)
750	.29818195(-03)	.29818216(-03)	.78447997(-04)	.78447955(-04)
800	.92028673(-03)	.92028706(-03)	.48430491(-04)	.48430286(-04)
850		.36995344(-03)		-.48633213(-04)

Tables 1 and 2 and they are used as the reference solutions. The upper
boundary integrals $I_{L+1,L+1}$ and $I_{L+1,L+2}$ are calculated for $L = 849$.
Comparing columns 1 and 2 of these tables, suggests that the present
procedure of solving a set of linear equations will yield Coulomb
integrals with an accuracy corresponding to the accuracy of the upper
boundary integrals; i.e., an accuracy corresponding to five to six

decimal places. This accuracy does not depend upon the value of α.

It is easy to see that the three-term recurrence relation (3.2) is equivalent to a tridiagonal system of linear equations comprising the main diagonal and two lower diagonals. Formulae based on LU decomposition show this; consequently, such a tridiagonal system will be unstable as well.   Relationship (3.2) can be rearranged as a tridiagonal system existing of the main diagonal and the two diagonals adjacent to it. Formulae produced by a LU decomposition will show that stable solutions can be obtained if the lower and upper values of the solution are known. The pentadiagonal system of linear equations (4.2) has, basically, the same favourable properties.

5. TEST CALCULATIONS AND DISCUSSION

The output of four test runs gives the electric multipole radial matrix elements calculated by upward recursion, as well as by solving a pentadiagonal system of linear equations. Both processor times are given too.

The results of test runs 1 ($\lambda = 1$, $k = 20.2$, $k' = 20.0$, $\eta' = 100$) and 2 ($\lambda = 2$, $k = 20.2$, $k' = 20.0$, $\eta' = 100$) show that with $k > k'$ the upward recursion is rather more stable for the lower-diagonal integrals than for the upper-diagonal ones; however, test run 3 ($\lambda = 2$, $k = 20.0$, $k' = 20.2$, $\eta = 100$) shows that with $k < k'$ the opposite is the case. It seems that the recursion shows this feature for higher λ values, too. For $\lambda = 1$ this can be understood by considering the coefficient of I_ℓ in the upper-diagonal recurrence relation (3.2)

$$(2\ell+1) \frac{k'}{k}^2 S_\ell^2(\eta') + (2\ell+3) \frac{k}{k'} S_\ell^2(\eta). \qquad (5.1)$$

The coefficient in the corresponding lower-diagonal recurrence relation (not given in this article) is

$$(2\ell+1) \frac{k}{k'} S_\ell^2(\eta) + (2\ell+3) \frac{k'}{k}^2 S_\ell^2(\eta'). \qquad (5.2)$$

For $k > k'$, the coefficient (5.2) will be smaller than the coefficient (5.1) and, since these coefficients play the same role as α in the approximated relation (3.4), the lower-diagonal recurrence relation will be more stable than the upper one. When $k < k'$, the coefficient (5.2)

will be greater than the coefficient (5.1) and, therefore, the lower-diagonal recurrence relation will be less stable than the upper one. We believe that for higher λ values similar considerations will hold.

Looking at the results of test run 4 ($\lambda = 2$, $k = 20.0$, $k' = 20.0$, $\eta = 100$) and comparing the $F_\ell G_\ell$ and $G_\ell F_\ell$ integrals which were obtained by upward recursion, as well as by solving band linear equations, the conclusion is confirmed once again more that the latter give more accurate results than the former.

6. NOTES ON THE PROGRAM

A flow diagram of the various subroutines is given in Fig. 3. Arrows in two directions imply calling and returning. The functions of each subprogram are described briefly below.

1) The main program reads the necessary input parameters and calls for subroutines RECMUD and RECLIP in order to calculate the radial matrix elements. Subsequently, it calls the subroutine RECPRN in order to print the results before ending the calculation.
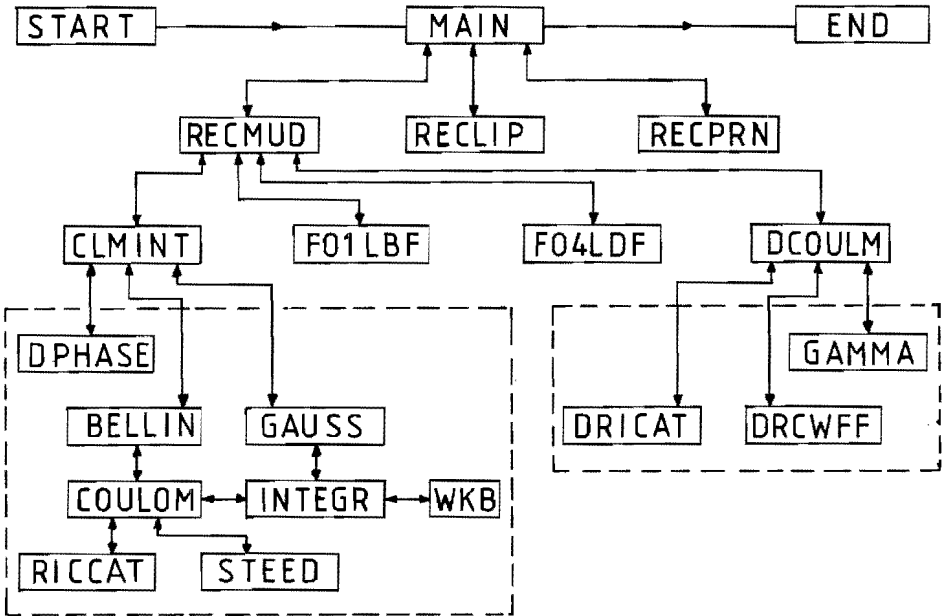
Fig. 3. Flow diagram illustrating calls and returns with respect to the subprograms used in the program.

2) RECMUD calls CLMINT to calculate the Coulomb integrals for four combinations of ℓ and $\ell' = \ell$, $\ell+1$. Then, it uses these integrals either, as initial values in an upward recursion, or as boundary values for solving a system of linear equations in order to calculate the main and upper-diagonal integrals $I_{\ell,\ell}^{(\lambda)}$ and $I_{\ell,\ell+1}^{(\lambda)}$ using Eqs. (2.3a) and (2.3b), respectively. The calling sequence is:

```
CALL RECMUD(DRM1 ,DRM2 ,DETI ,DWNI ,DETF ,DWNF ,LAMB ,LMIN ,LMAX  ,
            IACC ,LINQ ,DMINT,DSINT,DA    ,DB    ,DAL  ,LXLN ,LXLNM2,
            FC   ,FDC  ,GC    ,GDC  ,SIGMA,IEXP ,
            DFI1 ,DGI1 ,DFF1 ,DGF1 ,DFI2 ,DGI2 ,DFF2 ,DGF2 ,LXCN  )
```

All the real variables and arrays are declared to be DOUBLE PRECISION. The type and meaning of the parameters are:

DRM1 ,DRM2   real, lower and upper integration limits R_1 and R_2, respectively.

DETI ,DETF   real, Sommerfeld parameters η and η', respectively.

DWNI ,DWNF   real, wave numbers k and k', respectively.

LAMB   integer, electric multipole moment λ.

LMIN ,LMAX   integer, minimum and maximum values, respectively, of the angular momentum range for which radial matrix elements are required.

IACC   integer, chosen from 0 or 1. See calling sequence CLMINT.

LINQ = 0   upward recursion.

LINQ = 1   solving a pentadiagonal system of linear equations.

DMINT,DSINT   real arrays, contain the main- and upper-diagonal radial matrix elements, respectively and should be dimensioned to at least to the size (LXLN,4).

DA,DB,DAL   real arrays, see for explanation the NAG-Library routines F01LBF and F04LDF. They should be dimensioned to the size (5,LXLNM2), (LXLNM2,4) and (2,LXLNM2), respectively.

LXLN   integer, equals to LMAX−LMIN+1+mod(λ,2)+λ/2.

LXLNM2   integer, equals to (LXLN-2)*2.

FC,FDC   real arrays, contain the output Coulomb wave functions F_ℓ,

GC,GDC F_ℓ', G_ℓ, G_ℓ', arranged by order, after calling the subroutine DCOULM. They should be dimensioned to the size LMAX+LAMB.

SIGMA   real array of dimension LMAX+LAMB for Coulomb phase shifts.

IEXP   integer array of dimension LXLNM2 for modulo exponent of Coulomb wave functions, also used in F01LBF and F04LDF.

DFI1 ,DFI2   real arrays, contain the regular Coulomb wave functions for
             η, kR_1 and η, kR_2, respectively.
DFF1 ,DFF2   real arrays, contain the regular Coulomb wave functions for
             η', $k'R_1$ and η', $k'R_2$, respectively.
DGI1 ,DGI2   real arrays, contain the irregular Coulomb wave functions for
             the same above-mentioned parameters. These Coulomb wave
             function arrays should be dimensioned to the size LXCN.
LXCN   integer, equals to LMAX-LMIN+1+λ.

3) RECLIP calculates the other Coulomb integrals, by means of λ-inplane
recursion, using Eqs. (2.4) and (2.5). The calling sequence is:
CALL RECLIP(DRM1 ,DRM2 ,DETI ,DWNI ,DETF ,DWNF ,LAMB ,LMIN ,LMAX ,
            LXLN ,LAP1 ,FFINT,FGINT,GFINT,GGINT,DMINT,DSINT,
            DFI1 ,DGI1 ,DFF1 ,DGF1 ,DFI2 ,DGI2 ,DFF2 ,DGF2 ,LXCN)
The type and meaning of the parameters is the same as in the calling
sequence of RECMUD, except for:
FFINT,FGINT real arrays, contain the required radial matrix elements $I_{\ell,\ell'}^{(\lambda)}$,
GFINT,GGINT for the four combinations $F_\ell F_{\ell'}$, $F_\ell G_{\ell'}$, $G_\ell F_{\ell'}$, $G_\ell G_{\ell'}$ of the
             Coulomb wave functions and should be given the dimension of
             (LXLN,LAP1).
LAP1   integer, equals to $\lambda+1$.
4) RECPRN prints the radial matrix elements $I_{\ell,\ell'}^{(\lambda)}$, in a λ-dependent format
In the output, they are denoted as M($-\lambda-1$, F_ℓ, $F_{\ell'}$), etc, corresponding
to a notation used in Refs. [11,14]. The calling sequence is:
CALL RECPRN(ETI,WNI,RM1,LMIN,LAMB,LINQ,ETF,WNF,RM2,LMAX,IACC,
            FFINP,FGINP,GFINP,GGINP,LXMLP,LAP1,LMDL)
The meaning of the parameters is the same as in the calling sequences of
RECMUD and RECLIP, except for:
FFINP,FGINP real temporary arrays, contain the radial matrix elements
GFINP,GGINP $I_{\ell,\ell'}^{(\lambda)}$, to facilitate their output as a function of ℓ with
             increment LMDL and should be given the dimension of
             (LXMLP,LAP1).
LXMLP   integer, at least the number of increments LMDL.
5) CLMINT calculates the radial matrix elements $I_{\ell,\ell'}^{(\lambda)}$, given by (1.1) for
a value of η, k and λ, and a single valued pair of (ℓ,ℓ'). This is done
for the four combinations of the Coulomb wave functions. Fig. 3 shows the
subprograms called by CLMINT (catalogue number: ACCM) [13].

6) DCOULM combines our double precision versions DRICAT and DRCWFF of the Coulomb wave functions subprograms RICATI (catalogue number: ABOQ) [21] and RCWFF (catalogue number: ABPC) [22,23], respectively, to use the most efficient one for some pair of η and kr values.

The main program, RECMUD and RECLIP share a less important COMMON block, labelled PRINT. Together with the DATA statement it gives the possibility to print out intermediate results in RECMUD and RECLIP. The concerning statements are self-explanatory.

Each test run requires five input data cards. The first one should contain a test run number. The second and fourth are similar and must contain DRM1, DRM2, DETI, DWNI, DWNF. The third and fifth must include LAMB, LMIN, LMAX, IACC, LINQ, LMDL. They differ only from the variable LINQ which is chosen equal to 0 and 1, respectively.

Finally, we notice that, although RECMUD and RECLIP can calculate the radial matrix elements of any multipolarity, the arrays in the main program have been dimensioned up to a λ value equal to 5. The same holds for the print facilities of RECPRN.

REFERENCES

[1] K. Alder and H.C. Pauli, Nucl. Phys. 128(1969)1931.

[2] J. Raynal, in Computing as a Language of Physics, edited by A. Salam (IAEA, Vienna, 1972), p. 292.

[3] K. Alder, F. Roesel and R. Morf, Nucl. Phys. A284(1977)145.

[4] M. Ichimura, M. Igarashi, S. Landowne, C.H. Dasso, B.S. Nilsson, R.A. Broglia and A. Winther, Phys. Lett. 67B(1977)129.

[5] L.D. Tolsma, Phys. Rev. C20(1979)592.

[6] M. Rhoades-Brown, M.H. Macfarlane and S.C. Pieper, Phys. Rev. C21(1980)2417.
    M. Rhoades-Brown, M.H. Macfarlane and S.C. Pieper, Phys. Rev. C21(1980)2436.

[7] J. Raynal, Phys. Rev. C23(1981)2571.

[8] R.G. Gordon, J. Chem. Phys. $\underline{51}$(1969)14.

R.G. Gordon, Quantum Scattering Using Piecewise Analytic Solutions, in: B. Alder, S. Fernbach and M. Rotenberg (eds), Methods in Computational Physics 10 (Academic, New York, 1971).

[9] L.Gr. Ixaru, Comput. Phys. Commun. $\underline{20}$(1980)97.

L.Gr. Ixaru, "Numerical Methods", D. Reidel Publishing Company, Dordrecht, 1984.

[10] L.C. Biedenharn, J.L. McHale and R.M. Thaler,
Phys. Rev. $\underline{100}$(1955)376

[11] K. Alder, A. Bohr, T. Huus, B. Mottelson and A. Winther.
Rev. Mod. Phys. $\underline{28}$(1956)432.

[12] G.H. Rawitscher and C.H. Rasmussen,
Comput. Phys. Commun. $\underline{11}$(1976)183.

[13] H.F. Arnoldus, Comput. Phys. Commun. $\underline{32}$(1984)421.

[14] M. Samuel and U. Smilansky, Comput. Phys. Commun. $\underline{2}$(1971)455.

[15] L.E. Wright, Phys. Rev. $\underline{C20}$(1979)393.

[16] Section IV of Ref. [7].

[17] M. Abramowitz and I.A. Stegun, Eds. "Handbook of Mathematical Functions", National Bureau of Standards, Washington, D.C.

[18] Note: Our definition of the Coulomb integral with $R_2 = \infty$ corresponds to Raynal's definition (25) in [7] as: $I^{(\lambda)}_{\ell,\ell'} = (kk')^{\lambda/2} M(H,K,R)^{-\lambda-1}_{\ell,\ell'}$.

[19] W. Gautschi, SIAM Review $\underline{9}$(1967)24.

[20] C.F. Fischer and R.A. Usmani, SIAM J. Numer. Anal. $\underline{6}$(1969)127.

[21] C. Bardin, Y. Dandeu, L. Gauthier, J. Guillermin, T. Lena,
J. M. Pernet, H.H. Wolter and T. Tamura,
Comput. Phys. Commun. $\underline{3}$(1972)73.

[22] A.R. Barnett, D.H. Feng, J.W. Steed and L.J.B. Goldfarb,
Comput. Phys. Commun. $\underline{8}$(1974)377.

[23] A.R. Barnett, Comput. Phys. Commun. $\underline{11}$(1976)141.

TEST RUN OUTPUT

TEST RUN 1

********** CALCULATION OF ELECTRIC MULTIPOLE RADIAL MATRIX ELEMENTS BY UPWARD RECURSION **********

ETI = .9900990100E+02   WNI = .2020000000E+02   RM1 = .5000000000E+02   LMIN = 0   LAMBDA = 1   LINQ = 0
ETF = .1000000000E+03   WNF = .2000000000E+02   RM2 = .1000000000E+04   LMAX = 850   IACC = 0   LMDL = 100

DIPOLE RADIAL MATRIX ELEMENTS M(-2,FLI,FLF)

LI	LF=LI-1	LF=LI+1	LI	LF=LI-1	LF=LI+1	LI	LF=LI-1	LF=LI+1
0	0.	.76025183893D 03	300	.36920099116D-03	.94648008329D-03	600	.45913655042D 03	.87424384189D-03
100	.89023756730D-03	.57316527953D 03	400	.87376303949D-03	.63565429531D-03	700	.65876360912D 03	.46919918693D-03
200	.28267318809D-03	.83326416928D 03	500	.10097263930D-02	.13754809053D-03	800	.89741581287D 03	.92028946197D-03

DIPOLE RADIAL MATRIX ELEMENTS M(-2,FLI,GLF)

LI	LF=LI-1	LF=LI+1	LI	LF=LI-1	LF=LI+1	LI	LF=LI-1	LF=LI+1
0	0.	.60938389225D 03	300	.93167644333D 03	.75029027073D-04	600	.92827891102D-03	.31063468009D-03
100	-.41336840430D-03	.77512717704D 03	400	.50054957715D 03	.68720366352D-03	700	.83252578223D-03	.80497513616D-03
200	.95310715462D-03	.47482508417D 03	500	.23220439613D 03	.93695135266D-03	800	-.64461023395D-03	.21516576202D-03

DIPOLE RADIAL MATRIX ELEMENTS M(-2,GLI,FLF)

LI	LF=LI-1	LF=LI+1	LI	LF=LI-1	LF=LI+1	LI	LF=LI-1	LF=LI+1
0	0.	.59812258432D 03	300	.92741753062D 03	.88973212097D-04	600	-.93969931950D-03	.32802583290D-03
100	.40240883703D 03	.78335423499D 03	400	.50698989943D 03	.69967486870D-03	700	-.85834888327D-03	-.79861876355D-03
200	.94520197549D-03	.48325173387D 03	500	.21962702695D 03	.92339992849D-03	800	.67694970129D-03	-.15641281879D-03

DIPOLE RADIAL MATRIX ELEMENTS M(-2,GLI,GLF)

LI	LF=LI-1	LF=LI+1	LI	LF=LI-1	LF=LI+1	LI	LF=LI-1	LF=LI+1
0	0.	.76548916816D 03	300	.38248603042D-03	.94607210238D-03	600	-.47831274437D-03	-.88837895121D-03
100	.89633152895D-03	.56369966566D 03	400	-.88781950588D-03	.64485770439D-03	700	.64085910186D-03	-.50012338230D-03
200	.29306346526D-03	.82329642733D 03	500	.99691906416D-03	-.12569671280D-03	800	.84789620493D-03	.909?0072313D-03

PROCESSOR TIME IS   9.6 SECONDS.

********** CALCULATION OF ELECTRIC MULTIPOLE RADIAL MATRIX ELEMENTS BY BAND LINEAR EQUATIONS **********

ETI = .9900990100E+02   WNI = .2020000000E+02   RM1 = .5000000000E+02   LMIN = 0   LAMBDA = 1   LINQ = 1
ETF = .1000000000E+03   WNF = .2000000000E+02   RM2 = .1000000000E+04   LMAX = 850   IACC = 0   LMDL = 100

DIPOLE RADIAL MATRIX ELEMENTS M(2,FLI,FLF)

LI	LF=LI-1	LF=LI+1	LI	LF=LI-1	LF=LI+1	LI	LF=LI-1	LF=LI+1
0	0.	.76025183893D-03	300	-.36920098664D-03	.94648005173D 03	600	.45913653114D-03	-.87424424721D-03
100	.89023757251D-03	.57316527253D-03	400	-.87376303349D-03	.63565422407D-03	700	.65876364867D-03	.46920018599D-03
200	.28267319279D 03	.83326415447D-03	500	-.10097263929D-02	.13754825813D 03	800	.89741589775D-03	.92028966528D-03

DIPOLE RADIAL MATRIX ELEMENTS M(2,FLI,GLF)

LI	LF=LI-1	LF=LI+1	LI	LF=LI-1	LF=LI+1	LI	LF=LI-1	LF=LI+1
0	0.	.60938389225D-03	300	.93167644872D 03	-.75028989473D 04	600	.92827888805D-03	-.31063419721D-03
100	.41336841051D 03	.77512718539D-03	400	.50054984531D-03	.68720357865D-03	700	.83252573785D-03	.80497632642D-03
200	.95310716021D 03	.47482510182D-03	500	.23220438410D-03	.93695115298D-03	800	.64461033507D-03	.21516873651D-03

DIPOLE RADIAL MATRIX ELEMENTS M(2,GLI,FLF)

LI	LF=LI-1	LF=LI+1	LI	LF=LI-1	LF=LI+1	LI	LF=LI-1	LF=LI+1
0	0.	-.59812258432D-03	300	.92741753767D 03	.88973162880D-04	600	-.93969928943D-03	.32802520083D-03
100	.40240884516D 03	.78335424591D-03	400	.50698990880D-03	.69967475760D-03	700	-.85834882159D-03	-.79862032154D-03
200	.94520198281D 03	.48325175697D-03	500	.21962701121D 03	.92339966712D-03	800	.67694983365D-03	-.15641671225D-03

DIPOLE RADIAL MATRIX ELEMENTS M(2,GLI,GLF)

LI	LF=LI-1	LF=LI+1	LI	LF=LI-1	LF=LI+1	LI	LF=LI-1	LF=LI+1
0	0.	.76548916816D-03	300	.38248603547D-03	.94607207412D-03	600	-.47831272711D-03	-.88837931414D-03
100	.89633153362D-03	.56369965939D-03	400	.88781950050D-03	.64485764060D-03	700	.64085913727D-03	-.50012427689D-03
200	.29306346947D-03	.82329641407D-03	500	-.99691905513D-03	.12569686287D-03	800	.84789628093D-03	.90969848753D-03

PROCESSOR TIME IS   51.4 SECONDS.

L. D. Tolsma

TEST RUN 2

********** CALCULATION OF ELECTRIC MULTIPOLE RADIAL MATRIX ELEMENTS BY UPWARD RECURSION **********

ETI = .9900990100E+02   WNI = .2020000000E+02   RM1 = .5000000000E+02   LMIN = 0   LAMBDA = 2   LINQ = 0
ETF = .1000000000E+03   WNF = .2000000000E+02   RM2 = .1000000000E+04   LMAX = 750   IACC = 0   LMDL =100

QUADRUPOLE RADIAL MATRIX ELEMENTS M(3 ,FLI ,FLF)

LI	LF=LI-2	LF-LI	LF-LI+2	LI	LF=LI-2	LF-LI	LF=LI+2
0	0.	0.	.15598390133D-04	400	.18320452692D-04	.43085302516D-05	.17858317835D-04
100	.70718031346D-05	.18785011694D-04	.52868706696D-06	500	.90540471227D-05	.16858565397D-04	.10352880562D-04
200	-.12656714123D-04	.17116203899D-04	.42350210757D-05	600	.73271640929D-05	.17475870373D-04	-.93407974710D-05
300	.19814413588D-04	.88088583360D-05	.12958997912D-04	700	.21978817927D-04	.24536395594D-05	-.15286711139D-04

QUADRUPOLE RADIAL MATRIX ELEMENTS M(3 ,FLI ,GLF)

LI	LF-LI-2	LF-LI	LF=LI+2	LI	LF-LI-2	LF-LI	LF=LI+2
0	0.	0.	.10925963142D-04	400	.91295887268D-05	.18605190273D-04	.19757886206D-07
100	-.18021499662D-04	.31295713701D-05	.18722665726D-04	500	.19323932099D-04	.98926487312D-05	-.14698395357D-04
200	-.15205915492D-04	.85625797646D-05	.18027955624D-04	600	.20387608116D-04	.83949005132D-05	-.14765225346D-04
300	-.35125954397D-05	.16984319007D-04	.12793394640D-04	700	.52217264139D-05	.19574561124D-04	.83694953330D-05

QUADRUPOLE RADIAL MATRIX ELEMENTS M(3 ,GLI ,FLF)

LI	LF-LI-2	LF-LI	LF-LI+2	LI	LF-LI	LF-LI	LF=LI+2
0	0.	0.	-.10703100664D-04	400	.92660222491D-05	.18904961352D-04	-.54901551095D-08
100	.17926607340D-04	.33771246000D-05	.18729720837D-04	500	-.18965400303D-04	.98783097882D-05	.14340089132D-04
200	.15269008735D-04	.83015764684D-05	.17977840899D-04	600	-.20810886494D-04	-.83158217736D-05	.15210918607D-04
300	.32488929198D-05	.17145435003D-04	.12618842218D-04	700	.58483405323D-05	.19807627945D-04	-.79229096273D-05

QUADRUPOLE RADIAL MATRIX ELEMENTS M(3 ,GLI ,GLF)

LI	LF-LI-2	LF-LI	LF-LI+2	LI	LF=LI	LF-LI	LF=LI+2
0	0.	0.	.15707541667D-04	400	.18597729254D-04	-.43852375540D-05	.18167819912D-04
100	.73043823552D-05	.18742051285D-04	.27746982511D-06	500	.90607533786D-05	-.16499583345D-04	.10318712831D-04
200	-.12403481085D-04	.17123352410D-04	.39786437645D-05	600	.71864719119D-05	-.17916106725D-04	-.93273069648D-05
300	.19905667025D-04	.85807559445D-05	.13177280926D-04	700	.21964724365D-04	.18687561488D-05	-.15734526963D-04

PROCESSOR TIME IS 10.4 SECONDS.

********** CALCULATION OF ELECTRIC MULTIPOLE RADIAL MATRIX ELEMENTS BY BAND LINEAR EQUATIONS **********

ETI = .9900990100E+02   WNI = .2020000000E+02   RM1 = .5000000000E+02   LMIN = 0   LAMBDA = 2   LINQ = 1
ETF = .1000000000E+03   WNF = .2000000000E+02   RM2 = .1000000000E+04   LMAX = 750   IACC = 0   LMDL =100

QUADRUPOLE RADIAL MATRIX ELEMENTS M(3 ,FLI ,FLF)

LI	LF-LI-2	LF-LI	LF-LI+2	LI	LF-LI	LF-LI	LF=LI+2
0	0.	0.	.15598390141D-04	400	.18320444610D-04	-.43086003330D-05	.17858652394D-04
100	.70718168725D-05	.18784999656D-04	.52870772023D-06	500	.90540375895D-05	-.16858697627D-04	.10353692249D-04
200	-.12656700982D-04	.17116179061D-04	.42350799433D-05	600	.73271782459D-05	-.17476136579D-04	-.93387965810D-05
300	-.19814404290D-04	.88088179452D-05	.12959138208D-04	700	.21978842005D-04	.24530777890D-05	-.15281715387D-04

QUADRUPOLE RADIAL MATRIX ELEMENTS M(3 ,FLI ,GLF)

LI	LF-LI-2	LF-LI	LF-LI+2	LI	LF-LI	LF=LI	LF=LI+2
0	0.	0.	.10925963131D-04	400	.91295764933D-05	-.18605084192D-04	.19251587676D-07
100	-.18021520492D-04	.31295895985D-05	.18722634493D-04	500	.19323917670D-04	-.98924485850D-05	-.14699623742D-04
200	-.15205935400D-04	-.85625421618D-05	.18027866553D-04	600	.20387586695D-04	.83953034377D-05	-.14765622346D-04
300	-.35126095179D-05	-.16984257863D-04	.12793182336D-04	700	.52216899733D-05	.19575411395D-04	.83619347265D-05

QUADRUPOLE RADIAL MATRIX ELEMENTS M(3 ,GLI ,FLF)

LI	LF-LI-2	LF=LI	LF-LI+2	LI	LF-LI	LF-LI	LF=LI+2
0	0.	0.	.10703100653D-04	400	.92660100134D-05	.18904855250D-04	-.49837254928D-08
100	.17926628165D-04	.33771428304D-05	.18729689590D-04	500	-.18965385869D-04	.98781096003D-05	.14341317826D-04
200	.15269028643D-04	.83015386600D-05	.17977751802D-04	600	-.20810865069D-04	.83162247849D-05	.15213947493D-04
300	.32489069995D-05	.17145373849D-04	.12618629856D-04	700	.58483040831D-05	.19808478403D-04	-.79153471611D-05

QUADRUPOLE RADIAL MATRIX ELEMENTS M(3 ,GLI ,GLF)

LI	LF-LI-2	LF-LI	LF-LI+2	LI	LF-LI	LF-LI	LF=LI+2
0	0.	0.	.15707541675D-04	400	.18597721171D-04	-.43853076421D-05	.18168154517D-04
100	.73043960901D-05	.18742039246D-04	.27749048397D-06	500	.90607438444D-05	-.16499715359D-04	.10319524629D-04
200	-.12403467944D-04	.17123327571D-04	.39787026423D-05	600	.71864860666D-05	-.17916372960D-04	-.93253058087D-05
300	.19905657728D-04	.85807155504D-05	.13177421243D-04	700	.21964748445D-04	.18681943151D-05	-.15729530555D-04

PROCESSOR TIME IS 42.9 SECONDS.

********** CALCULATION OF ELECTRIC MULTIPOLE RADIAL MATRIX ELEMENTS BY UPWARD RECURSION **********

ETI = .1000000000E+03 WNI = .2000000000E+02 RM1 = .5000000000E+02 LMIN = 0 LAMBDA = 2 LINQ = 0
ETF = .9900990099E+02 WNF = .2020000000E+02 RM2 = .1000000000E+04 LMAX = 750 IACC = 0 LMDL =100

QUADRUPOLE RADIAL MATRIX ELEMENTS M(-3,FLI,FLF)

LI	LF=LI-2	LF=LI	LF=LI+2	LI	LF=LI-2	LF=LI	LF=LI+2
0	0.	0.	.16169152034D-04	400	.18152099033D-04	-.43085829275D-05	.18504793596D-04
100	.35270058473D-06	.18785002687D-04	.68088008519D-05	500	.10648156426D-04	-.16858664850D-05	.87684753914D-05
200	.38219693700D-05	.17116185270D-04	.12655611825D-04	600	-.88727159925D-05	.17476070662D-04	.76059509124D-05
300	.12941349538D-04	.88088280054D-05	.20021096024D-04	700	-.15781137543D-04	.24532167920D-05	.22327308974D-04

QUADRUPOLE RADIAL MATRIX ELEMENTS M(-3,FLI,GLF)

LI	LF=LI-2	LF=LI	LF=LI+2	LI	LF=LI-2	LF=LI	LF=LI+2
0	0.	0.	.98442299146D-05	400	-.39128393515D-06	.18904880878D-04	.94313319454D-05
100	.18776231667D-04	-.33771383566D-05	.18173321173D-04	500	.14481650074D-04	.98781578795D-05	.19461517372D-04
200	.18010296222D-04	-.83015480142D-05	.15062532008D-04	600	-.15017837173D-04	.83161277038D-05	.20260163344D-04
300	-.13018100202D-04	.17145388659D-04	.32115510149D-05	700	-.79188741397D-05	.19808273674D-04	.48084329780D-05

QUADRUPOLE RADIAL MATRIX ELEMENTS M(-3,GLI,FLF)

LI	LF=LI-2	LF=LI	LF=LI+2	LI	LF=LI-2	LF=LI	LF=LI+2
0	0.	0.	.10067055815D-04	400	.25067535581D-06	.18605109801D-04	.94409114723D-05
100	.18684203595D-04	.31295851246D-05	.18177277782D-04	500	-.14123278444D-04	.98924968141D-05	.19103900019D-04
200	.18076607200D-04	-.85625513101D-05	.15009158868D-04	600	-.15444161408D-04	.83952064351D-05	.20708037724D-04
300	.12753196230D-04	.16984272670D-04	-.30399421692D-05	700	.72919839056D-05	.19575206845D-04	.52678100142D-05

QUADRUPOLE RADIAL MATRIX ELEMENTS M(-3,GLI,GLF)

LI	LF=LI-2	LF=LI	LF=LI+2	LI	LF=LI-2	LF=LI	LF=LI+2
0	0.	0.	.16278378179D-04	400	.17876905862D-04	-.43852902383D-04	-.18195119883D-04
100	.58642918138D-06	.18742042290D-04	.65575169044D-05	500	.10635036807D-04	-.16499682798D-04	-.88090691339D-05
200	.40743815358D-05	.17123333792D-04	-.12911328017D-04	600	-.90040278085D-05	.17916307015D-04	.76293941184D-05
300	.12853629845D-04	.85807256084D-05	.19800497407D-04	700	-.15777044991D-04	.18683333846D-05	.21892815032D-04

PROCESSOR TIME IS   10.2 SECONDS.

********** CALCULATION OF ELECTRIC MULTIPOLE RADIAL MATRIX ELEMENTS BY BAND LINEAR EQUATIONS **********

ETI = .1000000000E+03 WNI = .2000000000E+02 RM1 = .5000000000E+02 LMIN = 0 LAMBDA = 2 LINQ = 1
ETF = .9900990099E+02 WNF = .2020000000E+02 RM2 = .1000000000E+04 LMAX = 750 IACC = 0 LMDL =100

QUADRUPOLE RADIAL MATRIX ELEMENTS M(-3,FLI,FLF)

LI	LF=LI-2	LF=LI	LF=LI+2	LI	LF=LI-2	LF=LI	LF=LI+2
0	0.	0.	.16169152051D-04	400	.18152179895D-04	-.43086003274D-05	.18504791585D-04
100	.35270538180D-06	.18784999658D-04	.68088045193D-05	500	.10648352737D-04	-.16858697625D-05	.87684730191D-05
200	.38219834904D-05	.17116179058D-04	.12655608484D-04	600	.88722319222D-05	.17476136575D-04	.76059544906D-05
300	.12941383388D-04	.88088179488D-05	.20021093689D-04	700	.15779928756D-04	.24530777925D-05	.22327314496D-04

QUADRUPOLE RADIAL MATRIX ELEMENTS M(-3,FLI,GLF)

LI	LF=LI-2	LF=LI	LF=LI+2	LI	LF=LI-2	LF=LI	LF=LI+2
0	0.	0.	.98442299063D-05	400	.39116483861D-06	.18904855249D-04	-.94313289837D-05
100	.18776224603D-04	-.33771428180D-05	.18173326576D-04	500	.14481939212D-04	.98781096059D-05	-.19461513877D-04
200	-.18010275426D-04	.83015388645D-05	.15062536928D-04	600	.15018550139D-04	-.83162247861D-05	-.20260158148D-04
300	.13018050346D-04	.17145373847D-04	.32115544410D-05	700	.79170937667D-05	.19808478404D-04	-.48084241231D-05

QUADRUPOLE RADIAL MATRIX ELEMENTS M(-3,GLI,FLF)

LI	LF=LI-2	LF=LI	LF=LI+2	LI	LF=LI-2	LF=LI	LF=LI+2
0	0.	0.	.10067055806D-04	400	.25055638662D-06	.18605084194D-04	.94409085129D-05
100	.18684196543D-04	.31295895839D-05	.18177283189D-04	500	-.14123567280D-04	.98924485824D-05	.19103896528D-04
200	.18076586430D-04	-.85625421662D-05	.15009163788D-04	600	-.15444873642D-04	.83953034304D-05	.20708032533D-04
300	.12753146430D-04	-.16984257869D-04	-.30399455937D-05	700	.72902051439D-05	.19575411388D-04	.52678011680D-05

QUADRUPOLE RADIAL MATRIX ELEMENTS M(-3,GLI,GLF)

LI	LF=LI-2	LF=LI	LF=LI+2	LI	LF=LI-2	LF=LI	LF=LI+2
0	0.	0.	.16278378184D-04	400	.17876986766D-04	-.43853076455D-05	-.18195117871D-04
100	.58643398269D-06	.18742039260D-04	.65575205708D-05	500	.10635233219D-04	-.16499715587D-04	-.88090667605D-05
200	.40743956648D-05	.17123327578D-04	-.12911324677D-04	600	-.90035434923D-05	.17916372958D-04	.76293976483D-05
300	.12853663714D-04	.85807155480D-05	-.19800495080D-04	700	-.15775835596D-04	.18681943217D-05	.21892821047D-04

PROCESSOR TIME IS   41.9 SECONDS.

TEST RUN 4

********** CALCULATION OF ELECTRIC MULTIPOLE RADIAL MATRIX ELEMENTS BY UPWARD RECURSION **********

ETI = .1000000000E+03 WNI = .2000000000E+02 RM1 = .5000000000E+02 LMIN = 0 LAMBDA = 2 LINQ = 0
ETF = .1000000000E+03 WNF = .2000000000E+02 RM2 = .1000000000E+04 LMAX = 750 IACC = 0 LMDL =100

QUADRUPOLE RADIAL MATRIX ELEMENTS M(3,FLI ,FLF)

LI	LF=LI-2	LF=LI	LF=LI+2	LI	LF=LI-2	LF=LI	LF=LI+2
0	0.	0	.10727668257D-03	400	.53269247717D-04	.11305895988D-03	-.52916723248D-04
100	.15439940010D-04	.10750911141D-03	.13763070934D-04	500	.47790826804D-04	.11714373619D-03	-.47374149793D-04
200	.37929399998D-04	.10849762229D-03	.38510164681D-04	600	.36948003186D-04	.12272941062D-03	-.37134949939D-04
300	.52260767357D-04	.11036544424D-03	.52108477512D-04	700	.20914393287D-04	.13174057826D-03	-.20326737291D-04

QUADRUPOLE RADIAL MATRIX ELEMENTS M(-3,FLI ,GLF)

LI	LF=LI-2	LF=LI	LF=LI+2	LI	LF=LI-2	LF=LI	LF=LI+2
0	0.	0.	.31117076502D-05	400	.97044730115D-04	.15116923247D-06	.97179359226D-04
100	-.10626077170D-03	.70697765856D-07	.10648818367D-03	500	.10254854727D-03	-.12728650410D-06	.10269732412D-03
200	-.10105817320D-03	.31382664864D-07	.10086432578D-03	600	.11011914634D-03	-.22757392097D-06	.11035566681D-03
300	-.95783239106D-04	.13634501365D-06	.95827740261D-04	700	.11965758833D-03	.99769238216D-07	.11977476595D-03

QUADRUPOLE RADIAL MATRIX ELEMENTS M(3,GLI ,FLF)

LI	LF=LI-2	LF=LI	LF=LI+2	LI	LF=LI-2	LF=LI	LF=LI+2
0	0.	0.	-.28718763419D-05	400	.97181647300D-04	-.15201535119D-06	-.97192739956D-04
100	.10643537803D-03	.71044260923D-07	.10672201991D-03	500	.10230514668D-03	-.12816958063D-06	-.10242385955D-03
200	.10129451087D-03	.30738412782D-07	.10112767109D-03	600	.11015506340D-03	-.22666842986D-06	-.11025983360D-03
300	.95924603160D-04	.13712441786D-06	.95817222843D-04	700	.11901360020D-03	-.10068928912D-06	-.11928770757D-03

QUADRUPOLE RADIAL MATRIX ELEMENTS M(3,GLI ,GLF)

LI	LF=LI-2	LF=LI	LF=LI+2	LI	LF=LI-2	LF=LI	LF=LI+2
0	0.	0.	.10720618757D-03	400	-.52988582657D-04	.11313545681D-03	-.53229537010D-04
100	.15623231310D-04	.10771892637D-03	.13665786805D-04	500	-.47521129722D-04	.11688446562D-03	-.47615375430D-04
200	.38045049801D-04	.10875343866D-03	.38505487857D-04	600	-.37400483259D-04	.12270034041D-03	-.36688695798D-04
300	.52017228705D-04	.11043354367D-03	.52390327065D-04	700	-.20969971126D-04	.13112586531D-03	-.20756413296D-04

PROCESSOR TIME IS 6.7 SECONDS.

********** CALCULATION OF ELECTRIC MULTIPOLE RADIAL MATRIX ELEMENTS BY BAND LINEAR EQUATIONS **********

ETI = .1000000000E+03 WNI = .2000000000E+02 RM1 = .5000000000E+02 LMIN = 0 LAMBDA = 2 LINQ = 1
ETF = .1000000000E+03 WNF = .2000000000E+02 RM2 = .1000000000E+04 LMAX = 750 IACC = 0 LMDL =100

QUADRUPOLE RADIAL MATRIX ELEMENTS M(3,FLI ,FLF)

LI	LF=LI-2	LF=LI	LF=LI+2	LI	LF=LI-2	LF=LI	LF=LI+2
0	0.	0.	.10727668257D-03	400	-.53269252990D-04	.11305896484D-03	-.52916728640D-04
100	.15439937316D-04	.10750911344D-03	.13763067936D-04	500	-.47790832204D-04	.11714374136D-03	-.47374155290D-04
200	-.37929404427D-04	.10849762597D-03	.38510169325D-04	600	-.36948008658D-04	.12272941593D-03	-.37134955492D-04
300	-.52260772380D-04	.11036544881D-03	.52108482690D-04	700	-.20914398805D-04	.13174058365D-03	-.20326742878D-04

QUADRUPOLE RADIAL MATRIX ELEMENTS M(-3,FLI ,GLF)

LI	LF=LI-2	LF=LI	LF=LI+2	LI	LF=LI-2	LF=LI	LF=LI+2
0	0.	0.	.31117077081D-05	400	.97044274174D-04	-.15159227428D-06	.97179813610D-04
100	-.10626052920D-03	.70871023304D-07	.10648842710D-03	500	.10254808162D-03	-.12772802279D-06	.10269778843D-03
200	-.10105778520D-03	.31060545273D-07	.10086471221D-03	600	.11011867526D-03	-.22712119623D-06	.11035613671D-03
300	-.95782802902D-04	.13673470188D-06	.95828174719D-04	700	.11965711394D-03	-.10022924206D-06	.11977523931D-03

QUADRUPOLE RADIAL MATRIX ELEMENTS M(3,GLI ,FLF)

LI	LF=LI-2	LF=LI	LF=LI+2	LI	LF=LI-2	LF=LI	LF=LI+2
0	0.	0.	-.28718763987D-05	400	.97181191289D-04	-.15159226936D-06	-.97191194356D-04
100	.10643513545D-03	.70870987429D-07	-.10672226331D-03	500	.10230468096D-03	-.12772802016D-06	-.10242432388D-03
200	.10129412279D-03	.31060562702D-07	-.10112805752D-03	600	.11015459226D-03	-.22712119747D-06	-.11026030353D-03
300	.95924166880D-04	-.13673469282D-06	-.95817657307D-04	700	.11901582574D-03	-.10022924172D-06	-.11928818096D-03

QUADRUPOLE RADIAL MATRIX ELEMENTS M(3,GLI ,GLF)

LI	LF=LI-2	LF=LI	LF=LI+2	LI	LF=LI-2	LF=LI	LF=LI+2
0	0.	0.	.10720618756D-03	400	-.52988587924D-04	.11313546177D-03	-.53229542403D-04
100	.15623228625D-04	.10771892840D-03	.13665783802D-04	500	-.47521135115D-04	.11688447079D-03	-.47615380926D-04
200	-.38045045221D-04	.10875344244D-03	-.38505492504D-04	600	-.37400488725D-04	.12270034571D-03	-.36688701350D-04
300	.52017233721D-04	.11043354824D-03	.52390332244D-04	700	-.20969976638D-04	.13112587070D-03	-.20756418882D-04

PROCESSOR TIME IS 17.2 SECONDS.

SOLVING LARGE SETS OF COUPLED EQUATIONS ITERATIVELY BY VECTOR PROCESSING ON THE CYBER 205 COMPUTER

L.D. TOLSMA

Department of Physics, Eindhoven University of Technology, Eindhoven, The Netherlands

The set of coupled linear second-order differential equations which has to be solved for the quantum-mechanical description of inelastic scattering of atomic and nuclear particles can be rewritten as an equivalent set of coupled integral equations. This set can be solved iteratively. A concept of vectorization of coupled-channel Fortran programs, based upon this integral method, is presented for the use of the Cyber 205 computer.

1. Introduction

In general, the quantum-mechanical description of inelastic scattering of atomic and nuclear particles leads to a set of coupled second-order differential equations of the partial wave radial functions ψ_{Il}^J of the following form:

$$
\left[\frac{d^2}{dr^2} + k_I^2 - \frac{l(l+1)}{r^2} - V_0(r) \right] \psi_{Il}^J(r)
$$
$$
= \sum_{I'l'} V_{Il;I'l'}^J(r) \psi_{I'l'}^J(r), \qquad (1)
$$

for a spinless projectile. Here J, l and I denote the total angular momentum, the orbital angular momentum and the spin of the target with excitation energy ϵ_I, respectively. In eq. (1) $V_0(r)$ is the spherical part of the interaction potential. The coupling matrix at the right-hand side contains the contribution of the multipole expansion of the interaction potential.

To obtain the solutions for $\psi_{Il}^J(r)$, two boundary conditions have to be fulfilled. At the origin, they must vanish and for large distances they must be related to an ingoing partial wave in the entrance channel plus outgoing partial waves in all relevant exit channels. The precise asymptotic form defines a scattering matrix.

In conventional coupled-channel calculations, the set (1) has to be solved as many times as the dimension N of the set for each J value in order

to satisfy the boundary conditions. Especially for large systems this procedure is time consuming and hardly feasible. In addition it generates a complete $N \times N$ scattering matrix, while in the physics context of a case often only a restricted number of columns of this matrix is needed, namely those elements which connect the entrance channel to all the experimentally relevant exit channels. This has been the motivation to study iteration methods for which the solutions are obtained directly without the need for solving the set (1) N times. The calculation of the solutions has been based upon the use of piecewise analytic reference solutions. This will be explained in the next section.

A concept of vectorization of coupled-channel Fortran programs, based upon the method to be explained, is presented for the use on the Cyber 205 computer. Finally, some results will be mentioned.

2. Concise description of the calculation procedure

Considering some interval of the integration range and introducing a reference potential U^{rf} for that interval, the Schrödinger equation (1) in compact notation [1] is

$$
\left[\frac{d^2}{dr^2} + k_i^2 - U_{ii}^{rf}(r) \right] \psi_i(r) = \sum_{j=1}^{N} W_{ij}(r) \psi_j(r),
$$
$$
i = 1, 2, \ldots, N. \qquad (2)
$$

Several forms of the reference potential have been considered, depending on the location on the integration range:
- Constant reference potential [2,3]

$$U^{rf}(r) = \overline{U},\qquad(3a)$$

where $\overline{U}$ is introduced as the average value of the diagonal potential for the interval. The reference solutions are the trigonometric and exponential functions.
- Linear reference potential [2]

$$U^{rf}(r) = \overline{U} + (r - \bar{r})\, dU/dr|_{r=\bar{r}},\qquad(3b)$$

where $\overline{U}$ is also the average potential over the interval, and $\bar{r}$ is the midpoint. The reference solutions are the Airy functions which can be efficiently evaluated numerically, as shown by Gordon [2].
- Coulomb reference potential

$$U^{rf}(r) = 2\eta k/r + l(l+1)/r^2,\qquad(3c)$$

with the wave number k and Sommerfeld parameter η. The reference solutions are the regular and irregular Coulomb wave functions.

If the right-hand side of eq. (2) is replaced by zero, each of the resulting decoupled equations has two linearly independent solutions:
1. The regular solution $G_i(r)$. This is defined to vanish at the origin and by the asymptotic form

$$G_i(r) \underset{r \to \infty}{\sim} \left(i/2\sqrt{k_i}\right)\left[H_i^-(\eta_i; k_i r)\right.$$
$$\left. - S_i^0 H_i^+(\eta_i; k_i r)\right].\qquad(4a)$$

2. The irregular outgoing wave solution $G_i^+(r)$. This is defined by the asymptotic form

$$G_i^+(r) \underset{r \to \infty}{\sim} \left(1/\sqrt{k_i}\right)H_i^+(\eta_i; k_i r).\qquad(4b)$$

The functions H^- and H^+ are the ingoing and outgoing Coulomb waves, respectively. They are given in terms of the well-known regular and irregular Coulomb wave functions.

The solutions (4) can be expressed in terms of the linearly independent reference solutions $A(r)$ and $B(r)$, which belong to a specific form of the reference potential (3).

$$G_i(r) = A_i(r)a_i + b_i(r)b_i\qquad(5a)$$

and

$$G_i^+(r) = A_i(r)a_i^+ + B_i(r)b_i^+.\qquad(5b)$$

The constant coefficients a_i, b_i and a_i^+, b_i^+ are determined by conditions of continuity at the interval boundaries.

Subsequently the Green's functions can be constructed and set (2) can be rewritten as an equivalent set of N coupled integral equations. With an ingoing wave in the entrance channel k, this gives

$$\psi_i^k(r) = G_i(r)\left[\frac{2}{i}\delta_{ik} - \int_r^\infty G_i^+(r')\right.$$
$$\times \sum_{j=1}^N W_{ij}(r')\psi_j^k(r')dr'\Bigg]$$
$$- G_i^+(r)\left[\int_0^r G_i(r')\sum_{j=1}^N W_{ij}(r')\psi_j^k(r')dr'\right].$$
$$(6a)$$

Equivalently,

$$\psi_i^k(r) = G_i(r)c_i(r) - G_i^+(r)c_i^+(r),\qquad(6b)$$

with the boundary conditions

$$c_i(\infty) = (2/i)\delta_{ik}\qquad(7a)$$

and

$$c_i^+(0) = 0.\qquad(7b)$$

The asymptotic value of the outgoing coefficients $c_i^+(r)$ are related to the S-matrix elements.

The set of coupled integral eqs. (6) can be solved by iteration. In this paper only an inward–outward iteration scheme has been applied [4,5]. In this scheme, the following set of coupled integral equations for the amplitudes $c_i(r)$ and $c_i^+(r)$ are considered:

$$c_i(r) = \frac{2}{i}\delta_{ik} - \int_r^\infty G_i^+(r')$$
$$\times \sum_{j=1}^N W_{ij}(r')G_j(r')c_j(r')dr'$$
$$+ \int_r^\infty G_i^+(r')\sum_{j=1}^N W_{ij}(r')G_j^+(r')c_j^+(r')dr',$$
$$(8a)$$

$$c_i^-(r) = \int_0^r G_i(r') \sum_{j=1}^N W_{ij}(r') G_j(r') c_j(r') dr'$$

$$- \int_0^r G_i(r') \sum_{j=1}^N W_{ij}(r') G_j^+(r') c_j^+(r') dr',$$

for $i = 1, 2, \ldots, N$.　　　　　　　　(8b)

To solve these equations we use the relatively slow variation of the amplitudes $c_i(r)$ and $c_i^+(r)$ with respect to the rapid oscillations of the functions $G_i(r)$ and $G_i^+(r)$ in the classically allowed region. The r dependence of the amplitudes is weak as long as the difference between the true potential and the reference potential is small. Thus, a choice of step size has to be made so that small variations of $c_i(r)$ and $c_i^-(r)$ over an interval can be neglected.

Expressing $G_i(r)$ and $G_i^+(r)$ in reference solutions, integrals are obtained of the form

$$\int_{r_1}^{r_2} A_i W_{ij} B_j dr.$$　　　　　　(9)

With the reference solutions which belong to the reference potentials (3), this type of integral can be evaluated analytically. Even in the case applying the Coulomb potential as a reference potential the corresponding integrals can be evaluated efficiently by making use of recursion relations [6].

3. Vector processing on the Cyber 205

The most computer-time consuming parts are the determination of the solutions G_i and G_i^+, the evaluation of the integrals (9) in the coupling

matrix and especially the iteration process for c_i and c_i^+, depending upon the number of iterations that are needed. These parts of our Fortran program have been coded directly in the vector Fortran offered by the Cyber 205 computer system. To get optimal performance special attention has been paid to the data structure being as contiguous as possible, which is the main demand in vector processing. However, the vector processing possibilities are highly determined by the structure of the coupling matrix. For large systems of coupled equations with N for instance equal to hundred or even a few hundred the coupling matrix is sparse. The structure of sparsity, i.e., the number and placements of zeros, depends on the physical model being studied. Due to this sparsity contiguity can only be obtained by the application of "data motion" primitives, the so-called Q8-routines [7]. See also the appendix.

The vector processing of the above-mentioned time consuming parts will be briefly explained.
- The determination of the solutions G_i and G_i^+ contains the determination of the reference solutions and the coefficients a_i, b_i and a_i^+, b_i^+. The calculation of these coefficients is a recursive process. Therefore, the maximum vector length can only be N. However, the calculation of the reference solutions can be performed in blocks with a vector length of $N \times K$, where K is a number of integration steps. This has not yet been done by us.
- The evaluation of the integrals (9) in the coupling matrix will be illustrated from a simple example for which the coupling matrix pictorially looks like

$$\begin{bmatrix}
a_{11} & a_{12} & a_{13} & a_{14} & & & & & & \\
a_{21} & a_{22} & a_{23} & & a_{25} & a_{26} & a_{27} & & & \\
a_{31} & a_{32} & a_{33} & a_{34} & & a_{36} & a_{37} & a_{38} & & \\
a_{41} & & a_{43} & a_{44} & & & a_{47} & a_{48} & a_{49} & \\
 & a_{52} & & & a_{55} & a_{56} & & & & \\
 & a_{62} & a_{63} & & a_{65} & a_{66} & a_{67} & & & \\
 & a_{72} & a_{73} & a_{74} & & a_{76} & a_{77} & a_{78} & & \\
 & & a_{83} & a_{84} & & & a_{87} & a_{88} & a_{89} & \\
 & & & a_{94} & & & & a_{98} & a_{99} & \cdot \\
 & & & & & & & & \cdot & \cdot & \cdot \\
 & & & & & & & & \cdot & \cdot & a_{N-2\,N-1} \\
 & & & & & & & & & \cdot & a_{N-1\,N-1} & a_{N-1\,N} \\
 & & & & & & & & & & a_{N\,N-1} & a_{N\,N}
\end{bmatrix}, \qquad (10)$$

where the explicit representation of the individual zeros is omitted.

The mathematical expressions of the diagonal and non-diagonal integrals are different. The diagonal integrals can be obtained by using in the expressions vector operations of length N. Since the coupling matrix is symmetric, only the left-lower part has to be considered. The number of non-zero elements in this part is supposed to be M. With the following row index vector for the lower non-diagonal coupling matrix elements

$$[2\ 3\ 4\ 3\ 5\ 6\ 7\ 4\ 6\ 7\ 8\ 7\ 8\ 9\ 6\ 7\ 8\ 9\ldots N-1\ N]$$
(11)

and the corresponding column index vector

$$[1\ 1\ 1\ 2\ 2\ 2\ 2\ 3\ 3\ 3\ 3\ 4\ 4\ 4\ 5\ 6\ 7\ 8\ldots N-2\ N-1]$$
(12)

the reference solutions in (5) are gathered into vectors with length M or $M \times K$. The non-diagonal integrals can now be evaluated by means of simple vector operations. Subsequently, the diago-

nal and non-diagonal integrals are merged and a sequence number is attached to the matrix elements in the following way

$$[1(11)\ 2(21)\ 3(31)\ 4(41)\ 5(22)\ 6(32)\ 7(52)$$
$$8(62)\ 9(72)\ 10(33)\ 11(43)\ 12(63)\ 13(73)\ 14(83)$$
$$15(44)\ 16(74)\ 17(84)\ 18(94)\ldots].$$
(13)

This sequence is reordered and supplemented with the corresponding sequence number belonging to the elements of the right-upper part of the matrix according to

$$[1\ 2\ 3\ 4\ 7\ 8\ 9\ 14\ 18\ldots 2\ 5\ 6\ 11\ 19\ 12\ 13\ 17\ 26\ldots$$
$$3\ 6\ 10\ 15\ 20\ 20\ 16\ 24\ 27\ldots$$
$$4\ 7\ 11\ 16\ 0\ 21\ 22\ 25\ 0\ldots].$$
(14)

The zeros in this and the subsequent sequence (16) correspond to inactive elements, which will be suppressed by the use of control vectors. By gathering the calculated integrals according to sequence (14), all the integrals of the coupling matrix are obtained. Pictorially the matrix (10) looks now like

$$\begin{bmatrix}
a_{11} & a_{12} & a_{13} & a_{14} & & & & \\
a_{21} & a_{22} & a_{23} & a_{25} & a_{26} & a_{27} & & \\
a_{31} & a_{32} & a_{33} & a_{34} & a_{36} & a_{37} & a_{38} \\
a_{41} & a_{43} & a_{44} & a_{47} & a_{48} & a_{49} & \\
a_{52} & a_{55} & a_{56} & & & & \\
a_{62} & a_{63} & a_{65} & a_{66} & a_{67} & & \\
a_{72} & a_{73} & a_{74} & a_{76} & a_{77} & a_{78} & \\
a_{83} & a_{84} & a_{87} & a_{88} & a_{89} & & \\
a_{94} & a_{98} & a_{99} & & & & \\
\cdot & & & & & & \\
\cdot & & a_{N-1\,N-2} & a_{N-1\,N-1} & a_{N-1\,N} & \\
\cdot & a_{N\,N-1} & a_{N\,N} & & & &
\end{bmatrix}$$
(15)

– The iteration process for $c_i(r)$ and $c_i^+(r)$ is recursive. Therefore the next considerations hold only for one integration step. The vector length of these coefficients is N. With the following column index vector (see (15))

$$[1\ 1\ 1\ 1\ 2\ 2\ 2\ 3\ 4\ldots 2\ 2\ 2\ 3\ 5\ 3\ 3\ 4\ 8\ldots$$
$$3\ 3\ 3\ 4\ 6\ 5\ 4\ 7\ 9\ldots 4\ 5\ 4\ 7\ 0\ 6\ 6\ 8\ 0\ldots]$$
(16)

they are gathered to a vector length equals the length of the sequence (14) or matrix (15). The multiplication of the matrices and vectors in (8) can now be performed. The new coefficients are obtained by the addition of parts with a length N of the result vector of this multiplication. The construction of the original coupling matrix in form (15) dispenses with the necessity for the use of the data motion primitive Q8SSUM.

4. Results

To analyse experimental data, the set (1) has to be solved in general for some hundreds of different J-values. Here the results will be mentioned of calculations for one arbitrary J-value of two distinct heavy ion nuclear collision test cases. A sparsity factor, i.e. the number of zeros in the coupling matrix compared to the total number of matrix elements can be given by

$$Sf = \left[N^2 - (2M + N) \right] / N^2. \tag{17}$$

In table 1 the processor time in seconds for the calculation of the solutions G_i and G_i^+, the integrals in the coupling matrix and the iteration process for c_i and c_i^+, beside the overhead and total-time, are shown for both test cases. For each test case the processor times for a highly optimized scalar mode can be compared with a vector mode of the program.

The table shows that the gain of the vector mode compared to the scalar mode for the solutions G_i and G_i^+ is restricted. The main reason is that for a part of the integration range a call to the Airy function subroutine has to be done which is not yet vectorized. In addition, this is a recursive process which allows only a maximum vector length of N. This is also the case with the iteration process, although a high sparsity factor favours the vector mode. However, the most important speed-up comes from the evaluation of the integrals in the coupling matrix. The table shows that for this part the explained vector algorithm is about 6 times faster than the original scalar algorithm, mainly due to the possibility of choosing here a maximum vector length of $M \times K$. This results in a overall speedup of about a factor of 2 to 2.5.

Table 1
Processor times in seconds

Mode ,Sol. G, G^+	Integrals	Iteration	Overhead	Total-time
Test case A with $N = 64$, $M = 516$, $K = 10$ and $Sf = 0.73$				
scalar 2.286	11.283	7.621	1.341	22.531
vector 1.861	2.107	6.448	1.361	11.777
Test case B with $N = 169$, $M = 588$, $K = 10$ and $Sf = 0.95$				
scalar 5.407	18.309	9.215	0.986	33.917
vector 4.803	2.788	5.233	1.073	13.897

Appendix

The Q8 intrinsic functions Q8VGATHR, Q8VMERG, Q8VCTRL, Q8SNCT, have been applied in our code. They are clearly described in the Fortran 200 Manual (chap. 10) [7]. Here a brief explanation of Q8VGATHR will be given, which is the most used Q8-function in our program. A call looks like

$$R(1; M) = Q8VGATHR(S(1; N), I(1; M);$$
$$R(1; M)),$$

where S is the source, I the index and R the result vector, respectively. Each element of the result vector corresponds to an element in the index vector. This means that the index vector has to be as long as the result vector. The elements in the index vector indicate which element of the source vector are assigned to the corresponding elements in the result vector. This is illustrated below, where the function is applied to gather the reference solution G_i by means of the index vector (11).

S-vector $[G_1 \ G_2 \ G_3 \ G_4 \ G_5 \ G_6 \ G_7 \ G_8 \ G_9 \dots]$,

I-vector $[2 \ 3 \ 4 \ 3 \ 5 \ 6 \ 7 \ 4 \ 6 \ 7 \ 8 \ 7 \ 8 \ 9 \dots]$,

R-vector $[G_2 \ G_3 \ G_4 \ G_3 \ G_5 \ G_6 \ G_7 \ G_4 \ G_6 \ G_7$
$G_8 \ G_7 \ G_8 \ G_9 \dots]$.

References

[1] L.D. Tolsma, Phys. Rev. C20 (1979) 592.
[2] R.G. Gordon, J. Chem. Phys. 51 (1969) 14.
[3] L.Gr. Ixaru, Comput. Phys. Commun. 20 (1980) 97.
[4] K. Alder, F. Roesel and R. Morf, Nucl. Phys. A284 (1977) 145.
[5] M. Ichimura, M. Igarashi, S. Landowne, C.H. Dasso, B.S. Nilsson, R.A. Broglia and A. Winther, Phys. Lett. 67B (1977) 129.
[6] L.D. Tolsma, to be published.
[7] Fortran 200 version 1 Reference Manual, Control Data (1984).

SOME APPLICATIONS

$E2$ and $E4$ transition moments in ^{163}Dy and ^{167}Er†

H. J. Wollersheim* and Th. W. Elze

Institut für Kernphysik, Universität Frankfurt/Main, Germany

L. D. Tolsma

Physics Department, Eindhoven University of Technology, Eindhoven, The Netherlands

(Received 7 September 1977)

Coulomb excitation by α particles is used to determine reduced $E2$ and $E4$ transition matrix elements between ground-band rotational states in ^{163}Dy and ^{167}Er. The following results are obtained for ^{163}Dy: $\langle 7/2\ 5/2\|M(E2)\|5/2\ 5/2\rangle = 3.83 \pm 0.10$ e b; $\langle 9/2\ 5/2\|M(E2)\|5/2\ 5/2\rangle = 2.31 \pm 0.02$ e b; $\langle 11/2\ 5/2\|M(E4)\|5/2\ 5/2\rangle = 0.60^{+0.42}_{-0.60}$ e b², and for ^{167}Er: $\langle 9/2\ 7/2\|M(E2)\|7/2\ 7/2\rangle = 4.38 \pm 0.08$ e b; $\langle 11/2\ 7/2\|M(E2)\|7/2\ 7/2\rangle = 2.24 \pm 0.01$ e b; $\langle 13/2\ 7/2\|M(E4)\|7/2\ 7/2\rangle = 0.77^{+0.39}_{-0.51}$ e b². Quadrupole and hexadecapole moments deduced from these values are compared with those of neighboring even-A nuclei.

> NUCLEAR REACTIONS ^{163}Dy(α,α'), ^{167}Er(α,α'), $E = 12$ MeV, measured $\sigma(E_{\alpha'}$, 160°). Deduced $E2$ and $E4$ matrix elements.

I. INTRODUCTION

In recent years much experimental information has become available on quadrupole and hexadecapole moments of even-A nuclei in both the rare earth and actinide regions of the Periodic Table. In most of these studies α particles of sufficiently low energy have been used to Coulomb excite the 2^+ and 4^+ levels of the ground-state rotational band. The reduced $E2$ and $E4$ transition matrix elements, $\langle 2^+\|M(E2)\|0^+\rangle$ and $\langle 4^+\|M(E4)\|0^+\rangle$, are determined by comparing the experimental excitation probabilities of the 2^+ and 4^+ rotational states with theoretical values calculated within the framework of a suitable theory of multiple Coulomb excitation.

The purpose of the present experiment is to extend the precise Coulomb excitation studies performed in this laboratory[1-4] and elsewhere[5-13] to odd-A nuclei. Owing to the higher-level density, generally, more ground-band levels are populated by Coulomb excitation with α particles than in the neighboring even nuclei. Thus one is enabled to determine additional $E2$ matrix elements and verify the validity of the nuclear model used in the analysis.

From the observed excitation probabilities of the various ground-band levels, the intrinsic quadrupole and hexadecapole moments are determined and compared with those of the neighboring even-A isotopes. Preliminary results were reported earlier.[14]

II. EXPERIMENTAL PROCEDURE

The experiments were performed by bombarding thin (10–30 μg/cm²) enriched (> 91%) targets

of ^{163}Dy and ^{167}Er with 12 MeV α-particles from the University of Frankfurt Van de Graaff accelerator. The elastically and inelastically scattered projectiles were detected at $\theta_L = 160°$ with
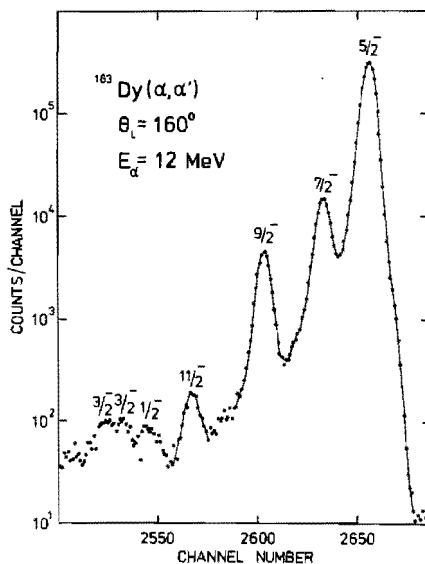

FIG. 1. Spectrum of 12 MeV α-particles scattered from ^{163}Dy.

– 151 –
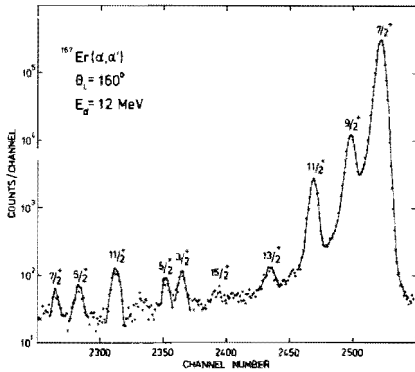
FIG. 2. Spectrum of 12 MeV α-particles scattered from ^{167}Er.

two cooled Si surface-barrier detectors positioned symmetrically to the beam direction. A peak-to-background ratio of better than 30 000:1 and an energy resolution of ~21 keV full width at half maximum (FWHM) have been achieved. Typical spectra are shown in Figs. 1 and 2.

The excitation cross section for the first excited state of the ground band was determined by means of a computer code which separated the respective peak from the elastic group in a self-consistent iterative procedure assuming identical line shapes. The intensities were simultaneously corrected for known impurities in the target material. At higher excitation energies a fourth-order polynomial fit was used to separate the peaks from the background. The excitation probabilities of the $\frac{9}{2}^{+}$, $\frac{11}{2}^{+}$, and $\frac{13}{2}^{+}$ levels in ^{167}Er were determined to an accuracy of 3.5%, 1.3%, and 8.7%, respectively. Similar uncertainties have been observed in ^{163}Dy.

III. ANALYSIS AND DISCUSSION

The reduced $E2$ and $E4$ transition matrix elements were obtained from the measured excitation probabilities by using both the quantum mechanical coupled-channels code JUPIGOR[15] and the semiclassical Winther-de Boer multiple Coulomb excitation code.[16] The calculations show

TABLE I. Results of the Coriolis calculation for ^{167}Er. Coriolis parameters: $E_{3/2}^{0} = 500.83 \pm 14.11$ keV, $E_{5/2}^{0} = 733.82 \pm 44.11$ keV, $E_{7/2}^{0} = -143.40 \pm 1.59$ keV, $\hbar^2/2\vartheta = 9.11 \pm 0.03$ keV, $A_{3/2\,5/2} = -10.81 \pm 4.69$ keV, $A_{5/2\,1/2} = -5.11 \pm 1.77$ keV.

Spin $I\,K^{\pi}\,(Nn_z\,\Lambda)$	Level energy (keV) Calc.	Exp.	Amplitude of wave function $\frac{3}{2}^{+}$ (651)	$\frac{5}{2}^{+}$ (642)	$\frac{7}{2}^{+}$ (633)
$\frac{7}{2}\,\frac{7}{2}^{+}$ (633)	−2.0	0.0	0.0009	0.0154	0.9999
$\frac{9}{2}$	81.5	79.3	0.0018	0.0234	0.9997
$\frac{11}{2}$	181.4	177.6	0.0029	0.0304	0.9995
$\frac{13}{2}$	299.4	293.7	0.0042	0.0371	0.9993
$\frac{15}{2}$	435.6	432.4	0.0057	0.0436	0.9990
$\frac{17}{2}$	589.9	592.0	0.0073	0.0500	0.9987
$\frac{19}{2}$	762.3	772.0	0.0093	0.0564	0.9984
$\frac{3}{2}\,\frac{3}{2}^{+}$ (651)	532.0	532.0	1.0000	$\cdots$	$\cdots$
$\frac{5}{2}$	578.0	574.5	0.9948	0.1021	$\cdots$
$\frac{7}{2}$	638.4	641.7	0.9880	0.1547	−0.0033
$\frac{9}{2}$	716.2		0.9799	0.1991	−0.0064
$\frac{11}{2}$	811.4		0.9711	0.2383	−0.0101
$\frac{5}{2}\,\frac{5}{2}^{+}$ (642)	816.0	812.5	−0.1021	0.9948	$\cdots$
$\frac{7}{2}$	883.3	874.0	−0.1547	0.9878	−0.0151
$\frac{9}{2}$	969.8	933.0	−0.1992	0.9797	−0.0225
$\frac{11}{2}$	1075.2		−0.2385	0.9707	−0.0289
$\frac{13}{2}$	1200.0	1205.0	−0.2735	0.9612	−0.0345

TABLE II. Reduced matrix elements $\langle I_f K_f \| M(E\lambda) \| I_i K_i \rangle$ in units of $e b^{\lambda/2}$ for levels populated by Coulomb excitation in the ^{163}Dy(α,α') and ^{167}Er(α,α') reactions.

^{163}Dy

$\langle \frac{7}{2} \, \frac{5}{2} \| M(E2) \| \frac{5}{2} \, \frac{5}{2} \rangle = 3.83 \pm 0.10$

$\langle \frac{9}{2} \, \frac{5}{2} \| M(E2) \| \frac{5}{2} \, \frac{5}{2} \rangle = 2.31 \pm 0.02$

$\langle \frac{11}{2} \, \frac{5}{2} \| M(E4) \| \frac{5}{2} \, \frac{5}{2} \rangle = 0.60 \pm^{0.42}_{0.60}$

^{167}Er

$\langle \frac{9}{2} \, \frac{7}{2} \| M(E2) \| \frac{7}{2} \, \frac{7}{2} \rangle = 4.38 \pm 0.08$

$\langle \frac{11}{2} \, \frac{7}{2} \| M(E2) \| \frac{7}{2} \, \frac{7}{2} \rangle = 2.24 \pm 0.01$

$\langle \frac{13}{2} \, \frac{7}{2} \| M(E4) \| \frac{7}{2} \, \frac{7}{2} \rangle = 0.77 \pm^{0.39}_{0.51}$

$\langle \frac{3}{2} \, \frac{3}{2} \| M(E2) \| \frac{7}{2} \, \frac{7}{2} \rangle = 0.49 \pm 0.03$

$\langle \frac{5}{2} \, \frac{3}{2} \| M(E2) \| \frac{7}{2} \, \frac{7}{2} \rangle = 0.42 \pm 0.02$

$\langle \frac{5}{2} \, \frac{5}{2} \| M(E2) \| \frac{7}{2} \, \frac{7}{2} \rangle = 0.53 \pm 0.03$

$\langle \frac{7}{2} \, \frac{5}{2} \| M(E2) \| \frac{7}{2} \, \frac{7}{2} \rangle = 0.44 \pm 0.04$

$\langle \frac{11}{2} \, \frac{11}{2} \| M(E2) \| \frac{7}{2} \, \frac{7}{2} \rangle = 0.70 \pm 0.02$

that the hexadecapole moment can be determined from the cross section of the third excited state, while its influence on the first and second excited states is negligibly small since the excitation of the latter two levels is governed by $E2$ transitions. For ^{167}Er two $E2$ matrix elements, $\langle \frac{9}{2} \, \frac{7}{2} \| M(E2) \| \frac{7}{2} \, \frac{7}{2} \rangle$ and $\langle \frac{11}{2} \, \frac{7}{2} \| M(E2) \| \frac{7}{2} \, \frac{7}{2} \rangle$, were determined from the excitation of the $\frac{9}{2}$- and $\frac{11}{2}$ levels by means of the quantum mechanical coupled-channels code. The ratio of these matrix elements was compared with the theoretical model predictions which are needed to calculate the entire $E2$ matrix. For both nuclei studied here, it

appears that the reduced transition probabilities are well described by the rigid-rotor model, without Coriolis mixing. Whether or not band mixing can be neglected was investigated in a three-band Coriolis calculation in which level energies were fitted to the experimental values by varying band-head energies, rotational parameter, and coupling strengths. The result of such a calculation, which included levels of the $K = \frac{7}{2}^+$, $\frac{5}{2}^+$, and $\frac{3}{2}^+$ bands in ^{167}Er, is shown in Table I. As can be seen, the coupling between the ground-state band and the higher bands is rather weak. A previously assigned $K = \frac{3}{2}^+$ band based on a level at 592 keV in ^{167}Er was not included in our Coriolis calculations, since Tveter *et al.*[17] have found that the $\frac{11}{2}^+$ state at 711 keV is the band head of a γ-vibrational band. This assignment is supported by the strong excitation of the 711 keV level in the present experiment. Similar results are obtained for the $K = \frac{1}{2}^-$, $\frac{5}{2}^-$, and $\frac{5}{2}^-$ bands in ^{163}Dy.

The influence of quantum mechanical effects on the cross sections was evaluated by calculating the excitation probabilities in terms of the $E2$ matrix with both the semiclassical and quantum mechanical coupled-channels code. The quantal effects reduced the differential cross sections of the $\frac{9}{2}^+$, $\frac{11}{2}^+$, and $\frac{13}{2}^+$ levels in ^{167}Er by approximately 1.6%, 1.7%, and 6.5%, respectively. These quantum mechanical corrections were then applied to the differential cross sections calculated with the semiclassical code as a function of the $E4$ matrix. The reduction of the excitation probability of the $\frac{13}{2}^+$ state by 6.5% was taken to be independent of the magnitude of the $\langle \frac{13}{2} \, \frac{7}{2} \| M(E4) \| \frac{7}{2} \, \frac{7}{2} \rangle$ matrix element. This is justified on the basis of the results shown in Fig. 2 of Ref. 1.

The $E2$ and $E4$ matrix elements obtained from the present study are listed in Table II. The sign

TABLE III. Comparison of the quadrupole and hexadecapole moments of ^{163}Dy and ^{167}Er with those of neighboring even-A nuclei.

	Q_{20} (b)	Q_{40} (b^2)	$\langle K' = K_{\text{g.s.}} \pm 2 | M(E2; \pm 2) | K_{\text{g.s.}} \rangle$ (e b)
^{163}Dy (Ref. 6)	7.36 ± 0.03	0.64 ± 0.24	
^{163}Dy	7.29 ± 0.13	$1.02 \pm^{0.71}_{1.02}$	
^{164}Dy (Ref. 1)	7.54 ± 0.04	$0.54 \pm^{0.24}_{0.25}$	
^{166}Er (Refs. 1 and 4)	7.67 ± 0.03	$0.52 \pm^{0.25}_{0.38}$	0.256 ± 0.005 ($K' = 2$)
^{167}Er	7.60 ± 0.10	$1.35 \pm^{0.57}_{0.56}$	0.248 ± 0.007 $(K' = \frac{11}{2})$ 0.249 ± 0.012 $(K' = \frac{3}{2})$
^{168}Er (Refs. 6 and 18)	7.61 ± 0.06	$0.47 \pm^{0.28}_{0.45}$	0.255 ± 0.005 ($K' = 2$)

of the $E4$ matrix element was taken to be positive, in analogy to the even-A neighboring nuclei. Also shown are interband matrix elements for ^{167}Er which have been determined from the measured cross sections by means of semiclassical calculations assuming identical intrinsic quadrupole moments[4] in the $K = \frac{3}{2}^+$, $\frac{5}{2}^+$, and $\frac{11}{2}^+$ rotational bands. The $E2$ matrix elements obtained are found to be in good agreement with previous measurements.[18]

Intrinsic quadrupole and hexadecapole moments derived from the measured reduced $E2$ and $E4$ matrix elements are compared with those of the even-A neighboring nuclei in Table III. It is seen that there is agreement of these values within the experimental uncertainties. In the case of the Er isotopes, the intrinsic interband matrix elements between the ground-state band and the γ-vibrational bands ($K_\gamma = K_{g.s.} \pm 2$) are also shown. In summary, the measured multipole moments indicate that the shapes of the strongly deformed odd-A nuclei ^{163}Dy and ^{167}Er are similar to those which have been determined for the respective neighboring even-A isotopes.

---

*Present address: Gesellschaft für Schwerionenforschung, Darmstadt, Germany.

[1] H. J. Wollersheim, W. Wilcke, Th. W. Elze, and D. Pelte, Phys. Lett. 48B, 323 (1974).

[2] H. J. Wollersheim, W. Wilcke, and Th. W. Elze, Phys. Rev. C 11, 2008 (1975).

[3] H. J. Wollersheim and Th. W. Elze, Nucl. Phys. A278, 87 (1977).

[4] H. J. Wollersheim and Th. W. Elze, Z. Phys. A280, 277 (1977).

[5] F. S. Stephens, R. M. Diamond, N. K. Glendenning, and J. de Boer, Phys. Rev. Lett. 24, 1137 (1970); F. S. Stephens, R. M. Diamond, and J. de Boer, ibid. 27, 1151 (1971).

[6] K. A. Erb, J. E. Holden, J. Y. Lee, J. X. Saladin, and T. K. Saylor, Phys. Rev. Lett. 29, 1010 (1972).

[7] W. Ebert, P. Hecking, K. Pelz, S. G. Steadman, and P. Winkler, Z. Phys. 263, 191 (1973).

[8] W. Brückner, J. G. Merdinger, D. Pelte, U. Smilansky, and K. Traxel, Phys. Rev. Lett. 30, 57 (1973).

[9] A. H. Shaw and J. S. Greenberg, Phys. Rev. C 10, 263 (1974).

[10] R. M. Ronningen, R. B. Piercey, R. S. Grantham, J. H.

Hamilton, A. V. Ramayya, B. van Nooijen, H. Kawakami, C. Maguire, L. L. Riedinger, and W. K. Dagenhart, Bull. Am. Phys. Soc. 21, 985 (1976).

[11] C. E. Bemis, Jr., F. K. McGowan, J. L. C. Ford, Jr., W. T. Milner, P. H. Stelson, and R. L. Robinson, Phys. Rev. C 8, 1466 (1973); F. K. McGowan, C. E. Bemis, J. L. C. Ford, Jr., W. T. Milner, R. L. Robinson, and P. H. Stelson, Phys. Rev. Lett. 27, 1741 (1971).

[12] C. Baktash and J. X. Saladin, Phys. Rev. C 10, 1136 (1974).

[13] J. H. Hamilton, L. Varnell, R. M. Ronningen, R. V. Ramayya, J. Lange, L. L. Riedinger, R. L. Robinson, and P. H. Stelson, Bull. Am. Phys. Soc. 19, 579 (1974).

[14] H. J. Wollersheim and Th. W. Elze, Verh. Dtsch. Phys. Ges. 11, 915 (1976).

[15] L. D. Tolsma, J. Comput. Phys. 17, 384 (1975).

[16] A. Winther and J. de Boer, in Coulomb Excitation, edited by K. Alder and A. Winther (Academic, New York, 1966), p. 303.

[17] A. Tveter and B. Herskind, Nucl. Phys. A134, 599 (1969).

[18] C. Baktash, J. X. Saladin, J. O'Brien, I. Y. Lee, and J. E. Holden, Phys. Rev. C 10, 2265 (1974).

Short Note

The Quadrupole Moment of ^{176}Lu*[1]

J. Gerl, K. Ronge, K. Venkata Ramaniah**, and Th.W. Elze
Institut für Kernphysik, Universität Frankfurt, D-6000 Frankfurt am Main,
Federal Republic of Germany

A. Hanser
Kernforschungszentrum Karlsruhe, Institut für Angewandte Kernphysik,
D-7500 Karlsruhe, Federal Republic of Germany

L.D. Tolsma
Physics Department, University of Technology, Eindhoven, The Netherlands

Abstract: The intrinsic quadrupole moment of
^{176}Lu has been determined by Coulomb excitation
with α-particles to be 6.98 ± 0.10 b. Evidence
for a new level at approximately 578 keV with
presumably collective structure is presented.

The electromagnetic properties of ^{176}Lu are
of much current interest since it has been pro-
posed to use the β-decay of its $K, I^{\pi} = 7, 7^-$
ground state to ^{176}Hf ($T_{1/2} = 3.6 \times 10^{10}$ y) as a
cosmic chronometer for s-process nucleosynthesis
(see e.g. [1] and references cited therein). The
ground-state decay, however, is complicated by
the $K, I^{\pi} = 0, 1^-$ isomeric state at 127 keV which
decays to ^{176}Hf with a half life of only 3.68 hr.
If, at stellar temperatures, this short-lived
isomer is linked to the ground state by electro-
magnetic interaction, then the total half life
against β-decay will be considerably smaller than
the known ground-state value and the applicabi-
lity of ^{176}Lu as cosmic clock may become ques-
tionable. In order to make estimates possible to
what extent the isomer can be excited, we have
initiated a general study of the electromagnetic
properties of ^{176}Lu, part of which is the precise
determination of its intrinsic quadrupole moment
reported in this communication.

The experiment was performed by exposing
thin (<10 µg/cm^2), isotopically pure ^{176}Lu tar-
gets to α-particle beams with energies of 9.5,
13.5 and 14.0 MeV obtained from the University of
Frankfurt Van de Graaff accelerator. The targets
were fabricated using the Karlsruhe isotope se-
parator. Elastically and inelastically scattered

α-projectiles were detected by two cooled and
collimated Si surface-barrier detectors position-
ed at ±164° with respect to the beam direction.
An energy resolution of typically 22 keV (FWHM)
was achieved. At the beam energy of 13.5 MeV two
separate measurements were performed and, hence,
a total of 8 spectra was obtained. A representa-
tive spectrum measured at 13.5 MeV is shown in
Fig. 1. This spectrum shows excitation of the
ground band up to and including the 10$^-$ state,
with an additional peak seen at 578 keV (marked
by "?"). This latter group is probably due to a
collective ^{176}Lu level which is reported here for
the first time. Since the intensity of this peak
strongly decreases with decreasing projectile
energy and, moreover, its position in the spec-
trum is independent of the projectile energy, it
is most unlikely that this peak is caused by a
target contaminant.

The excitation cross section of the 8$^-$ state
was obtained relative to the elastic-scattering
strength by using a computer code that separated
the 8$^-$ and 7$^-$ peaks in an iterative, selfconsis-
tent procedure assuming identical line shapes.
The intensities of the other groups were obtained
by fitting third-order polynomials to the back-
ground below and above each peak.

To deduce the intrinsic quadrupole moment
from the measured excitation probabilities, semi-
classical Coulomb-excitation cross sections were
calculated using the Winther-de Boer code [2].
All E2 matrix elements which connect the 7$^-$, 8$^-$,
9$^-$ and 10$^-$ levels were included in these calcula-
tions, with the rigid-rotor formula [3] used to
relate the reduced matrix elements to the intrin-
sic quadrupole moment Q_0,

$$\langle I_f K || M(E2) || I_i K \rangle = \sqrt{(2I_i+1)\ 5/16\pi}\ (I_i K 20 | I_f K) e Q_0.$$

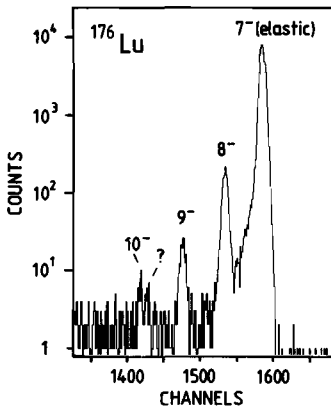*Fig. 1: Spectrum of α-particles scattered elastically and inelastically from a ^{176}Lu target. Projectile energy $E_\alpha = 13.5$ MeV, $\Theta_{lab} = 164^O$. The group labelled "?" ($E_{exc} \approx 578$ keV) is presumably due to a collective state in ^{176}Lu reported here for the first time.*

The quadrupole moment Q_0 was derived by adjusting the entire E2 matrix to fit the measured excitation probability of the 8^- level. The E2 matrix obtained in this way was found to reproduce also the experimental excitation cross sections of the 9^- and 10^- levels within their experimental uncertainties. This result justifies in turn the application of the rigid-rotor model to describe the lowest states of ^{176}Lu.

Several corrections were applied to the semi-classical calculations just described, the most important of which is due to quantal effects. This correction was evaluated by calculating the excitation cross sections with a quantum-mechanical coupled-channels code [4] and comparing the results to the semi-classical calculations. Quantal effects were found to enhance the quadrupole moment deduced from the excitation probability of the 8^- state measured at 13.5 MeV by 1.4%. Further corrections which are due to atomic screening, vacuum polarization and dipole polarization of the target nucleus have been applied following the prescription given in ref. [5]. The sum of these corrections, all of which act in the same direction, reduce the quadrupole moment by $\approx 1.1\%$ to 1.4% depending on the projectile energy. The E4 excitation, however, has been neglected as it has virtually no effect ($< 0.1\%$) on the quadrupole moment deduced, assuming an either positive or negative intrinsic hexadecapole moment as found in the neighbouring ^{176}Yb and ^{176}Hf nuclei, respectively [6,7].

Table 1 shows the results for the intrinsic quadrupole moment Q_0 obtained from the individual measurements performed at different bombarding energies, together with their statistical errors. The sign of Q_0 was chosen to be positive accord-

ing to the prolate deformation observed in this mass region. The result obtained at the highest projectile energy (14.0 MeV) is seen to be considerably smaller than the values deduced at lower bombarding energies. This fact is attributed to the onset of interference effects between the Coulomb and nuclear interactions. Also included in Table 1 is the weighted average $<Q_0>$

Table 1: Intrinsic quadrupole moment Q_0 of ^{176}Lu as derived from the individual Coulomb-excitation measurements performed at different bombarding energies and the resulting average value $<Q_0>$

E (MeV)	Q_0 (b)	$<Q_0>$ (b)
9.5	6.99 ± 0.09 ⎫	
13.5	6.94 ± 0.05 ⎬	6.98 ± 0.10
	7.02 ± 0.06 ⎭	
14.0	6.69 ± 0.08	

obtained from the measurements at 9.5 and 13.5 MeV. The error associated with $<Q_0>$ as given in Table 1 has been chosen to be approximately twice the statistical uncertainty in order to account for the fact that the 578 keV level has been neglected in the Coulomb-excitation calculations. Inclusion of this state in the data analysis was found to alter the quadrupole moment only within these error limits when either E2 or E3 excitation was assumed and matrix elements were used that reproduce all of the measured excitation cross sections. A more detailed discussion of the results described in this communication, together with additional data on the electromagnetic properties of ^{176}Lu will be the subject of a forthcoming publication.

**   On leave from Physics Department, Andhra University, Visakhapatnam, India

[1] H. Beer, F. Käppeler, K. Wisshak and R. A. Ward, Astrophys. J. Suppl. 46, 295 (1981)

[2] A. Winther and J. de Boer, in Coulomb Excitation, K. Alder and A. Winther ed., New York: Academic Press, 1966

[3] A. Bohr and B. R. Mottelson, Nuclear Structure, Vol. 2, New York: W. A. Benjamin, 1975

[4] L. D. Tolsma, Phys. Rev. C 20, 592 (1979)

[5] K. Alder and A. Winther, Electromagnetic Excitation, Amsterdam: North Holland, 1975

[6] H. J. Wollersheim, W. Wilcke and Th. W. Elze, Phys. Rev. C 11, 2008 (1975)

[7] R. M. Ronningen et al., Phys. Rev. C 16. 2208 (1977)

SUMMARY

The quantum-mechanical description of inelastic scattering processes with multiple excitation induced by atomic particles requires the numerical solution of the Schrödinger equation, which can be reformulated as a set of coupled linear second-order radial differential equations. In this thesis, the computational aspects of solving the Schrödinger equation are investigated for small, as well as for large sets.

For small sets the investigation deals with the accuracy of the numerical integration process. The sets are solved as many times as the dimension of the set with linearly independent regular starting values for each of the solution vectors. A method has been used successfully for measuring the accuracy of the regular solution subspace spanned by the solution vectors, rather than the accuracy of the solution vectors themselves, in order to investigate the accuracy of the integration process. This method computes the principal angles between two solution subspaces obtained under different numerical conditions (varying integration step length and stabilization strategy). One of the subspaces is constructed under optimal conditions so that it is considered to be the reference subspace, the other being the subspace to be investigated. In this method, the quality of a solution subspace obtained by a numerical procedure, can be measured, e.g., the extent to which solution vectors, as a basis of the solution subspace, remain linearly independent in the range from the origin to the matching radius R_m during the integration.

The computation of the principal angles can be used to inspect the loss of accuracy in the integration range originating from the truncation error inherent in the difference formula used and to detect the possible sources of deficiencies in the numerical process for solving the Schrödinger equation. A method has been developed and applied with which deficiencies caused by discontinuities in the potential matrix can be avoided.

The loss of accuracy due to the tendency of the solution vectors to become "nearly linearly dependent" during the integration through a classically forbidden region as an effect of round-off errors, can be examined by determining the principal angles, too. This loss of accuracy requires stabilization of the set of solution vectors. We found that, in our test cases of alpha particle scattering from ^{28}Si, including some with an energy near the Coulomb barrier, stabilization in only a few well-chosen mesh points was sufficient to obtain an S-matrix accuracy adequate for practical purposes.

In order to take into account the long range of the Coulomb coupling effectively, an integration method has been applied based upon piecewise analytic reference solutions.

To describe heavy-ion reactions, large sets will occur together with a rapidly oscillating behaviour of the solution function within the classically allowed region of the integration range and with an even longer range of the Coulomb coupling. In order to investigate the computational aspects of these sets, the set of coupled differential equations of the partial-wave radial solutions is rewritten in integral form. Decomposing these solutions into two basis functions, the corresponding amplitudes satisfy a set of coupled integral equations. Expressing the basis functions in terms of appropriately chosen piecewise analytic reference solutions, the integrals appearing in this set can be evaluated analytically. The goniometric and Airy functions, as well as the Coulomb wave functions are used as reference solutions. The integrals containing Coulomb wave functions can be determined efficiently using recurrence relations. The coupled set of amplitude equations is solved iteratively. The efficiency of two iteration methods, the inward-outward and the sequential one, has been investigated for test cases dealing with multiple Coulomb excitation of ^{238}U by 385 MeV ^{84}Kr up to high spin states of the ground-state rotational band. The Coulomb and nuclear excitation of ^{238}U by 286 MeV ^{40}Ar and 718 MeV ^{84}Kr has been considered too. Padé approximants to the S-matrix elements were also included in both of the iteration methods. It turns out that the inward-outward iteration method converges much faster than the sequential one. In many cases, the inward-outward method does not need Padé acceleration at all, while the sequential method does. It even happens sometimes that convergent cases in the inward-outward method diverge in the sequential method aided by Padé approximants. The excitation probabilities as a function of the scattering angle were calculated for the aforementioned heavy-ion reactions.

A method for vectorization of coupled-channel Fortran programmes, based upon these integral equations, has been investigated for use on the Cyber 205 computer (with one vector-pipeline). Results are given for the excitation test cases of ^{238}U by ^{40}Ar and ^{84}Kr. In these cases with dimensions of the set of 64 and 169, respectively, it appears that the vector algorithm gives a partial speed-up of 4 to 8, resulting in an overall factor of 2 to 3 speed-up as compared with a highly optimized scalar algorithm.

Finally, the intrinsic quadrupole and hexadecapole moments of some odd-A nuclei have been determined in collaboration with a group from the university of Frankfurt (BRD).

SAMENVATTING

De quantummechanische beschrijving van inelastische verstrooiings-
processen met meervoudige excitatie geinduceerd door atomaire deeltjes
vereist de numerieke oplossing van de Schrödinger-vergelijking. Deze ver-
gelijking kan worden geschreven als een stelsel gekoppelde lineaire dif-
ferentiaalvergelijkingen van de tweede orde voor de radiale golffuncties.
In dit proefschrift worden aspecten onderzocht die een rol spelen bij het
oplossen van de Schrödinger-vergelijking voor zowel kleine als grote
stelsels.

Het onderzoek van kleine stelsels heeft betrekking op de nauwkeurig-
heid van het numerieke integratieproces. Volgens de standaardprocedure
wordt het stelsel zo vaak opgelost als zijn dimensie bedraagt, met
lineair onafhankelijke reguliere startwaarden voor ieder van de oplos-
singsvectoren. Om de nauwkeurigheid van het integratieproces te onder-
zoeken is met succes een methode gebruikt om de nauwkeurigheid te meten
van de oplossingsruimte, opgespannen door de oplossingsvectoren, in
plaats van de nauwkeurigheid van die vectoren zelf. Deze methode berekent
de kanonieke hoeken tussen twee oplossingsruimten die onder verschillende
numerieke omstandigheden verkregen zijn. Een van de ruimten wordt onder
optimale omstandigheden berekend en dient als referentieruimte, terwijl
de tweede de ruimte is die wordt onderzocht. Met deze methode kan de kwa-
liteit van een oplossingsruimte, verkregen met een numerieke procedure,
gemeten worden; bijvoorbeeld, de mate waarin de lineaire onafhankelijk-
heid van de oplossingsvectoren als basis van een oplossingsruimte gehand-
haafd blijft tijdens de integratie van de oorsprong tot de straal R_m.

De berekening van deze hoeken kan worden gebruikt om het verlies aan
nauwkeurigheid in het integratie-interval, als gevolg van de afbreekfout
die inherent is aan de gebruikte differentieformule, na te gaan. Tevens
kunnen mogelijke onvolkomenheden in het numerieke proces worden waargeno-
men. Een methode is ontwikkeld en toegepast waarmee gebreken, veroorzaakt
door discontinuiteiten in de potentiaalmatrix, kunnen worden vermeden.

Het nauwkeurigheidsverlies ten gevolge van de neiging van de oplos-
singsvectoren om tijdens de integratie door een klassiek verboden gebied
"bijna lineair afhankelijk" te worden door afrondfouten, kan ook door
bepaling van de kanonieke hoeken worden onderzocht. Dit verlies vereist
stabilisatie van het vectorstelsel. Het bleek dat in onze testgevallen
van alpha-verstrooiing aan ^{28}Si, waarvan enkele met een energie in de
buurt van de Coulomb-barrière, stabilisatie slechts in een klein aantal
goedgekozen integratiepunten nodig was om een nauwkeurigheid van de
S-matrix te verkrijgen, die voldoende is voor practische toepassingen.

Om met de lange dracht van de Coulombkoppeling effectief rekening te houden, is een integratiemethode toegepast gebaseerd op intervalsgewijs te bepalen analytische referentieoplossingen.

Bij de beschrijving van zware-ionenprocessen komen grote stelsels voor met een snel oscillerend gedrag van de oplossingsfunctie in het klassiek toegankelijke gebied van het integratie-interval en met een nog langere dracht van de Coulombkoppeling. Om de berekeningsaspecten van deze stelsels te onderzoeken wordt het stelsel gekoppelde differentiaal-vergelijkingen voor de radiale partiële-golfoplossingen geschreven in integraalvorm. Door deze oplossingen in twee basisfuncties te ontwikkelen voldoen de overeenkomstige amplitudes aan een stelsel gekoppelde inte-graalvergelijkingen. De integralen die in dit stelsel voorkomen kunnen analytisch worden bepaald door de basisfuncties intervalsgewijs uit te drukken in geschikt gekozen analytische referentieoplossingen. Zowel goniometrische en Airyfuncties als Coulombgolffuncties worden als refe-rentieoplossingen gebruikt. De integralen met Coulombgolffuncties kunnen efficiënt met recursierelaties worden bepaald. Het gekoppelde stelsel van amplitudevergelijkingen wordt iteratief opgelost. De efficiëntie is onderzocht van twee iteratieschema's, de inwaarts-uitwaarts-methode en de sequentiële, voor testgevallen van meervoudige Coulomb-excitatie van ^{238}U door 385 MeV ^{84}Kr tot aan hoge spintoestanden van de grondtoestand rotatieband. Tevens is de Coulomb-kern-excitatie van ^{238}U door 286 MeV ^{40}Ar en 718 MeV ^{84}Kr bekeken. Ook werd in beide iteratiemethoden Padé-approximatie op de S-matrixelementen toegepast. Het blijkt dat de inwaarts-uitwaartse iteratiemethode veel sneller convergeert dan de sequentiële. In veel gevallen heeft de inwaarts-uitwaartse methode in het geheel geen Padé-versnelling nodig in tegenstelling tot de sequentiële methode. Voor bovengenoemde zware-ionenreacties werden de excitatie-waarschijnlijkheden als functie van de verstrooiingshoek berekend en voor zover mogelijk vergeleken met het experiment.

Een methode voor vectorisatie van gekoppelde-kanalen Fortranprogram-ma's, gebaseerd op deze integraalvergelijkingen, is voor gebruik op de Cyber 205 supercomputer (met één vectorpijplijn) onderzocht. Resultaten worden gegeven voor de testgevallen waarin ^{238}U geëxciteerd wordt door ^{40}Ar and ^{84}Kr. Voor deze gevallen, met een stelsel van dimensie 64, respectievelijk 169, blijkt dat het vectoralgoritme een partiële versnelling geeft van 4 tot 8, resulterend in een totale versnellings-factor van 2 tot 3 vergeleken met een geoptimaliseerd scalair algoritme.

Tenslotte zijn de intrinsieke quadrupool- en hexadecapoolmomenten van enige oneven-A kernen bepaald in samenwerking met een groep van de universiteit te Frankfurt (BRD).

DANKWOORD

Het onderzoek dat aan dit proefschrift ten grondslag ligt kon slechts tot stand komen door bijdragen die andere personen hieraan hebben geleverd. Langs deze weg wil ik dan ook graag een woord van dank aan hun adres uitspreken.

Dit geldt op de eerste plaats voor mijn beide promotoren, de professoren Dr. B.J. Verhaar en Dr. G.W. Veltkamp. Door mij deelgenoot te maken van hun kennis en inzicht in het onderhavige onderwerp en mij daarop kritisch te bevragen, hebben zij mede richting en inhoud van het onderzoek bepaald. De soms moeizame discussies met hen waren toch een voortdurende stimulans voor mij.

Het beschreven onderzoek kon niet worden uitgevoerd zonder uitgebreid en langdurig rekenwerk, dat op de Burroughs 7700/7900 computers van de Technische Hogeschool moest worden verricht. Hiervoor bleek het nodig om het onderste uit de computerkan te halen, wat nooit gelukt zou zijn zonder de hulp van medewerkers van het Rekencentrum, met name van Gertjan Visser, Henk van de Langenberg, Carel Braam en Piet Tutelaers. Ook de medewerking, voor o.a. de speciale weekend-arrangementen, die ik van Loek van de Putte en zijn medewerkers ondervond, heb ik zeer op prijs gesteld. In een later stadium van het onderzoek zijn berekeningen uitgevoerd op de Cyber 205 supercomputer van het Academisch Rekencentrum te Amsterdam. Ook een aantal medewerkers van dit rekencentrum ben ik zeer erkentelijk voor de verleende assistentie.

Een gewaardeerde bijdrage aan de vormgeving van dit proefschrift is geleverd door Ruth Gruijters en incidenteel ook door de heer C. Quak, die het tekenwerk voor hun rekening heben genomen. Dr. Peter Attwood ben ik zeer erkentelijk voor zijn bijstand bij het vinden van de juiste formuleringen in het engels.

Tenslotte dank ik stagiairs en afstudeerders voor hun bijdrage aan het onderzoek en mijn collega's uit de groep Experimentele Kernfysica voor hun vriendschap die van grote morele betekenis voor mij was.

Allen, van harte bedankt !!!

CURRICULUM VITAE

17 juli 1937   Geboren te Magelang, Indonesië.

Juli   1950   Definitieve vestiging in Nederland.

1950 - 1956   Middelbare schoolopleiding aan het Sint-Joris College te Eindhoven.

1956 - 1958   Vervulling militaire dienstplicht.

1958 - 1965   Studie aan de Technische Hogeschool Eindhoven, aangevangen in de afdeling der Electrotechniek. Na het afleggen van het kandidaatsexamen in deze afdeling is de studie voortgezet in de afdeling der Technische Natuurkunde. Het ingenieursdiploma is behaald met afstudeerwerk verricht in de groep Kernfysica.

1966 - heden   Wetenschappelijk medewerker aan de Technische Hogeschool Eindhoven, afdeling der Technische Natuurkunde, in de groep Kernfysica, later in de werkgroep Theoretische Kernfysica van de vakgroep Deeltjesfysica, en sinds 1983 in de vakgroep Theoretische Natuurkunde.

1979 - 1985   Lid van de Hogeschoolraad, waarvan twee jaar als plaatsvervangend voorzitter.

STELLINGEN

behorende bij het proefschrift van

L.D. Tolsma

Eindhoven, 13 juni 1986.

1. Conclusies met betrekking tot de geldigheid van benaderingen als de Bornapproximatie, toegepast op de "modulerende amplitudes", welke zijn gebaseerd op berekeningen waarin de grondtoestand met slechts één aangeslagen toestand wordt gekoppeld, gelden niet a priori voor gekoppelde-kanalenberekeningen met meervoudige excitatie.

   M. Rhoades-Brown, M.H. Macfarlane and S.C. Pieper,
   Phys. Rev. C21(1980)2417.

2. M. Rhoades-Brown e.a. maken een vergelijking tussen de geschatte rekentijden, die enerzijds nodig zijn voor een door hen toegepaste iteratiemethode voor het oplossen van grote stelsels differentiaal-vergelijkingen en anderzijds voor de standaardmethode. De voor hun aanpak gunstig uitvallende conclusie is onjuist.

   M. Rhoades-Brown, M.H. Macfarlane and S.C. Pieper,
   Phys. Rev. C21(1980)2436.

3. De zogenoemde lambda-up recursierelatie voor electrische-multipool radiale matrixelementen is, vanuit numeriek oogpunt beschouwd, voor veel toepassingen nauwelijks bruikbaar.

4. Een grote mate van symmetrie in berekende S-matrixelementen is geen garantie voor een even grote numerieke nauwkeurigheid van deze elementen.

   R.G. Gordon, "Quantum Scattering Using Piecewise Analytic Solutions" in: Methods in Computational Physics 10, Atomic and Molecular Scattering, eds. B. Alder et al. (Academic, New York, 1971), p.81; Dit proefschrift, hoofdstuk 3.

5. De analyses van experimentele resultaten met behulp van het in brede kring gebruikte computerprogramma JUPITOR hebben hun waarde niet verloren ondanks de deficiënties hierin die met de in dit proef-schrift beschreven methode zijn waargenomen.

   T. Tamura, Oak Ridge National Laboratory Report No.ORNL-4152(1967); H. Rebel and G.W. Schweimer, Kernforschungszentrum Karlsruhe Report No. KFK-1333(1971).

6. Het oplossen van een stelsel differentiaalvergelijkingen

$$\frac{d^2}{dr^2} \psi_i(r) = \sum_j^n V_{ij}(r) \psi_j(r), \qquad i = 1,2,\ldots,n$$

met een integratiemethode gebaseerd op een differentieformule waar-
van de afbreekfout van hoge orde is, moet zinloos worden geacht als
de potentiaalfunctie $V_{ij}(r)$ discontinuiteiten in lage afgeleiden
bevat.

N.M. Clarke, Comput. Phys. Commun. 27(1982)365;
Dit proefschrift, hoofdstuk 3.

7. De bijdrage die universiteiten en technische hogescholen moeten
leveren aan technologische innovatie en versterking van de economie
dient niet ten koste te gaan van wat er van hun universaliteit nog
over is. Deze laatste dreigt opnieuw aangetast te worden door de
beleidsvoornemens van de minister om de activiteiten op het gebied
van de lichamelijke, sociaal-culturele en geestelijke vorming van
studenten niet meer tot de universitaire taken te rekenen.

Notitie inzake het beleid betreffende studentenvoorzieningen,
Ministerie van Onderwijs en Wetenschappen, juni 1985.
Commentaar op de notitie van het Landelijk Overleg Studenten-
pastoraat, Humanistisch Studentenraadswerk, Joods Studentenwerk
IJAR, october 1985.

8. De wijze waarop de universiteiten in Japan tegen een zeer geringe
vergoeding gebruik kunnen maken van supercomputers steekt schril af
bij het hier te lande gehanteerde doorberekeningssysteem van de
gemaakte rekenkosten. Dit zal verstrekkende gevolgen hebben voor de
ontwikkeling van wetenschap en techniek.

K.G. Wilson, "Science, Industry, and the New Japanese Challenge" in:
Supercomputers – their impact on science and technology,
Proceedings of the IEEE 72(1984)6.
J.M. van Kats, R. Llurba en A.J. van der Steen, Reisverslag bezoek
aan Japan, verschijnt in ACCU-reeks, Academisch Computer Centrum
Utrecht, 1986.

9. De Technische Hogeschool Eindhoven dient in overweging te nemen om ten behoeve van onderwijs en onderzoek een multiprocessor parallel-computer aan te schaffen met een architectuur zoals een, die gebaseerd is op de hyperkubus topologie.

dimensie	0	1	2	3	4	5
processoren	1	2	4	8	16	32
verbindingen	0	1	4	12	32	80
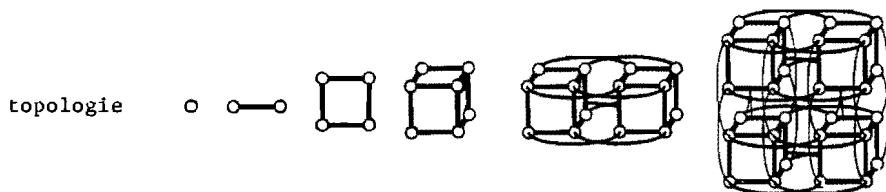
topologie

De hyperkubus topologie

10. Zo er al sprake is van een beleid van de zijde van het Nederlandse Episcopaat ten aanzien van het pastoraat onder studenten van het Wetenschappelijk en Hoger Beroeps-Onderwijs dan wordt dit tot nu toe gevoerd onder het motto "over hen, zonder hen". De kerkgeschiedenis leert dat het ook anders kan.

11. De door priesters geleide rooms-katholieke lekenorganisatie Opus Dei, die haar activiteiten met name richt op studerende jongeren, gaat uit van een spiritualiteit die geen ruimte laat voor de vorming van een persoonlijk geweten.

J. Escriva de Balaguer, de Weg, o.a. de alinea's 457, 777 en 945.

12. Ook al is Neelie's bod nog zo snel,
Het gaspedaal overtroeft óók dit wel.